

MICROCOPY RESOLUTION TEST CHART  
NATIONAL BUREAU OF STANDARDS 1963 A

(6)

AD

AD-A148 743

STABILITY OF EMBANKMENTS  
ON SOFT CLAY

Final Technical Report  
Part 3 of 3: Centrifuge tests  
and Numerical Analysis

by

M S S Almeida and R H G Parry

November 1984

United States Army

EUROPEAN RESEARCH OFFICE OF THE U S ARMY

London, England

DTIC  
SELECTED  
DEC 14 1984  
S D E

CONTRACT NUMBER DAJ A37-82-C-0177

Cambridge University Engineering Department

approved for Public Release, distribution unlimited

DTIC FILE COPY

84 12 05 024

Unclassified

SECURITY CLASSIFICATION OF THIS PAGE (When Data Entered)

REPORT DOCUMENTATION PAGE		READ INSTRUCTIONS BEFORE COMPLETING FORM
1. REPORT NUMBER	2. GOVT ACCESSION NO AD-A148743	3. RECIPIENT'S CATALOG NUMBER
4. TITLE (and Subtitle) Stability of Embankments on Soft Clay Part 3 of 3: Centrifuge Tests and Numerical Analysis		5. TYPE OF REPORT & PERIOD COVERED Final Technical Report June 82 - Sep 84
		6. PERFORMING ORG. REPORT NUMBER
7. AUTHOR(s) M.S.S. Almeida and R.H.G. Parry		8. CONTRACT OR GRANT NUMBER(s) DAJA37-82-C-0177
9. PERFORMING ORGANIZATION NAME AND ADDRESS Engineering Department Cambridge University Cambridge CB2 1PZ, UK		10. PROGRAM ELEMENT, PROJECT, TASK AREA & WORK UNIT NUMBERS 61102A-IT161102-BH57-01
11. CONTROLLING OFFICE NAME AND ADDRESS USARDSG-UK PO BOX 65, FPO NY, NY 09510		12. REPORT DATE Sep 84
		13. NUMBER OF PAGES 157
14. MONITORING AGENCY NAME & ADDRESS (if different from Controlling Office)		15. SECURITY CLASS. (of this report) Unclassified
		15a. DECLASSIFICATION/DOWNGRADING SCHEDULE
16. DISTRIBUTION STATEMENT (of this Report) Approved for public release; distribution is unlimited.		
17. DISTRIBUTION STATEMENT (of the abstract entered in Block 20, if different from Report)		
18. SUPPLEMENTARY NOTES		
19. KEY WORDS (Continue on reverse side if necessary and identify by block number) Centrifuge, CRISP, displacements, dissipation, effective stress, embankment, granular columns, normal consolidation, numerical modelling, overconsolidation, permeability pore pressure, settlement, shear modulus, soft clay, stability, stage construction, stress history, total stress, undrained shear strength.		
20. ABSTRACT (Continue on reverse side if necessary and identify by block number) Centrifuge tests have been conducted to study the behaviour of embankments on soft clay and to provide quantitative data against which to test the predict- ive power of the Cambridge CRISP program. Soft clay foundations were prepared with an overconsolidated crust over normally consolidated kaolin clay. Methods of conducting site investigation tests on this clay have been described in Parts 1 and 2. Tests were performed both with embankments constructed during flight in stages and in a single lift to failure, with measurements of pore pressures at		

selected locations, and displacements using a marker grid. Some tests were performed with the clay foundation strengthened using granular columns. An embankment built in a single life, on unstrengthened clay, failed at a height of 11.6m before inducing failure. Heights of 13m were achieved with stage constructed embankments on strengthened foundations, but without any failure occurring. Unexpected large lateral displacements were measured in unstrengthened clay during consolidation periods. Large displacement increases are a good indicator of factor of safety below about 1.3. At corresponding loading the use of strengthened foundations decreased lateral and vertical movements by about 50%.

In numerical computation using CRISP, particular attention was given to the influences of assumed shear modulus and permeability. Prediction of ground level settlements, pore pressure generation and pore pressure dissipation were good, but horizontal movements and vertical movements of depth tended to be overpredicted. Total stress and effective stress stability analyses were made for embankments on both unstrengthened and strengthened clay foundations. In the latter case allowance was made for the strength of the columns. It was found for the wide spacing of columns, used, the increased pore pressure dissipation due to the presence of the columns had a much greater strengthening effect than any intrinsic strength of the columns themselves. Calculated effective stress factors of safety of failed embankments were found to be 0.9 for unstrengthened and 0.87 for strengthened foundations, the difference between these figures and unity is probably due to a side friction on the box. Total stress analyses significant pore pressure dissipation was occurring during construction.

Accession For	
NTIS GRA&I	<input checked="" type="checkbox"/>
DTIC TAB	<input type="checkbox"/>
Unannounced	<input type="checkbox"/>
Justification	
By _____	
Distribution/ _____	
Availability Codes	
Avail and/or	
Dist	Special

**A-1**

## Contents

1. Introduction	1
2. Review and Objectives	2
2.1 Embankments on soft clays	2
2.2 Single lift embankments	3
2.3 Stability of embankments on soft clays	4
2.3.1 Total stress analysis	4
2.3.2 Effective stress analyses	6
2.4 Stage constructed embankments	6
2.4.1 Stability analysis	6
2.4.2 Time settlement analysis	7
2.5 Soil strengthening with granular columns	8
2.6 Analytical tools	10
2.7 Numerical modelling	11
2.8 Experimental tools	14
2.9 Centrifugal modelling	15
2.9.1 Principles	15
2.9.2 Applications to embankments on soft clays	17
2.9.3 Clay beds for centrifuge tests	18
2.10 Objectives and programme	19
2.10.1 Objectives	19
2.10.2 Outline of the report	20
3. CENTRIFUGAL MODELLING	21
3.1 Apparatus and technique used	21
3.1.1 Clay models with granular columns	21
3.1.2 Pore pressure measurements	24
3.1.3 Photography and displacement measurements	25
3.2 Centrifuge tests	27
3.2.1 Geometries and loading sequences	27
3.2.2 Description of the tests	28
3.2.3 Objectives of the tests	30
3.3 Displacements and strains data	31
3.3.1 Displacement vectors	32
3.3.2 Horizontal displacements	32
3.3.3 Vertical displacements	34
3.3.4 Strains data	35

3.3.5 Discussion of the results	36
3.4 Pore pressure data	39
3.4.1 Location of the pore pressure transducers	39
3.4.2 Results for tests MA3 and MA6	40
3.4.3 Results for test MA5	44
3.5 Summary and conclusions	45
4. Numerical modelling	47
4.1 CRISP program	47
4.2 In situ stress state	47
4.3 Modelling the clay foundation	49
4.3.1 Cam-clay parameters	49
4.3.2 Shear moduli	51
4.3.3 Coefficients of permeability	53
4.4 Modelling the sand layer and the embankment	54
4.5 Finite element analyses	55
4.5.1 Finite element mesh	55
4.5.2 Analyses performed	56
4.6 Predicted and measured displacements	57
4.6.1 Results	57
4.6.2 Discussion	58
4.7 Predicted and measured pore pressures	60
4.8 Stress distribution in the clay foundation	62
4.9 Conclusions	64
5. Stability analyses	65
5.1 Introduction	65
5.2 Total and effective stress analyses	66
5.2.1 Undrained strength parameters	66
5.2.2 Effective stress strength parameters	67
5.3 Strengthening effect of the columns	67
5.4 Stability of tests MA3 and MA6	69
5.4.1 Results	69
5.4.2 Discussion	70
5.5 Stability analysis of test MA5	73
5.6 Summary and conclusions	75
6. Conclusions	77
6.1 Experimental observations	77
6.2 Analytical studies	77
6.3 Concluding remarks	79
7. References	80

Tables 3.1, 3.2, 4.1, 4.2

Plates 3.1 to 3.14

Figures 2.1, 3.1 to 3.40, 4.1 to 4.20, 5.1 to 5.8

## LIST OF SYMBOLS

$c_u$	undrained shear strength
$c_h, c_v$	coefficients of consolidation in the horizontal and vertical directions
$c'$	cohesion in terms of effective stress
$\bar{c}'$	cohesion of the composite foundation
$e$	voids ratio
$e_{cs}$	voids ratio at critical state line for $p'=1$ kPa
$h_u$	excess head of water (in meters)
$k_h, k_v$	permeability in the horizontal and vertical directions
$m$	relative stress distribution between column and soil
$n$	stress concentration ratio
$p'$	mean normal effective stress $=(\sigma'_1 + \sigma'_2 + \sigma'_3)/3$
$p'_c$	isotropic preconsolidation pressure
$p'_o$	mean in-situ effective stress $=(\sigma'_{vo} + 2\sigma'_{ho})/3$
$p_o$	pressure acting around the cone tip
$q^*$	generalized deviatoric stress $=((\sigma'_1 - \sigma'_2)^2 + (\sigma'_2 - \sigma'_3)^2 + (\sigma'_3 - \sigma'_1)^2)^{1/2}$
$t$	time
$u$	pore water pressure
$z$	depth
$A_c$	area of clay per granular column
$A_s$	area of stone or sand column
$\bar{B}$	pore pressure coefficient $(=\delta u / \delta \sigma'_v)$
$C_c$	gradient of the compression line in the $e:\log p'$ plot
$C_s$	gradient of the swelling line in the $e:\log p'$ plot
$C_k$	slope of the $e:\log k_v$ line
$E$	Young's modulus
$F_s$	factor of safety
$G$	shear modulus
$H$	total depth of the clay foundation
$I_D$	relative density
$K'$	bulk modulus in terms of effective stress
$K_o$	coefficient of lateral earth pressure at rest

$K_{nc}$	coefficient of lateral earth pressure at rest in the normally consolidated state
N	gravity scaling factor (centrifuge acceleration $Ng$ )
OCR	overconsolidation ratio ( $=\sigma'_{vm}/\sigma'_v$ )
$T_v$	time factor for vertical water flow
$\gamma$	soil specific weight
$\delta_h, \delta_v$	horizontal and vertical displacements
$\delta u$	incremental excess pore pressure
$\eta$	ratio $q^*/p'$
K	gradient of the swelling line in the $e:\ln p'$ plot
$\lambda$	gradient of the compression line in the $e:\ln p'$ plot
$u_c, u_s$	ratio of stresses acting on the clay and sand column to the applied embankment pressure
$\nu'$	Poisson's ratio in terms of effective stress
$\sigma$	applied embankment pressure
$\sigma_c, \sigma_s$	stresses acting on clay and sand column, respectively
$\sigma'_1, \sigma'_2, \sigma'_3$	principal effective stresses
$\sigma'_h, \sigma'_v$	horizontal and vertical effective stresses
$\sigma'_{ho}, \sigma'_{vo}$	in-situ horizontal and vertical effective stresses
$\sigma_v$	total vertical stress
$\sigma'_{vm}$	maximum vertical effective stress
$\phi'$	angle of friction in terms of effective stress
$\phi'_{cs}$	angle of friction corresponding to critical state conditions
$\phi'_c, \phi'_s$	angle of friction of clay and sand column
$\bar{\phi}'$	angle of friction of the composite foundation
$\Delta$	increment
$\Delta u$	excess pore pressure
M	critical state frictional constant

## 1. INTRODUCTION

Although a good deal of attention has been given in recent years to the problem of embankments on soft clay, a number of factors still require close investigation. These include the influence of anisotropy and partial drainage during construction, and methods of predicting pore pressure generation and deformations, particularly horizontal movements. Centrifuge techniques allow models to be prepared with soil stress histories and loading conditions corresponding reasonably well with those in the field; and, at the same time give much greater control over the conduct of the test and over the recording of the behaviour. Data obtained under these closely controlled conditions give a basis against which predictive methods can be assessed.

A series of tests investigating the performance of embankments on soft clays has been performed on the Cambridge centrifuge. An essential feature of this work is the correct determination of the undrained shear strength of the soft clay. Previous reports (Almeida and Parry 1983a,b) have dealt with vane and penetrometer tests performed in laboratory and during centrifuge operation. This report, the last of this series, is concerned with centrifugal and numerical modelling of stage constructed embankments on soft clays. The numerical model used here is the Cambridge CRISP program which is based on critical state concepts. Opportunity has also been taken in the centrifuge testing programme of assessing the benefit of strengthening the soft clay foundation with granular columns.

In section 2 previous work related to centrifugal and numerical modelling are reviewed and objectives and programmes are stated. Section 3, on which this report is based, presents displacements and pore pressure data of centrifuge tests of embankment construction on both unstrengthened and strengthened soft clay foundation. Numerical analyses of a stage constructed embankment on unstrengthened soft clay are presented in section 4 and stability analyses are presented in section 5. Conclusions of the research work are presented in section 6.

## 2. REVIEW AND OBJECTIVES

### 2.1 Embankments on soft clays

When soft soils are encountered below a proposed earth embankment, the geotechnical engineer has four alternatives:

- (a) bypass the soft soil by relocating the embankment structure;
- (b) remove the soft soil and replace it with a good one;
- (c) design the embankment structure for the soft soil;
- (d) treat the soil to improve its properties.

As good sites and materials get scarce, the last two alternatives increase in importance.

If stability requirements prevent construction of an embankment in a single lift, a number of methods can be used for the design of the embankment-foundation system. Some common methods of construction are use of stabilizing berms or lightweight fills, preloading, surcharge loading, construction in stages and dynamic compaction. Sand drains or prefabricated drains associated with stage construction or surcharge loading are commonly used when the acceleration of settlements and rapid increase of the foundation strength are important requirements.

Alternatively the weight of the embankment can be transferred to more competent layers by stone columns, lime columns or embankment piles, or redistributed to the clay foundation by the use of reinforcement under the embankment. Thermal stabilization such as heating and freezing, grouting and electro-osmosis are less common procedures used for improvement of the foundation soil under embankments.

The methods for construction and treatment of foundation soils under embankments as outlined above have been described in detail by Broms (1979) and Mitchell and Katti (1981) amongst others, and it is beyond the scope of this report to discuss them further. Factors which lead to the choice of the most suitable method for construction or treatment of the foundation soil for a particular problem will depend on technical, economical and political aspects.

This report examines the behaviour of stage constructed embankments on untreated clay foundations and on clay foundations reinforced with stone columns. Attention is also given to the behaviour of embankments quickly constructed on untreated foundations.

The experimental tool used in this report is mainly centrifugal modelling. The analytical tool employed is numerical modelling based on critical state soil mechanics theory. Limit equilibrium stability analyses of embankment failures are also performed.

Since single lift on untreated foundations is the most common type of embankment construction procedure used, this is discussed first.

## 2.2 Single lift embankments

Current practice for the design of embankments on soft clays usually separates short term behaviour during and immediately after construction and long term post construction behaviour.

The assessment of the short term embankment stability is generally made by means of the total stress,  $\phi = 0$  analysis, the undrained strength being measured by means of vane tests. However as a number of embankments have failed with factors of safety in excess of unity (Parry, 1971; Bjerrum, 1972), correction factors to vane strength as a function of the plasticity index (Bjerrum, 1972) or liquid limit (Pilot, 1972) have been proposed.

Effective stress analyses are sometimes performed with estimated pore pressures and with  $c'$  and  $\phi'$  determined from triaxial tests. Predictions of pore pressures generated during construction are made by means of stress computations by elasticity theory and use of pore pressure parameters (Skempton, 1954; Henkel, 1960) obtained from triaxial tests. Other methods for pore pressure calculation have been proposed by Hoeg et al (1969), Burland (1971) and Leroueil et al (1978), but these methods have not yet found widespread use.

Short term settlements are in practice estimated by means of a Young's modulus determined from undrained triaxial tests and the Poisson's ratio is assumed to be 0.5, consistent with undrained behaviour. More rarely numerical analysis by means of the finite element method are performed and a more complete pattern of displacements is obtained.

The design for the post construction phase requires estimates of the final settlements and the development of settlements with time. Oedometer values of coefficients of compressibility  $C_c$  and swelling  $C_s$  are used for the computations of final settlements. The Terzaghi 1-D consolidation theory is the basis of time-settlement analysis, using the coefficient of consolidation  $c_v$ . Since  $c_v$  is not a soil constant and there are practical difficulties in the definition of drainage boundaries and thin sand layers, as discussed by Rowe (1972), time-settlement analysis is not a straightforward exercise. Difficulties in the use of  $c_v$  are further discussed below. Brenner et al (1982) compared a number of methods of settlement calculation with field observations and concluded that in many cases it is not too difficult to find a combination of procedures and soil parameters which produces a good fit to the observed data.

### 2.3 Stability of embankments on soft clays

#### **2.3.1 Total stress analysis**

Since Parry (1971) and Bjerrum (1972) have pointed out the difficulties in the evaluation of the stability of embankments on soft clays, a major effort has been concentrated in the clarification of this problem. The use of total stress,  $\phi = 0$  analysis with vane strengths corrected as proposed by Bjerrum (1972) or Pilot (1972) has been the method most widely used. However the theoretical basis of these corrections have been questioned and, as an attempt to reduce empiricism, other approaches to the total stress analysis have been proposed (Ladd and Foot, 1974; La Rochelle et al, 1974; Trak et al, 1980), though the vane correction proposed by Bjerrum (1972) is still largely used. Tavenas and Leroueil (1980) have added a number of recent cases to the factor of safety-plasticity index plot and have suggested a slightly different procedure for application of the vane correction.

The approach recommended by Ladd and Foot (1974) is the SHANSEP method applied by Ladd and his co-workers to the analysis of a number of failed embankments (e.g. Lacasse et al, 1978). One of the most contentious aspects of this method is the procedure of consolidating specimens beyond the preconsolidation pressure, so limiting the method to uncemented

unsensitive clays. The method has been criticized (Mesri, 1975, Leroueil et al, 1979) for natural clays in general, as they possess some intrinsic structure as a result of the geologic process, which is destroyed by the application of high consolidation pressures.

La Rochelle et al (1974) have suggested the measurement of the undrained strength at large strains (USALS method) in undrained triaxial tests. Difficulties of application of this method are associated with the magnitude of the corrections for cross sectional variation of the sample and membrane effects at large strains. Unlike SHANSEP, USALS method has not been widely applied.

Trak et al (1980) have proposed a semi-empirical approach based on an interpretation of the Bjerrum's data made by Mesri (1975), which led to the observation that the available strength at failure under an embankment is nearly independent of the plasticity index and is a function of the preconsolidation pressure  $\sigma'_{vm}$ . The equation  $c_u = 0.22\sigma'_v$  has been shown to be applicable to sensitive Canadian clays.

As an illustration to the above discussion, the field undrained strength of the Rio de Janeiro soft clay has been determined (Almeida, 1981) by field vane tests, undrained triaxial tests, SHANSEP, the method proposed by Trak et al (1980) and by critical state theory (CST), as shown in fig. 2.1. All methods, except that proposed by Trak et al, have produced, for this particular case, fairly close strengths below the crust. However the field vane test was the only one to detect the high strength at the crust. Total stress stability calculations of a trial embankment on Rio de Janeiro clay using uncorrected vane strengths have produced a safety factor close to unity (Ramalho-Ortigao et al, 1983). The fact that the Rio de Janeiro clay has an average plasticity index of 80%, for which the vane correction is supposed to be high, highlights the uncertainties still involved in total stress stability analyses. Nevertheless in general the stability of single lift embankments can presently be carried out with a reasonable degree of reliability by the use of total stress approaches calibrated regionally.

### **2.3.2 Effective stress analyses**

Less attention has been given to effective stress analysis to evaluate embankment stability. In view of the difficulties involved with the total stress analyses, Parry (1971) suggested that the effective stress analysis can be more reliable, provided realistic values of pore pressures can be obtained. Parry argued that some of the factors affecting the total stress analysis have a smaller effect on the effective stress analysis, in particular strain rate effects. In the light of effective stress analyses performed by Parry and McLeod (1967), it was suggested that  $c'$  values measured in the laboratory should be ignored in calculating stability, unless definite evidence to the contrary is available.

Effective stress analysis of the embankment failure on the Rio de Janeiro soft clay produced a factor of safety for peak strength parameters different to that given by the total stress analysis (Ramalho-Ortigao et al, 1983). Improvements were obtained using critical state strength parameters (Almeida, 1984).

Pilot et al (1982) have pointed out that reliable effective stress analyses are necessary in two important situations:

(a) construction of embankment in stages, discussed below, in which estimates of the increase of undrained strength with consolidation is difficult;

(b) control of construction of high embankments on soft compressible soils by means of in-situ measurements of pore pressures.

## **2.4 Stage constructed embankments**

### **2.4.1 Stability analysis**

Incremental or stage construction is a common method employed for embankments on soft ground. The consolidation of the foundation following each stage of construction increases progressively the shear strength of the foundation. Assessment of the stability for each stage of construction is an important aspect in the design of such structures.

Tavenas et al (1978) have suggested that the only way of obtaining an estimate of the true stability condition at any stage of construction is by means of effective stress analysis using the actual pore pressures

observed in the foundation and  $c'$  and  $\phi'$  obtained at large strains. However pore pressures are not always measured and reliable methods of pore pressure prediction are still necessary for the application of effective stress stability methods.

Alternatively, for total stress analysis, Tavenas and Leroueil (1980) have suggested computing the clay strength according to  $c_u = 0.22\sigma'_v$  where  $\sigma'_v$  is obtained from an elastic stress analysis combined with in situ pore pressure observations. Ladd and Foot (1980) have argued that the use of the above equation might be overconservative since much of the soil strengthening will occur beneath the embankment crest where an active-compression mode of failure leads to a shear strength increment higher than  $0.22\Delta\sigma'_v$ . Ladd and Foot (1980) have suggested that the above equation is more suitable for a simple shear type of failure which occurs roughly under the slope and that a passive-extension type of failure developing outside the embankment toe leads to a shear strength increment lower than  $0.22\Delta\sigma'_v$ .

#### 2.4.2 Time settlement analysis

The Terzaghi consolidation theory is commonly employed for time-settlement analysis under embankments on soft soils as discussed previously. The theory is based on assumption of linear elastic soil behaviour and of one dimensional drainage and settlement. The construction of an embankment in stages rarely causes such one dimensional behaviour but generally nonlinear consolidation involving lateral displacement and drainage.

The two basic theories commonly used for multi-dimensional consolidation are the Terzaghi-Rendulic theory (Terzaghi, 1943) based on the diffusion theories and the Biot (1941) theory developed from elasticity theory. The development and application of these theories have been reviewed in the literature (e.g., Murray, 1978). The basic criticism of the Terzaghi-Rendulic theory, is the assumption that total stresses remain constant during consolidation. This is not the case since differential strains developing through the soil require changes in total stresses to satisfy the stress-strain laws. Biot's theory is preferable from this point of view because it couples total stress equilibrium to strain compatibility during consolidation. It also displays the Mandel-Cryer

effect which is observed experimentally (Gibson et al, 1963).

Although Biot's theory is amenable to analytical treatment of simple problems, a numerical method such as finite differences and finite elements must be applied to solve more complicated problems. The theory is in most cases formulated in terms of the coefficient of consolidation  $c_v$ . The value of  $c_v$  is determined from oedometer tests for the range of stresses corresponding to the initial and final effective stress under the embankment and is considered a constant. However  $c_v$  is not an intrinsic soil parameter but a combination of permeability and deformability as given by

$$c_v = \frac{k(1+e)\sigma'_v}{0.434 \gamma_w C_c} \quad (2.1)$$

During consolidation the voids ratio  $e$ , the effective stress  $p'$  and the coefficient of permeability  $k$  vary so that  $c_v$  is not a constant. The coefficient of compressibility  $C_c$  sometimes varies as well over large stress increments.

Alternatively, Biot's theory can be formulated by means of the coefficient of permeability, as described by Small, Booker and Davis (1976). This formulation, used in the CRISP program (Gunn and Britto, 1983) employed later in this report can also be generalized to include a coefficient of permeability dependent on the voids ratio, as proposed in section 4.

Most of the early applications of Biot's theory have been for linear elastic material and only more recently (e.g. Thompson, 1976) has the theory been used with more realistic elasto-plastic strain hardening models such as Cam-clay models. Numerical analyses of embankments on soft clays are further discussed below.

## 2.5 Soil strengthening with granular columns

The work described in this report includes the modelling of embankments on soft clays strengthened with granular columns. Stone columns are used mainly to transfer the embankment load to the more competent soil stratum underneath the soft clay deposit. Therefore granular columns under embankments on soft clays increase the bearing

capacity and reduce settlements. The rate of consolidation of the foundation soil is also increased since the granular columns also act as vertical drain in the soil. A blanket of sand or gravel is usually placed over the top of the columns and serves both as a drainage layer and to distribute stresses from structures above.

Methods used for the construction of granular columns in soft soils have been reviewed recently by Greenwood and Kirsch (1983) and only the main features of these methods are outlined below.

Construction techniques for sand columns have been developed in Japan (Tanimoto, 1973) and consist of a casing pipe driven into the soil to the desired depth by a vibrator located at the top of the pipe. A sand-gravel plug at the bottom of the pipe prevents the soil from entering during driving. Sand is then introduced into the pipe which is then withdrawn part way while compressed air is blown inside the casing to hold the sand in place. The pipe is then vibrated down to compact the sand column and increase its diameter. The process is repeated until the pipe reaches the ground surface. The resulting piles are usually 0.6 m to 0.8 m in diameter and are placed in a triangular pattern with a spacing of 1.5 m to 2.2 m.

Most stone column installations are made using the vibro-replacement method, a variant of the technique of vibroflotation used to compact granular soils. The technique is in essence similar to the construction of sand columns described above. Major differences are in the shape of the pipe which is usually conical and in the application of water jet for soil replacement, though a dry process is sometimes used. Diameters of stone columns are usually about 0.6 m for stiff clays and about 1.0 m for soft clays. Square or triangular grid patterns are used and column spacings vary from 1.5 to 3.5 m.

The radial displacement of the soil during installation of the granular columns by vibration methods may reduce the shear strengths of the surrounding soil. Thornburn (1975) has suggested the use of a non-displacement method if the shear strength of the surrounding soil is less than 20 kPa.

Stone columns are not commonly employed to improve the shearing resistance under slopes of embankments, although a few examples of such applications have been presented by Rathgeb and Kutzner (1975) and Aboshi

et al (1979). Bishop (1976) has argued that for a significant improvement a considerable replacement in terms of area ratio is necessary, together with substantial overburden pressure to mobilize the frictional strength of the columns. Studies of embankments on granular columns performed here are concentrated on the suitability of the use of granular columns with low area replacement ratio under slopes of embankments to improve the shearing resistance.

## 2.6 Analytical tools

The distinction commonly made between the design for undrained construction and for drained long term behaviour is convenient for the geotechnical engineer, but do not give a full understanding of the behaviour of embankments on soft clays. Partial drainage behaviour is often important in the field (Leroueil et al, 1978) and should be taken into account. Considering the number of assumptions and parameters left to the choice of the geotechnical analyst, it is not surprising to see the number of good type C1 predictions (Lambe, 1973) published in the literature. On the other hand when type A predictions are called, MIT (1975) the agreement is generally poor apart from a few cases.

Alternatively, by using critical state soil mechanics (Schofield and Wroth, 1968; Roscoe and Burland, 1968), a smaller number of parameters is required. Strength and compressibility are treated within the framework of the elasto plastic strain hardening Cam-clay models and the same soil parameters are used for both drained and undrained analyses. Partial drained behaviour can be also modelled numerically by a Biot coupled consolidation analysis, as used in the CRISP program.

Some common criticisms (e.g. Tavenas, 1981) to the original Cam-clay models are:

(a) the assumption of a yield locus centred on the isotropic compression line whereas anisotropic consolidated clays exhibit yield loci approximately centred on the  $K_0$  consolidation line (e.g. Parry and Nadarajah, 1973)

(b) the assumption of isotropic rather than anisotropic behaviour inside the yield locus

(c) the assumption of associated flow rule which can be acceptable for

isotropic soils but does not properly represent the behaviour of anisotropic natural clays.

Despite the above criticisms the original Cam-clay models have been continuously used at Cambridge. The reasons are that they retain the mathematical simplicity and use a small set of parameters obtained from standard laboratory tests. Wood (1980) used a simple Cam-clay model and was able to deduce the shape of the yield locus of the in situ soil as well as predicting stress paths and pore pressures under the centre line of a tank loading test.

### 2.7 Numerical modelling

One strong feature of the Cam-clay models is the reasonable modelling of the behaviour of lightly overconsolidated clays under stress paths corresponding to embankment loading (Wood, 1982). Therefore the comparison of the theoretical computations with the good quality data provided by the highly instrumented centrifuge tests offers an excellent opportunity to check the performance of the critical state numerical predictions.

In the past some amount of success (e.g. Wroth, 1977) has been obtained in predicting the behaviour of embankments on soft soils by means of critical state finite element computations. A brief review of prior numerical analyses using critical state models is presented below.

The first finite element program employing models of soil behaviour based on critical state soil mechanics was developed by Simpson (1973). One of the applications of the program was to the analysis of the Kings Lynn trial embankment. Drained and undrained analysis using the same soil parameters were carried out. Good agreement for short and long term settlements were obtained from the two analyses. Computed pore pressure showed less agreement with field measurements than displacements, and poor agreement was obtained between measured and computed movements outside the toe of the embankment. The results of these analyses were also presented by Wroth and Simpson (1972).

Thompson (1976) improved Simpson's (1973) program and applied it to a class A prediction of the MIT trial embankment (MIT, 1974). The predictions were good in general but pore pressure computations in particular were better than those presented by the other predictors. The other

participants in the prediction symposium used non linear elastic programs with pore pressures computed from total stresses and pore pressure parameters. The results of this analyses have also been discussed by Wroth (1977).

Making use of the findings of these two workers and others (notably Naylor, 1975), Zytynski (1976) developed CRISTINA (Critical State Numerical Algorithm). Basset et al (1981) used a later version of that program with coupled consolidation to predict the behaviour of centrifuge constructed embankments. Excess pore pressures generated by the embankment construction and their rates of dissipation were fairly well predicted. However the settlements during consolidation were substantially overpredicted.

CRISP program (Gunn and Britto, 1981), the more recent version of the critical state finite element program developed at Cambridge, has been used by Almeida (1981, 1982).

A coupled consolidation analysis of the month long construction period was performed and good agreement was observed between predicted and measured settlements and pore pressures. Undrained and drained analyses have also been performed to obtain the two limit conditions of behaviour. Results of the undrained analysis under predicted settlement and overpredicted pore pressure. Long term settlements produced by the drained analysis compared well with settlements obtained from standard oedometer test computations. Results have also been compared (Almeida and Ramalho-Ortigao, 1982) with numerical predictions using an elastic non-linear model and the superiority of critical state numerical predictions which accounted for the soil consolidation was made evident.

Davies (1981) also used CRISP for the numerical analyses of stage constructed embankments during centrifuge flight. Predictions of pore pressures were quite reasonable with a trend towards overprediction near the centre line and underprediction beyond the embankment toe. Displacements were in general overpredicted and a much deeper pattern of displacements was predicted by the numerical computations. This was attributed by Davies to the high artificial stiffness of the sand surcharge layer, but can equally be explained by the consideration of a constant permeability for the whole clay foundation, which remained unchanged throughout the embankment construction. It has been observed

that compressible clay layers under high embankments experience a considerable consolidation during stage construction. Therefore if the permeability is made dependent on the voids ratio, some improvement can possibly be obtained.

The previous review shows that the higher expectations of good agreement between sophisticated numerical analyses and centrifuge tests of embankment construction have not always been satisfied, hence pointing to the need for further comparisons between centrifuge tests and numerical analyses.

Other critical state finite element programs have been developed elsewhere. Truong and Magnan (1977) developed the Rosalie program and used it for predictions of the Cubzac-les-Ponts B trial embankment constructed on a foundation of soft clay. They noted that their predictions were sensitive to the in situ values of  $K_0$  assumed in the analysis. It was found in general that the computations underestimated the observed settlements. Drained analyses allowed 50% consolidation settlements to be estimated.

Magnan et al (1982a) have modified the Rosalie program to include: coupled consolidation, yield locus centred on the  $K_0$  line, anisotropic elastic behaviour inside the yield locus and non-associative flow rule. Analyses of the Cubzac-les-Ponts B embankment produced better predictions of settlements based on the modified Cam-clay model than using the new model. However lateral displacements have been better predicted by the new model. Pore pressures have been reasonably predicted by both models, although observed pore pressure dissipations were faster than numerical results.

Magnan et al (1982b) have also used the new Rosalie to analyse the Cubzac-les-Ponts A embankment taken quickly to failure. The new model produced good predictions of settlements but overpredicted lateral displacements. Pore pressures have been systematically overpredicted. For both cases of embankments A and B, Magnan and co-workers have partly explained the discrepancies by the lack of complete saturation of the foundation soil ( $S = 96\%$ ) and to the poor quality data of the permeability measurements. This highlights the advantages of using centrifuge tests to check numerical methods, as discussed below.

## 2.8 Experimental tools

Field trials are commonly used to improve the understanding of the behaviour of general prototype structures and particularly of embankments on soft clays.

Initially the chosen clay deposit is thoroughly investigated by means of in situ and laboratory tests. The instrumentation installed to monitor field behaviour consists basically of piezometers for pore pressure measurements and of a number of instruments such as settlement plates, extensometers, inclinometers, to measure horizontal and vertical displacements. The embankment with known material properties is then built at a chosen loading rate and instrument readings recorded.

The results of the measurements are then analysed, usually in relation to undrained short term and drained long term behaviour, as outlined previously. The theories for prediction of the embankment behaviour are checked and ranked according to ease and accuracy with which correct predictions are made. The field observational method (Peck, 1969), as outlined above for the case of embankments on soft clays, is one of the methods by which progress has been made in geotechnical engineering.

Alternatively, progress can be achieved in the laboratory by performing model tests of soils in their simplest states (e.g. well graded sands and saturated reconstituted clays), so that their properties can be defined by the minimum possible number of parameters, these soil parameters being measured under a wide variety of imposed stress or strain paths by suitable soil testing equipment. This latter approach has been pursued at Cambridge over the last three decades (Roscoe, 1970; Schofield, 1980).

Advantages of model tests over full-scale work are (Bassett, 1980):

(a) because of their small size they are relatively cheap and quick to carry out,

(b) they can be taken to failure with no catastrophic or expensive results,

(c) the soil properties can be chosen and are more controllable, hence soils are more uniform,

(d) more repeatability of experiments can be achieved.

Model tests can be divided into three categories as defined by James (1971):

(a) Category I: model test simulating real prototypes. All boundary conditions, i.e. soil strata, ground water conditions must be suitably simulated in the model.

(b) Category II: model test considered to be prototype in its own right and its behaviour compared with some method of analysis. A typical requirement of tests in this category is the soil uniformity.

(c) Category III: model test of an idealised artificial prototype designed to reveal detailed stress and deformation information about a problem.

Most of the model experiments reported by Roscoe (1970) fall into Category III and they have provided important strain data information on the behaviour of earth retaining structures. The majority of soil mechanics model testing falls into Category II and involves situations where the boundary forces of the soil mass outweigh the self weight effects of the soil. Examples of Category I type tests are given by Lydon and Schofield (1970) on the short term stability of slopes on overconsolidated clays and by Bassett (1973, 1974) and Bassett and Horner (1979) on the deformation of embankments on soft clays. These workers have used centrifuge tests since self weight dominate stress level and hence stress paths.

The experimental work described here involves centrifugal modelling of embankments on clay foundations. The model tests fall into Category II above since no particular prototype problem was modelled by the tests. However, corresponding prototype dimensions and boundary conditions could be easily found in practice.

## 2.9 Centrifugal modelling

### **2.9.1 Principles**

The scaling laws applied to model testing have been stated by Rocha (1957) and reviewed by Roscoe (1968). The advantages of the centrifuge to achieve self weight and stress path similarity have been discussed by Schofield (1980). In essence, if a model  $N$  times smaller than the prototype is subjected to an acceleration  $N$  times the earth gravity field, then the density of all materials in the model will be increased by  $N$  and the

stresses at a depth  $z/N$  will be identical to the stress in the prototype at a depth  $z$ . If materials with the same stress-strain behaviour are used in both model and prototype, strain similarity is also achieved in both model and prototype.

An additional advantage of a centrifuge test is the shortening of time-dependent processes. According to the Terzaghi consolidation theory the time for dissipation of excess of pore pressure is proportional to the square of the drainage path. As stresses in the centrifuge are the same magnitude as the prototype but the model dimensions are reduced by  $N$  times, the drainage path is also  $N$  times shorter. Hence the model time is  $N^2$  times shorter than in the prototype. This relationship has obvious implications for the centrifuge modelling of stage constructed embankments on soft clays.

Complete similarity for modelling purposes would also require the ratio of the dimensions of particle sizes, between model and prototype dimensions, to be observed. However, in order to model correctly the stress-strain responses of soils in a centrifuge test, natural soils must be used. Hence, particle sizes are not scaled down and complete similarity cannot be achieved, as pointed out by Ovesen (1980).

Roscoe (1968) quoting x-ray and electron microscope results stated that the thickness of failure surfaces was in the region of 10 to 20 particle diameters. Hence the shear band thickness is a function of the particle size rather than of the size of the overall body of soil and is incorrectly modelled in centrifuge tests. This point is not particularly important for clay models since the typical particle size of the kaolin clay used here is 0.002 mm. Consequently the use of coarse granular materials in sand model tests, such as the 14/25 Leighton Buzzard sand, should be avoided. The embankment material used in the model tests performed here is the 30/52 Leighton Buzzard sand also used by Horner (1982) and Davies (1981), with grain sizes ranging from 0.3 to 0.5 mm. Scarpelli (1981) investigated shear bands of the 30/52 sand using a 330 mm long direct shear box. In the radiographs taken during the tests it was shown that the band width reached a value of ten times the average grain size only after dilation had ceased and critical state was being approached. Hence, according to Scarpelli's figure, the thickness of the failure zone through the embankment would be of about 4 mm. This

corresponds to 0.4 m at 100 g, the chosen acceleration field for the tests to be performed here. The significance of errors introduced by the non-scaling of shear band thicknesses are not very clear but are expected to be of minor importance for the tests performed here.

Settlements due to secondary consolidation or drained creep are not scaled either during centrifuge tests. However because centrifuge test times are relatively short, those settlements will be negligible during test periods.

### 2.9.2 Applications to embankments on soft clays

Avgherinos (1969) initiated centrifuge studies of embankment failures at Cambridge and was mainly concerned with slope failures by rapid drawdown of reservoirs. Endicott (1971a) followed Avgherinos and performed embankment tests on clay foundations. While the centrifuge was stationary the embankment was placed on the foundation and the construction was simulated by increasing the centrifuge acceleration in stages over a period of time. Hence the model embankment height was equivalent to the height of the prototype at each centrifuge acceleration level. However the stress history imposed on the clay foundation was not exactly the same as in the equivalent prototype, as discussed below. This construction technique was used by Bassett (1973, 1974) and Endicott (1971b) for modelling real prototype embankments.

Beasley (1973) developed the in-flight embankment construction technique and compared it with the accelerating technique. It was found that the stress conditions were similar at the end of construction but that at intermediate stages the excess of pore pressures did not compare because the samples were subjected to different loading sequences. The method of construction developed by Beasley (1973) consists of pouring sand from a hopper mounted on the centrifuge package while the centrifuge is running at a constant speed. This more realistic technique of embankment construction has since been used by Davies (1981) and Horner (1982) and is also used here.

All the above research workers have conducted plane strain model tests. A perspex plate used to form one side of the centrifuge model container allows the side face of the model to be observed from above the centrifuge arm while the centrifuge is spinning. This visible section is

instrumented by inserting a regular grid of small silver spheres which allows pictures to be taken and subsequent displacement and strain fields to be computed, using the technique described by James (1973). When using the technique of embankment construction by hopper pouring, no displacement information can be obtained in the embankment section itself.

Pore pressures are recorded using miniature pore pressure transducers inserted into the clay bed at locations similar to those likely to be selected for pore pressure monitoring in a prototype. Pore pressure transducers used here are provided with silicon chips, hence offering very fast response times, of the order of 0.1 sec. Full descriptions of the apparatus and techniques used for displacements and pore pressure measurements are presented in section 3.

### **2.9.3 Clay beds for centrifuge tests**

Bassett (1974) used centrifuge modelling techniques to predict the behaviour of the trial embankment at the MIT (1974) prediction symposium. He resorted to a single model test using local natural soil to achieve what would be an acceptable engineering decision, but not the closest answer. This approach raised questions about how to achieve material properties representative of the most likely conditions in the ground. Bassett (1980) subsequently suggested a bracketing approach in which the worst and the better samples from a site are chosen and tested, and thus the corresponding prototype behaviour is likely to be bounded by the two model tests. This approach has been successfully used by Bassett and Horner (1979). Difficulties in interpreting of centrifuge tests using heterogeneous natural soils can be avoided by using reconstituted or laboratory prepared soils (Schofield, 1980) and this is the basic reason why reconstituted kaolin and Gault clay are used in the clay models here.

Clay foundations under embankments usually consist of a stiffer highly overconsolidated clay layer over a soft lightly overconsolidated clay layer with shear strength increasing with depth. Most soft clay deposits have not experienced any erosion of overburden and causes of overconsolidation of such deposits are probably water level lowering or fluctuation, secondary consolidation and desiccation stresses close to the surface, which are responsible for the high strength at the crust. Since the behaviour of embankments on soft clays is likely to be influenced by

the existence of the overconsolidated clay crust, attempts have been made to produce clay models for centrifuge tests consisting of a stiff clay layer over a soft clay layer. Horner (1982) and Bassett and Horner (1979) produced a number of such models in which the ratio of thickness of stiff to soft clay layer was varied to produce a range of strength profiles. The stiffer layer was separately consolidated in the laboratory and placed over the softer layer, and the complete clay model was then reconsolidated under centrifuge acceleration. However results indicated that relative displacements occurred between both layers during embankment construction.

Davies (1981) developed a technique of producing a single sample with a stiff layer over a soft layer. The stiff crust was achieved by consolidating together from slurry a layer of Gault clay on top of the kaolin, followed by an additional partial consolidation aiming to subject the top half of the clay model to higher effective stresses. This technique, successfully developed by Davies (1981), is used here and described in detail Almeida and Parry (1983b).

## 2.10 Objectives and programme

The previous sections have examined the behaviour of embankments on soft clays and reviewed the associated work on centrifugal and numerical modelling techniques.

### **2.10.1 Objectives**

The objectives of the research described in this report, with consideration to the previous points are:

(a) conduct a number of centrifuge tests of stage constructed embankments on untreated clay foundations and on clay foundations treated with granular columns, using the same stress history in all clay models to allow direct comparison of the results;

(b) compare measurements of pore pressures, displacements and strains taken during centrifuge tests with predictions obtained by a critical state numerical method;

(c) perform total and effective stress stability analyses of embankments constructed in stages on treated and untreated foundations, as

well as of an embankment taken quickly to failure.

### 2.10.2 Outline of the report

Results of pore pressures and displacements of stage constructed embankment on virgin foundations and on foundations treated with granular columns are presented in section 3.

The programme for analysis of the centrifuge tests of embankment loading consisted of:

(a) numerical analyses using the CRISP program, as described in section 4, consisting of comparisons of predicted and observed pore pressures and displacements data of a stage constructed embankment on untreated foundation

(b) stability analyses of the embankment construction, as described in section 5, consisting of total and effective stress analyses of:

(a) embankment quickly taken to failure in a quasi-undrained condition,

(b) embankment constructed in stages over an untreated clay foundation and taken to failure at the end of the test,

(c) embankment constructed in stages on foundation treated with granular columns.

Effective stress analyses have been performed using measured pore pressures during embankment construction and effective stress strength parameters. Total stress analyses have made use of undrained strengths measured by the vane apparatus during centrifuge operation.

Section 6 presents the conclusions of the research work.

### 3. CENTRIFUGAL MODELLING

Centrifugal modelling of embankments on soft clays is the subject of this section. Centrifuge tests to be described are MA3, MA4, MA5 and MA6. Tests MA3, MA4 and MA6 were of stage constructed embankments and test MA5 was of a foundation taken quickly to failure by successive embankment loading. Clay foundations treated with granular columns were used in tests MA4 and MA6. Tests MA3 and MA5 were of embankments on untreated foundations. Data of displacements and pore pressures of the different tests are compared and discussed.

#### 3.1 Apparatus and technique used

Apparatus and techniques for preparing clay beds for embankment construction during flight and for site investigation have already been described (Almeida and Parry, 1983b). This section complements the description of apparatus and techniques used, including: a) the process of installation of the granular columns; b) the instrumentation to measure pore pressures and displacements.

##### **3.1.1 Clay models with granular columns**

###### Material and geometry

Models MA4 and MA6 (see description below) were provided with a grid of granular columns in the position of the clay bed under the embankment slope.

The 30/52 Leighton Buzzard sand, also used for the embankment and the top surcharge layer, was used for the columns. Particle sizes of the 30/52 sand range from 0.3 to 0.5 mm and centrifuge model tests were performed at 100 g. Hence the sand in the columns had a corresponding diameter at prototype scale varying from 30 to 50 mm, which is within the range used for stone columns.

An essential feature of the stone columns is that they are stiffer than the surrounding soil so that, by arching, the embankment load is transferred to the more competent sand layers below the clay foundation.

Hence sand columns have been prepared here in dense conditions, by dry pouring, as described subsequently. Additionally by being prepared with high relative densities, the granular columns are more effective as elements to improve the shearing resistance.

Clay models without granular columns were provided with filter paper and porosint at the bottom of the liner to act as drainage elements. However since clay models with granular columns would have increasing water flow, it was decided to provide these with an additional 5 mm thick layer of 80/120 Leighton Buzzard sand to act as underdrainage.

Diameter of stone columns in soft clays range from 0.75 m to 1.5 m. Model granular columns were chosen to have 10 mm diameter, equivalent to 1.0 m at prototype scale. Grid spacings ranged from 1.5 to 3.5 m, closer grids being used for softer clays.

As stated in section 2, one of the objectives of the experimental work carried out in this dissertation was to investigate the feasibility of low area replacement ratios. Therefore it was decided to perform two tests with equivalent prototype grid spacings of 3.0 m and 4.0 m.

Column grids used in clay models MA4 and MA6, fig. 3.1, have approximate square grids of 30 mm and 40 mm of distance between centres, respectively. The grid lay-out had to leave clear the centre line down which the penetrometer probe would be driven, and columns had to be not too close to the boundaries. In order to accommodate these restrictions column grids could not be all made of exact squares. The location of the column grids with respect to the embankment is given below where results of centrifuge tests of embankment construction are discussed.

#### Installation of the granular columns

In field conditions the installation of stone columns causes in general significant disturbance to the surrounding soil, as discussed in section 2. Under laboratory conditions, installation of columns can be performed with negligible clay disturbance, which is desirable with respect to analysis and comparisons with embankment tests on untreated clay.

The phase of model preparation in the laboratory was the same for all clay models, including those provided with granular columns. The granular columns were installed following the consolidation run during centrifuge

flight to achieve the required stress history.

Before stopping the centrifuge, solenoid valves connected to the external water reservoirs were operated and the free water available in ducts, pipes and drainage layers was dumped into the centrifuge pit. The purpose of this operation was to avoid excessive swelling of the clay model, hence minimizing the time for reconsolidation of the clay model in the second phase of the centrifuge test after installation of the sand columns.

After stopping the centrifuge, the strong box and swing platform were lifted to the preparation room. The sand layer in the region of the grid was removed and a rig to help with the installation of the granular columns was positioned inside the strong box, as shown in fig. 3.2a. The sequence of events, fig. 3.2b, d, for installation of the sand drains consisted of:

- 1 - driving of a 0.5 mm thick open ended tube guided by the rig inside the clay model, fig. 3.2b;

- 2 - twisting and subsequent lifting of the tube with the clay inside, fig. 3.2c;

- 3 - positioning of a tube with funnel just above the top of the open hole and pouring the sand at a fixed slow rate to achieve a dense packing, fig. 3.2d;

- 4 - extrusion of the clay from inside the tube and cleaning of the tube with a brush;

- 5 - internal and external spraying of a silicone fluid to ease driving and minimize disturbance.

Events 1 to 5 above were repeated for each column of a row and for each row. The amount of sand to be used in each sand column was estimated in advance and placed in a number of envelopes corresponding to the number of existing columns. This made possible a careful control of the density of each granular column. The average relative density of the sand columns was 89% for both tests.

After installation of the sand columns the sand layer was re-placed in the region of the columns. The strong box and the rest of the centrifuge apparatus were rebolted to the centrifuge arm and the centrifuge restarted. The time lapse between stopping and restarting the centrifuge was of about 4 hours in both tests. The time taken for re-equilibrium of

pore pressures after restart of the centrifuge was 120 min for test MA4 and 140 min for test MA6.

In model MA4 the time taken for re-equilibrium of pore pressures should have been much shorter since it was provided with more granular columns. However in model MA4 the solenoid valve did not operate at 100 g but only at about 50 g, thus water was drawn into the clay model and a significant swelling took place. In model MA6 a new solenoid valve was used which operated satisfactorily at 100 g. It is assumed here that the reconsolidation of the clay models provided with granular columns was of minor importance and that stress histories of models with and without granular columns are essentially the same. Hence comparisons can be made of results of embankment loading tests for all clay models.

### 3.1.2 Pore pressure measurements

After consolidation in laboratory was completed under the final pressure the pressure was removed and miniature pore pressure transducers were inserted through the back of the clay model. The consolidometer back plate was carefully removed from the consolidometer and the transducers inserted into a hole augered into the clay and then backfilled with thick slurry, a technique commonly used at Cambridge, as described in detail by Davies (1981). A wooden template clamped to the side of the model was very effective not only for the temporary support of the auger and transducer leads, thus minimizing clay disturbance, but also for the correct positioning of the transducers. The position of the transducers inside the clay model was checked by radiographs taken after the test.

Miniature pore pressure transducers used were the PDCR81 transducers manufactured by Druck Ltd. They are 6.35 mm diameter by 12 mm long, fig. 3.3, and utilise semiconductor strain gauges to measure the strains of a silicon diaphragm. The back of the diaphragm is bonded to a glass isolating ring and is vented to the atmosphere. The front of the diaphragm has a small gap between it and a porous stone which prevents effective soil pressures from acting on the diaphragm. In order to achieve a rapid response the stone and the gap between it and the diaphragm need to be saturated with water. To achieve this the transducers were placed into a blown glass chamber which was filled with de-aired water and subjected to a pressure of -0.9 atmospheres using a vacuum pump. During saturation the

transducers were powered up and connected to a digital voltmeter for control. It was found that by applying and removing the vacuum a number of times the effectiveness of the de-airing operation could be assessed by checking the response time.

The transducers were calibrated in a rig commissioned by D.V. Maddocks which allowed simultaneous calibration of 5 transducers at any time. The pressure was applied by a remote air/water interface and recorded in a Druck DPI 100 digital pressure meter. For the maximum range of pressure of 350 kPa the output was about 100 mV for a power supply of 5 volts.

### 3.1.3 Photography and displacement measurements

#### Model face preparation

Following the laboratory consolidation and transference of the model to the strong box, the front face of the model was prepared with two grids for photographic observation: a square grid of dark brown clay and a grid of 3 mm diameter silver markers superimposed on the former. The objective of the clay grid was to allow observation of discontinuities such as failure planes. The silver markers allowed measurements of displacements to be performed after the test.

A melinex template was placed on the face of the model with the strong box tilted to  $45^{\circ}$ , as shown in plate 3.1. The clay powder was sprinkled from a sieve over the template, the powder adhering to the clay model by drawing moisture from it. Excess powder was vacuumed and the template removed to expose the clay grid.

Silvered markers inside plastic cups were then carefully pressed into each of the squares formed by the clay grid, hence forming a 15 mm centres array, as shown in plate 3.2. When photographed using the flash system outlined previously, these silvered markers reflected the flash and appeared as dark spots on the film negative. Silver markers were also fixed at the liner base and served as fiducial markers for film measurement.

### Displacement measurements

Photographs of the model were taken during flight using a Hasselblad 500 EL/M camera. The camera is mounted above the centrifuge pit, and views the package through the perspex window, hence producing photographs equivalent to a cross sectional view of the prototype. A 20 Joule flash synchronized to the centrifuge rotor is triggered by a microswitch attached to the axis of the centrifuge. The duration of the flash is 2  $\mu$ s. At model travelling speeds of 50 m/s, the model movement during flash is of only 0.1 mm which does not affect the quality of the picture. Polaroid type photographs taken during the test provide a visual record of the model at different stages of a test. Standard type photographs allow measurement to be made of displacements at the boundaries of the model. The film used was Kodak Plux-X 70 mm Aerographic film 2648 (estar base) also used for aerial photography.

The film negatives were measured using the film measuring machine developed at Cambridge by James (1973) and recently modified to include a video system (see Davies, 1981). The coordinates of the centre of each mark are recorded on punched paper tape and transferred to the University IBM computer to be processed by a program developed initially by Smith (1972). Full details of the program may be found in Britto (1983). The program maps the measured points of each film on to the same reference axes set by the user. By overlaying data of two films in this way measurements referring to the same point are detected and the relative displacement of the corresponding points are calculated. Vertical and horizontal displacements of the markers are printed and the displacement vectors plotted.

For the purpose of strains computations the program divides the lead shot grid into rectangles and these are divided into triangles. Strains are assumed to be constant within the triangular elements and are computed from the displacements of the vertices. Small changes of geometry is one of the hypothesis for strains computations and small increments of strains are calculated from the initial and final configurations of the triangle. Cumulative strains are calculated by summing incremental strains of the intermediate films. The program prints and plots principal strains; volumetric strains are also printed. A program written by Philips (1984) to plot displacements and strains isocontours resulting from numerical analyses was changed by the writer to handle the film measurement data.

Errors associated with film measurements have been discussed by a number of research workers. Mair (1979) reports errors of  $\pm 10$  microns depending on the quality of the image. According to Davies (1981) this error can be reduced to  $\pm 5$  microns using the new TV monitor. For a 10:1 reduction between model and image this is equivalent to  $\pm 50$  microns (i.e. 0.05 mm) which at prototype scale ( $N = 100$  g) corresponds to 5 mm. Soft clay models tested here have experienced deformations much in excess of 0.05 mm and quite often of about 5 mm. Hence errors in displacements measurements can be as low as 1%, but considering the other sources of errors (e.g. Beasley, 1973), that figure might substantially increase.

Errors associated with strains computed from displacements are more serious. Displacements errors of  $\pm 50$  microns in a 15 mm grid silvered markers result in shear strain errors of 0.66%. However it was found that poor quality of some markers greatly affected local computation of strains thus changing considerably the strain pattern. According to Mair (1979) shear strains can be accurate to within 2%, but for poor quality markers errors could be accurate of within 4%. Taylor (1984) reports errors associated with shear and volumetric strains of about 5%. Considering the above findings and that errors associated with strains are within the magnitude of measurements made here, it has been decided to give limited attention to strains data. Therefore strain data will be used here to compare results amongst different tests but not for comparisons with numerical predictions.

## 3.2 Centrifuge tests

### **3.2.1 Geometries and loading sequences**

The geometries of centrifuge model tests MA3, MA4, MA5 and MA6 are shown in fig. 3.4 a to d. The right wall of the strong box is ideally smooth, thus it is a plane of symmetry. Hence cross section of models shown in fig. 3.4 represent half of the corresponding prototypes. Fig. 3.4 also shows locations of the pore pressure transducers in all tests but MA4, since pore pressure data for this test are not presented here, as discussed in section 3.3.

Embankment slopes in fig. 3.4 vary from about 1(V):4(H) to 1(V):1.5(H) and embankment heights vary from about 50mm (5.0m) after lift 2 to 130mm (13.0 m) at full height. At prototype scale the full embankment base and the platform are 80m and 40m wide, respectively, all the above dimensions being easily found in modern road construction works. Departures from usual prototype behaviour shown in fig. 3.4, regarding embankment profile and increase of the slope angle with the increase of height of embankment, are mainly due to the Coriolis effect and to difficulties involved in hopper operation, but are of minor importance.

Embankment densities vary for each lift due to factors such as time of hopper opening and amount of sand available in the hopper. It is possible to estimate the average density of the embankment at the end of the test by computing weight and volume of sand used. The average density measured was  $16.3 \text{ KN/m}^3$  which corresponds to a voids ratio of 0.595 and a relative density of 78%, for the 30/52 Leighton Buzzard sand.

Models MA4 and MA6 were provided with granular column grids of 56 and 20 columns respectively, as described above. Nominal centre to centre spacings of the square grids used in models MA4 and MA6 were 40mm (4.0m) and 30mm (3.0 m), respectively.

Loading histories used for stage constructed embankments MA3, MA4 and MA6 are shown in fig. 3.5 in terms of average height of embankment against time of construction. Construction times used here are shorter than used by Davies (1981), and can be easily duplicated in practice (e.g. Tavenas et al, 1978). Centrifuge tests MA3, MA4, MA5 and MA6 are described below.

### **3.2.2 Description of the tests**

#### (a) Test MA3

Model MA3 was constructed in stages from lift 1 to lift 3 and was then taken quickly to failure. This occurred 10s after lift 5 was poured, at an average height of 116mm (11.6m). Photographs taken during flight at the start and end of lift 3 are shown in plates 3.3 and 3.4. Plates 3.5 and 3.6 show lift 5 just after pouring and at the start of failure, respectively. The complete embankment failure is shown in plate 3.7, a photograph taken after the test. Because the hopper operation was not stopped in time, another lift was poured after failure had occurred.

However this was of minor importance as all data from before, during and after failure were obtained.

(b) Test MA4

In test MA4 the shortest construction time, fig. 3.4b, and the highest embankment, fig. 3.5, were achieved. This was possible because a large area of the clay foundation was treated. Plate 3.8 shows a photograph of the test at the end of the third stage of construction. Comparison of plates 3.4 and 3.8 show clearly the smaller displacements existing in test MA4. After the test the clay model was cut in sections through the granular columns, to allow these to be examined. Examination proved that the process of installation of the granular columns was very effective, as shown in plate 3.9.

(c) Test MA5

Test MA5, fig. 3.4c, was an embankment quickly loaded to cause foundation failure. The overall construction time was 60 seconds, corresponding closely to 7 days construction time at prototype scale. The first two lifts were poured at 20 second intervals and the last two lifts at 10 second intervals. The photograph after pouring lift 3 was missed, thus that is not represented in fig. 3.4c. However for the purposes of stability analyses the geometry of lift 3 could be figured out based on the times used for hopper operation and geometries of lifts 2 and 4. Failure occurred on placing lift 4 at a height of 65mm (6.5m). Plate 3.10 presents a picture of the embankment at the start of the failure and plate 3.11 shows the failure completed. It is interesting to notice that the initial local slip surface under the embankment slope, plate 3.10, was followed by a generalized failure, plate 3.11, developing outside the initial slip failure. The two failure surfaces more or less coincided at their lowest point and a wedge was formed in between both surfaces under the embankment, as seen more clearly in plate 3.12 taken after the test.

(d) Test MA6

Test MA4 was a pilot test for test MA6 and the experience gained from the former was used for planning the latter. Test MA6, fig. 3.4c, used a smaller foundation area subjected to treatment than test MA4, and within

the treated area a larger column spacing was adopted. In test MA6 a loading sequence, fig. 3.5, similar to test MA3 was adopted, but the construction time was shorter.

No failure occurred in model MA6, but stability computations to be discussed in section 5 show that a low factor of safety of about 1.1 was achieved just after lift 5, fig. 3.4d, was poured, at an embankment height of 131mm (13.1m). Plate 3.13 shows a picture of test MA6 at the end of stage 3. Comparison of plate 3.13 with plates 3.4 and 3.8 of tests MA3 and MA4, respectively illustrates how granular columns can substantially modify the pattern of displacements of otherwise untreated foundations.

Plate 3.14 shows a sectional view through clay model MA6 in which the granular columns were sectioned. The integrity of the columns after the test is very clear, apart from the natural distortion due to embankment loading.

Tests MA4 and MA6 should ideally have allowed for full consolidation of lift 5 to obtain long term displacements data. Unfortunately, however, the tests had to stop early during stage 5 of construction due to difficulties of manning.

### **3.2.3 Objectives of the tests**

The objectives of tests MA3, MA4 and MA6 were:

#### (a) Test MA3

1. to provide good quality data for comparisons with numerical analysis, to be described in section 4,
2. to provide information for stability analysis to be performed in section 5,
3. to compare performances of tests on untreated and treated foundations.

#### (b) Test MA4

1. to test the feasibility of the process of installation of the granular columns,
2. to allow a preliminary check on the effectiveness of the columns,

3. to be a pilot test for test MA6.

(c) Test MA6

1. to provide displacements and pore pressure data to allow direct comparison with those of test MA3,

2. to provide data for stability analysis of embankments on stone columns and comparisons with stability analysis of test MA3.

The basic purpose of test MA5 was to provide data for stability analysis of a quickly constructed embankment. These data were essentially geometry of the embankment and pore pressures developed during construction. Hence less attention is given to displacements data of test MA5, though these are also briefly described.

Results of displacements and pore pressures of the centrifuge tests are presented in the following sections. The tests to be presented in more detail are in order of emphasis MA3, MA6, MA4 and MA5 for the reasons presented above.

3.3 Displacements and strains data

Results of displacements can be presented in the following forms:

- a) displacement vectors;
- b) contours of horizontal and vertical displacements;
- c) horizontal and vertical displacements under the embankment base;
- d) inclinometer plots;
- e) settlement profiles;
- f) settlements with time.

Displacement vectors are useful to give a general idea about the pattern of displacements and allow straightforward comparisons for the same test or between different tests. Contour plots indicate both pattern and magnitude of displacements. The remaining plots make possible localized quantitative comparisons and have also a practical interest as are the plots usually obtained from field tests.

All the above types of plots are explored here to give an overall idea of the results of the tests. Results of settlement with time are presented in section 5 together with results of numerical analysis. An overall discussion of the results is presented at the end of the section.

### 3.3.1 Displacement vectors

Displacements vectors for test MA3 just after constructing lift 3 and at the end of the stage are presented in fig. 3.6a,b. It can be seen that not only consolidation settlements occurred, but also horizontal displacements and heave in front of the embankment. Displacements for test MA3 just after pouring of lift 4 and for lift 5 before failure (corresponding to plate 3.5) are shown in fig. 3.7 a,b. Displacement at the end of tests MA4 and MA6 are shown in figs. 3.8 and 3.9, respectively. Displacement scales used in the plots of figs. 3.8 and 3.9 are twice those used in fig. 3.7. Comparisons of figs. 3.7, 3.8 and 3.9 show very clearly the beneficial effect of the granular columns in tests MA4 and MA6 in restraining heave and horizontal displacements. Patterns of displacements for tests MA4 and MA6 are similar, though quite different from test MA3.

Displacements for test MA5 at the moment the failure started (corresponding to plate 3.12) are seen in fig. 3.10. The region of large displacements in fig. 3.10 defines clearly a slipping surface very close to a circular shape. The moment the measurements were taken (plate 3.12) the sliding was just starting, this being probably the reason for the incomplete pattern of displacements shown at the bottom of fig. 3.10.

### 3.3.2 Horizontal displacements

It has been suggested (Marche and Chapuis, 1974) that lateral displacements can be considered good indicators of the development of failure conditions in clay foundations. Marche and Chapuis (1974) studying lateral displacements under a number of embankments quickly built, showed that large lateral deformations develop when the factor of safety of the embankment is lower than 1.3. Therefore particular attention is given here to the results of horizontal displacements to investigate, amongst other aspects, whether the above findings are also applicable to stage constructed embankments.

#### (a) Contour plots

Contour plots of horizontal displacements for tests MA3 and MA6 are shown in figs. 3.11 and 3.12, respectively. Points to be noticed from these figures are:

- a) the very large increase of displacements during stage 3 of test

MA3, maximum displacements varying from 6mm (0.6m) at the start of stage 3 to 13mm (1.3m) at the end of stage 3.

b) the much smaller increase of displacements during stage 3 of test MA6, partly due to the smaller consolidation time, but mainly due to the treatment with granular columns.

c) the overall larger displacements for test MA3 also associated with high gradient of displacements with depth, mainly at the later stages of the test.

Contour plots for test MA4 at the end of stage 2 and at the end of the test are shown in fig. 3.13. Similar magnitudes and patterns of displacements were obtained for tests MA6, fig. 3.12, and MA4, fig. 3.13, with foundation treatment. However a strict comparison between the two tests is difficult mainly because of the different construction histories, fig. 3.5, used in those tests.

Horizontal displacements for test MA5 at lift 2 and at lift 4 just before failure are presented in fig. 3.14a,b. Particularly noticeable are the relatively small displacements due to quick embankment loading, about 3mm (0.3m), compared with the large displacements at the start of failure, about 15mm (1.5m). At lift 2 the height of embankment was about 50mm (5.0m) and at failure was 65mm (6.5m). Test MA4, reached a height of 70mm (7.0m) at lift 2, fig. 3.13a. Comparison of figs 3.13 and 3.14 shows clearly the beneficial effect of the granular columns associated with stage construction for decreasing horizontal displacements.

#### (b) Displacements at the embankment base

Horizontal displacements at the horizontal plane 5mm (0.5m) below the clay surface are presented in figs. 3.15, 3.16 and 3.17 for tests MA3, MA6 and MA4, respectively. Plots are for below the clay surface, as there are practical difficulties of positioning the reflective markers, used for displacement measurements, coincidentally with the clay surface. Curves for test MA3, fig. 3.15, are for beginning and end of stages 2 and 3 and at lift 5 just before failure. Points to be noticed in fig. 3.15 are:

- a) the large increase of displacements taking place during stage 3,
- b) the comparatively smaller immediate displacements occurring just after loading of lift 3,
- c) the trend of the curves forming a plateau under the embankment

slope,

d) the rapid decrease of horizontal displacements away from the embankment slope.

Plots of horizontal displacements 5mm (0.5m) below the clay surface for test MA6, fig. 3.16, and for test MA4, fig. 3.17 are for end of stages 2 and 3 and end of the test at stage 5. Displacements at the end of lifts 2 and 3 are bigger for test MA4, but at the end of the tests magnitudes are about the same. Larger displacements for test MA4 at the intermediate stages are due to higher lifts of embankment associated with shorter time of construction, as seen in fig. 3.5. The similar magnitude of final horizontal displacements, about 8mm (0.8m), might be fortuitous since different construction histories and column lay-out were used in each of the tests, although the final embankment heights were almost the same.

#### (c) Equivalent inclinometer plots

Equivalent inclinometer plots for tests MA3 and MA6 are shown in figs. 3.18 and 3.19, respectively, at three positions I1, I2 and I3 under the embankment slope. Locations of inclinometers I1, I2 and I3 have been chosen to be approximately the same in the two figures to make direct comparisons possible. Results for test MA3, fig. 3.14, are for beginning and end of lifts 2 and 3, just after pouring of lift 4 and at lift 5 just before failure. Results for test MA6, fig. 3.15 are for the end of lifts 2,3,4 and 5. Comparison of figs. 3.18 and 3.19 show:

- a) larger displacements for test MA3,
- b) in test MA3 small immediate displacements due to embankment loading, compared with those occurring during consolidation,
- c) greater gradients of displacements with depth for test MA3.

#### **3.3.3 Vertical displacements**

Contour plots for tests MA3, MA6, MA4 and MA5 are shown in figs. 3.20, 3.21, 3.22 and 3.23, respectively. Figs. 3.24 to 3.26 present vertical displacements at the horizontal plane 5mm (0.5m) below the clay surface. Profiles of vertical displacements with depth are shown in fig. 3.27 a,b for tests MA3 and MA6 at two vertical lines under the embankment.

The relevant comments about figs. 3.20 to 3.27 are:

a) the larger settlements and clay heave observed in test MA3, fig. 3.24, compared with the others,

b) the large settlements due to consolidation but much smaller immediate settlements just after embankment loading in test MA3, fig. 3.27a,

c) the larger settlements during the test MA4 compared with corresponding results for test MA6,

d) the very small heave in test MA4 and moderate but still small heave in test MA6, which is consistent with the larger area of the foundation subjected to treatment in test MA4,

e) that for test MA6 heave as well as settlements increased more rapidly after stage construction stopped at the end of lift 3 and quick embankment loading proceeded to lift 5,

f) the points of maximum vertical settlements for tests with granular columns are located outside the region treated with granular columns, illustrating the benefit of these for reducing settlements,

g) the smaller gradient of vertical displacements with depth observed for tests MA6 as compared with test MA3,

h) the small vertical displacements during lift 2 of test MA5 fig. 3.23a, the larger displacements just before failure at lift 4, fig. 3.23b, and the vertical displacements bigger than horizontal displacements, fig. 3.14, at both lifts 2 and 4.

### 3.3.4 Strains data

Since computed strains from measured displacements have limited accuracy (see section 4.6.2), strains data have to be used with caution, thus being invoked here for the purpose of supporting the displacements observations.

Average volumetric and shear strains of the tests described here are presented in table 3.1. Average strains computed for the entire foundation [1] can give an approximate idea about the straining taking place during each moment of the test, as discussed below. Results of tests MA3 and MA6, to be compared, are given at similar instants of the tests. Volumetric and shear strains just before failure in test MA3 are 3.6% and

---

[1] Considering all centroids of the triangle formed by the lead shots (see section 3.1.3).

15.5% respectively, and the corresponding values at the end of test MA6 are 2.8% and 10.7%. Thus, strains for test MA3 are generally greater than for test MA6. Fig. 3.28a shows contours of shear strains just before failure in test MA3. The region of large shear strains, 25% in magnitude, is very close to the region of the sliding mass.

Average value of maximum shear strains of 10.3% at the end of the test MA4 are almost the same as for test MA6. Average volumetric strains at the end of test MA4 are by coincidence the same as before failure in test MA3. Since the construction time for test MA4 was shorter than for test MA3, the same volumetric strains for both tests imply that the granular columns in the former have accelerated consolidation, despite embankment load in test MA4 being higher.

Table 3.1 also presents average shear and volumetric strains for test MA5, at lift 2 and at the start of the failure in lift 4. During lift 2 volumetric strains are zero, but shear strains are quite high, 7.8%. At the start of failure the shear strains about double reaching 16.8%, which is similar as just before failure in test MA3. Average volumetric strains at the start of failure are 0.84%, suggesting a quasi-undrained type of behaviour. Contours of shear strains at the start of failure are shown in fig. 3.28b. Similar to test MA3, fig. 3.28a, the sliding mass is bounded by shear strains of 25% in magnitude. However, a region of unexpectedly high shear strains, of 50% in magnitude, is enclosed within the global sliding mass and corresponds closely to the wedge formed between the initial and final slip surfaces. The plots of fig. 3.28 illustrate the difficulties of interpreting results of strains computed from displacements, as pointed out in section 3.1.

### 3.3.5 Discussion of the results

Displacements and strains for the centrifuge tests of embankment construction have been presented in the previous sections and a discussion about the results is presented below.

#### (a) Test MA3

A pattern of displacements associated with large shear and volumetric strains has developed during stage 3 of test MA3. A similar behaviour, though much less accentuated than in stage 3, occurred during

stage 2, but was not observed during stage 1. Therefore it is apparent that following stage 1 most of the top half of the clay layer under the embankment becomes normally consolidated, leading to the larger deformations. The very large magnitude of displacements observed at the end of stage 3 - maximum horizontal and vertical displacements of about 13 mm (1.3 m) and heave of about 5 mm (0.5 m) - correspond to a serviceability limit stage condition, intolerable at prototype conditions. The same magnitude of settlements occurred in the stage constructed embankments reported by Tavenas et al (1978), though horizontal displacements were smaller and no information about heave was given.

It might appear that wall friction is influencing the pattern of settlements for test MA3, as seen in figs.3.20 and 3.24. However it is likely that side friction is only of minor importance and that large shear strains associated with low factors of safety are the causes for the distortional pattern of displacements. These arguments are supported by numerical and stability analyses performed in sections 4 and 5.

#### (b) Tests MA4 and MA6

Entirely different patterns of displacements from test MA3, were obtained for tests MA4 and MA6 with granular columns. Heave and horizontal displacements were substantially decreased as a result of placing the granular columns under the embankment slope in those two tests. Heave which was about 5 mm (0.5 m) at the end of stage 3 in test MA3 was just 1 mm (0.1 m) at the corresponding stage in test MA6 and even smaller in test MA4. Maximum horizontal displacements which reached 13 mm (1.3 m) for test MA3 at the end of stage 3 were of only 4 mm (0.4 m) at the corresponding stage in test MA6 and of 7.5 mm (0.75 m) in test MA4.

Horizontal displacements close to the clay surface, at the top of inclinometer I2, for tests MA3 and MA6 are plotted in the non-dimensional plot of fig. 3.29a. Results of this plot illustrate that the columns have reduced horizontal displacements by more than 50%.

Granular columns placed only under the embankment slope, were less effective in reducing settlements. This is illustrated in fig. 3.29b where maximum settlements for tests MA3 and MA6 are plotted against height of embankment in a non-dimensional plot. However a non-dimensional plot of differential vertical displacements given by the difference between

maximum settlement and maximum heave, fig. 3.29c, is a better way of assessing the efficiency of the granular columns than the plot of fig. 3.29b. Fig. 3.29c illustrates that granular columns have decreased differential settlements also by about 50%.

If in tests MA3 and MA6 embankment construction had stopped at the end of stage 3 where embankment heights were about the same for both tests, long term settlements close to the centre line would probably have been not very different in magnitude for the two tests. Maximum settlements for tests MA4 and MA6 occur just outside the treated area and mid-way between the embankment toe and the prototype centre line. Again what might appear to be an influence of wall friction in figs. 3.25 and 3.26 is likely to be a marked influence of the draining boundaries in tests MA4 and MA6. The region subjected to larger settlements in these two tests is under the direct influence of top and bottom drainage layers and granular columns, hence settlements are accelerated in that region. If full dissipation of pore pressures was allowed during each lift more even curves of settlements would probably have been obtained. However because all tests described here produced similar settlement curves under the embankment and also no full dissipation of pore pressure was allowed, a definite conclusion about the above points cannot be obtained.

On the other hand, if granular columns had been placed under the whole embankment settlements would have been substantially reduced due to the arching effect produced by the columns. However the use of granular columns with the primary purpose of limiting settlements is not within the scope of this dissertation.

#### (c) Test MA5

In test MA5 a circular slip failure was obtained at lift 4, 60 seconds (7 days) after construction started, the height of embankment at failure being 65mm (6.5m). Maximum horizontal displacements at lift 2 were about 3 mm (0.3 m) but increased to 15 mm (1.5 m) at the start of the failure, vertical displacements being generally about 2/3 the horizontal displacements. This leads to a distortional pattern of displacements with average shear strains in the clay model of 16.8% at failure and average volumetric strains of 0.84%, suggesting a quasi-undrained behaviour.

Davies (1981) performed centrifuge tests of an embankment constructed in a single lift in which failure occurred 6 seconds after construction. His height of embankment at failure was the same as here, 65 mm (6.5 m). Davies's model was 180 mm deep and was just made with kaolin only having a less stiff crust. These differences seem to have counterbalanced, so that same heights of embankment at failure were obtained. Maximum shear strains reported by Davies before failure were 20%, compared with 25% measured here just after failure had started, as shown in fig. 3.28b.

### 3.4 Pore pressure data

Pore pressure results for tests MA3, MA5 and MA6 are presented in this section. Pore pressure data for test MA4 had a similar pattern to that of test MA6, thus not being presented here.

#### **3.4.1 Location of the pore pressure transducers**

The location of the pore pressure transducers in each of the tests is shown in fig. 3.4. The following points were considered for the location and the number of pore pressure transducers:

- a) that only 11 channels were available for pore pressure measurement,
- b) that pore pressure results should cover most of the foundation under the embankment,
- c) that some transducers should be placed close to the centre line of the corresponding prototype to provide pore pressure data in a region with negligible principal stress rotation,
- d) that some transducers should be placed under the embankment slope, an important region to be monitored for stability analyses,
- e) that transducers should be evenly distributed with depth, to assist in the control of the partial consolidation performed in laboratory as well as the consolidation run to achieve equilibrium of pore pressures,
- f) that transducers should be placed inside and just outside the region treated with stone columns to monitor the pore pressure diffusion in that region.

Pore pressure data from tests MA3 and MA6 are to be compared, but because of the above reasons it was not possible to have the transducers in both models at the same positions. However this was not particularly important as far as comparisons to be undertaken here are concerned. Models MA3 and MA6 each had 11 transducers, but model MA5 had only 8 transducers, the reason being that models MA5 and MA6 were tested in the same week. However for the purpose of stability calculations the pore pressure data available from test MA5 was sufficient. Transducer P5 in test MA3 and transducer P8 in test MA6 shown in figs. 3.4a and 3.4c respectively, by open circles, malfunctioned and no outputs were produced. However the remaining 10 transducers in each test worked very satisfactorily.

Pore pressure data for tests MA3 and MA6 are presented together in the next section and for test MA5 are presented in a subsequent section.

#### **3.4.2 Results for tests MA3 and MA6**

The variations of excess pore pressure with time for tests MA3 and MA6 are presented in fig. 3.30 to fig. 3.34 and results at approximately similar locations in both tests are represented by the same symbol to make comparisons easier. Profiles of pore pressure with depth and contours of pore pressure in the clay foundation are also presented to give a complete picture of the pore pressure development during the tests.

Pore pressures observations are discussed below under the following headings:

a) Pore pressure response immediately after loading; b) Pore pressure dissipation; c) Granular columns and pore pressures; d) Redistribution of pore pressures.

##### (a) Pore pressure response immediately after loading

Results presented in figs. 3.30 to 3.34 show that pore pressures increased after embankment loading and for some transducers, particularly in test MA3, continued to rise after the end of construction. Transducers closer to the prototype centre line generally peaked more quickly than the transducers closer to the embankment toe.

The delayed peak type of response can be seen more clearly plotting the continuous output recorded in magnetic tape, using the FLY-14 program

developed by Dean (1983). Pore pressure response after loading lift 2 in test MA3 is shown in fig. 3.35. It is seen that although all transducers respond immediately to loading, not all transducers peak at the completion of load application. Pore pressures carry on increasing after end of loading in transducers P3, P8, P9 and P11.

Delay between end of construction and peak pore pressure is mainly due to redistribution of pore pressure from a zone of higher excess pore pressure to zones of lower excess pore pressure, but the Mandel-Cryer effect (Gibson et al, 1963) might also have some influence in the pore pressure response after loading. The time for peak pore pressure varied from transducer to transducer and ranged between a few seconds to 2min (14 days). A more pronounced delay in response was observed by Davies (1981).

Peak excess pore pressures in tests MA3 and MA6 following embankment loading were of similar magnitude for transducers at the same distance from the centre line of the prototype. Ratios of increment of excess pore pressure to increment of vertical applied pressure  $\bar{B} = \delta u / \delta \sigma_v$  have been computed for transducers under the embankment platform for tests MA3 and MA6. The increment of applied pressure was computed from the difference between successive average embankment heights. Values of  $\bar{B}$  following lift 1 are presented in table 3.2 and vary between 1.01 and 1.12 for lift 2 in test MA3 and between 0.95 and 1.03 for lift 2 in test MA6. Values of  $\bar{B}$  around unity show that pore pressure generation for soil elements close to the prototype centre line resemble behaviour observed in 1D consolidation tests.

During lifts 3 and 4 in test MA3 values of  $\bar{B}$  were of the order of 0.8 - 1.0, but during the last lift were of the order of 0.7 - 0.9. These reduced values of  $\bar{B}$  might be associated with the development of arching as the embankment settles under the platform and heave takes place close to the embankment toe, resulting in a non-uniform stress distribution as discussed by Parry (1971). Because of this arching the total stress increase induced by the construction is reduced under the centre of the embankment, but additional stresses are thrown onto the toe of the embankment. Indeed values of  $\bar{B}$  at transducers P6, P7 and P8 under the embankment slope are larger during lift 5 than during the previous lifts.

Even more reduced values of  $\bar{B}$  resulted during the last lifts of test MA6, as seen in table 3.2. Values of  $\bar{B}$  are of the order of 0.8 - 0.9 at

lift 3, of the order of 0.6 - 0.8 at lift 4 and of the order of 0.5 - 0.6 at lift 5. This phenomenon is consistent with the more accentuated arching taking place in test MA6 due to the stiffening influence of the granular piles placed under the embankment slope. Leroueil et al (1978) suggest determining values of  $\bar{B}$  during each construction phase and using these to predict the pore pressures for the next construction stage. This procedure might be adequate in cases where small distortions and thus negligible arching occurs. However where substantial arching occurs, as in test MA3 reported here, or when some sort of reinforcement is used under the embankment slope, as in test MA6, the above procedure should lead to overestimation of pore pressures in view of the trend of decreasing  $\bar{B}$  for the later stages of construction.

#### (b) Pore pressure dissipation

The plots presented in fig. 3.30 to 3.34, show that full dissipation of excess pore pressures was not allowed during each stage of construction. For test MA6 more rapid dissipation of pore pressures took place in the region of the granular columns, as discussed later.

Pore pressure dissipation was quicker for transducers located at the bottom half of the clay foundation than for transducers located at the top half. This feature was common in both tests MA3 and MA6 and was due to the presence of the top 40mm of Gault clay, which has lower permeability than kaolin (see section 7.4).

Comparing transducers P1 and P2 in test MA3, fig. 3.30a, located the same distances from top and bottom draining layers, the faster rate of dissipation of the bottom transducer P2 illustrates this point. Similar comparison can be made with transducers P3 and P4 and at the same distance from top and bottom, and again transducer P4 dissipates faster, as shown in fig. 3.31a. Transducer P11, fig. 3.34a, located between transducer P3 and P4, but closer to P3, dissipated (during stages 3 and 4) faster than transducer P3 which was closer to the draining boundary, but embedded within Gault clay.

Similar results have been found for transducers P1, P2 and P3 in test MA6. Transducers P1 and P3, fig. 3.30b were at the same distance from top and bottom draining layers and transducer P3 dissipated faster than P1. Transducer P2, fig. 3.34b, between P1 and P3 dissipated at a slower rate

than P3 and at a similar rate to P1. This was because P1 was at the top half of foundation and within Gault clay, whereas P2 and P3 were both embedded in kaolin.

Profiles of excess pore pressures with depth for tests MA3 and MA6 are shown in fig. 3.36a,b. Excess pore pressures at the start and end of stages 1,2 and 3, as well as just after pouring lifts 4 and 5 are shown. The arrows in the above figures indicate pore pressure dissipation during the stage. Some interpolation has been necessary to draw profiles of pore pressure with depth. An important feature illustrated in fig. 3.36 is the faster dissipation of pore pressure for transducer in the bottom half clay layer. The inclined shape of the isochrones at the later stages of the tests highlights the faster dissipation of pore pressure of the bottom layer following subsequent loading.

#### (c) Granular columns and pore pressures

Transducers in test MA6 with granular columns showed generally faster dissipation of pore pressure than in test MA3. Transducers P6 and P7 placed between the columns, fig. 3.4d, at the centre of the square grid, produced particularly fast dissipation of pore pressures. The response of P7 located at mid depth was unexpectedly faster than P6 located 15mm below the clay surface, though the fact that P6 was embedded within Gault clay was responsible for its comparatively slow rate of dissipation. Transducer P7 dissipated almost fully during construction stages 1, 2 and 3. On the other hand transducers P1, P2 and P3 placed close to the centre line of the corresponding prototype were not much affected by the presence of the columns under the embankment slope.

The influence of the granular columns in changing the pattern of pore pressure within the clay foundation is well illustrated by comparing contours of excess pore pressure for tests MA3 and MA6. Excess pore pressures in meters of water,  $h_u$ , at start and end of stage 2, are presented in figs. 3.37 and 3.38 for tests MA3 and MA6, respectively.

Maximum values of  $h_u$  at the start of stage 2 are 8m, at prototype scale, for both tests, though a larger area of model MA3 is subjected to the maximum value of  $h_u$  than in test MA6. At the end of stage 2 maximum values of  $h_u$  are 7m for test MA6 and 6m for test MA3, but the pattern is quite different in test MA6, since pore pressures are very small under the

embankment slope. It is important to notice that the time for consolidation of lift 2 in test MA6 was about 60% of that for test MA3, and that average embankment heights were 54mm (5.4m) for test MA3 and 58mm (5.8m) for test MA6. The implications of low pore pressures under the embankment slope with respect to the stability analysis will be made evident in chapter 8.

#### (d) Redistribution of pore pressures

Transducer P10 in test MA3, close to the embankment toe and 30mm (3.0m) below the clay surface, fig. 3.4a, produced an output different from the remaining transducers. During stage 2, fig. 3.33a, the quick initial dissipation after loading was followed by a steady increase in pore pressure and stabilization at the end of the stage. In stage 3 the response of P10 was slightly different; the pore pressure generated after loading remained constant throughout the rest of the stage.

Transducer P9 in test MA6, close to the embankment toe and 15mm (1.5m) below the clay surface fig. 3.4d, at a similar location to transducer P10, test MA3, showed an initial dissipation at a high hydraulic gradient followed shortly by a dissipation at a lower gradient, as shown in fig. 3.33b. The proximity of transducer P9 to the granular columns is the reason for the difference in response from transducer P10 in test MA3. However the general cause for pore pressure increase after initial dissipation or marked decrease in the rate of dissipation is the bi-dimensional pore pressure redistribution under the embankment from the zones of high excess pore pressure to the zones of lower excess pore pressure. Hence, close to the embankment toe, increasing pore pressures or decreasing pore pressure gradients are due to the horizontal pore pressure redistribution from under the embankment.

#### **3.4.3 Results for test MA5**

The complete response of the pore pressure transducers during loading of test MA5 is shown in fig. 3.39. Excess pore pressure  $\Delta u$  increased just after loading of each lift and kept about constant till the next lift was placed. Failure occurred 10 seconds after lift 4 was poured when the recording of the data was stopped. Transducers P1, P2 and P3 showed some decrease of pore pressure after lift 4 was applied. Transducer

P4 showed an unexpected decrease of pore pressure during loading of lift 4, followed by an increase in pore pressure till failure took place. The reason for the response is not clear. Transducer P8 outside the embankment toe presented a continuous increase of pore pressures during loading, but apart from lift 1 there was no marked increase in pore pressures just after embankment loading, though during lift 4 the delayed increase in pore pressure is quite clear. Profiles of  $\Delta u$  with depth for transducers P1 to P5 are shown in fig. 3.40. The curved shape of the isochrones suggests that some drainage might have taken place during loading. A slight departure from the undrained type of loading was also suggested by the results of volumetric strains discussed above. The drop in pore pressures for transducers P1 to P3 after pouring of lift 4 and the unexpected increase in pore pressures for transducers P4 and P5 are shown in fig. 3.40.

### 3.5 Summary and conclusions

Pore pressure and displacement data of centrifuge tests of embankments on soft clays have been presented in this chapter. Tests MA3, MA4 and MA6 were performed using stage construction techniques and were taken to average prototype embankment heights of 11.6, 13.0 and 13.1 meters, respectively. Model MA3 was taken to failure at the end of the test whereas embankment in model MA5, built quickly, failed at 6.5m.

Displacements during and after stage 2 of test MA3 on virgin foundation were very large and were associated with large shear and volumetric strains. Contrary to the classical scheme of large distortions developed during construction, followed by an oedometer-like consolidation behaviour, large increase of lateral displacements occurred during stages 2 and 3 of construction, which had factors of safety varying between 1.0 and 1.2 (to be presented in section 4). Lateral displacements approximately doubled during each stage of construction, delayed deformations being much larger than construction deformations. Results indicated that large lateral displacements are good indicators of the passage of the clay to a normally consolidated state, i.e., a phenomenon not necessarily related to incipient failure but which might be associated with low factors of safety or to a serviceability limit state condition, both of

which occurred in test MA3. However as far as quickly constructed embankments are concerned, large lateral displacements can be good indicators of impending failure, as suggested by results of test MA5.

The use of granular piles under the embankment slope in test MA6 resulted in 50% decrease of both horizontal and vertical displacements, compared with test MA3. Granular columns have also acted as draining elements and changed the pore pressure pattern in the foundation, particularly under the embankment slope. Results of test MA4 also on granular columns confirmed the beneficial influence of the columns in decreasing displacements.

Pore pressure dissipation was faster in the bottom clay layer due to the presence of the less permeable Gault clay at the top. The pore pressure coefficient  $\bar{u}$  for transducers close to the prototype centre line for tests MA3 and MA6 was close to unity during loading of lifts 2 and 3 but decreased significantly at the subsequent lifts, particularly in test MA6. This was attributed to arching in the embankment-foundation interaction which was more accentuated in test MA6 due to the presence of the columns.

#### 4. NUMERICAL MODELLING

Numerical modelling has been made of a stage constructed embankment on unstrengthened soft clays, and is the subject of this section. Numerical predictions of displacements, strains and pore pressures for test MA3 are presented and compared with the observations reported in section 3.

##### 4.1 CRISP program

Constitutive models included in CRISP (Gunn and Britto, 1983) are Cam-clay models, elastic perfectly-plastic models and linear elastic models. The clay foundation has been modelled here as a modified Cam-clay material (Roscoe and Burland, 1968). The embankment and sand layer have been modelled as linear elastic materials. The soil parameters prescribed to each of the materials are described below.

A number of triangular and quadrilateral elements are available in the program. Elements with displacement unknowns at the nodes or with both pore pressures and displacements unknowns are provided. The latter type of element is required in coupled consolidation analyses and the specific types of elements used are discussed later.

The formulation of consolidation is based on Biot's 3-D consolidation theory. Physical non-linearity is handled by a purely incremental approach which requires the use of a large number of increments. The equations are assembled numerically, using a fast stiffness formulation (Sloan, 1981) and are solved using a frontal scheme.

##### 4.2 In situ stress state

Clay models prepared here for centrifuge tests, undergo the stress history described by Almeida and Parry (1983b). A soil element close to the clay surface experiences loading in the laboratory and continuous swelling as it is unloaded and then subjected to 100g acceleration, eventually reaching equilibrium. On the other hand, a soil element at the bottom of the clay model experiences loading followed by unloading and subsequent reloading to a normally consolidated condition as it reaches equilibrium at  $N = 100$ .

Under the above circumstances, it is difficult to estimate exactly the horizontal effective stresses in situ  $\sigma'_{ho} = K_o \cdot \sigma'_{vo}$ , particularly for the soil elements in the upper over-consolidated clay layer. The reason for this is that the coefficient of earth pressure at rest  $K_o$  is not just dependent on OCR but differs from unloading to reloading (Mayne and Kulhawy, 1982).

Experimental values of the coefficient of earth pressure at rest  $K_{nc}$  for the normally consolidated Speswhite kaolin have been determined by Manson (1980) and Airey (1984) and both have found an average value of 0.69. A comprehensive study of the variation of  $K_o$  with OCR has not yet been undertaken, but limited data is provided by Manson (1980). For Gault clay, the data is more limited. Thompson (1962) found  $K_{nc}$  in the normally consolidated Gault clay I of around 0.72 but Airey (1984) reports a value of about 0.60 for Gault clay II. A value of  $K_{nc} = 0.69$  is used here for Gault clay II.

There are several proposed relationships between  $K_o$  and OCR and these have been reviewed by Mayne and Kulhawy (1982). Mayne and Kulhawy proposed a general equation which accounts for unload-reload histories. However, their equation requires the estimate of the minimum vertical pressure under unloading, which is difficult or uncertain for the clay models prepared for centrifuge tests. The correlation between  $K_o$ , OCR and plasticity index proposed by Brooker and Ireland (1965) is one of the most widely used. It was based on results of five soils, none of which was kaolin and so their relationships might not be relevant to the models prepared here.

The equations given by Wroth (1975) fit well the experimental data on Spestone kaolin by Nadarajah (1973) as shown by a number of research workers (e.g. Francescon, 1983) and also the data of Gault clay I as shown by Davies (1981). It is preferred by most research workers at Cambridge working with reconstituted clays. Parry (1982) has suggested the use of the following empirical equation

$$K_o = K_{nc} (\text{OCR})^{\phi'} (\text{radians}) \quad (4.1)$$

in which  $K_{nc}$  is assumed equal to 0.69. Values of  $K_o$  computed with eq. 4.1 using  $\phi' = 23^\circ (= 0.401 \text{ radians})$  are presented in table 4.1 together with

the values given by Brooker and Ireland (1965)'s correlation and Wroth (1975)'s equations. It is interesting to see that values given by eq. 4.1 are virtually equal to the values given by Wroth's equations with the advantage that the former is much simpler than the latter.

The variation of OCR with depth for the clay foundation and the variation of  $K_0$  with depth given by eq. 4.1 are shown in fig. 4.1a. Values of the in situ horizontal and vertical effective stresses  $\sigma'_{ho}$  and  $\sigma'_{vo}$  are shown in fig. 4.1b. The third curve in fig. 4.1b is the isotropic preconsolidation pressure  $p'_c$  required for Cam-clay models to locate the position of the yield locus at each integration point. Values of  $p'_c$  have been computed from the stress history ( $\sigma'_{ho}$ ,  $\sigma'_{vo}$  and OCR) using the equation of the modified Cam-clay yield locus.

Gunn (1983) investigated the effect of assumptions related to the initial stress state and concluded that when a significant amount of yielding takes place, the actual stress conditions in a soil body depend more on the applied loads and critical state parameters than on the assumed initial conditions. Therefore, despite some uncertainties about the values of  $K_0$  for the over-consolidated clay, the adopted initial stress conditions, fig. 4.1b, should be quite satisfactory since significant yielding took place during test MA3, as discussed in section 3.

### 4.3 Modelling the clay foundation

#### 4.3.1 Cam-clay parameters

Cam-clay models used for the clay foundation require four critical state parameters:  $\lambda$ ,  $K$ ,  $M$  and  $e_{cs}$ , plus an elastic parameter. This can be the Poisson ratio  $\nu'$  or the shear modulus  $G$ . The latter is used here for reasons to be discussed below. For coupled consolidation analysis the program also requires values of the coefficients of permeability in the vertical ( $k_v$ ) and horizontal ( $k_h$ ) directions.

The model clay foundation is composed of Speswhite kaolin and Cambridge Gault clay. Critical state parameters for both materials have been reported by a number of research workers (e.g. Mair, 1979; Davies, 1981; Houlsby, 1981; Airey, 1984) and it is out of the scope of this dissertation to review these in detail. However, values of shear modulus

and of coefficients of permeability are reviewed in more detail in separate sections, since less attention has been given to these parameters. Critical state parameters assigned to kaolin and Gault clay are described below.

(a) Speswhite kaolin

Values of  $\lambda$  and  $K$  for Speswhite kaolin largely accepted at Cambridge (e.g. Mair, 1979, Randolph et al, 1979) as representative of the behaviour of this material, are  $\lambda = 0.25$  and  $K = 0.05$ , and they are adopted here. A series of undrained triaxial tests on Speswhite kaolin subjected to different stress histories by Davidson (1980) gave a value of 0.88 for  $M$ . On this basis, a value of 0.9 was adopted for  $M$  in the finite element analyses. The value for  $e_{cs}$  computed from tests by Knoyle (1979) was 2.39 which compares with  $e_{cs} = 2.44$  adopted by Randolph et al (1979). This last value is adopted here.

(b) Gault clay

The Gault clay II used in the tests described here has also been used by Airey (1984) and by Davies (1981) but it is different from the Gault clay I used by Thompson (1962), since the latter contains some amount of fine sand. The material properties assigned by Davies (1981) to his Gault clay were taken from Thompson (1962) and are shown in table 4.2.

Values of  $\lambda$  and  $K$  determined from the 1-D consolidation test for preparation of Gault clay beds for site investigation tests described in section 3.5, were  $\lambda$  equal to 0.207 and  $K$  varying between 0.010 and 0.014. These give ratios  $\lambda/K$  between 14 and 20, which are out of the expected range for clays. Airey (1984) found a curved 1-D consolidation line for specimens consolidated in the simple shear apparatus. For the range of pressure of the centrifuge tests values of  $\lambda$  and  $K$  were found to be 0.219 and 0.035, which give a more common  $\lambda/K$  ratio of 6.5, and these values are adopted here. The parameter  $e_{cs}$  was assumed to be 1.96 based on the 1-D consolidation test of the large specimen performed for site investigation tests.

Due to the lack of triaxial test data on Gault clay II, the adopted value of  $M$  was based on results of simple shear tests performed by Airey (1984), in the light of the following arguments:

a) values of  $q'_{cs}$  computed by Airey are  $21.5^\circ$  for Speswhite kaolin and  $23.7^\circ$  for Gault clay II;

b)  $\phi'_{cs}$  is not directly measured in the simple shear test, but if internal consistency of the results is expected, the difference of about  $2^\circ$  between kaolin and Gault clay should hold;

c) the accepted value of  $\phi'_{cs}$  for kaolin is  $23^\circ$  (e.g. Randolph et al, 1979), hence  $\phi'_{cs} = 25^\circ$  seems to be a reasonable value for Gault clay II, considering also the small amount of fine sand present in it.

d) the relationship between M and  $\phi'_{cs}$  for compression condition is (Parry, 1971)

$$M = \frac{6 \sin \phi'_{cs}}{3 - \sin \phi'_{cs}} \quad (4.2)$$

thus  $M = 1.0$  for  $\phi'_{cs} = 25^\circ$ .

Values of  $\lambda$ , K,  $e_{cs}$  and M adopted for kaolin and Gault clay are summarized in table 4.1.

#### 4.3.2 Shear moduli

Critical state models usually describe the elastic behaviour within the yield locus by a pressure-dependent bulk modulus given by

$$K' = \frac{(1 + e) p'}{K} \quad (4.3)$$

and either a constant shear modulus G or a constant Poisson's ratio,  $\nu'$ . It appears that neither of the assumptions of G or  $\nu'$  constant is satisfactory as discussed below.

The use of constant Poisson's ratio in connection with a variable bulk modulus results in a pressure dependent shear modulus given by

$$G = \frac{3(1-2\nu')}{2(1+\nu')} \cdot K' = \frac{3(1-2\nu')}{2(1+\nu')} \cdot \frac{(1+e)p'}{K} \quad (4.4)$$

Zytnski et al (1979) have pointed out that the above equation leads to non-conservative behaviour, unless the bulk modulus depends on the shear

stress. Since experimental evidence (Wroth et al, 1979) suggest that G varies with the mean pressure, the use of a constant G in numerical calculations may be unrealistic and a compromise is necessary.

Houlsby (1981) has shown that the use of a shear modulus proportional to mean normal effective stress  $p'$  or to preconsolidation pressure, has provided a much better fit to his triaxial tests in Speswhite kaolin than a constant shear modulus. However, it was not possible to distinguish which was the better between these two possibilities. Houlsby (1981) also showed that the use of a shear modulus proportional to the preconsolidation pressure implied slight but unimportant changes in the shape of the yield locus. For the analyses carried out here, the shear modulus has been assumed to be dependent on the mean current pressure  $p'$ . For Speswhite kaolin, tests by Davidson (1980), summarized by Houlsby (1981), have resulted in

$$G = 75 p' \quad (4.5)$$

Values of G corresponding to the initial in-situ stress state

$p' = (2\sigma_{ho} + \sigma_{vo})/3$ , are shown in fig. 4.2.

In fact, using acceptable values of  $e = 1.5$ ,  $k = 0.05$  and  $v' = 0.33$  in eq. 4.4, it gives  $G = 18.8 p'$  which is about one fourth of  $G = 75 p'$  as given by the experimental equation 4.5. Due to the lack of shear modulus data for Gault clay, eq. 4.5 is also used to compute values of G for the Gault clay crust and the results are shown by dashed lines in fig. 4.2. The variation of shear modulus with depth shown in fig. 4.2 is valid, just for the start of the analysis. Equation 4.5 was implemented in CRISP program and as effective stresses increased due to consolidation, values of G were automatically updated. Preliminary numerical analyses showed that the Gault clay crust was being made excessively stiff with respect to G computed using eq. 4.5. Thus in the absence of G data for Gault clay, it was assumed  $G = 2250$  kPa (see fig. 4.2) for the Gault clay throughout the analysis; and eq. 4.5 was used just for the kaolin layer underneath.

Values of G computed by eq. 4.4, assuming  $v'=0.3$ , are also shown in fig. 4.2, and are much lower than those given by eq. 4.5. The ratio  $G/C_u$  is a good guide for the estimated values of G. Davidson (1980) found values of  $G/c_u$ , fig.4.3, varying between 130 and 230. The ratio  $G/c_u$  given by values of G

computed by eq. 4.4 vary between 27 and 74, fig.4.3, whereas the same ratio given by values of G computed by eq. 4.5 vary between 72 and 270, fig.4.3. Thus values of G for kaolin given by eq. 4.5 seem to be quite realistic, whereas use of eq. 4.4 might lead to excessively low values of G. Davies (1981) used values of G given by eq. 4.4 and this might be a reason why displacements were overpredicted.

#### 4.3.3 Coefficients of permeability

Coefficients of permeability for kaolin have been measured by a number of research workers at Cambridge. Kusakabe (1982) measured  $k_v = 1.7 \times 10^{-9}$  m/s from flow measurements under a vertical pressure of 130 kPa. Davies (1981) reports a value of  $k_v = 2.52 \times 10^{-9}$  m/s from consolidation tests conducted at stress levels experienced in his centrifuge tests. Maddocks and Savvidou (1982) report  $k = 2.11 \times 10^{-9}$  m/s from flow measurements in isotropically consolidated specimens in triaxial tests under stress levels relevant to those experienced by the models tested here.

Manson (1980) obtained  $k_v$  values in the range  $0.44-1.6 \times 10^{-9}$  m/s from 1-D consolidation tests. She also fitted straight lines to the plot of  $\log k_v$  against voids ratio. For an initial voids ratio of about 1.5 the backfigured value of  $k_v$  from Manson's tests was  $2.5 \times 10^{-9}$  m/s. Considering all the results presented above,  $k_v = 2.0 \times 10^{-9}$  m/s has been adopted in the case in which the permeability is assumed to remain constant throughout the analysis. However an analysis with permeability varying with the voids ratio have also been performed, as discussed below.

The coefficient of permeability is not a soil constant as discussed in chapter 1. In situations in which large loads are applied and significant consolidation takes place, changes in voids ratio can lead to important changes in the coefficient of permeability. This point might be important during stage construction of embankments on soft clays and is investigated here.

The equation adopted here to correlate the coefficient of permeability with the voids ratio and which was implemented in the CRISP program is the well known linear relationship between  $\log k_v$  and e given by

$$k_v = k_{v0} \cdot 10^{(e-e_0)/C_k} \quad (4.6)$$

where  $k_{v0}$  is the initial permeability,  $e_0$  is the initial voids ratio and  $C_k$  is the slope of the  $\log k_v:e$  plot which, for kaolin, was found to be 0.604 as determined from Manson's oedometer tests. Values of  $k_{v0}$  adopted for kaolin were based on the initial voids ratio  $e_0$  and varied between  $1.4 \times 10^{-9}$  m/s at the bottom clay layer to  $3.7 \times 10^{-9}$  m/s just below the Gault clay.

In the absence of values of the coefficient of permeability for Gault clay II, this has been computed from the 1-D consolidation test of the large specimens used to perform piezocone tests, discussed in section 3.5. For the average OCR of 1.9 and  $c_v = 1.05 \text{ mm}^2/\text{s}$ , the backfigured value of  $k_v$  was  $9.37 \times 10^{-10}$  m/s, which compares with  $k_v = 3.16 \times 10^{-10}$  m/s obtained by Thompson (1962) for the Gault clay I. For the analysis in which equation 4.6 was used to update  $k_v$  with the voids ratio, a value of  $C_k = 0.60$  has been adopted, based on tests by Thompson (1962).

Values of the coefficient of permeability in the horizontal direction,  $k_h$  were assumed to be 1.5 times higher than  $k_v$ , according to results obtained by Chan (1975) for Spestone kaolin.

#### 4.4 Modelling the sand layer and the embankment

The correct modelling of the embankment material is an important step in the achievement of good numerical results. Ramalho-Ortigao et al (1980) studied the influence of the embankment stiffness using an hyperbolic model for the embankment. Horizontal and vertical displacements were shown to increase when the embankment stiffness was halved. Stronger influence was observed when the embankment stiffness was made negligible, which is similar to applying distributed load instead of adding layers of finite elements to simulate the embankment construction. The influence of the embankment stiffness on foundation displacements is further discussed below. Bassett et al (1981) have modelled the embankment simply as an applied distributed load. Davies (1982) assumed the embankment as a linear elastic material ( $E = 7 \text{ MPa}$ ) and the sand layer as a Cam-clay material with equivalent bulk modulus of 30 MPa.

In numerical analysis of embankments on soft clays there is usually more concern with the influence of the embankment on the soft clay than with the accurate modelling of the stress-strain behaviour of the embankment itself. Hence the writer believes that the embankment material should be reasonably well modelled using a simple non-linear elastic assumption such as the hyperbolic model by Duncan and Chang (1970).

Since in the CRISP program elastic non-linear models are not available, a study of the suitability of models available in CRISP to be used for the embankment was performed by Almeida (1981). A linear elastic model used for the embankment placed some restraint on the development of horizontal displacements in the upper part of the clay foundation. The use of a Mohr-Coulomb elastic perfectly-plastic model did not result in significant improvement, since the embankment only started yielding at the later stages of construction. Cam-clay model was then used for the embankment producing reasonable results. However the shortcoming of using Cam-clay model for the embankment is that it requires an initial stress state. Hence a small and fictitious stress state has to be assigned to elements to be incorporated into the analysis at a later stage, which was not considered entirely satisfactory. Thus a routine was written for a hyperbolic model and preliminary analyses were encouraging, though some numerical problems appeared. Hence it was decided to use linear elastic embankment and sand layer, and values assigned were  $E = 3$  MPa for embankment and  $E = 2$  MPa for sand layer. A Poisson's ratio of  $\nu' = 0.3$  was used for both materials.

#### 4.5 Finite element analyses

##### **4.5.1 Finite element mesh**

As described previously, CRISP provides triangular and quadrilateral elements, with displacements unknown, and also pore pressure unknowns in the case of coupled consolidation analysis. Unlike previous analyses performed using CRISP program, three different types of elements have been used in the finite element mesh adopted here. For the clay foundation subjected to embankment loading and consolidation, the six noded linear strain triangle with linear variation of pore pressure across the element,

fig.4.4a, has been used. The total number of degrees of freedom for this element is 15, 12 ( $2 \times 6$ ) being for displacements and 3 being for pore pressures at the vertex nodes. On the other hand, elements with displacement-only degrees of freedom have been used for both sand layer and sand embankment. These linear strain triangles and quadrilaterals, fig.4.4b,c, are used according to the requirements of the embankment geometry at each stage of construction.

The finite element mesh with the type of elements mentioned above is presented in fig. 4.5. It is composed of a total of 130 elements, 85 being in the clay foundation, 12 in the sand layer and 33 in the embankment. The embankment consisted of four lifts, lift 5 being simulated by distributed load on the top of lift 4, in order to make the analyses cheaper. The total number of nodes in the mesh was 319 and the maximum number of degrees of freedom in the solution was 694. It is quite common (e.g., Davies, 1981) not to mix different types of elements. Using only consolidation type triangular elements for the whole mesh the total number of elements would be 158 as opposed to 130 and the total number of degrees of freedom would increase from 694 to 789. Thus it is apparent that the mesh with mixed elements should produce cheaper analyses than the single element mesh.

Boundary conditions adopted in the analysis, fig.4.5, are those existing inside the centrifuge model container and consist of sides restrained horizontally but allowed to move vertically, and bottom restrained in both horizontal and vertical directions. Drainage was permitted at top and bottom of the clay model throughout the analysis, i.e., during both loading and consolidation.

#### **4.5.2 Analyses performed**

The analysis was performed by applying the self weight under the centrifuge acceleration for each lift onto the mesh and allowing for dissipation of pore pressures under that load. Times for both loading and consolidation were exactly the same as in the centrifuge test. The addition of each lift and the consolidation that followed corresponded to one stage of the complete finite element analysis. This allowed for checks on the progress of the analysis and plots of the results were examined before continuing with the next stage. For this purpose the stop/restart facility of the CRISP package through magnetic tapes was used.

Numerical analyses have been carried out for three cases using different assumptions related to the coefficient of permeability, as summarized in table 4.3. Fig. 4.6b shows the two types of initial distribution of the coefficient of vertical permeability  $k_{v0}$  assumed in the analysis. The distribution b is based on the distribution of voids ratio shown in fig. 4.6a. The distribution a consists simply of adopting average values of  $k_{v0}$  for each of the two types of clays used. The coefficient of horizontal permeability  $k_h$  was assumed to be equal to 1.5 times the value of  $k_v$ , as discussed previously. The coefficient of permeability was constant in cases B and C but varied in case A according to eq. 4.6.

Unless otherwise stated, comparisons between predictions and measurements are made based on the numerical computations of case A. Cases B and C are only used for specific comparisons.

Results of numerical analyses are presented in the next two sections and compared with the measurements reported in section 3.

#### 4.6 Predicted and measured displacements

##### 4.6.1 Results

Predicted vertical displacements at the top of the clay surface, and measured displacements 5mm (0.5m) below the clay surface are compared in fig.4.7 a to c. Plots are given at start and end of lifts 2 and 3 as well as just after construction of lift 5. Magnitudes of both settlement under the embankment and heave in front of the embankment are generally very well predicted. As far as surface settlements are concerned, the only factor of discrepancy is related with the shape of the curves under the embankment. Possible reasons for this difference are discussed later.

The variation of settlements with time is shown in fig.4.8 for a point 22.5 m away from the prototype centre line. The few available measured data confirm that the variation of settlements with time is being well predicted. However the variation of settlements with depth is not as well predicted as surface settlements, as shown in fig.4.9. The numerical analysis produces gradually decreasing displacements with depth, displacements at great depths beings largely overpredicted.

Equivalent inclinometer plots I1, I2 and I3 are presented in figs.4.10 and 4.11 for lifts 2,3 and 5. Maximum horizontal displacements are well predicted at inclinometers I1 and I3 but not so well at inclinometer I2. Maximum computed horizontal displacements were located at a depth ratio  $z/H$  of the order of 0.25-0.4, whereas observed maximum values were at a depth ratio of the order of 0.0-0.2. Similar to the vertical displacements, observed horizontal displacements had a more pronounced gradient with depth than computed values, hence displacements at great depths were overpredicted.

Contours of computed vertical and horizontal displacements at the end of stage 3 are presented in fig.4.12a,b. The general agreements in magnitude between predictions and measurements, but deeper pattern of predicted displacements, are quite clear by comparing predictions of fig.4.12 with measurements presented in figs. 3.11 and 3.20.

Contours of maximum shear strains and of volumetric strains are presented in fig.4.13a,b for the end of stage 3 of construction. Maximum shear strains are 30% and occur under the embankment slope, as expected. Maximum volumetric strains are 9% and occur close to the bottom draining layer, as also expected. Predicted and measured strain are not compared in view of the errors involved in the computations of the latter, as discussed in section 3.

#### 4.6.2 Discussion

Maximum magnitudes of both heave in front of the embankment and settlement under the embankment were very well predicted at all stages of the test. Also, maximum magnitudes of horizontal displacements were fairly well predicted. However both vertical and horizontal displacements were somewhat overpredicted at greater depths. Computed horizontal displacements appeared to be restrained at the clay surface, thus differing in shape from the measured curves. Difficulties associated with predictions of lateral deformations of foundations were discussed by Poulos (1972). Predicted horizontal displacements are usually larger than measurements and Poulos listed the possible reasons for the discrepancies: (1) the difficulty of estimating Poisson's ratio of the soil; (2) anisotropy of the soil; (3) non-linear stress-strain behaviour of soil; (4) nonhomogeneity of soil; (5) neglect of certain factors such as the

effect of embankment stiffness and foundation roughness, or more generally, incorrect assumptions made regarding the stresses applied to the soil by the foundation or embankment. Factor (1) above is important in the context of linear and non linear soil models but much less for the Cam-clay models used here for the foundation. Also factors (3) and (4) are not relevant here for obvious reasons. Thus factors (2) and (5) are the relevant ones here.

Factor (2), regarding soil anisotropy, is recognizedly (see section 2.6) a drawback of the simple Cam-clay model adopted here. Indeed anisotropic elastic behaviour, might be particularly important for the initially overconsolidated top clay layer (see Parry and Wroth, 1977). On the other hand, anisotropy in the shape of the yield locus for 1-D consolidated soil is generally relevant for the whole foundation. Considering that when yielding takes place plastic strains are considerably greater than elastic strains, it appears that the bottom clay layer is yielding more than expected, thus plastic strains and consequently displacements are being overpredicted there.

The modelling of the embankment also seemed to be unsatisfactory, as suggested in (5) above. Indeed, not only a linear elastic model does not properly model the variation of embankment stiffness with stress level, but also the embankment-clay foundation interaction is not being correctly modelled, as discontinuity of displacement between embankment and foundation should possibly be allowed. Therefore it is apparent that a more correct modelling of the embankment material should improve the shape of the settlement curves under the embankment and the profiles of lateral deformations and settlements with depth. Poulos (1972) also pointed out that the sensitivity of the horizontal movements to the factors listed above is considerably greater than that of vertical displacements.

The importance of the stiffness of the embankment and sand layer is illustrated in fig. 4.14a,b. Deformed meshes for case A, fig. 4.14a, and for a case D, fig. 4.14b, with the same parameters as case A but with a 20% less stiff embankment and sand layer are presented. Node displacements have been magnified by the same amount in both plots shown in fig. 4.20 to allow a straightforward comparison between results. It is seen that settlements under the embankment slope are almost doubled but settlements at the embankment centre line have hardly increased. Thus the pattern of the

settlement curve under the embankment obtained for case D is similar to that obtained for measured settlements, though these are overpredicted. Heave in front of the embankment and lateral deformations are more affected by the 20% drop in the embankment- sand layer stiffness than settlements, and both roughly increase by two to three times.

The discussion by Poulos (1972) was made in the context of quickly built embankments. In the case of stage constructed embankment, the hypotheses regarding the consolidation of the clay foundation might also be important, as suggested by the analyses performed here. It was observed that the consideration of permeability constant throughout the analyses (cases B and C) has an effect of increasing lateral deformations [1] as compared to the consideration of permeability varying with voids ratio (case A).

#### 4.7 Predicted and measured pore pressures

Excess pore pressures  $\Delta u$  measured during test MA3 are compared in this section with values of  $\Delta u$  computed at the integration point nearest to the pore pressure transducers.

Measured and predicted variations of excess pore pressure with time are presented in figs. 4.15 and 4.16 for eight out of the ten transducers monitored. The agreement is generally good for both generation and dissipation of pore pressures. Computed pore pressures had a trend of reaching peak values at the end of loading whereas measured pore pressures showed some peak delay, as discussed in section 3. However computed  $\Delta u$  at some transducers peaked after the end of loading. That is the case of transducer P6, fig.4.15c, where despite the poor agreement, both predicted and measured pore pressures peaked after the end of loading lifts 1,2 and 3.

At transducer P9, fig. 4.16b, computed pore pressures showed a continuous rise after the end of loading lift 1, maximum values being obtained at the end of the stage. Also at transducer P10 computed  $\Delta u$  remained stable for some time at the beginning of stages 2 and 3, which was also the case for the early moments of stage 2 in transducer P11. The

---

[1] as also increases settlements

delayed peak response as well as the continuous rise in pore pressure at the end of loading are a consequence of both the two-dimensional pore pressure redistribution in the clay foundation and Mandel-Cryer effect, which are reflected in the computational method.

At transducer P6, fig.4.15c, the agreement was not particularly good, as predicted dissipation was slightly faster than measured, particularly in stage 3. Computed dissipation of  $\Delta u$  at transducer P1, fig. 4.15a, located at similar depth as P6, i.e., close to the interface between Gault clay and kaolin, was also faster than measured during stage 3. Similar disagreement was also obtained at transducer P10 (also located within Gault clay) during stages 2 and 3. Predicted pore pressure responses of the remaining transducers located within kaolin were generally very good and particularly noticeable are the excellent agreements obtained for transducers P2 and P9, respectively shown in figs. 4.15b and 4.16b. Thus it appears that the few existing discrepancies between predictions and measurements are not particularly related with the computational model adopted but rather with difficulties in defining exactly the input soil parameters for the less well studied Gault clay. If lower values of coefficients of permeability are adopted for Gault clay, the predicted dissipation should improve.

The influence of the hypotheses regarding variation of the coefficient of permeability given by cases A and C, table 4.3, is shown in fig.4.17. Comparisons are made for transducers P2, P3, P6 and P9, respectively at 8, 17.5, 26 and 3.5 meters away from the prototype centre line. As expected, the difference between the two cases gradually increases for points closer to the centre line, as these are subjected to greater overburden pressures, hence experiencing larger changes in voids ratio.

As demonstrated above, agreement between measurements and case A predictions were generally very good. However as computed-case C pore pressure dissipate faster than for case A, agreement between case C and measurements is not as good as for case A. For instance the good agreement obtained for P2 and P9 under case A is not repeated under case C. Analogously the not so good agreement obtained under case A for P6 is worsened if case C is used for comparison. Results for case B were intermediate between case A and C but closer to C. Thus it appears that it

is not only important to assume the correct initial values of  $k_{v0}$  and  $k_{h0}$  but even more important to assume the permeability varying with voids ratio. The effect of the variation of permeability was less significant on the displacements than pore pressures, though both horizontal and vertical displacements were greater for cases B and C compared with case A.

#### 4.8 Stress distribution in the clay foundation

Contours of computed  $\Delta u$  at the end of lift 3, presented in fig.4.18a, show a decrease of  $\Delta u$  from mid depth to top and bottom draining layers and from the prototype centre line to the embankment toe, as expected. Values of the incremental mean effective stress  $\Delta p'$ , fig.4.18b, are greater at the boundaries than at mid depth, as also expected. Both pore pressures and stresses vary linearly within the LST elements adopted for the analysis, fig.4.4a. Curves of pore pressures, fig.4.18a are smoother since they are computed directly at the nodes whereas stresses are by-product of displacements, thus being less accurate, as suggested by the contours presented in fig.4.18b.

Computed incremental vertical effective stresses  $\Delta \sigma'_v$  are presented at fig.4.19a. Stresses have increased under the embankment but decreased in front of the embankment. The decrease of  $\Delta \sigma'_v$ , which is about 20kPa in maximum absolute value, is consistent with the extension type of loading existing in front of the embankment. Accumulated vertical effective stresses  $\sigma'_v$ , fig.4.19b, added to the total pore pressures  $u$  give the total vertical stresses  $\sigma_v$ , fig. 4.19c. Values of  $u$  outweigh  $\sigma'_v$ , this being the reason for the slightly smoother curves of  $\sigma_v$  contours compared to  $\sigma'_v$ .

Computed stress paths in the  $p':q^*$  diagram are plotted at the location of the pore pressure transducers P1, P2, P7, P8, P10 and P11 (see fig.3.4a), and are shown in fig.4.20, where  $q^*$  is the generalized deviatoric stress as defined by Roscoe and Burland (1968). The critical state line (csl) and the modified Cam-clay yield locus are also plotted in the  $p'-q^*$  diagram.

Points P1, P10 and P11 are located in the top overconsolidated clay layer, thus stress paths of these points start inside the yield locus. Conversely, points P2, P7 and P8 are in the bottom normally consolidated clay layer and their stress paths initiate on the yield locus. Stress paths at the above points provide a general idea about the consequences of

the succession of loading and consolidation on the whole of foundation under the embankment, this being the reason why they were chosen.

Computed stress paths indicate that all three points initially at the overconsolidated state reach yielding conditions during stage 2 of construction; point P11, the less over consolidated of the three, started yielding in lift 1, but P1 and P10, both at initial  $K_0$  conditions very close to unity, reached yield conditions in lift 2. Inspection showed that most of the clay foundation under the embankment was at a normally consolidated state at the end of stage 2, which explains why both computed and measured deformations increased more rapidly following completion of stage 3 loading.

Stress paths shown in fig.4.20 consist basically of :a) during loading, vertical or inclined stress paths with increasing  $q^*$ , generally moving towards the critical state line, and :b) during consolidation a predominantly horizontal line with increasing  $p'$ , thus moving away from the critical state line. Slight departures from these typical patterns are seen in the initially more over consolidated points P1 and P10, as consolidation during stage 1 was at P1 associated with increase in  $q^*$  and only marginal increase in  $p'$ , and at P10 was associated with a slight decrease in  $q^*$  while  $p'$  held constant. Vertical stress paths inside the yield locus during loading are consistent with the negligible drainage taking place during the short time of construction. Stress paths at P1 and P10 after completion of stage 2 loading followed the more typical pattern depicted above.

At points P8, P10 and P11 under the embankment slope, stress paths moved very close to the critical state line, particularly on completion of stages 3 and 5 loading. At points P2 and P7, located at greater depths, stress paths during loading were predominantly vertical and never approached close to the critical state line. The ratio  $\eta/M$ , when  $\eta=q^*/p'$ , is an indicator of the proximity to the critical state condition, where  $\eta/M$  is close to unity. At P2, located close to the prototype centre line,  $\eta/M$  remained within the narrow range of 0.33-0.47, whereas at P7, very close to the bottom draining layer,  $\eta/M$  experienced just a slight increase from 0.44 to 0.69.

#### 4.9 Conclusions

Critical state numerical analysis of stage constructed embankment test MA3 has been presented here. Close attention has been given to the influences of the shear modulus  $G$  and permeability of  $k_v$  of the clay foundation, as there is some confidence in the critical state parameters  $\lambda$ ,  $K$ ,  $M$  and  $e_{cs}$  assigned for both kaolin and Gault clay. Rather than using  $G$  and  $k_v$  constant throughout the analysis, as is more common, values of  $G$  were made dependent on the mean effective stress  $p'$  and values of  $k_v$  were related to the voids ratio, as these more realistic assumptions appeared to be important in the case of stage constructed embankments.

Indeed, reasonable overall agreement of maximum magnitudes of horizontal and vertical displacements and of pore pressure variation with time have been obtained. Agreement was particularly good for settlements at ground surface, and of pore pressure generation and dissipation in the kaolin clay. Agreement was less satisfactory for displacements at greater depths, where both horizontal and vertical displacements were overpredicted. Shapes of predicted and measured lateral deformation profiles with depth were also different. Reasons for the differences seem to be related to the modelling of the embankment as a linear elastic material and also that anisotropy of the clay foundation is not considered in the simple Cam-clay model. Agreement of pore pressures at the top Gault clay layer was less satisfactory than for the kaolin layer which was attributed to the insufficient data on consolidation and permeability of the Gault clay.

## 5. STABILITY ANALYSES

### 5.1 Introduction

An essential aspect of embankment design is the assessment of the stability during construction. Difficulties associated with stability analyses of embankments on soft clays have been reviewed in section 2.

Stability analyses of three different types of embankment tests are presented in this section:

- (a) embankment quickly taken to failure in a quasi-undrained condition - test MA5;
- (b) embankment constructed in stages and taken to failure at the end of the test - test MA3;
- (c) embankment constructed in stages on foundation treated with sand columns - test MA6.

Stability analysis of the embankment tests were performed using the simplified Bishop (1955) method. The computer program BISPO (Moraes Jr, 1975; Palmeira and Almeida, 1980) was used for both effective and total stress analyses. As pointed out by Fredlund and Krahn (1977) the simplified Bishop method presents several advantages over other more sophisticated methods and this is the reason it is widely used. The problems associated with the mathematical solution, as pointed out by Whitman and Bailey (1967) and Duncan and Poulos (1977), are considered in the program. In cases where the forces at the base of slices are computed to be negative - a situation frequently encountered in the zone near the embankment toe when high pore pressures are measured - the program sets the negative values to zero. Some other features of the program are:

- (a) 12 layers of soil can be considered,
- (b) material properties can vary linearly with depth,
- (c) pore pressures can be given either by assigning values of  $u$  to each layer of soil or by defining a mesh of total head of water, the latter option being adopted here,
- (d) the minimum factor of safety  $F_s$  can be found either by allowing the mesh of the centre of the circles to be successively displaced in

search of minimum values of  $F_s$  or by defining a fixed mesh of centres. The fixed mesh was adopted here and plots of isofactors of safety were automatically generated for each analysis performed.

## 5.2 Total and effective stress analyses

Total stress analyses have been performed using undrained strength profiles; effective stress analyses have been performed using effective stress strength parameters  $c'$  and  $\phi'$  and pore pressures measured during embankment construction. Soil parameters for the clay foundation used in total and effective stress analyses are discussed below. In both total and effective stress analyses the sand layer and sand embankment have been assumed to behave in a fully drained way.

The sand embankment was poured with an average density of  $16.3 \text{ KN/m}^3$  which corresponded to a voids ratio of 0.595 and a relative density of 78% for the 30/52 Leighton Buzzard sand. At this density the angle of friction under plane strain condition is estimated to be  $45^\circ$ . The material properties assigned for the top 9 mm saturated sand layer were:  $\gamma = 20.6 \text{ KN/m}^3$  and  $\phi' = 45^\circ$ .

### **5.2.1 Undrained strength parameters**

Undrained strength profiles used in the total stress analyses computation are given by vane tests performed during centrifuge flight as well as design strengths, both of which are presented in fig. 5.1. In situ undrained strength profiles are relevant for stability analyses of single lift constructed embankments.

Total stress analyses (TSA) of stage constructed embankments require the estimate of the gain of strength during each stage which involves some assumptions. Considering the relative simplicity of effective stress analyses (ESA) when pore pressure data are available, stability analyses of stage constructed embankments MA3 and MA6 have been limited to the ESA. Total stress analyses have been performed only for test MA5, taken to failure in a quasi undrained condition and for the lift 1 of test MA3. Results of total and effective stress analyses have been compared in these instances.

### 5.2.2 Effective stress strength parameters

Effective stress strength parameters use for kaolin and Gault clay are  $\phi'_{cs} = 23^\circ$  and  $\phi'_{cs} = 25^\circ$ , respectively, and are consistent with values of  $M = 0.9$  and  $M = 1.0$  used in critical state finite element computations. It is recognized that a small cohesion may exist in the more overconsolidated Gault clay, though it is likely to be insignificant in the lightly overconsolidated ( $1 < OCR < 2$ ) kaolin. However in view of the difficulties in estimating the small value of  $c'$  and considering that an unconservative estimate of  $c'$  may considerably affect the computed factors of safety, values of  $c' = 0$  have been assumed for both kaolin and Gault clay. The clay density used in both total and effective stress analysis was  $15.4 \text{ kN/m}^3$ .

### 5.3 Strengthening effect of the columns

Before going into the analysis of the reinforcing effect of the granular columns, it is helpful to discuss the load sharing between columns and the soft soil.

The stresses shared between the columns and the clay foundation depend on the relative stiffness of the two materials, the cross sectional area of the columns and their spacing. The stress concentration ratio,  $n$ , may be defined as the ratio of the vertical stress of the stone or sand column  $\sigma_s$  to that in the clay soil,  $\sigma_c$ , fig. 5.2,

$$n = \sigma_s / \sigma_c \quad (5.1)$$

According to Mitchell and Katti (1981), stress ratios  $n$  are in the range of 2 to 6, with values of 3 to 4 usual. Defining now the replacement ratio  $a_s$  as

$$a_s = A_s / (A_s + A_c) \quad (5.2)$$

where  $A_s$  is the cross sectional area of the granular columns and  $A_c$  is the plan area of clay per column, fig. 5.2.

From stress equilibrium the following equations can be derived

$$\sigma = \sigma_s \cdot a_s + \sigma_c \cdot (1 - a_s) \quad (5.3)$$

$$\sigma_c = \sigma / (1 + (n-1) \cdot a_s) = \mu_c \cdot \sigma \quad (5.4)$$

$$\sigma_s = n\sigma / (1 + (n-1) \cdot a_s) = \mu_s \cdot \sigma \quad (5.5)$$

where  $\mu_c$  and  $\mu_s$  are the ratio of stresses in clay and sand to the average load intensity  $\sigma$ .

Stability analyses of embankments on granular columns are usually performed on the basis of the composite shear strength based on the undrained strength of the clay, the transverse shear strength of the columns and the replacement ratio. As the shear strength of the columns depends primarily on the normal stress on the shear plane, and this stress is not readily determined due to arching effects, assumptions and approximations are required. Both Priebe (1978) and Aboshi et al (1979) have presented methods for making these computations.

The Aboshi et al (1979) method requires the determination of the increment of stress due to surface loading using elasticity theory. The method by Priebe (1978) is more readily applicable and is suitable for both total and effective stress analyses, thus being adopted here. The method, which is a combination of elasticity and Rankine earth pressure theory, uses composite values of  $\bar{c}'$  and  $\bar{\phi}'$ , which are determined by

$$\text{tg } \bar{\phi}' = m \cdot \text{tg } \phi'_s + (1 - m) \cdot \text{tg } \phi'_c \quad (5.6)$$

$$\bar{c}' = (1 - m) \cdot c \quad (5.7)$$

where  $c$  and  $\phi'_c$  are the strength parameters of the unimproved soil mass and  $\phi'_s$  is the friction angle of the stone column. The parameter  $m$  is the relative stress distribution between soft soil and column defined by

$$m = a_s \cdot \frac{\sigma_s}{\sigma} = a_s \mu_s \quad (5.8)$$

Graphs based on the replacement ratio  $a_s$  and  $\phi'_s$  are given by Priebe for the rapid determination of  $m$ . For test MA6 with centre spacing of 40 mm and

column diameter of 10 mm the replacement ratio  $a_s$ , eq.5.2 is 0.049. Using this value of  $a_s$  and  $\phi'_s = 45^\circ$  the computed value of  $m$  according to Priebe's graphs is 0.142.

Alternatively,  $m$  could be estimated using eq.5.8 with  $\mu_s$  computed by eq.5.5 and the fact that  $n$  is likely to be in the range of 3 to 4 (Mitchell and Katti, 1981). Values of  $m$  according to eqs.5.8 and 5.5 vary between 0.137 and 0.152 for  $n$  varying between 3 and 4. Thus the computed value of  $m = 0.142$  according to Priebe's graphs implies a stress ratio  $n$  just above 3.

Substituting in eq.5.6  $m = 0.142$ ,  $\phi'_s = 45^\circ$  and  $\phi'_c = 23^\circ$ , the composite value of  $\bar{\phi}'$  for kaolin is  $26.8^\circ$ . Similarly the composite value for Gault clay,  $\phi'_c = 25^\circ$ , is  $\bar{\phi}' = 28.5^\circ$ . Stability analysis of test MA6 has been performed adopting the above values of  $\phi'_c$  and  $\bar{\phi}'$  respectively. Soil parameters adopted in the stability analysis of test MA6 are shown in fig. 5.3.

Since in design the reinforcing effect of the columns is usually neglected and assumed to contribute for an additional factor of safety (Greenwood and Kirsch, 1983), such analysis is also performed and compared with that in which the reinforcing effect of the columns is taken into account.

#### 5.4 Stability of tests MA3 and MA6

##### **5.4.1 Results**

Factors of safety for tests MA3 and MA6 have been computed at the following moments of the tests:

- (a) just after pouring lifts 1, 2 and 3,
- (b) at the end of stages 1, 2 and 3,
- (c) just after pouring lift 4,
- (d) just after pouring lift 5, at the instant of failure, for test MA3,
- (e) at the beginning and end of lift 5, for test MA6, the latter situation corresponding to the moment the test was finished.

Effective stress analyses have been performed for all the above situations using relevant pore pressure data. Total stress analyses have also been performed for lift 1, test MA3, to allow comparison with results of effective stress analyses. Since large deformations occurred throughout

test MA3, these were considered in defining the geometry of embankment and clay foundation. Similar consideration was applied for the later stages of test MA6.

Results of total and effective stress stability analyses of test MA3 are shown in fig. 5.4a,e where minimum factors of safety for each lift and corresponding slip circles are presented. Factors of safety for TSA at the start of lift 1 are lower than the corresponding value obtained from the ESA. These results are discussed later together with those of test MA5, in which a similar discrepancy was found.

Values of  $F_s$  for lift 1 vary between 1.61 and 1.81 but values of  $F_s$  obtained for stages 1 and 3, were just above unity after construction, increasing to about 1.2 at the end of the stages. Thus the increase in factor of safety was about 0.2 during stages 1, 2 and 3. Values of  $F_s$  for quick loading to failure were 1.05 for lift 4 and 0.91 at the moment of failure in lift 5. It is seen in fig. 5.4e that theoretical and observed slip surfaces are very close in test MA3. A discussion about the magnitude of values of  $F_s$  is presented later.

Results of effective stress stability analyses for test MA6 are presented in fig. 5.5. Values of  $F_s$  for stage 1 are again much higher than for the other stages and vary from about 2.15 to 2.96. The value of  $F_s$  following lift 1 was 1.04 just after pouring lift 2, which was unexpectedly low, and increased to 1.87 at the end of stage 2. During stage 3 values of  $F_s$  varied between 1.26 to 1.59. The value of  $F_s$  for lift 4 was 1.23 and for lift 5 was 1.00 after construction, increasing to 1.15 at the end of the test.

#### 5.4.2 Discussion

Centres of the critical slip circles for tests MA3, fig. 5.4, and MA6, fig. 5.5, are generally at the level of the embankment platform or just above it. Location of the slip circles are dictated mainly by the pore pressures regime of the foundation and by the component of embankment resistance. Thus, as far as embankment resistance is concerned, the minimum  $F_s$  will be found for low centred circles which owing to their short length of arc will mobilize smaller shearing resistances.

Stability analyses for test MA3 and MA6 are summarized in fig. 5.6a,b in plots of factor of safety against height of embankment. Upward arrows

for constant height of embankment denote increase of factors of safety during each stage. Comparison of the plots for the two tests show:

- (a) generally larger values of  $F_s$  for test MA6,
- (b) larger values of  $F_s$  during stage 1 in both tests, which reflect the shallow embankment and gentle slope angle used,
- (c) larger increase of  $F_s$  during each stage in test MA6, owing to the larger dissipation of pore pressure in the region of the granular columns under the embankment slope, despite the fact that construction time was shorter than for test MA3,
- (d) in test MA6, larger increase of  $F_s$  during stage 1 than during stage 3,
- (e) in test MA3 a constant increase in  $F_s$  of about 0.2 for stages 1, 2 and 3.

As the consolidation time for stage 1 in test MA6 was slightly smaller than for stage 3, the larger dissipation of pore pressures during stage 1, reflected by its larger increase in factor of safety, seems to be associated with larger values of  $c_v$  for the in situ overconsolidated top clay layer and decrease in values of  $c_v$  as the clay becomes normally consolidated following stage 1. In test MA3 as the consolidation time for stage 3 was about four times that of stage 1, and for stage 2 was intermediate between 1 and 3, an approximate constant increase of  $F_s$  in each of the stages reflects the decrease of  $c_v$  during the test.

Fig. 5.6 also presents results of stability analyses for test MA6 in which the strengthening effect of the granular columns is neglected. In other words, using values of  $\phi'_c$  for the whole of the clay foundation rather than adopting composite values of  $\bar{\phi}'$  for the treated region. It is seen in fig. 5.6 that the use of uncorrected values of  $\phi'_c$  leads to only slight reductions in calculated factors of safety in the present case in which low replacement ratio of granular columns has been adopted. Hence the stability of the embankments on granular columns was much more strongly influenced by the pore pressure regime under the embankment slope, due to the presence of the columns, than due to the strengthening effect of the columns.

The underprediction of the value of  $F_s = 0.91$  at failure for test MA3 is because the side friction of the model against the internal walls of the strongbox was neglected in the computations. The side friction of the clay foundation against the box is supposed to be very small, since

silicone grease was used (see section 4.5). Hence the main component of friction should be given by the sand embankment. Computed values of  $F_s$  just after pouring lift 5 were 0.91 at failure for test MA3, and  $F_s = 1.00$  for test MA6. Assuming similar magnitudes of side friction developed in both tests, it is likely that the actual value of  $F_s$  for lift 5, test MA6 is about 1.10. Displacements and strains data presented in section 3 suggested that test MA6 was close to failure following pouring of lift 5, and this is confirmed by the results presented above. However as shown in fig. 5.6, differences in values of  $F_s$  between the two tests were larger for stages before lift 5.

It has been shown above that ESA is a reliable way of assessing at any moment the stability of stage constructed embankments, provided actual pore pressures are measured. This approach has been successfully used (Margason and Symons, 1969; Tavenas et al, 1978) to accelerate the construction schedule of road embankments. Margason and Symons(1969) developed stability charts relating minimum factor of safety for different embankment heights to the pore pressure condition in the subsoil. These charts were prepared as part of the design procedure and provided a convenient method of site control of the rate of construction. Tavenas et al (1978) suggested that factors of safety computed by ESA should be kept in excess of 1.3 or preferably 1.4 to avoid the initiation of local failure. This suggestion while being confirmed by the results of test MA3, do not appear to be a strong need in the case of stage constructed embankments on granular columns. Indeed results of test MA6 have shown that short time duration values of  $F_s$  close to unity at the start of the stage do not necessarily imply local failure, due to the strengthening effect of the columns, as indicated by displacements and strains data shown in chapter 6. Also, low factors of safety occur just during a short time since the draining influence of the columns allows a quick increase of the factor of safety with time.

### 5.5 Stability analysis of test MA5

Results of total and effective stress stability analyses for test MA5 are presented in fig.5.7, where corresponding factors of safety and slip circles are presented for each of the four lifts of construction. Results of the analyses are summarized in fig.5.8, where factors of safety are plotted against height of embankment.

Values of  $F_s$  for ESA, fig.5.8, decrease from 1.2 for lift 1 to 0.87 for lift 4 when failure took place. The latter value compares with  $F_s = 0.91$  obtained for test MA3 at failure. Thus values of  $F_s$  for ESA are being systematically underpredicted by about the same amount, as a result of the side friction developing inside the centrifuge model container.

Values of  $F_s$  from TSA are lower than for ESA, thus confirming the similar discrepancy obtained for lift 1 of test MA3. The departure of values of  $F_s$  for ESA and TSA for the successive embankment lifts, clearly shown in fig. 5.8, suggests that some drainage might have taken place during the 60 secs (7 days) construction time. Nevertheless differences between ESA and TSA using measured vane strengths are larger than expected.

Critical slip circles for TSA and ESA are quite different, as shown in fig. 5.7. Circles for ESA are enclosed within TSA circle and also have smaller radius and lower centres. Also the TSA circle is closer to the observed generalized slip circle than the ESA circle, though part of the latter is quite close to the localized initial slip surface. The above findings are consistent with recent field observations as explained below.

Pilot et al (1982) have performed TSA and ESA of four well known case histories of embankment failures. In all four cases critical slip circles for ESA were enclosed within TSA circles. Moreover in all four cases the latter were close to the observed slip circle than the former. Another interesting field observation was the failure mechanism which is also supported by test MA5. In two out of the four cases studies, Pilot et al observed that critical circles from ESA were close to the initial failure surface but that the final failure surface, resulting from the extension of the first slide was close to the TSA circle. In all cases studied by Pilot et al (1982) values of  $F_s$  calculated by the ESA were closer to unity than the values obtained by the TSA, thus also confirming the findings obtained here.

Effective stress stability analyses performed by Davies (1981) of his single lift embankment built to failure resulted in a  $F_s = 0.80$  which compares with  $F_s = 0.87$  obtained here for test MA5. Total stress analyses performed by Davies using vane strengths resulted in a  $F_s = 0.96$ . Davies used a  $c_u$  profile given by the vane Mark I in which, due to shaft friction  $c_u$  is overestimated by 10% to 30%, depending on factors such as depth of test and clay strength. Therefore it is to be expected that the value of  $F_s$  determined by Davies would have possibly been 20% lower than 0.96, thus 0.77, which compares with 0.69 obtained here and is lower than 0.80 obtained for his ESA. No information about relative positions of the critical and observed circles was given by Davies.

In field situations vane strengths are usually corrected, as discussed in Chapter 1. Corrections (e.g. Bjerrum, 1972) are made on the basis of strain rate effects and influence of the anisotropy. Strain rate effects arise when the difference between the vane testing rate and the rate of embankment construction is large. It appears that both rates are of the same order of magnitude, as suggested by Davies (1981) and confirmed here. The shear strain rate in vane tests performed here is  $2.5 \text{ min}^{-1}$ , [1] according to an expression derived by Randolph (1980) in which the simplifying hypotheses of clay behaving as a linear elastic material, and vane rotating a cylinder of soil of the same diameter as the vane, are adopted.

As far as loading rates are concerned, average increments of shear strains during lift 4 in test MA5 were about 5% and the construction took 0.7 seconds. Thus the resulting strain rate was of about  $5 \text{ min}^{-1}$ , which is of the same order of magnitude as the vane strain rate, thus confirming previous findings by Davies (1981).

The other important factor of discrepancy between in situ and vane strengths is the effect of anisotropy. It is well known (e.g. Duncan and Seed, 1966) that the undrained strength of clays vary with the direction along which the clay is sheared, amongst other factors. The different modes of failure - compression, simple shear and extension - intervening in a slip surface were briefly discussed in section 2. Although differences of undrained strengths for the above modes of failure may not be too

---

[1] for a rate of rotation of  $72^\circ/\text{min}$  (see Almeida and Parry, 1983b).

important for the normally consolidated kaolin (Airey, 1984), it is not clear how important they are for overconsolidated kaolin and Gault clay, and also if the vane strength represents the average undrained strength along the slip surface. All the above uncertainties added to the possible occurrence of drainage during embankment construction has resulted in an unsatisfactory total stress analysis of test MA5.

#### 5.6 Summary and conclusions

Stability analyses of two stage constructed embankments, tests MA3 and MA6, and of an embankment quickly taken to failure, test MA5, have been presented in this section. Effective stress analyses of tests MA3 and MA6 were performed at the start and end of each stage using relevant pore pressure data. For test MA5 both total and effective stress analyses were carried out.

For the stability analyses of test MA6 on granular columns the strengthening effect of the columns was taken into account by making assumptions with respect to the load distribution between columns and soil. Stability analyses were also performed neglecting the strengthening effect of the columns. As far as stability is concerned, the strengthening effect of the columns was not important, but rather the higher rate of pore pressure dissipation under the slope due to the presence of the granular columns. It is expected that the strengthening effect becomes more important for larger area replacement ratios.

Factors of safety for test MA6 were higher than for test MA3 and also experienced a larger increase during each stage as a result of the larger dissipation of pore pressures in the region of the granular columns.

Results of stability analyses associated with displacements and strains data show that in the case of embankments on granular columns, small factors of safety of the order of 1.1 to 1.2 can be tolerated at the start of each stage of construction. However, in the case of untreated foundations, the use of such small factors of safety can lead to large displacements, and to a serviceability limit state condition, as shown in section 3.

Effective stress stability analyses for failure conditions in tests MA3 and MA5 have produced factors of safety of 0.91 and 0.87, respectively.

Factors of safety below unity are a consequence of neglecting the side friction inside the centrifuge model container.

Results of total stress stability analyses produced excessive low factors of safety. One of the apparent reasons for the low values was the possible drainage taking place during construction. Other possible reasons are anisotropy of the clay foundation and representativity of the strength measured by the vane as the average undrained strengths mobilized at the critical failure circles.

On the other hand reasonable results of effective stress stability analyses of single lift embankment have been obtained, which suggests that these are not only theoretically more correct than TSA, but also more reliable, as far as results obtained here are concerned.

## 6. CONCLUSIONS

### 6.1 Experimental observations

It was observed that the strengthening of the soft clay under the embankment slope with granular columns resulted in about 50% decrease in both horizontal and vertical displacements, compared to a case where no strengthening was adopted. Granular columns have also acted as draining elements and changed the pore pressure regime in the clay foundation under the embankment slope.

Ground movements of a stage constructed embankment on unreinforced foundation were large and associated with large shear and volumetric strains and with factors of safety close to unity. It was observed that lateral displacements approximately doubled during each stage of construction, delayed displacements being generally larger than construction displacements. Large lateral displacements appeared to be good indicators of the amount of yielding taking place in the clay foundation.

An embankment built quickly failed at approximately half the height reached by stage constructed embankments and in that case large lateral displacements appeared to be good indicators of the impending failure.

### 6.2 Analytical studies

Analytical studies for interpretation of the embankment tests involved:

- a) coupled consolidation numerical analysis of the stage constructed embankment on an untreated foundation, using the CRISP program and;
- b) total and effective stress analyses of an embankment quickly taken to failure and of embankments constructed in stages on reinforced and unreinforced clay foundations.

#### a) Numerical analyses

Ground displacements were generally well predicted by the numerical analyses, though displacements at greater depths were generally

overpredicted. Pore pressures were better predicted than displacements, particularly in the kaolin clay. The superiority of the numerical analyses presented here over previous analyses of centrifuge tests of embankments on soft clays appears to be related to the close attention given to the influences of the shear modulus and permeability of the clay foundation; these were made dependent on the stress level throughout the analysis.

Overall agreement between numerical predictions and measurements are likely to be further improved if anisotropy is included into the Cam-clay model and the non-linear stress strain behaviour of the embankment is taken into account.

#### b) Stability analyses

Factors of safety computed by effective stress stability analysis for the embankment on granular columns were higher than for the embankment on untreated foundation. The main reason for this was the higher rate of dissipation of pore pressure under the slope due to the presence of the columns; this also contributed to a large increase in the factor of safety during each stage of construction. The direct contribution of the granular columns to the shearing resistance was rather less important than as draining elements because of the low area replacement ratio adopted. The reinforcing effect would become more important for larger area replacement ratios.

Experimental and analytical observations showed that in the case of embankments on granular columns, factors of safety of the order of 1.1 to 1.2 can be tolerated immediately after loading each lift. However, in the case of embankments constructed on virgin foundation, such small factors of safety can lead to large displacements and to a serviceability limit state condition.

Effective stress analyses for failure conditions underpredicted factors of safety by about 10%, and were a consequence of neglecting the side friction inside the centrifuge container. Effective stress analyses appear to be a reliable way of controlling the rate of construction in stages provided pore pressures are monitored. Total stress analyses require the measurement or estimate of the undrained strength during stage construction, which appear to be less satisfactory than pore pressure measurements.

Total stress stability analyses of an embankment which was taken quickly to failure produced excessively low factors of safety; this was attributed to the possible drainage taking place during construction. Effective stress analysis gave a factor of safety of 0.87 at failure, which again suggests the influence of the walls of the centrifuge container.

### 6.3 Concluding remarks

One of the objectives of this research has been to compare the performance of stage constructed embankments on treated and untreated clay foundations. Treated clay foundations consisted of granular columns with low area replacement ratio used under the embankment slope. Centrifuge tests of models made of clay foundations subjected to realistic stress history and embankment loading allowed an uncommon technique of ground treatment to be assessed.

Another important objective of this research was to check, against centrifuge test data, the reliability of available design tools used for stage constructed embankments: a) numerical modelling using a simple Cam-clay model coupled with consolidation theory to predict displacements and pore pressures; b) effective stress methods to assess the stability and allow control of the rate of construction using measured pore pressures. Advances have been made with the application of both design tools, although there is room for improvements, particularly with respect to the numerical analysis.

The combination of centrifugal modelling, numerical modelling and stability computations has provided an important insight into the problem. Centrifugal modelling can be particularly invaluable in cases of novel conditions or unusual design and construction problems, where there is little or no experience, such as the techniques recently adopted for ground improvement. Numerical modelling is more easily available to the geotechnical engineer but needs to be validated against reliable data. The number of field case-histories with adequate observations and sufficient data regarding the geotechnical properties are regrettably few. Detailed observations of centrifuge models constructed with well known documented soils under known effective stress conditions can provide a rich data-base for testing numerical design tools.

## 7. REFERENCES

- Aboshi, H., Ichimoto, E., Harada, K. and Emoki, M. (1979). The composer: a method to improve characteristics of soft clays by inclusion of large diameter sand columns. Colloque Inter. sur le Renforcement des Sols, ENPC-LCPC, Paris, pp.211-216.
- Airey, D. (1984), Clays in circular simple shear apparatus. Ph.D thesis, University of Cambridge.
- Almeida, M.S.S. (1981), "Analysis of the Behaviour of an Embankment on Soft Clay", M.Phil. thesis, University of Cambridge, England, 1981.
- Almeida, M.S.S. (1982a) The undrained behaviour of the Rio de Janeiro clay in the light of critical state theories. Technical Report, Cambridge University, CUED/D - (SOILS) TR 119(1982).
- Almeida, M.S.S. (1982b), "Critical State Finite Element Analyses of a Field Test Embankment on soft Ground", presented at the June 1982 Workshop on the Implementation of Critical State Soil Mechanics in finite Element Computations, University of Cambridge, England.
- Almeida, M.S.S. and Ramalho-Ortigao, J.A. (1982), "Performance and Finite Element Analyses of a Trial Embankment on Soft Clay", International Symposium on Numerical Models in Geomechanics, Zurich, 1982, pp.548-558.
- Almeida, M.S.S. and Parry, R.H.G. (1983a) Technical Report, Cambridge University, CUED/D-(SOILS) TR141
- Almeida, M.S.S. and Parry, R.H.G. (1983b) "Studies with vane and penetrometer tests during centrifuge flight", Technical Report, Cambridge University, CUED/D-(SOILS) TR142
- Almeida, M.S.S. (1984) Discussion, Embankment failure on clay near Rio de Janeiro, submitted Jour. Geot.Eng.Div., ASCE
- Avgherinos, P.J. (1969). Centrifuge testing of models made of soil, Ph.D thesis, University of Cambridge.
- Bassett, R.H. (1973). Centrifugal model tests of embankments on soft alluvial foundations. Proc. 8th. Int. Conf. Soil Mech. and Found. Eng., 1973, Vol.2.2, pp.23-30.
- Bassett, R.H. (1974). Description of method of prediction, Proc. of Found. Deformation Pred. Symp., MIT, November 1974.
- Bassett, R.H. (1980). The use of physical models in design. Proc. 7th Eur. Conf. Soil Mech. and Found. Eng., Brighton, 1979, Vol.5, pp.253-270.
- Bassett, R.H. and Horner, J. (1979). Prototype deformations from centrifugal model tests, Proc. 7th Europ. conf. Soil Mech. and Found. Eng., Brighton 1979, Vol.2.
- Bassett, R.H., Davies, M.C.R., Gunn, M.J. and Parry, R.H.G. (1981) Centrifugal models to evaluate numerical methods. Proc. Int. Conf. on Soil Mech. and Found. Eng. Vol. 1, pp.557-562

- Beasley, D.H. (1973). Centrifugal modelling of soft clay strata subject to embankment loading, Ph.D. thesis, University of Cambridge.
- Bishop, A.W. (1955). The use of the slip circle in the stability analysis of slopes. *Geotechnique*, 5, pp.7-17
- Bishop, A.W. (1976). Discussion, Ground Treatment by Deep Compaction. *Inst. Civil Eng., London*, 1976, 138-140
- Biot, M.M. (1941) General theory of three-dimensional consolidation. *J. Appl. Phys.*, 12, pp. 155-164.
- Bjerrum, L. (1972). Embankments on soft ground *Proc. Spec. Conf. on Performance of Earth and Earth Supported Structures, Prudue Univer., Vol.2*, pp.1-54.
- Brenner, R.P., Balasubramanian, A.S., Varaurairut, V. and Sivandran, C. (1982). Methods of settlement prediction for embankment on soft clay: a case study. *Proc. VII Southeast Asian Geotech. Conf., Nov. 1982, Hong Kong*, pp.675-690.
- Britto, A.M. (1983). A user's guide to the soils STRAIN calculating program, Internal Report, CUED.
- Brooker, E.W. and Ireland, H.O. (1965). Earth pressure at rest related to stress history. *Canadian Geotechnical Journal*, vol.2(1),pp. 1-15.
- Broms, B.B. (1979). Problems and solutions to construction in soft clay, *Proc. 6th Asian Regional Conf. Soil Mech. Found. Eng., Vol.2*, 3-38
- Burland, J.B. (1971). A method of estimating the pore pressures and displacements beneath embankments on soft natural clay deposits. *Proc. Roscoe Memorial Symposium*, pp. 505-536.
- Chan, K.C. (1975). Stresses and strains induced in soft clay by a strip footing, Ph.D. thesis, University of Cambridge.
- Davidson, C.S. (1980) The shear modulus of clays. Part II Research Report, Cambridge University Engineering Department, England.
- Davies, M.C.R. (1981) Centrifugal modelling of embankments on clay foundations. Ph.D. Thesis, Cambridge University Engineering Department, England.
- Dean, E.R. (1983). Private communication.
- Duncan, J.M. and Seed, H.B. (1966). Strength variations along failure surfaces in clay. *Jour. Soil Mech. Found. Eng.*, 92, SM6, pp.81-104.
- Duncan, J.M. and Chang, C.Y. (1970). Non linear analysis of stresses and strain in soils. *ASCE, JSMFD*, vol. 96, SM5, pp. 1629-1653.

- Duncan, J.M. and Poulos, H.G. (1977). Modern techniques of analysis of engineering problems on soft clay. General Report, International Symposium on Soft Clay, Bangkok.
- Endicott, L.J. (1971a). Centrifugal testing of soil models, Ph.D. thesis, University of Cambridge.
- Endicott, L.J. (1971b). A centrifugal model test of the trial embankment at King's Lynn, Technical Report, Cambridge University Engineering Department, CUED/C-SOILS/ TR12 (1971).
- Fredlund, D.G. and Krahn, J. (1977). Comparison of slope stability methods of analysis, Can. Geot. Jour., 14(3), pp.429-439.
- Gibson, R.E., Knight, K. and Taylor, P.W. (1963). A critical experiment to examine theories of three-dimensional consolidation, Proc. Europ. Conf. on Soil Mech. and Found. Eng., Weisbaden, Vol.1, pp.69-76.
- Greenwood, D.A. and Kirsch, K. (1983). Specialist ground treatment by vibratory and dynamic methods, State of the Art, Conf. on Advances in Piling and Ground Treatment for Foundations, Int. of Civil Engineers, London, March 1983, pp.17-45.
- Gunn, M.J. (1983). Using Cam-clay in a finite element analysis, Symposium on Application of Critical State Soil Mechanics, June 1983, Emmanuel College, Cambridge.
- Gunn, M.J. and Britto, A.M. (1981). CRISP - User's and programmers' manual. Cambridge University Engineering Department.
- Gunn, M.J. and Britto, A.M. (1983). CRISP - Users' and Programmers' Manual, Cambridge University Engineering Department.
- Henkel, D.J. (1960). The shear strength of saturated remoulded clays. ASCE, Proc. Conf. on Shear Strength of Cohesive Soils, Boulder, Colorado, pp. 533-544.
- Hoeg, K., Andersland, O.B. and Rolfsen, E.N. (1969). Undrained behaviour of quick clay under load test at Asrum. Geotechnique, vol. 19(1), pp. 101-115.
- Horner, J.N. (1982) Centrifugal modelling of multilayer clay foundations subjected to embankment loading. PhD thesis, King's College, University of London.
- Houlsby, G.T. (1981). A study of plasticity theories and their applicability to soils, Ph.D. thesis, University of Cambridge.
- James, R.G. (1971). Some aspects of soil mechanics testing, stress strain behaviour of soils, Ed. R.H.G. Parry, Foulis, London, pp.417-440.
- James, R.G. (1973). Determination of strains in soils by radiography, CUED/C SOILS LN1(a), Department of Engineering, University of Cambridge.

- Knogle, D.S. (1979). The influence of pore water tension on the undrained shear strength of kaolin, University of Cambridge, Eng. Dept., Part II Research Report.
- Kusakabe, O. (1982). Stability of excavations in soft clay, Ph.D. thesis, University of Cambridge, England.
- Lacasse, S.M., Ladd, C.C. and Baligh, M.M. (1978). Evaluation of field vane, dutch cone penetrometer and piezometer testing devices. Res. Report, Dept. of Civil Eng., MIT.
- Ladd, C.C. and Foott, R. (1974). New design procedure for stability of soft clays. ASCE, JGED, 100(7), pp. 763-786.
- Ladd, C.C. and Foot, R. (1980). Discussion on the behaviour of embankments on clay foundations, Can. Geot. Jour. Vol.17, pp.454-460.
- Lambe, T.W. (1973). Predictions in soil engineering, Geotechnique, Vol.23, No.2, pp.149-202.
- La Rochelle, P., Track, B., Tavenas, F. and Roy, M. (1974). Failure of a test embankment on a sensitive Champlain clay deposit, Can. Geot. Jour., Vol.11, pp.142-181.
- Leroueil, S., Tavenas, F., Brucy, F., Rochelle, P. and Roy, M. (1979). Behaviour of destructed natural clays. ASCE, JGED, vol. 105(GT6), pp. 759-778.
- Leroueil, S., Tavenas, F., Mieussens, C. and Peignaud, M. (1978). Construction pore pressures in clay foundations under embankments. Part II: generalized behaviour. Canadian Geotechnical Journal, 15, pp. 66-82.
- Lyndon, A. and Schofield, A.N. (1970). Centrifugal model test of a short term failure in London clay, Geotechnique, Vol.20, No.4, pp.440-442.
- Maddocks, D.V. and Savvidou, C. (1982). Ocean disposal of high level radioactive waste - centrifuge modelling research - Preliminary tests, October 1981 - March 1982 - Report to the Department of Environment, University of Cambridge.
- Magnan, J.P., Humbert, P., Belkeziz, A. and Mouratidis, A. (1982a). Finite Element Analysis of Soil Consolidation, with Special Reference to the Case of Strain Hardening Elastoplastic Stress-strain Models, Proc. IV Int. Conf. on Num. Met. in Geomechanics, Edmonton, Canada, June 1982, pp.327-336.
- Magnan, J.P., Humbert, P. and Mouratidis, A. (1982b). Finite element analysis of soil deformations with time under an experimental embankment at failure, Proc. Int. Symp. on Num. Met. in Geomechanics, Zurich, September 1982, pp.601-609.
- Mair, R.J. (1979) Centrifugal modelling of tunnel construction in soft clay. Ph.D. Thesis, Cambridge University Engineering Department, England.

- Mak, K. (1984). Modelling the effects of a strip load behind rigid retaining walls, Ph.D. thesis, University of Cambridge.
- Manson, S.M. (1980). An investigation of the strength and consolidation properties of 'speswhite kaolin, University of Cambridge, Eng. Dept., Part II Research Report.
- Marche, R. and Chapuis, R. (1974) Controle de la stabilite des remblais par la mesure de deplacements horizontaux, Can. Geot. Jour., Vol.11(1), pp.182-201.
- Margason, G. and Symons, I.F. (1969). Use of pore pressure measurements to control embankment construction on soft foundations, Proc. 7th Int. Conf., Soil Mech., Mexico, 1969, 2, pp.307-315.
- Mayne, P.W. and Kulhawy, F.H. (1979). Ko-OCR relationships in soil, ASCE, Jour. Geot. Eng. Div., Vol.108, GT6, June 1982, pp.851-872.
- Mesri, G. (1975). Discussion on new design procedure for stability of soft clays. ASCE, JGED, 101(GT4), pp. 409-412.
- Meyerhof, G.G. and Sastry, V.V.R.N. (1978) Bearing capacity of piles in layered soils. Part 2. Sand overlying clay. Can. Geot. Jour., 15(2), pp.183-189
- MIT (1974). Proc. Foundation Deformation Prediction Symposium. Research Report FHWA-RD-75-515/516, 2 vol.
- Mitchell, J.K. and Katti, R.K. (1981). Soil improvement - state-of-the-art report, Proc. of the XX Int. Conf. on Soil Mech. and Found. Eng., Stockholm, 1981, Vol.4.
- Moraes Jr., L.J. (1975). Algumas consideracoes praticas a respeito da analise de estabilidade de taludes. M.Sc. thesis (in portuguese), Fed. Univ. of Rio de Janeiro, Brazil.
- Murray, R.T. (1978). Two and three-dimensional consolidation theory, Chapter 4 of Developments of Soil Mechanics, Ed. C.R. Scott, pp.103-147.
- Nadarajah, V. (1973). Stress-strain properties of lightly overconsolidated clay. Ph.D. thesis, University of Cambridge, England.
- Naylor, D.J. (1975). Non-linear finite elements for soils. Ph.D. thesis. Dept. of Civil Engineering, University College of Swansea.
- Ovesen, N.K. (1980). Discussion, Design Parameters in geotechnical Engineering, Proc. 7th Eur. Conf. on Soil Mech. and Found. Eng., 4, pp.318-323
- Palmeira, E.M. and Almeida, M.S.S. (1979). Atualizacao do programa BISPO para analise de estabilidade de taludes. Research Report (in portuguese), Brazilian Road Research Institute, IPR-DNER, Rio de Janeiro, Brazil.

- Parkin, A., Holden, J., Aarnot, K., Last, N. and Lunne, T. (1980). Laboratory investigations of CPT's in sand. 31 pp., Norwegian Geotechnical Institute, Report 52108-9.
- Parry, R.H.G. (1982) Stress state and stress paths, Lecture Notes 5, CUED, March 1982
- Parry, R.H.G. and McLeod, J.H. (1967). Investigation of slip failure in flood levee at Launceston, Australia. 5th Australian-New Zealand Conf. Soil Mech. and Found. Eng., Auckland.
- Parry, R.H.G. (1971). Stability of low embankments on soft clays. Proc. Roscoe Mem. Symp. Stress Strain Behaviour of Soils. Foulis Pub., 1971, pp. 643-668.
- Parry, R.H.G. and Nadarajah, V. (1973). Observations in laboratory prepared lightly overconsolidated kaolin, *Geotechnique*, Vol.24, pp.345-357.
- Parry, R.H.G. and Wroth, C.P. (1977). Shear properties of soft clays. Report presented at Symp. on Soft Clay, Bangkok, Thailand.
- Peck, R.B. (1969) 'Advantages and limitations of the observational method in applied soil mechanics' *Geotechnique* Vol.19 pp 171-87.
- Philips, R (1984). Private communication.
- Pilot, G. (1972). Study of five embankment failures on soft soils. Proc. ASCE Specialty Conference on Earth and Earth-supported Structures, Purdue Univ., vol. 1.1, pp. 81-99.
- Pilot, G., Trak, B. and La Rochelle, P. (1982), "Effective Stress Analysis of the Stability of Embankments on Soft Soils", *Canadian Geotechnical Journal*, Vol.19, No.4, Nov. 1982, pp.433-450.
- Poulos, H.G. (1972). 'Difficulties in Prediction of Horizontal Deformations of Foundations'. ASCE, JSMFD, 98 (SMB), pp.843-848.
- Priebe, H. (1978). Abschätzung des Scherwiderstandes eines durch Stopverdichtung verbesserten Baugrundes. *Die Bautechnik*, Vol.55, No.8, pp.281-284.
- Ramalho-Ortigão, J.A., M.L.G. Werneck & W.A. Lacerda (1983) Embankment failure on clay near Rio de Janeiro, *Jour. Geot. Eng. Div., ASCE*, Vol. 109, 11, 1460-1479
- Ramalho-Ortigão, J.R., Lacerda, W.A., Almeida, M.S. and Palmeira, E.N. (1980). Aterro experimental levado a ruptura sobre argila cimza do Rio de Janeiro, parte II: Análise do comportamento, (in portuguese), Internal Report, IPR-DNER, Rio de Janeiro, Brazil.
- Randolph, M.F. (1980). Piles subjected to torsion, *Jour. Geot. Eng. Div., ASCE*, 107, GT8, pp.1095-1111.

- Randolph, M.F., Steenfelt, J.S. and Wroth, C.P. (1979). The effect of pile type on design parameters for driven pile, Proc. 7th. Eur. Conf. on Soil Mech. and Found. Eng., Brighton, Vol.2, pp.107-114.
- Rathgeb E. and Kutzner C. (1975) Some applications of the vibro-replacement process, Geotechnique, Vol. 25, pp. 45-50
- Rocha, M. (1957). The possibility of solving soil mechanics problems by the use of models, Proc. 4th. Int. Conf. Soil Mech. Found. Eng., Vol.1, pp.183.
- Roscoe, K.H. (1968). Soils and model tests, Jour. Strain Analysis, Vol.3, No.1, pp.57-64.
- Roscoe, K.H. (1970). The influence of strains in soil mechanics, Geotechnique 20, No.2, pp.129-170.
- Roscoe, K.H. and Burland, J.B.(1968). On the generalized behaviour of 'wet' clay. Engineering plasticity, Ed. Heyman, J. and Leckie, F., Cambridge University Press, pp. 535-609.
- Rowe, P.W. (1971). Large scale laboratory model retaining wall apparatus. Stress-strain behaviour of soils, Ed. R.H.G. Parry, Publ. G.T. Foulis & Co., pp.441-449.
- Rowe, P.W. (1972). The relevance of soil fabric to site investigation practice. Geotechnique, vol. 22, pp. 193-300.
- Scarpelli, G. (1981). Shear bands in sands, M. Phil. thesis, University of Cambridge.
- Schofield, A.N. and Wroth, C.P. (1968). Critical state soil mechanics. McGraw Hill, London.
- Schofield, A.N. (1980). Cambridge geotechnical centrifuge operations. Geotechnique, vol. 30(3), pp. 227-268.
- Simpson, B (1973) Finite element computations in soil mechanics. Ph.D. thesis, University of Cambridge.
- Skempton, A.W. (1954). The pore pressure coefficients A and B. Geotechnique, 4(4), pp. 143-147.
- Sloan, S.W. (1980) 'A fast stiffness formulation for finite element analysis of two dimensional solids' Cambridge University Engineering Department, Technical Report 87 unpublished).
- Small, J.C., Booker, J.R. and Davis, E.H. (1976). Elastoplastic consolidation of soil. Int. J. Solids Structures, vol. 12(6), pp. 431-488.
- Smith, I.A.A. (1972). Stress and strain in a sand mass adjacent to a model wall, Ph.D. thesis, University of Cambridge.

- Tanimoto, K. (1973). Introduction of the sand compaction pile method as applied to stabilization of soft foundation grounds, Commonwealth Scient. and Res. Organ., Australia, 1973.
- Tavenas, F., Blanchet, R., Garneau, R. and Leroueil, S., (1978). "The Stability of Stage-Constructed Embankments on Soft Clays", Canadian Geotechnical Journal, Vol.15, 1978, pp.283-305.
- Tavenas, F., Trak, B. and Leroueil, S. (1980). Remarks on the validity of stability analysis. Canadian Geotechnical Journal, 17, pp.61-73.
- Tavenas, F. and Leroueil, S. (1980) The behaviour of embankments on clay foundations. Can. Geot. Jour. 17, pp. 236-260
- Tavenas, F. (1981). Some aspects of clay behaviour and their consequences on modelling techniques, laboratory shear strength of soil, ASTM STP 740, pp.667-677.
- Taylor, R.N. (1984). Ground movements associated with tunnels and trenches, Ph.D. thesis, University of Cambridge.
- Thompson, S.A. (1976). Application of finite elements to plane strain deformation and consolidation of soils. Ph.D. thesis, Cambridge University Engineering Department, England.
- Thompson, W.J. (1962). Some deformation characteristics of Cambridge Gault clay, Ph.D. thesis, University of Cambridge, England.
- Thorburn, S. (1975) Building structures supported by stablized ground. Geotechnique, (25), 1, 83-94.
- Trak, B., La Rochelle, P., Tavenas, F., Leroueil, S. and Roy, M. (1980). A new approach to the stability analysis of embankments on sensitive clays. Canadian Geotechnical Journal, 17, pp. 526-544.
- Terzaghi, K.V. (1943). Theoretical Soil Mechanics, John Wiley and Sons, New York.
- Truong, D.M. and Magnan, J.P. (1977). Application des modeles elastoplastiques de l'Universite de Cambridge au calcul du comportement d'un remblais experimental sur sols mous. Rapport de Recherche LPC No 74, Lab. Cental des Ponts et Chaussees.
- Whitman, R.V. and Bailey, W.A. (1967). Use of computers for slope stability analysis. ASCE, JSMFD, 93(4), pp. 475-498.
- Wood, D.M. (1980). Yielding in soft clay at Backebol,Sweden. Geotechnique, 30, No 1, pp. 49-65.
- Wood, D.M. (1982). Choice of Models for Geotechnical Predictions, Technical Report CUED/D - SOILS TR126 (1982), University of Cambridge, Engineering Department.

- Wroth, C.P. (1975). In-situ measurements of initial stresses and deformation characteristics, ASCE Specialty Conf. on In-situ Measurement of Soil Properties, North Carolina State University.
- Wroth, C.P. (1977). The predicted performance of soft clay under a trial embankment loading based on the Cam-Clay model. Chapter 6, Finite Elements in Geomechanics, Ed. Gudehus.
- Wroth, C.P. (1984). In-situ measurements of soil properties, 24th Rankine Lecture, March 1984.
- Wroth, C.P., Randolph, M.F., Houlsby, G.T. and Fahey, M. (1979). A review of the engineering properties of soils with particular reference to the shear modulus. Cambridge University Engineering Department, Technical Report No 75.
- Wroth, C.P. and Simpson, B. (1972). An induced failure at a trial embankment: part II finite element computations. Proc. Conf. on the Performance of Earth and Earth Supported Structures, ASCE, pp 65-79.
- Zytynski, M. (1976). First year research report. Cambridge University Engineering Department.
- Zytynski, M., Randolph, M.F., Nova, R. and Wroth, C.P. (1978). On modelling the unloading-reloading behaviour of soils. Intern. Journal for Num. and Analytical Methods in Geomechanics, vol. 2, pp. 87-94.

Table 3.1 - Average volumetric and shear strains

Test	lift	vol. strains (%)	maximum shear strains (%)
MA3	2-end	1.2	6.3
	3-start	1.3	9.0
	3-end	2.3	12.9
	5-failure	3.6	15.5
MA6	2-start	0.3	6.3
	3-start	1.3	7.9
	3-end	1.7	8.0
	4-start	2.3	8.7
	5-end	2.3	10.7
MA4	3-start	0.67	7.1
	5-end	3.6	10.3
MA5	2-start	0.001	7.3
	4-failure	0.84	15.3

Table 3.2. Values of  $\bar{B} = \Delta u / \Delta \sigma_v^{(1)}$  for transducers under the embankment platform

Test	Transducer	lift 2	lift 3	lift 4	lift 5
MA3	P1	1.12	1.05	0.90	0.33
	P2	1.13	0.86	0.79	0.58
	P3	1.01	0.35	0.99	0.73
	P4	1.07	0.36	1.08	0.94
	P11	1.09	0.95	0.96	0.33
MA6	P1	1.03	0.91	0.37	0.56
	P2	1.02	0.94	0.34	0.58
	P3	0.95	0.92	0.79	0.52
	P4	0.99	0.32	0.58	0.53
	P5	0.99	0.34	0.72	0.63

NOTE: (1)  $\bar{B} = \Delta u / \Delta \sigma_v$  is the ratio between increment pore pressure to the increment of applied vertical stress.

AD-A148 743

STABILITY OF LOW EMBANKMENTS ON SOFT CLAY PART 3  
CENTRIFUGE TESTS AND NUM. (U) CAMBRIDGE UNIV (ENGLAND)  
DEPT OF ENGINEERING M S ALMEIDA ET AL. NOV 84

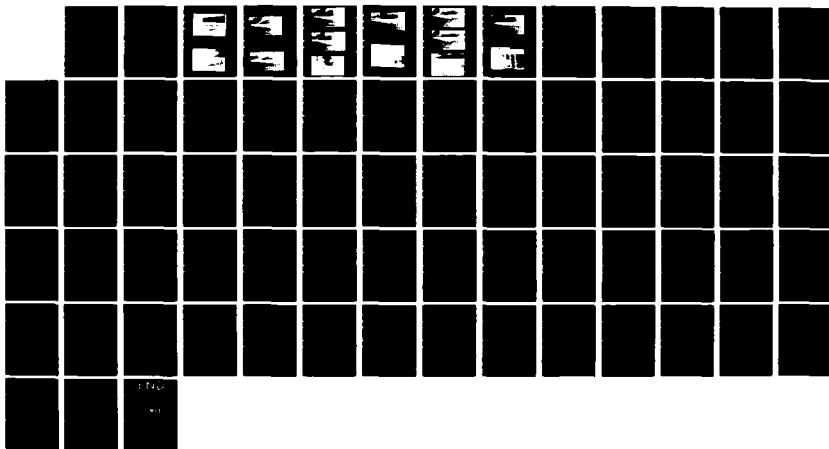
2/2

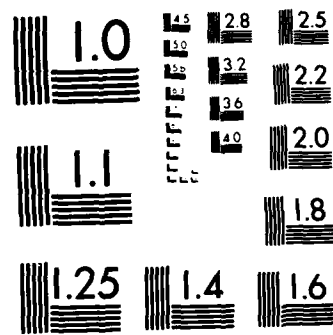
UNCLASSIFIED

DAJA37-82-C-0177

F/G 8/13

NL





MICROCOPY RESOLUTION TEST CHART  
NATIONAL BUREAU OF STANDARDS-1963-A

Table 4.1 - Variation of  $K_o$  with OCR

OCR	$K_o$		
	Brooker and Ireland (1975)	Wroth (1975)	Parry (1982)
1	0.69	0.69	0.69
2	0.88	0.91	0.91
4	1.16	1.20	1.20
8	1.38	1.57	1.59
16	1.69	2.08	2.09

Table 4.2 Critical state parameters

	$\lambda$	$K$	$e_{cs}$	$M$
Speswhite Kaolin	0.25	0.05	2.44	0.90
Gault clay I <sup>(1)</sup>	0.175	0.0435	1.99	0.896
Gault clay II	0.219	0.035	1.96	1.0

(1) after Thompson (1962)

Table 4.3 Numerical analyses performed

Case	$k_{v0}$	$k_v$ ( $k_h$ ) during consolidation
A	b	variable
B	b	constant
C	a	constant

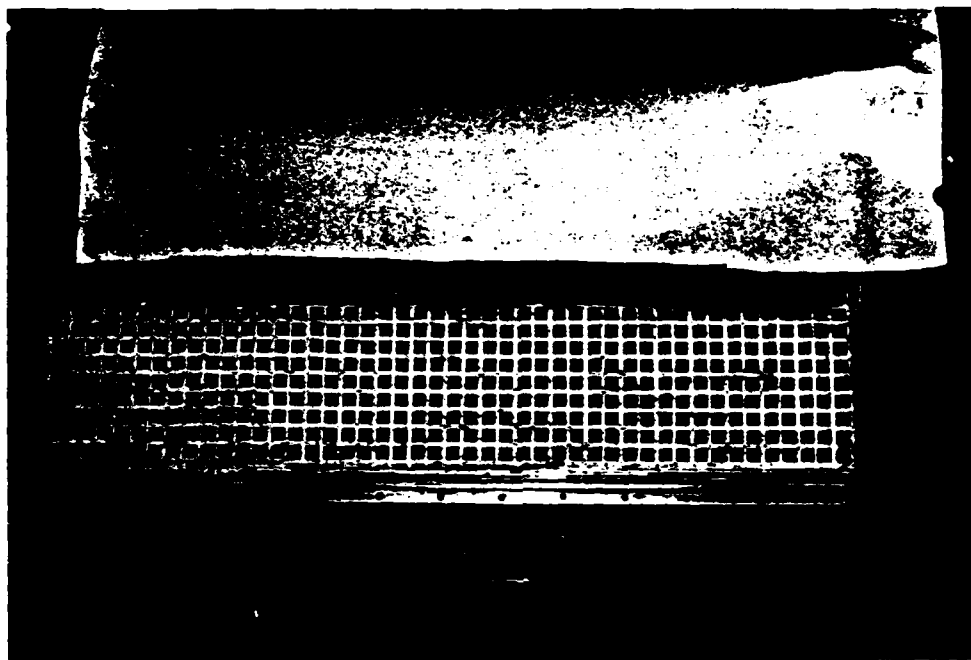


Plate 3.1 - Model face preparation, brown clay grid

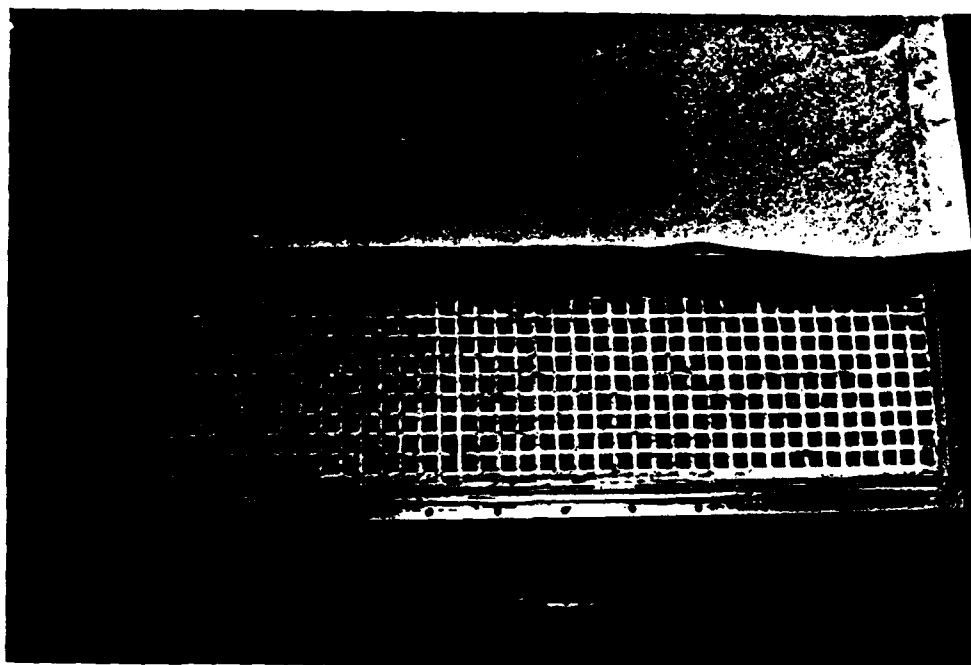


Plate 3.2 - Model face with silvered marks

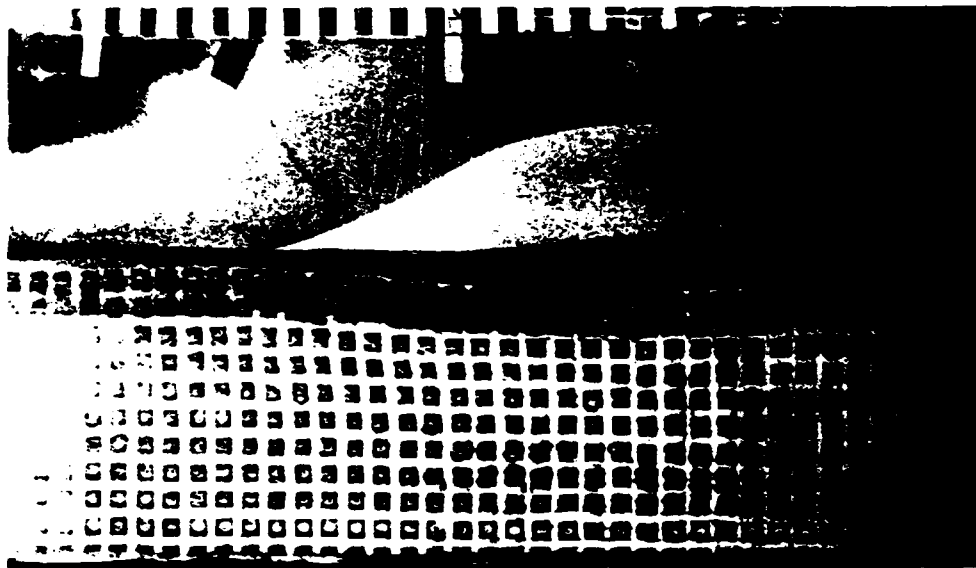


Plate 3.3 - Test MA3, start of stage 3

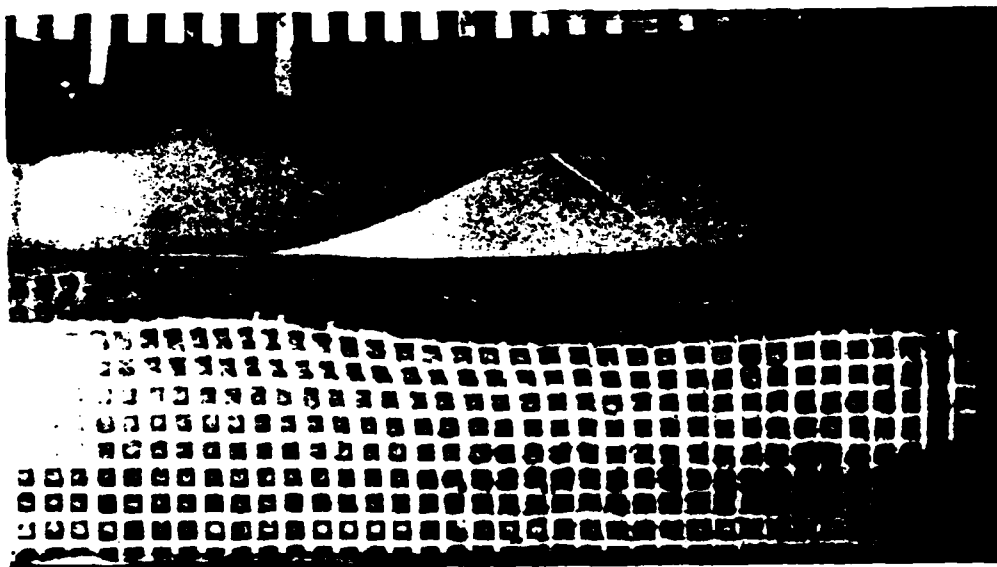


Plate 3.4 - Test MA3, end of stage 3

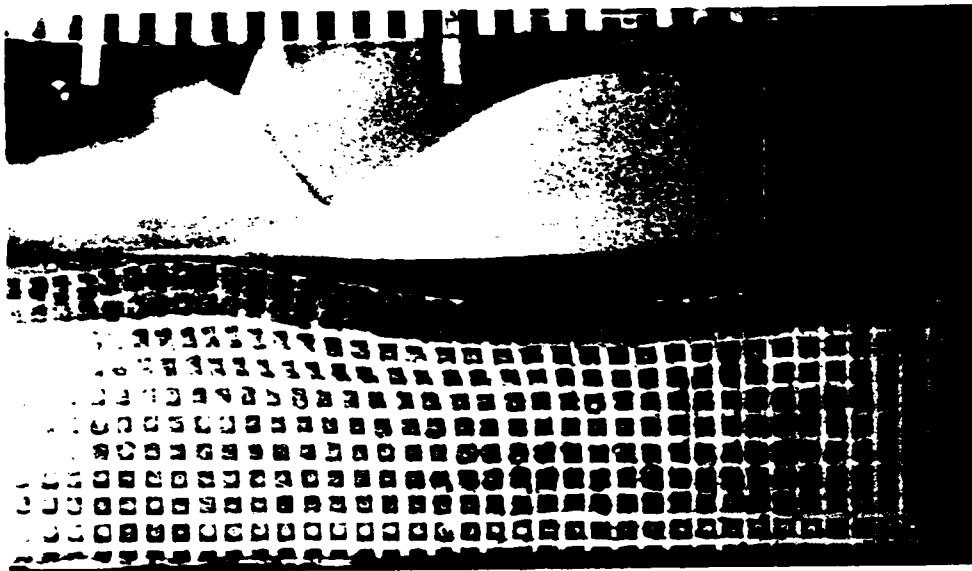


Plate 3.5 - Start of lift 5, test MA3

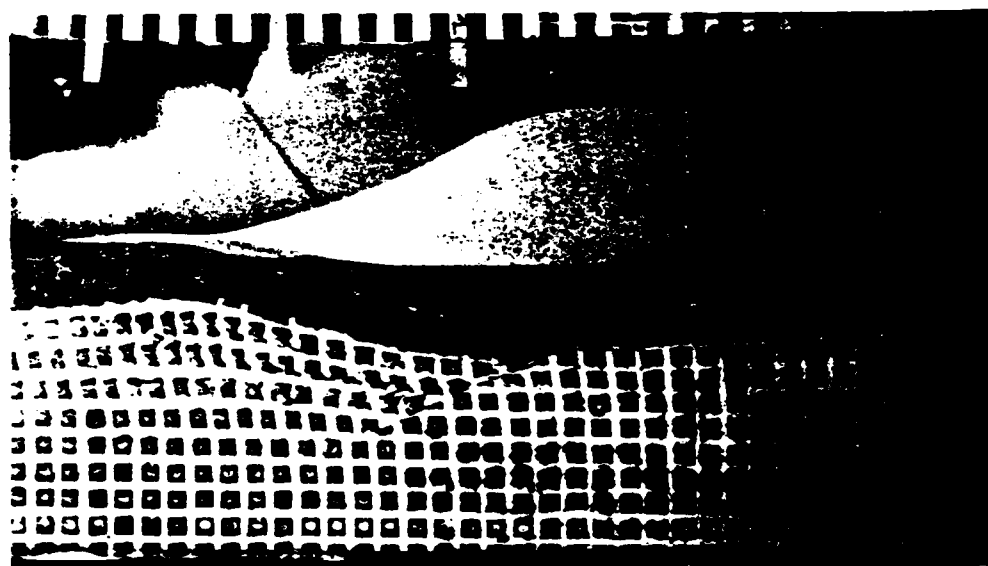


Plate 3.6 - Start of failure, lift 5, test MA3



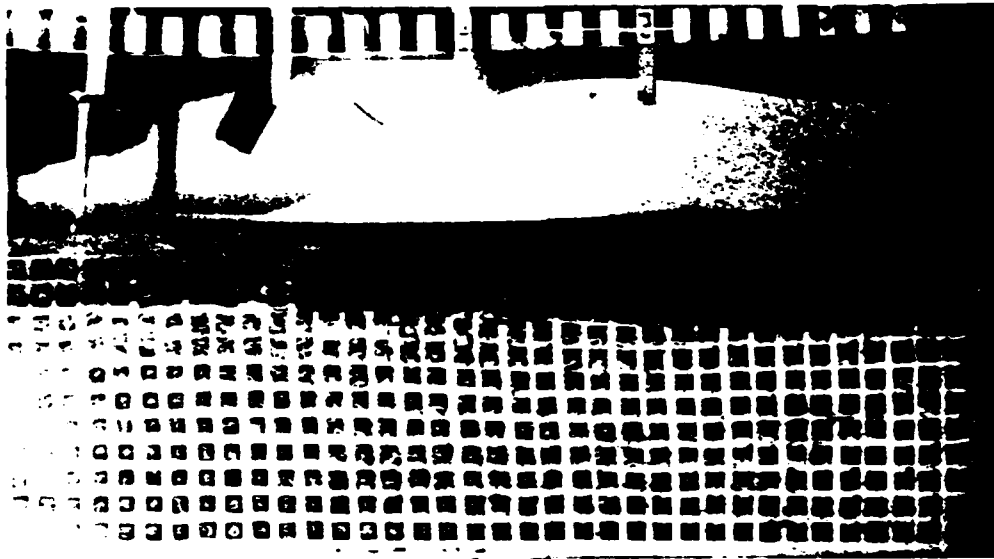


Plate 3.8 - Test MA4, end of stage 3

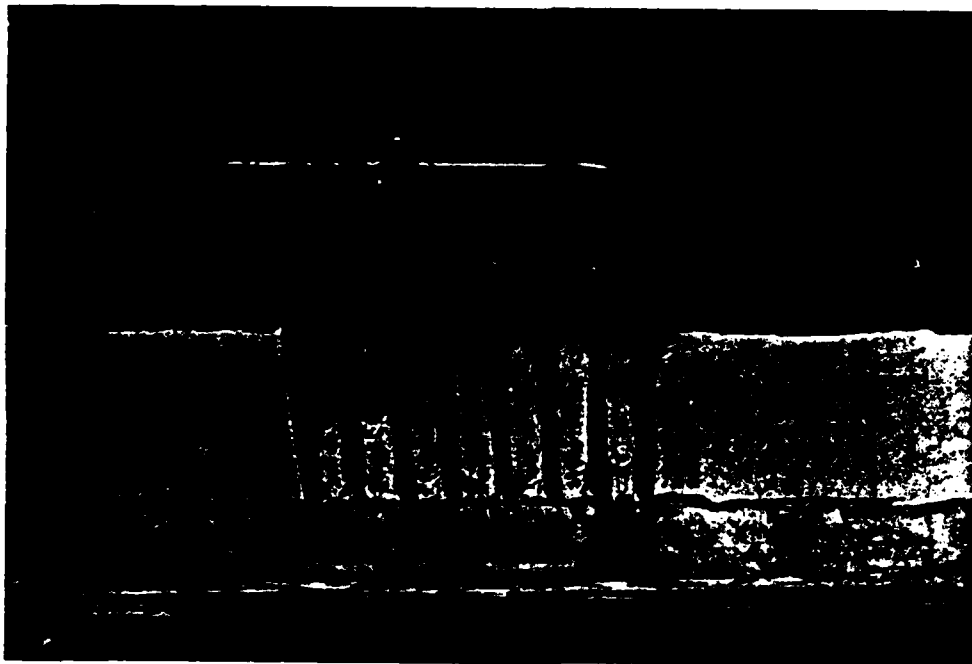


Plate 3.9 - View of clay foundation after test MA4

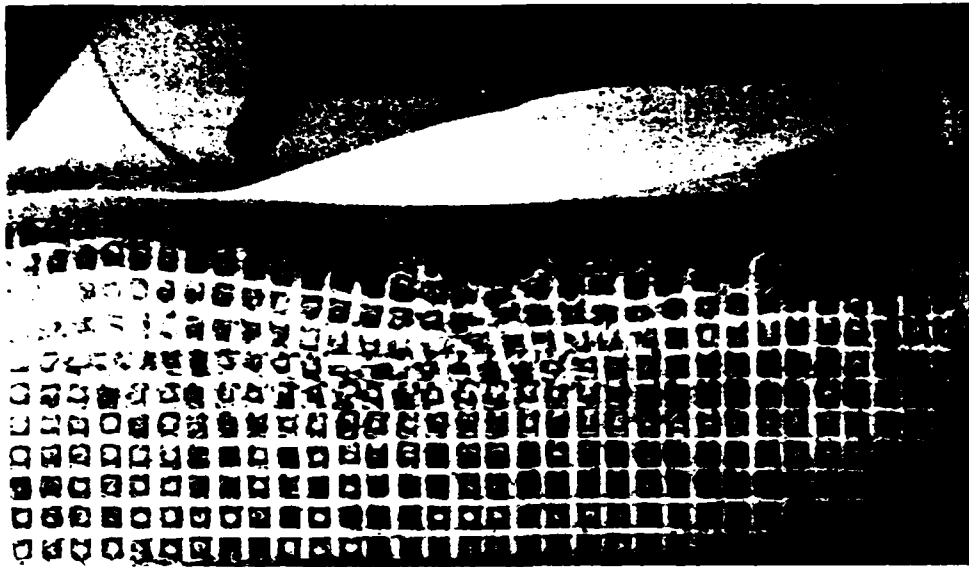


Plate 3.10 - Start of failure, test MA5

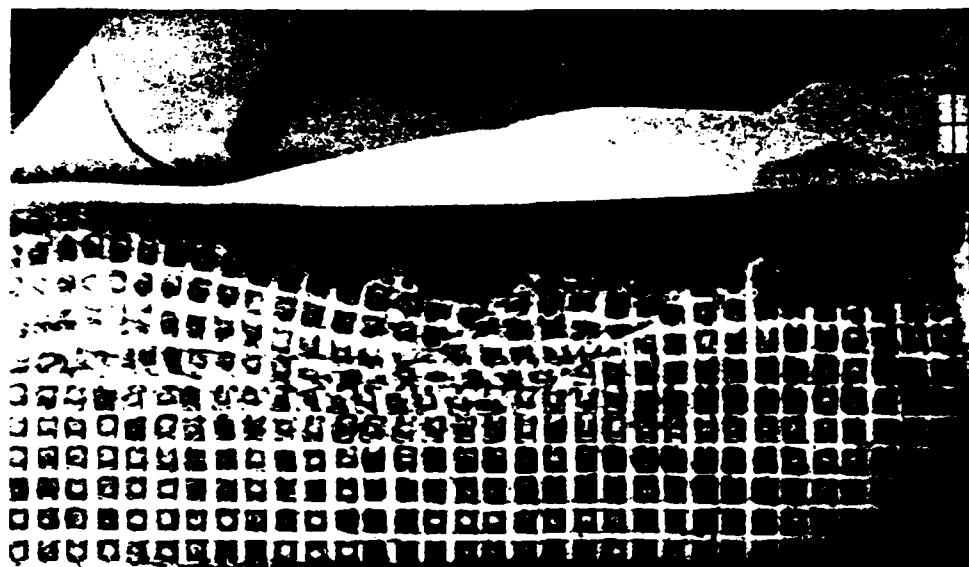


Plate 3.11 - End of failure, test MA5



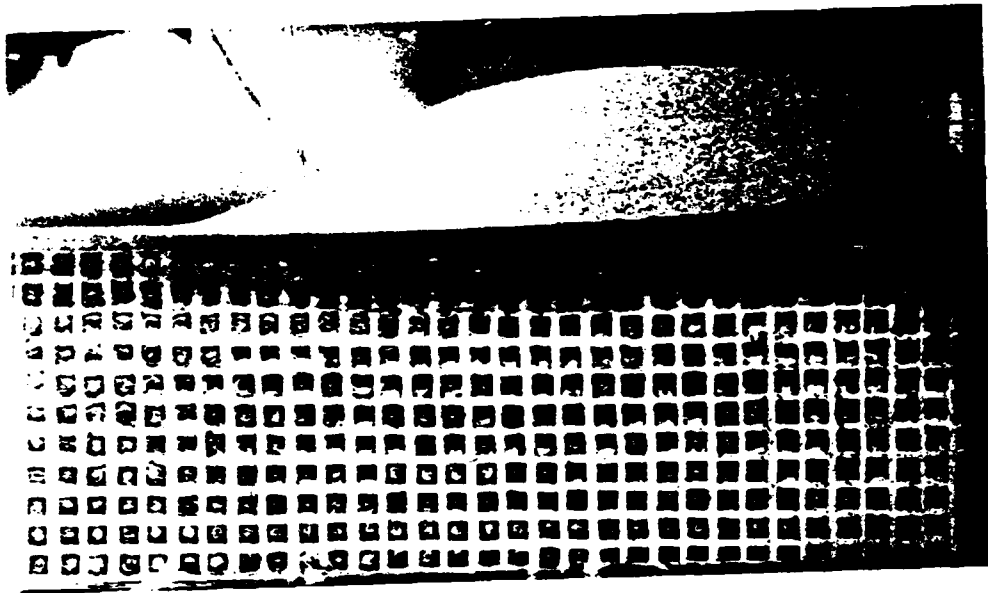


Plate 3.13 - Test MA6, end of stage 3

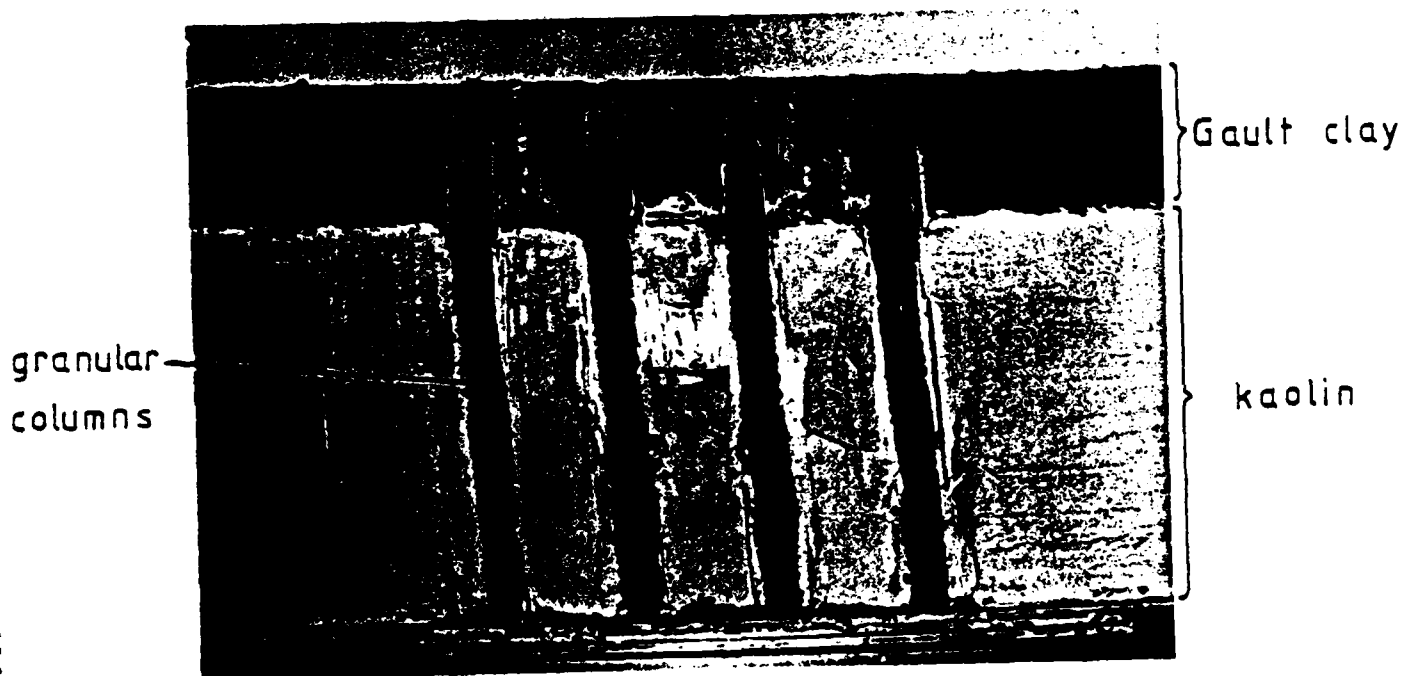
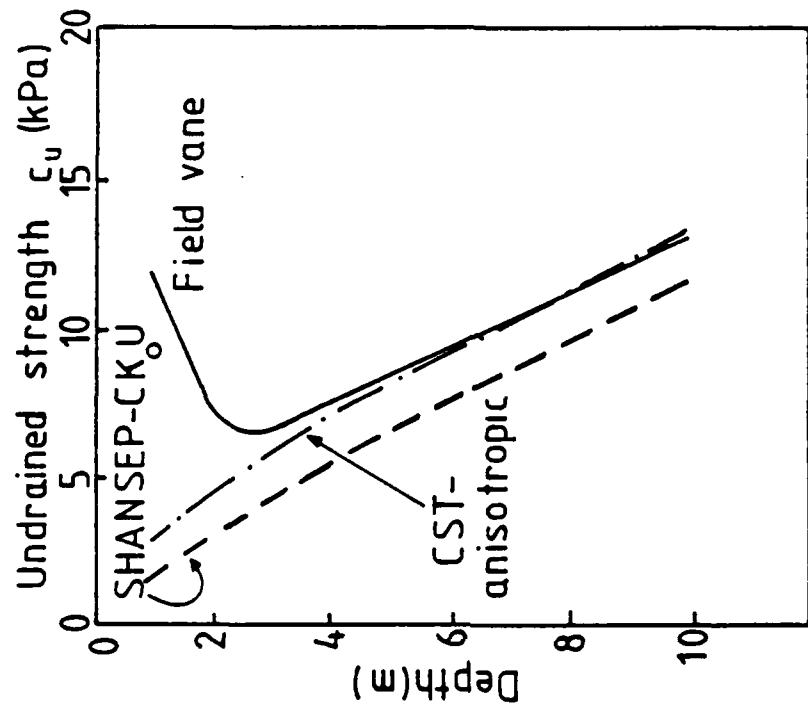
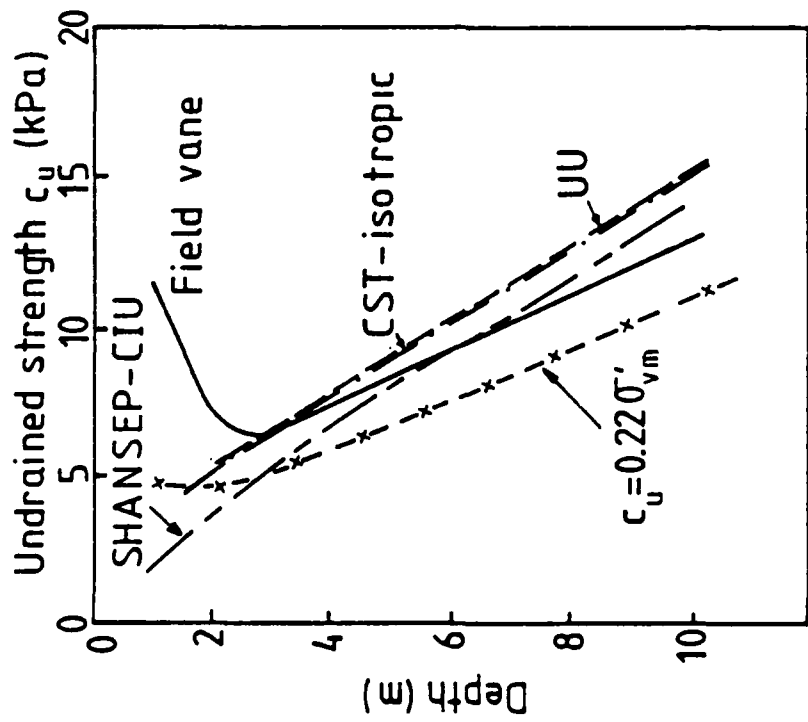


Plate 3.14 - Sectional view of clay foundation MA6 after test



a)



b)

Fig. 2.1 - Undrained strength of the Rio de Janeiro soft clay (after Almeida, 1981)

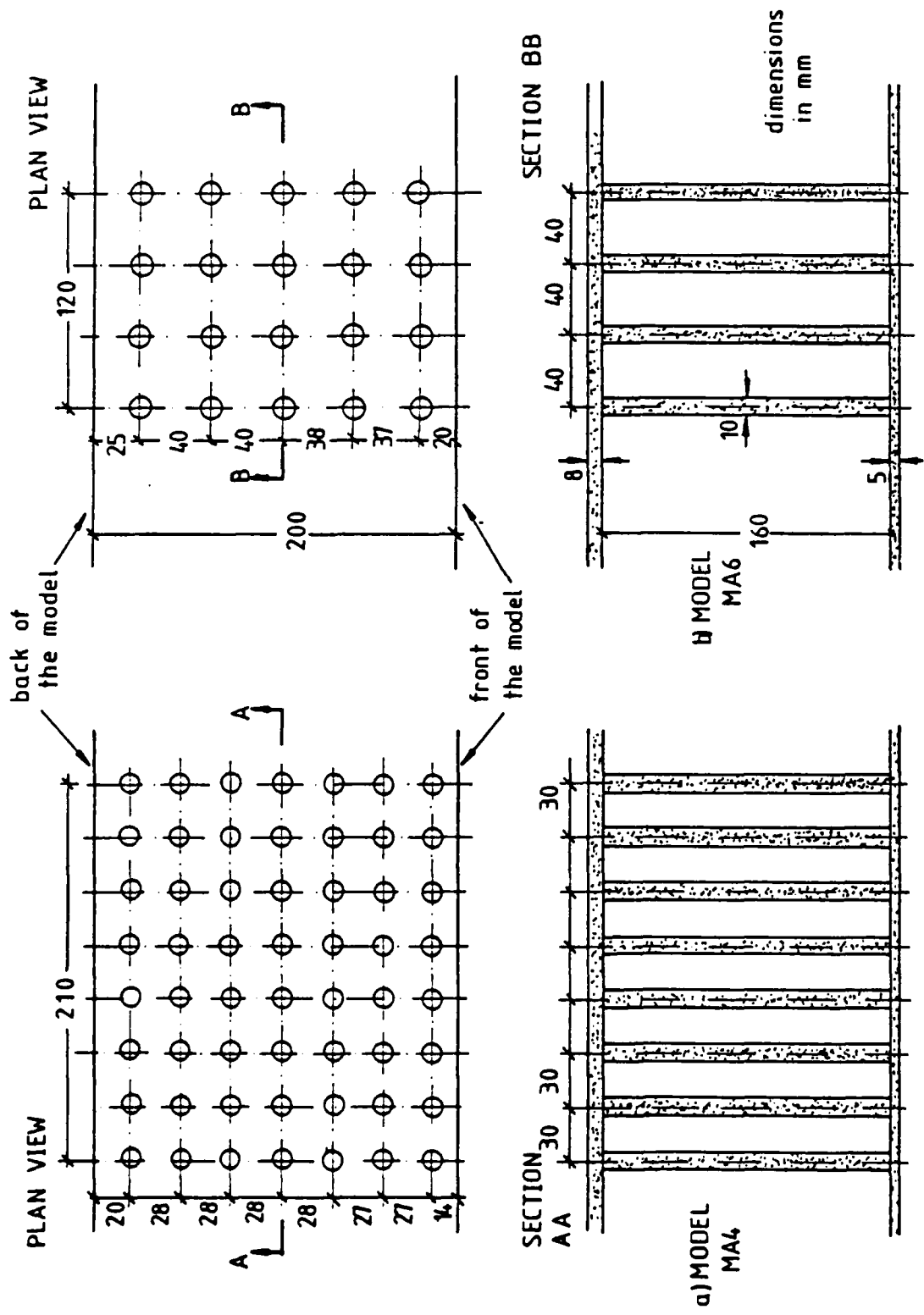


Fig. 3.1 - Column grids for models MA4 and MA6

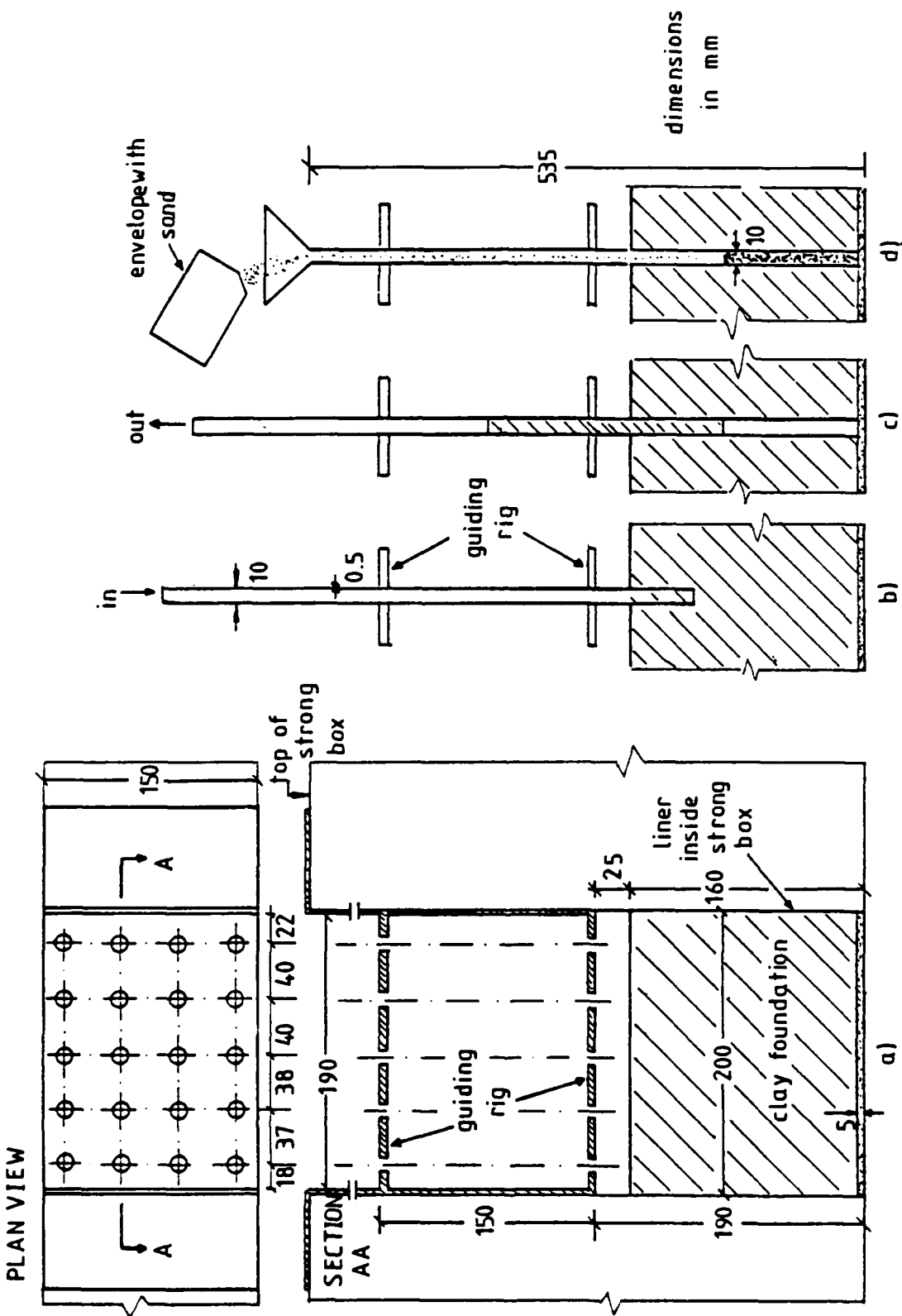


Fig. 3.2 - Installation of the granular columns

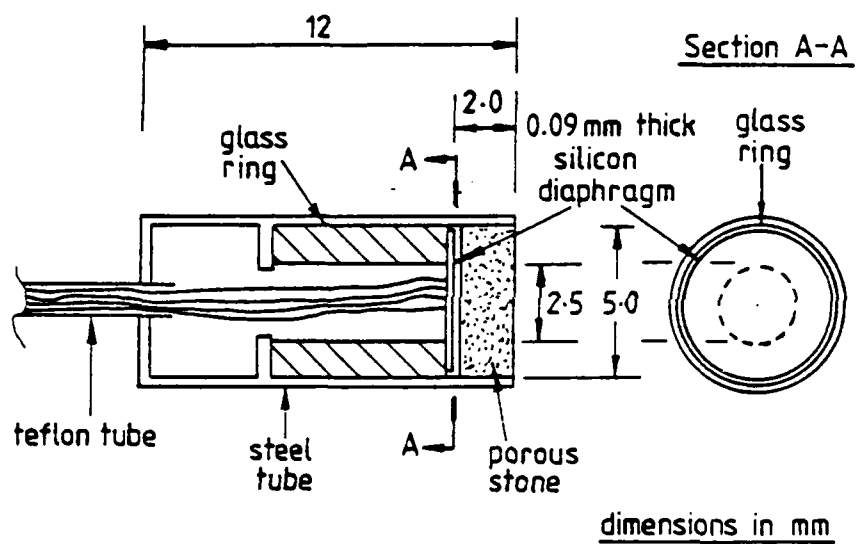


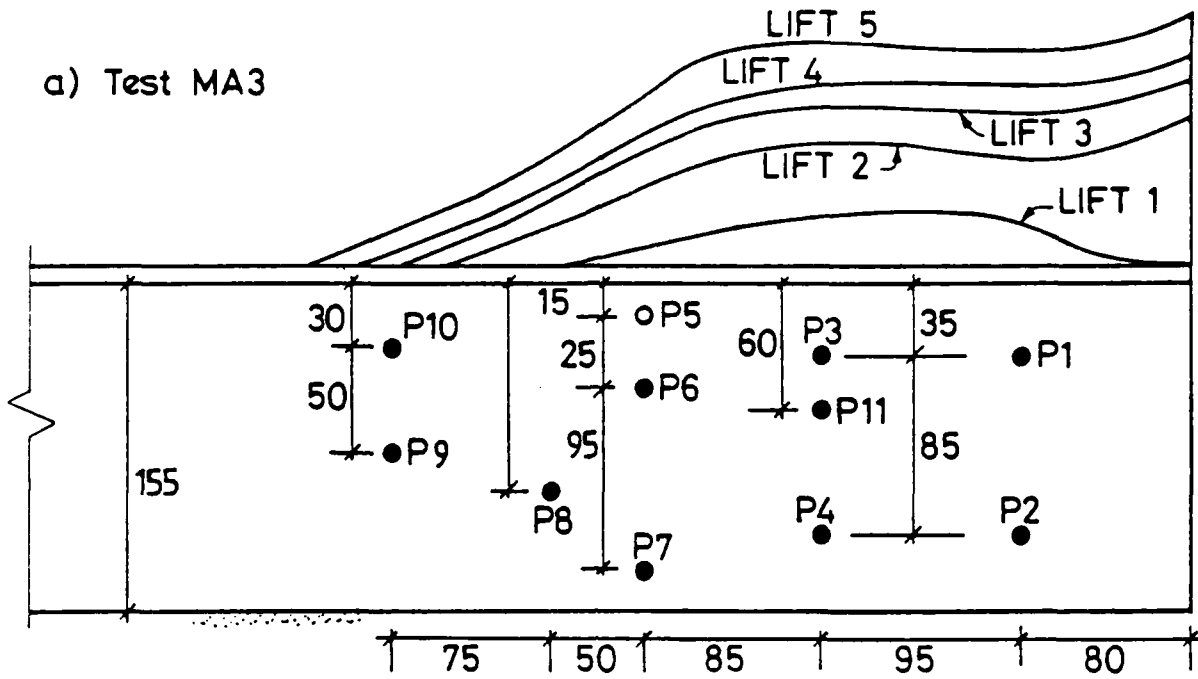
Fig. 3.3 - Druck pore pressure transducer

scale

0 50 100mm (model)

0 5 10m (prototype)

a) Test MA3



all dimensions shown  
are for the model

b) Test MA4

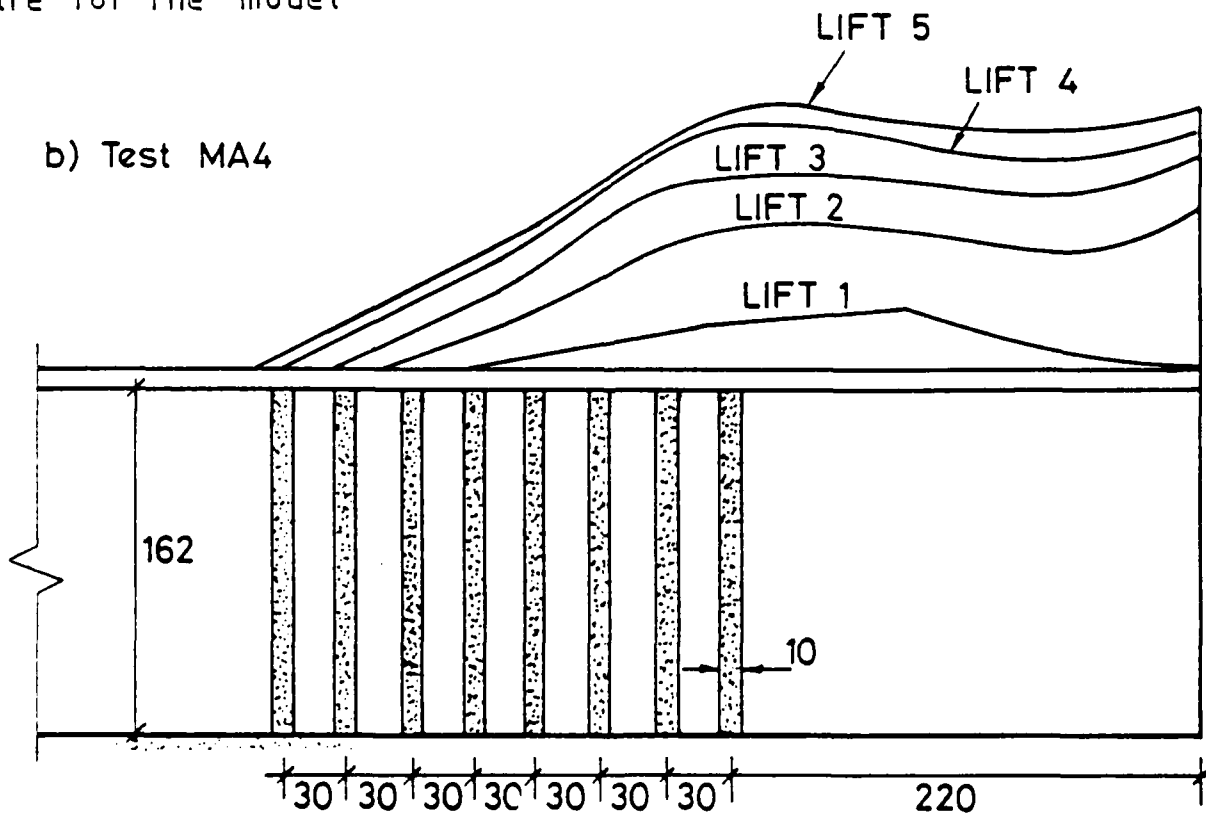


Fig. 3.4 - Centrifuge tests of embankments on soft clays

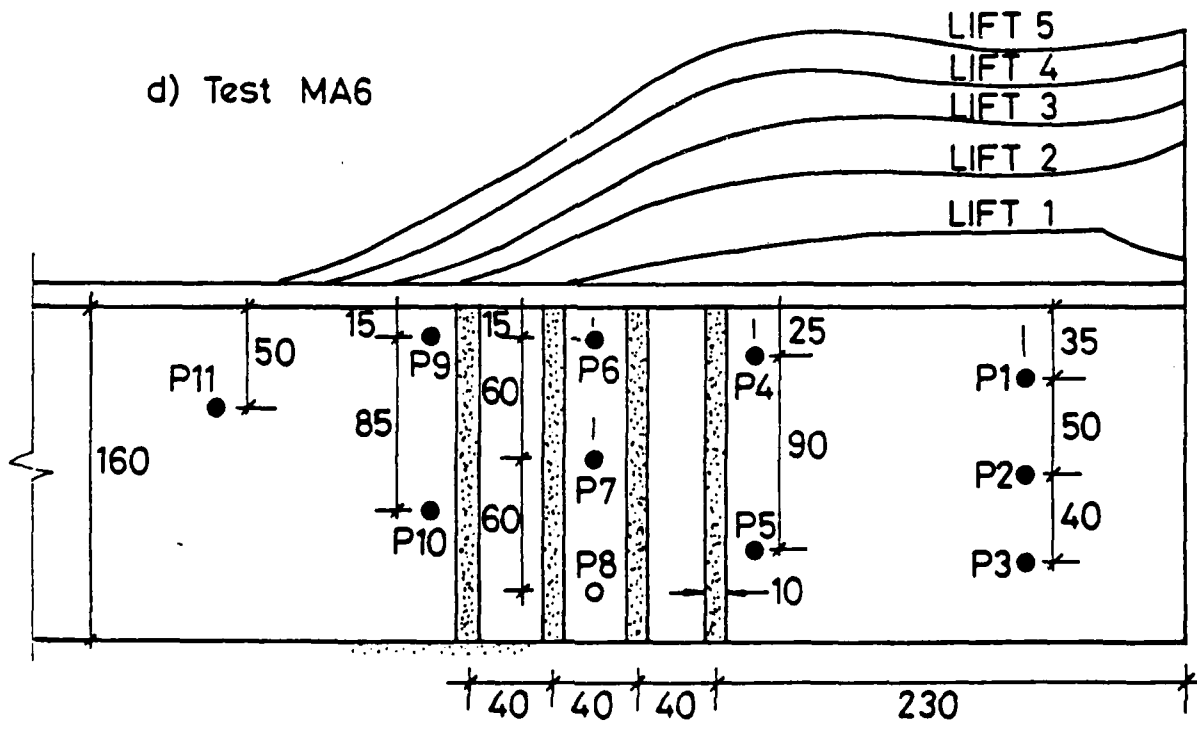
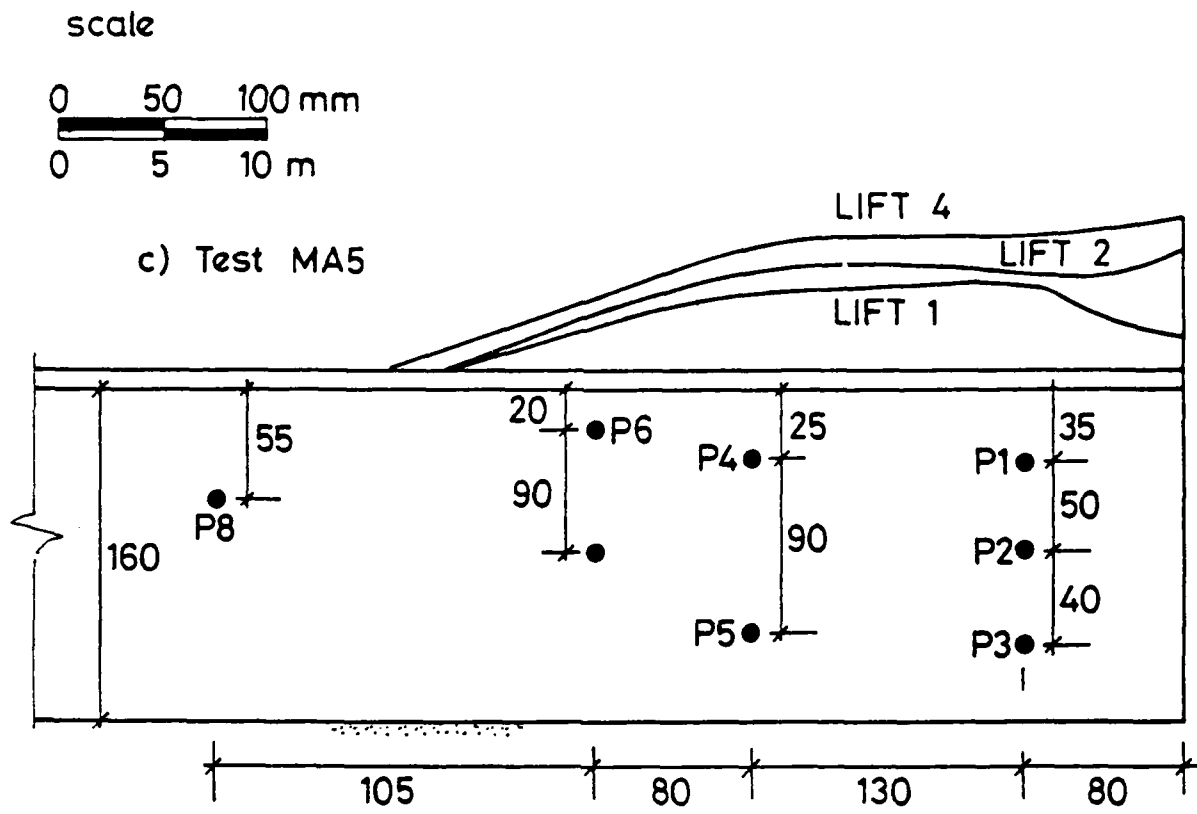


Fig. 3.4 (contn.) - Centrifuge tests of embankments on soft clays

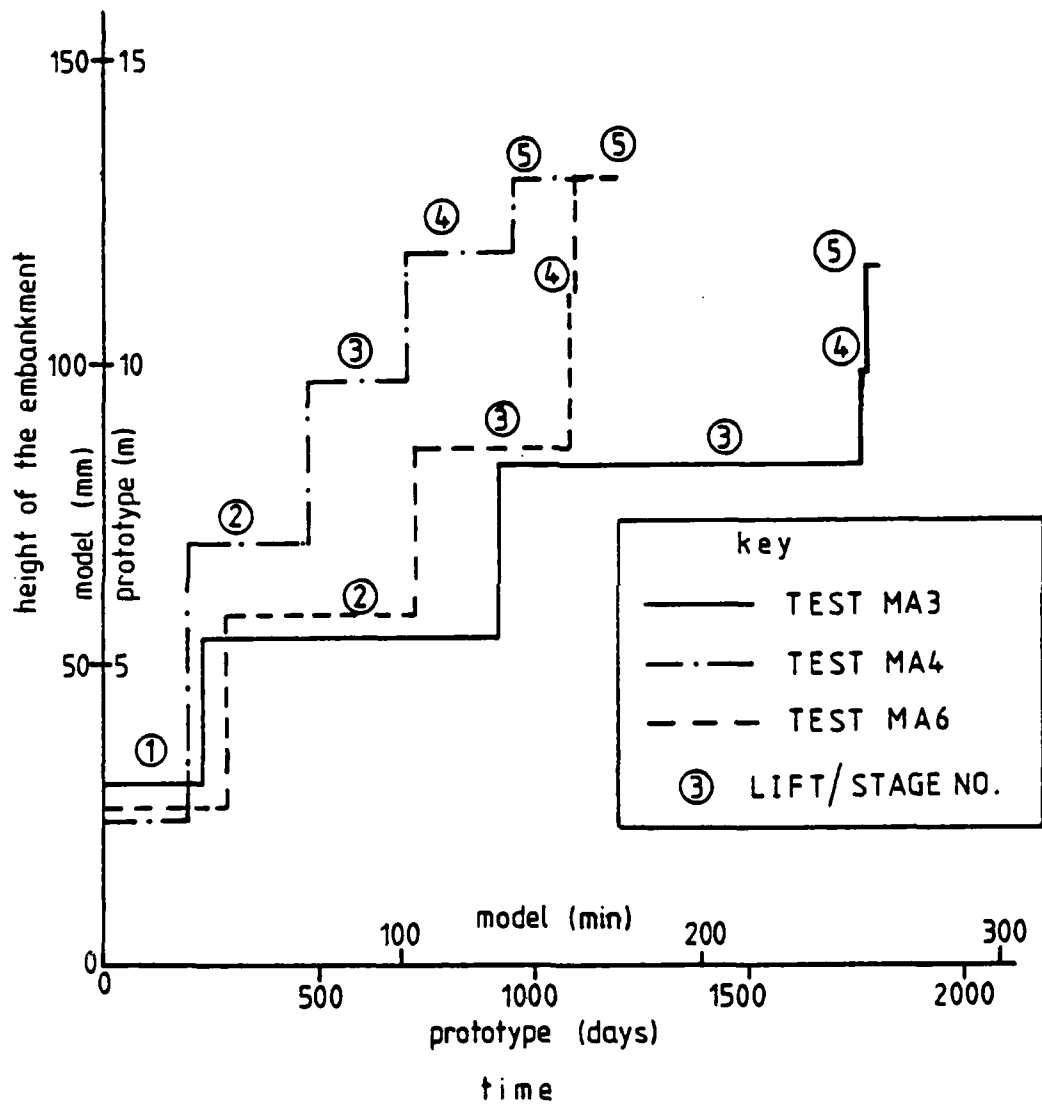
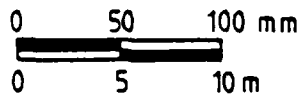
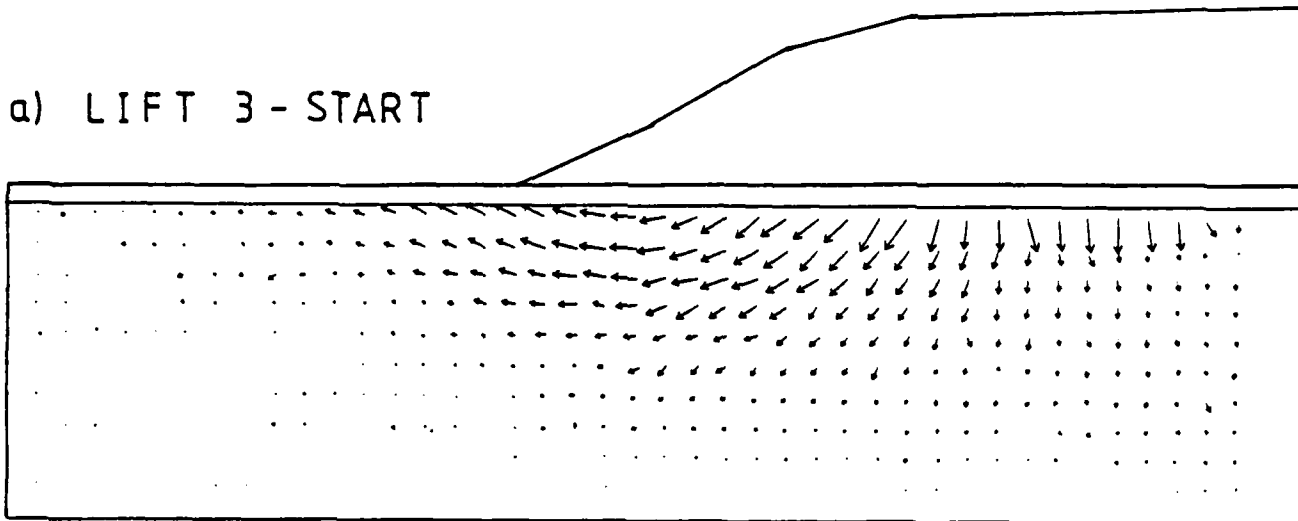


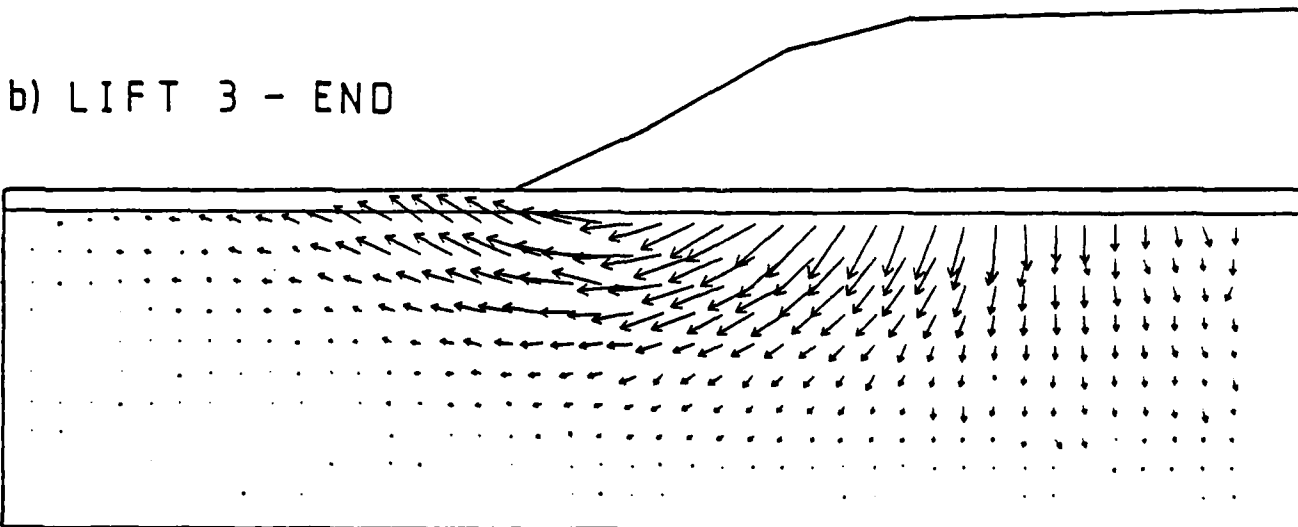
Fig. 3.5 - Construction history for stage constructed embankments



a) LIFT 3 - START



b) LIFT 3 - END



DISPLACEMENTS

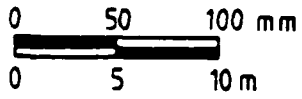
MAGNIFICATION FACTOR = 2.0

TEST MA3

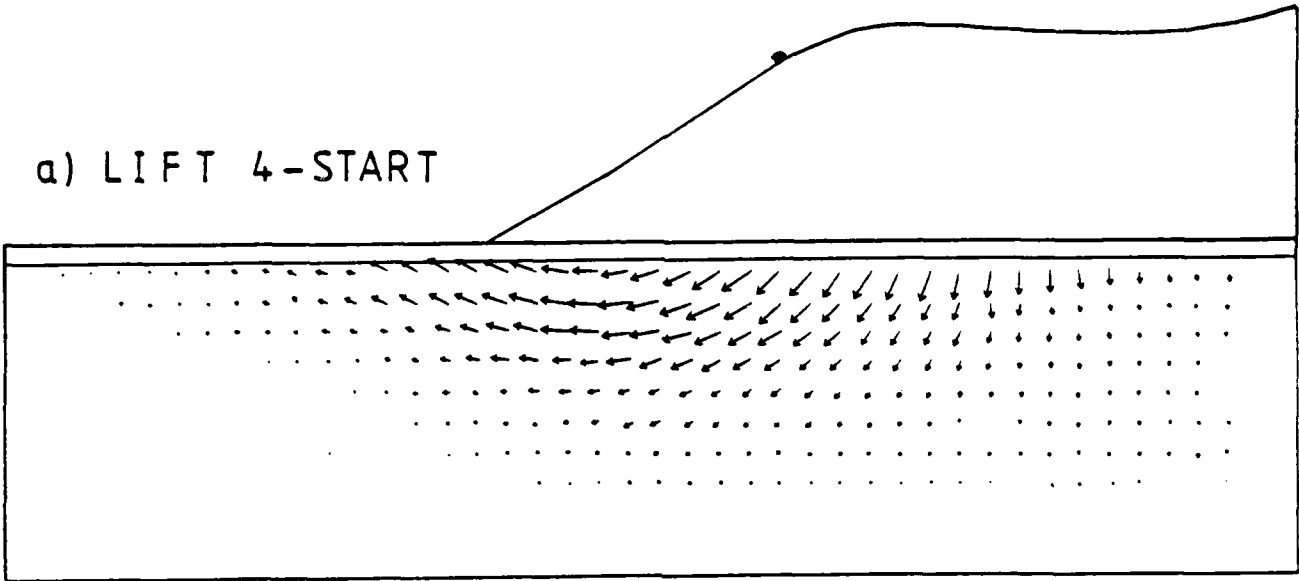
DISP. OF 10 MMS =



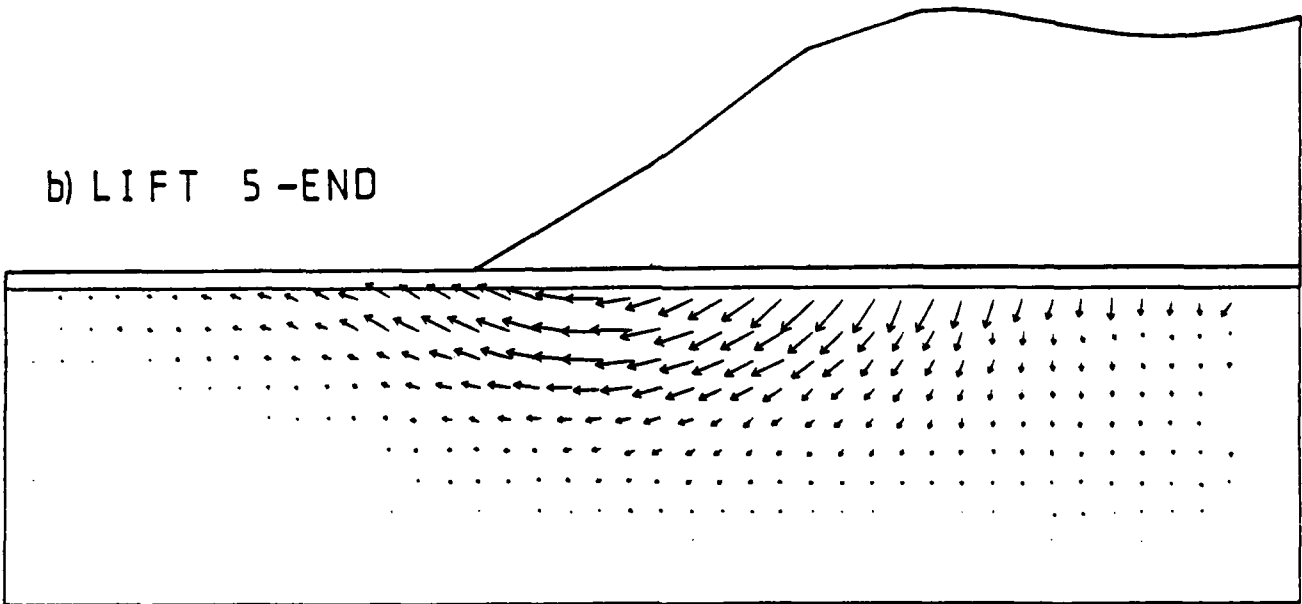
Fig. 3.6 - Displacement vectors - test MA3



a) LIFT 4-START



b) LIFT 5-END



DISPLACEMENTS

MAGNIFICATION FACTOR = 1.0

TEST MA3

DISP. OF 10 MMS =



Fig. 3.7 - Displacement vectors - test MA3

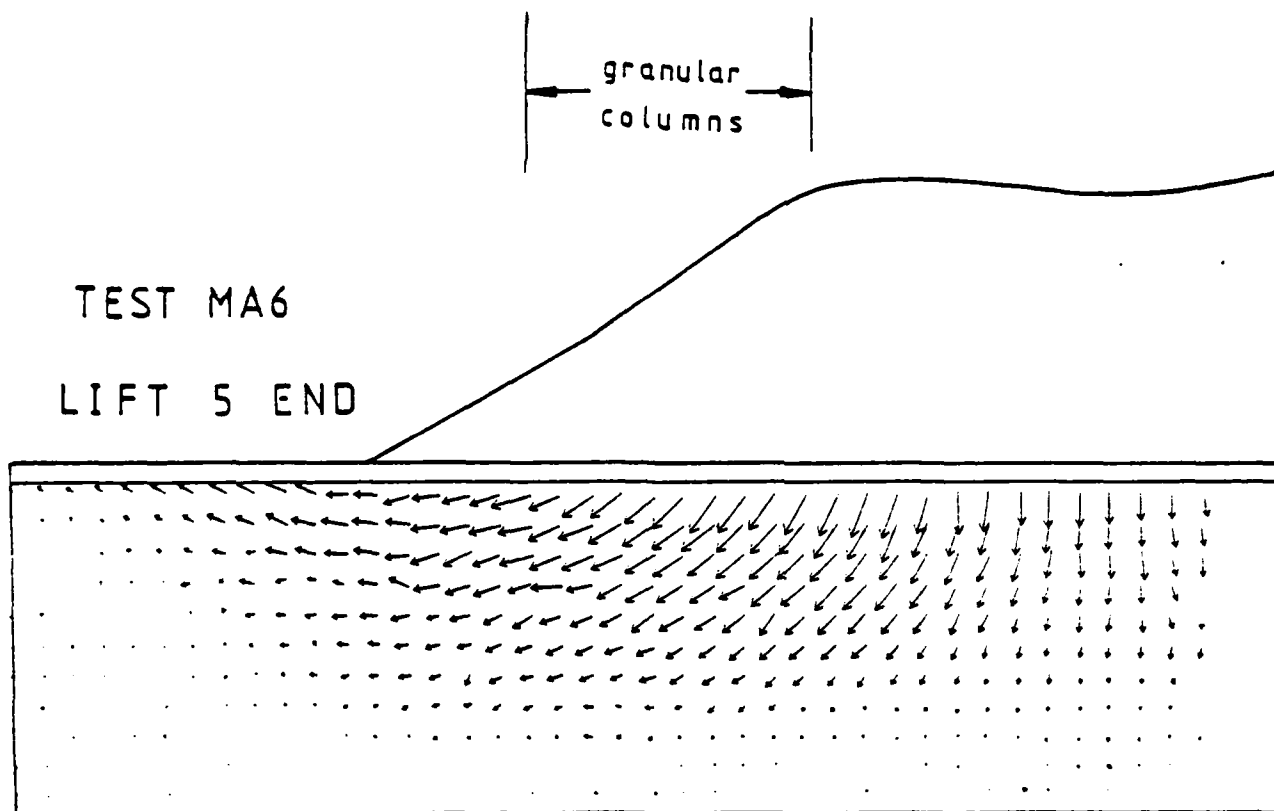
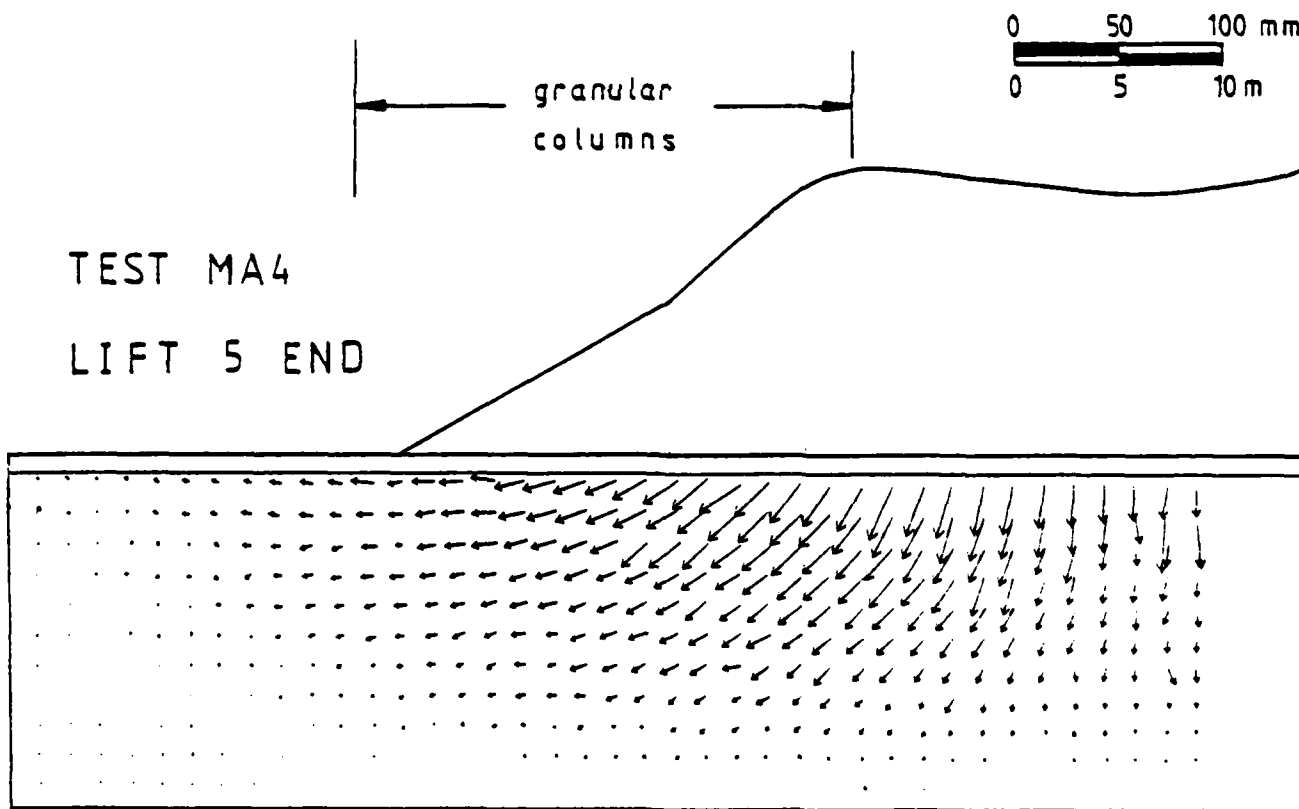


Fig. 3.8 - Displacement vectors - test MA6



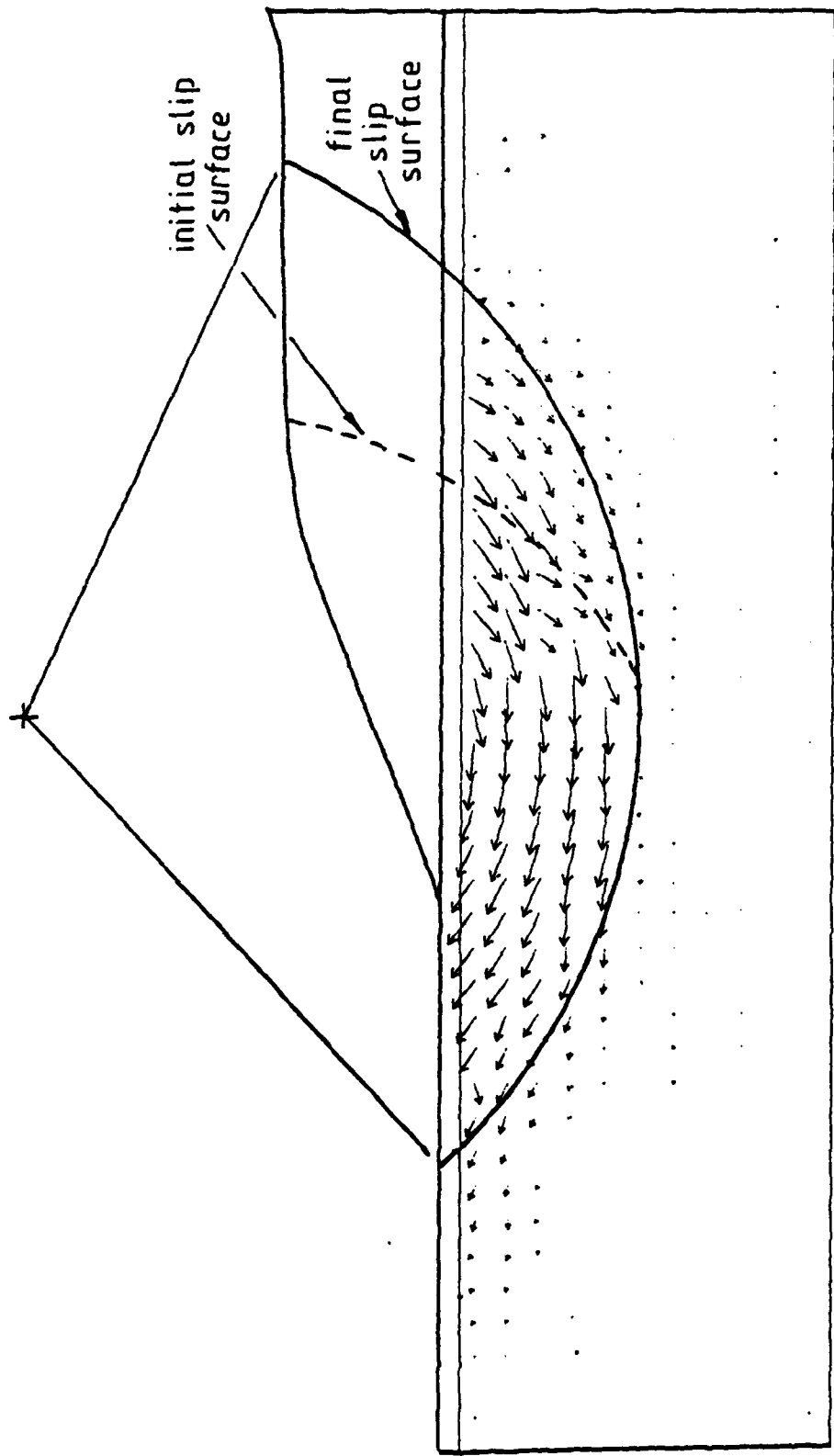
DISPLACEMENTS

MAGNIFICATION FACTOR = 2.0

DISP. OF 10 MMS =



Fig. 3.9 - Displacement vectors - test MA4



DISPLACEMENTS

MAGNIFICATION FACTOR = 2.0

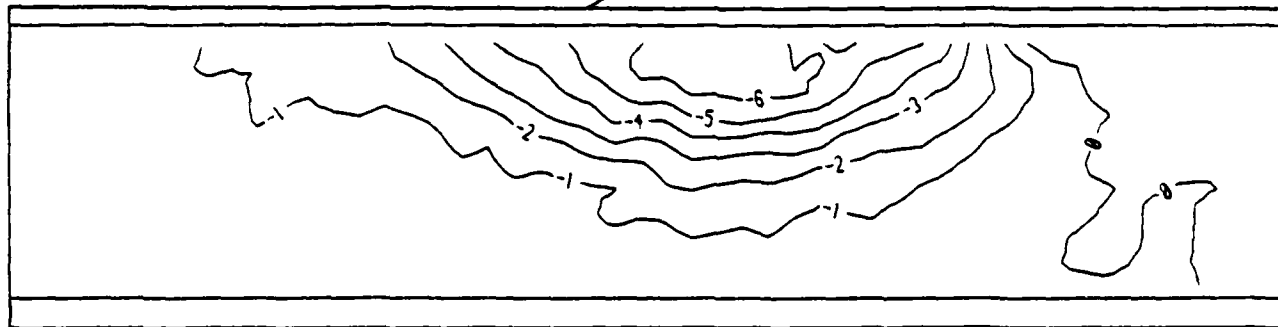
TEST MA5 LIFT 4

DISP. OF 10 MMS =

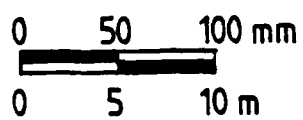
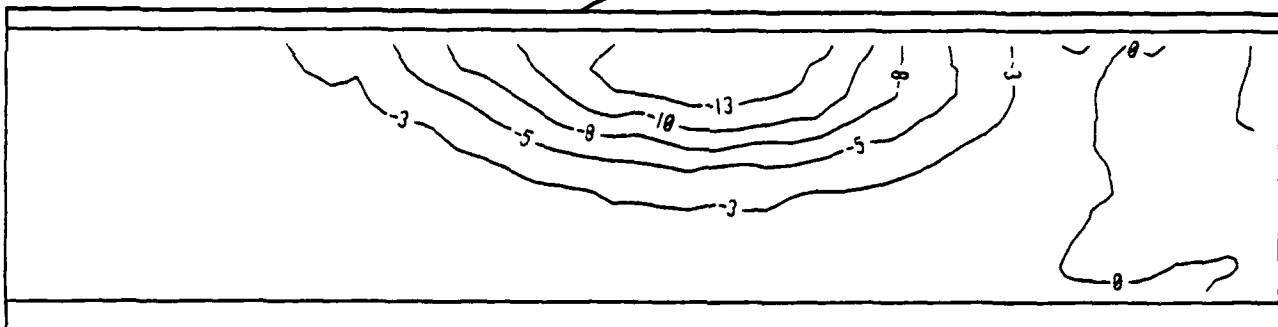


Fig. 3.10 - Displacement vectors at the start of failure - test MA5

a) LIFT 3 - START



b) LIFT 3 - END



c) LIFT 5 - END

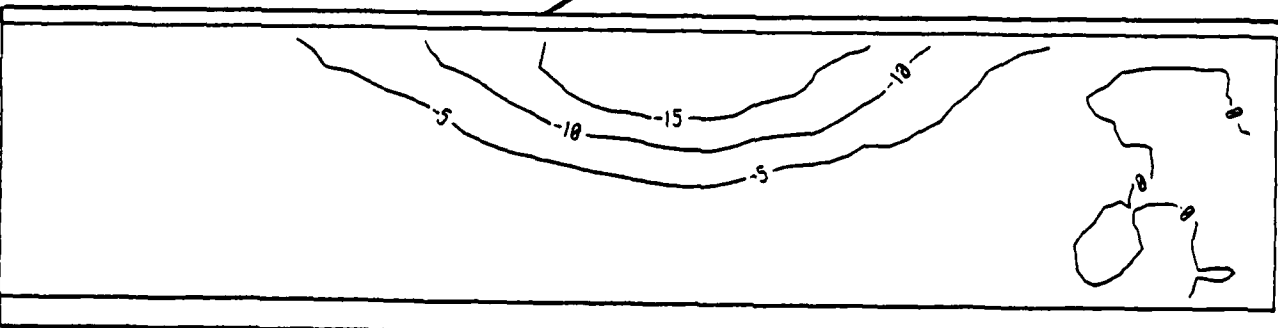


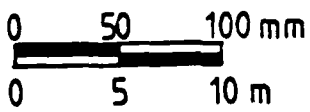
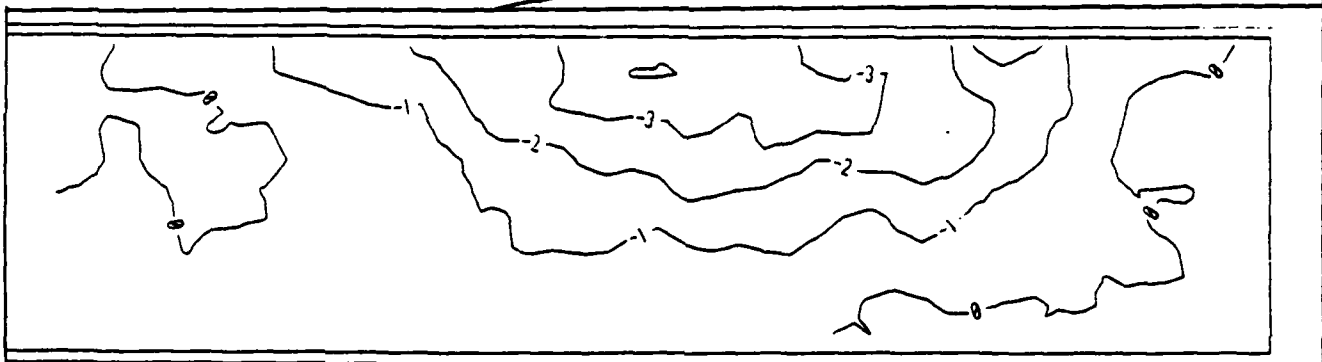
Fig. 3.11 - HORIZONTAL DISPLACEMENTS - TEST MA3

a) LIFT 3 START



granular columns

b) LIFT 3 END



c) LIFT 5 END

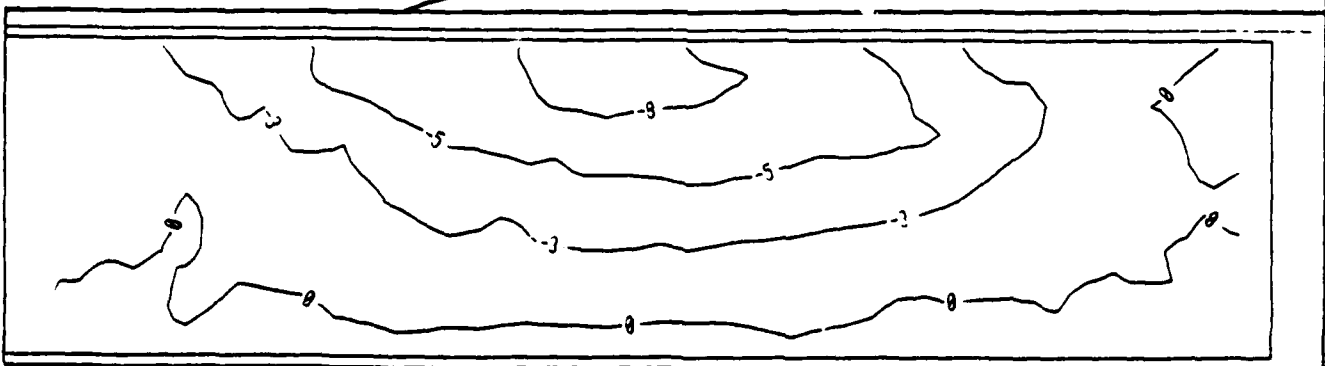
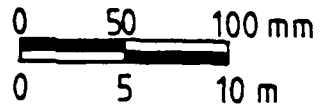
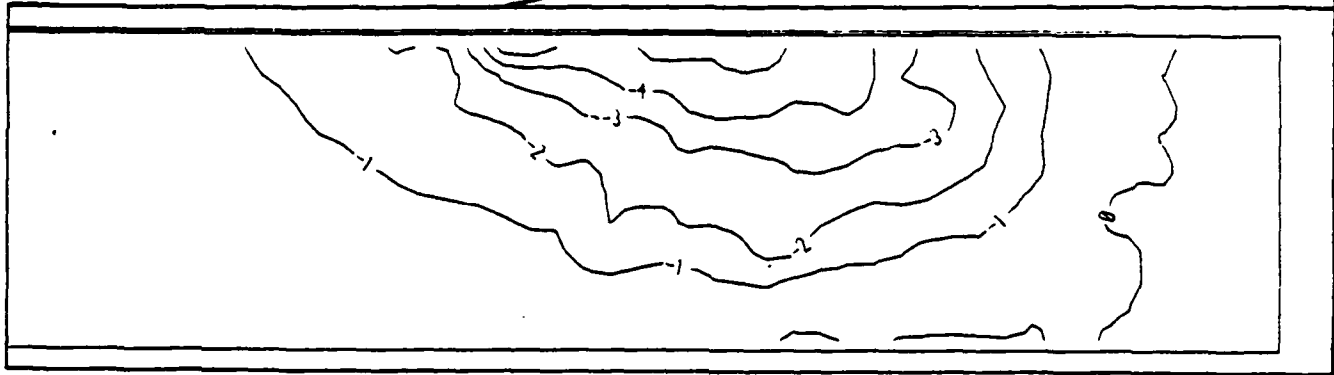


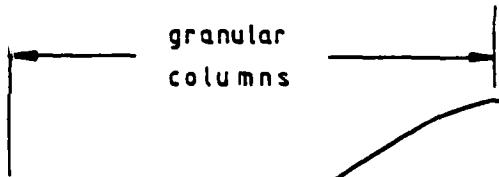
Fig. 3.12 - HORIZONTAL DISPLACEMENTS TEST MA6



a) LIFT 2 - END



granular  
columns



b) LIFT 5 - END

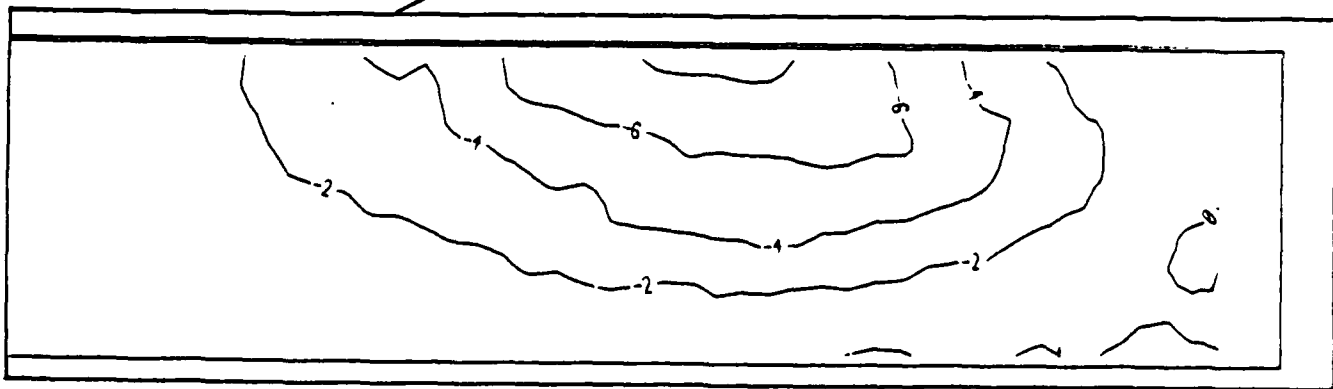
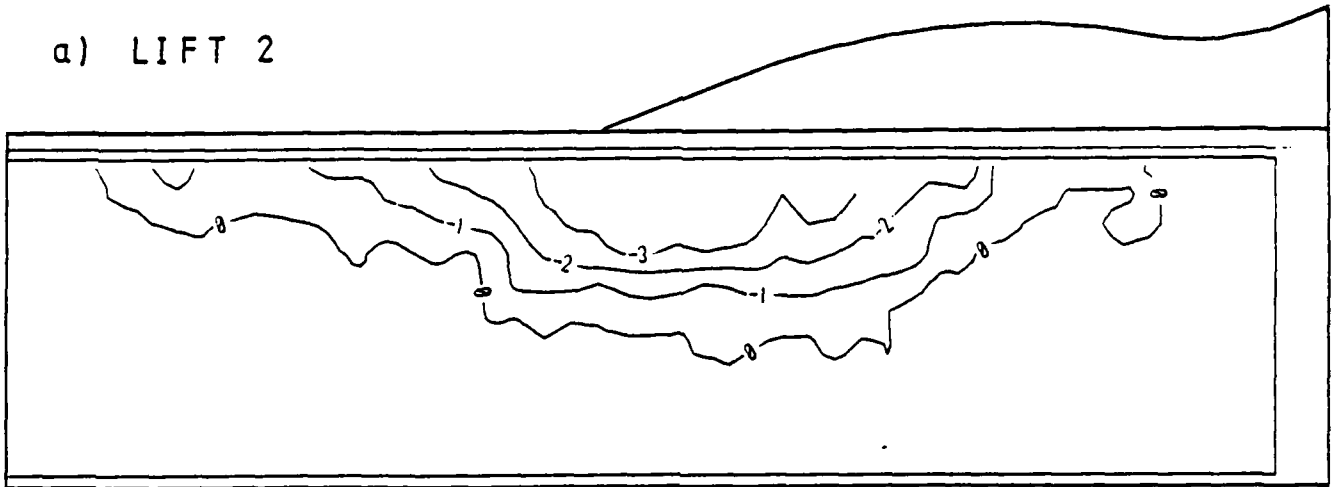


Fig. 3.13 - HORIZONTAL DISPLACEMENTS - TEST MA4

a) LIFT 2



b) LIFT 4

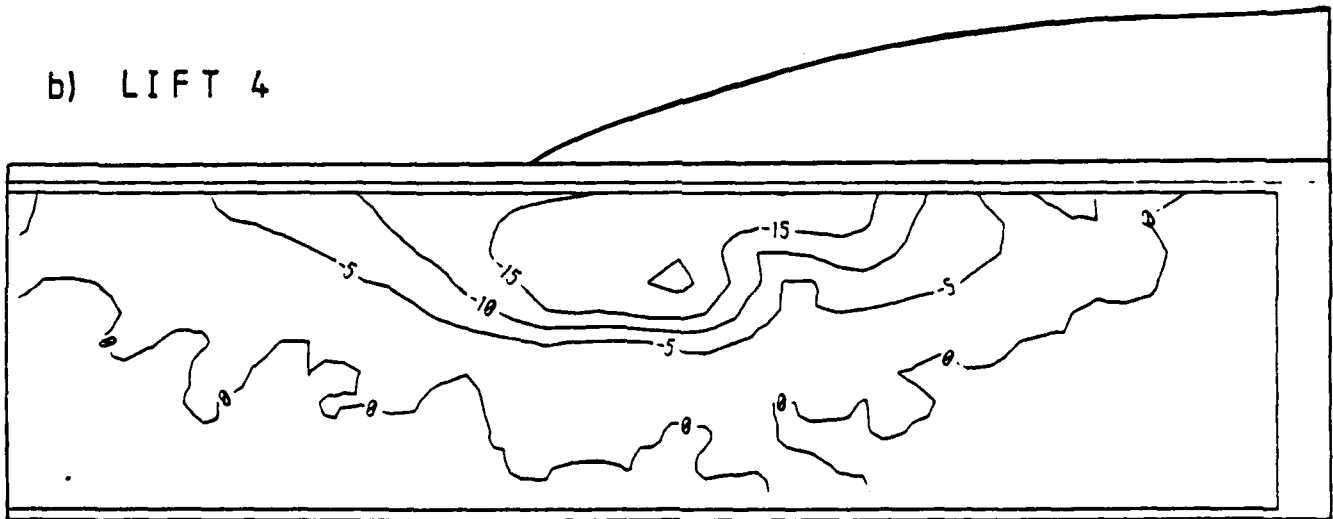


Fig. 3.14 - HORIZONTAL DISPLACEMENTS - TEST MAS

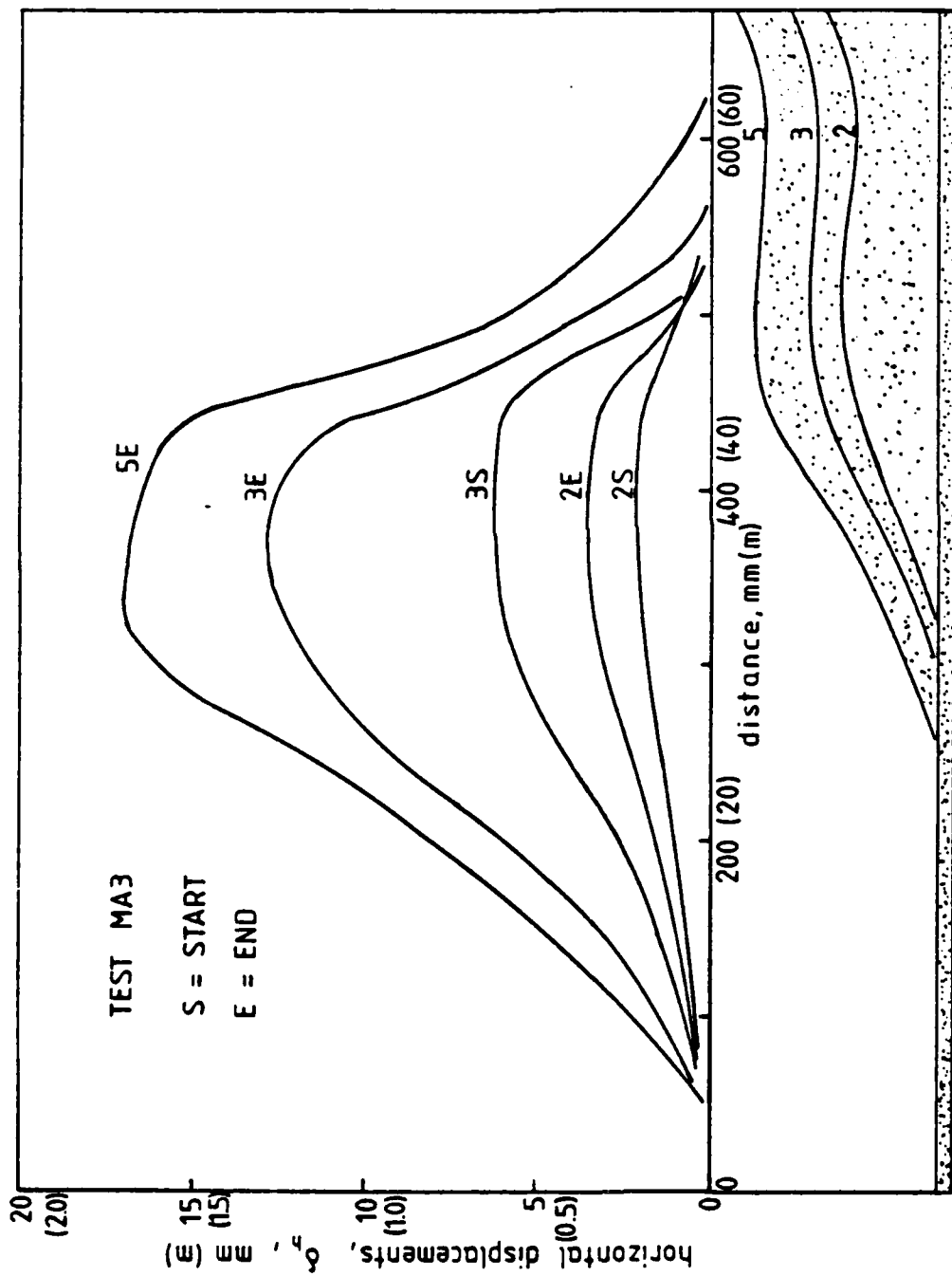


Fig. 3.15 - Horizontal displacements 5 mm (0.5 m) below clay surface - test MA3

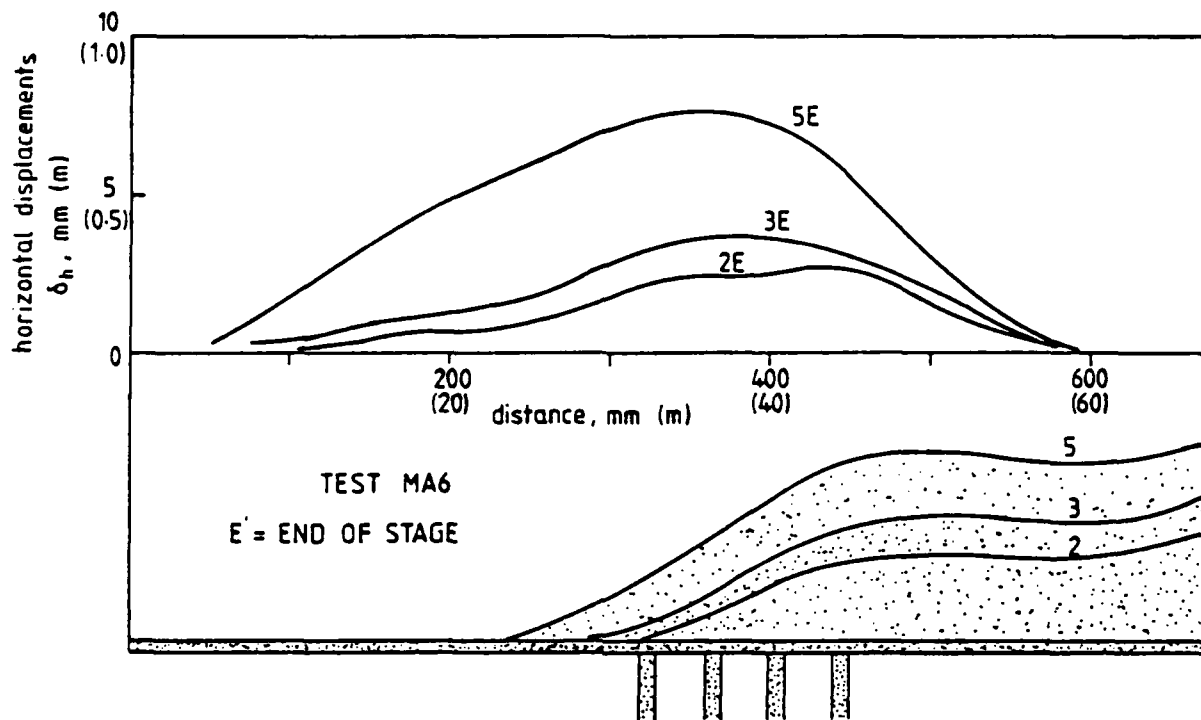


Fig. 3.16 - Horizontal displacements 5 mm (0.5 m) below clay surface - test MA6

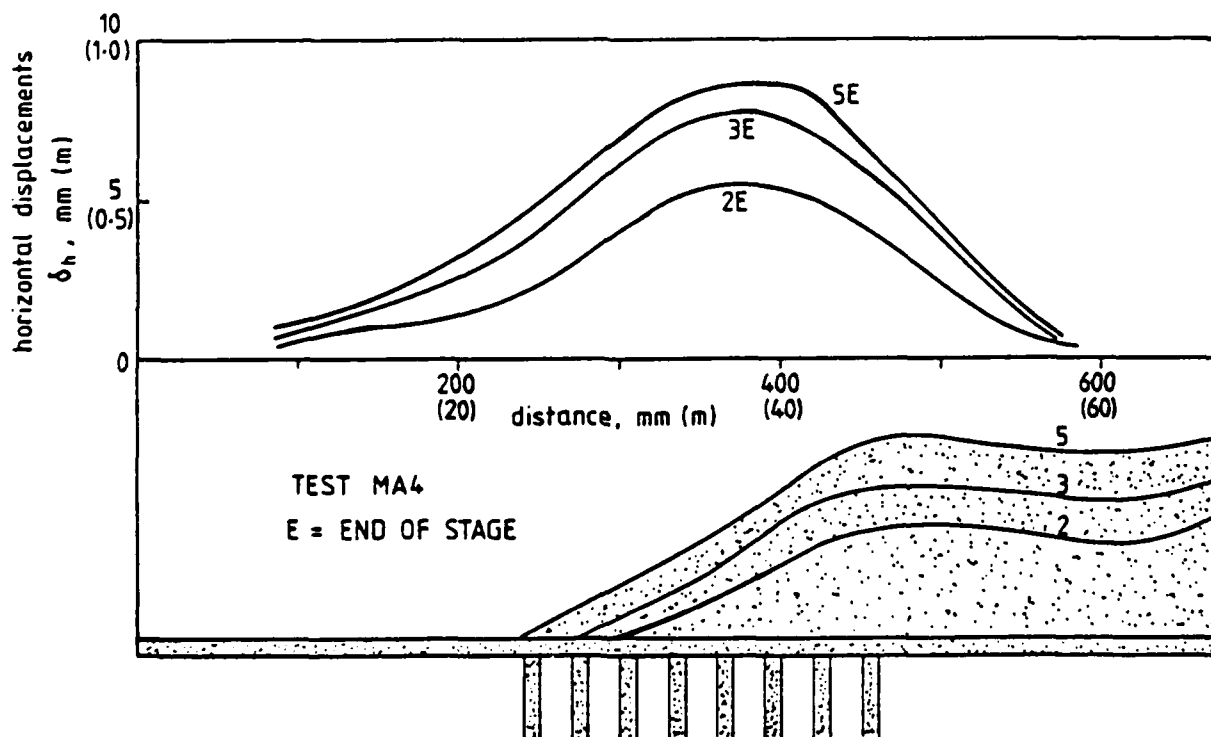


Fig. 3.17 - Horizontal displacements 5 mm (0.5 mm) below clay surface - test MA4

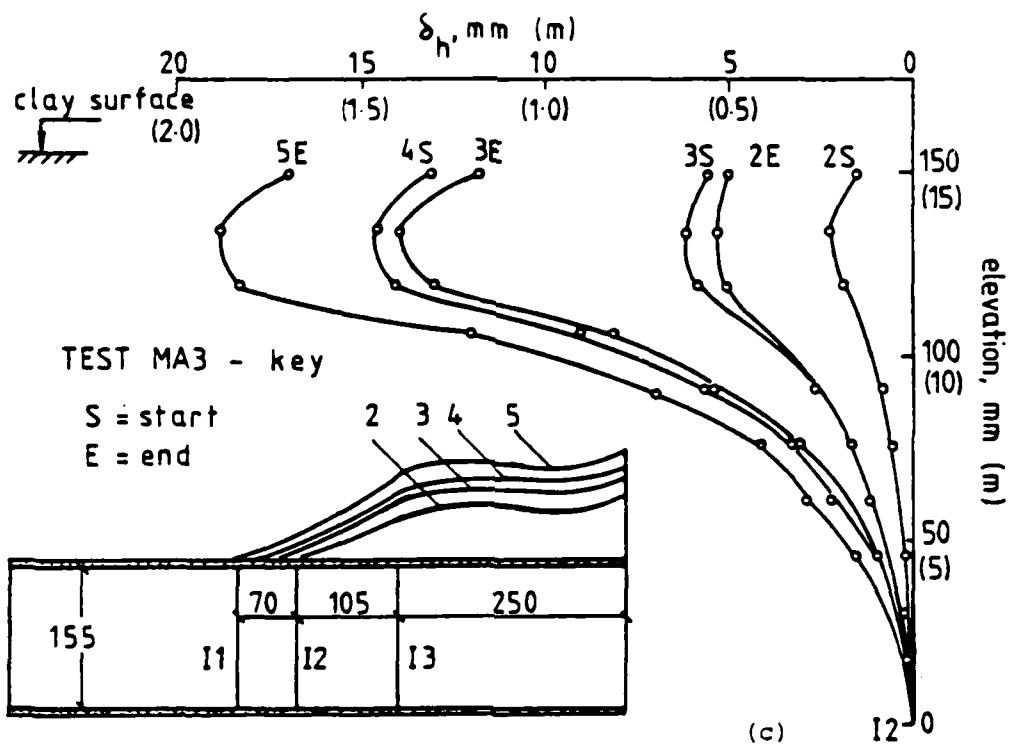
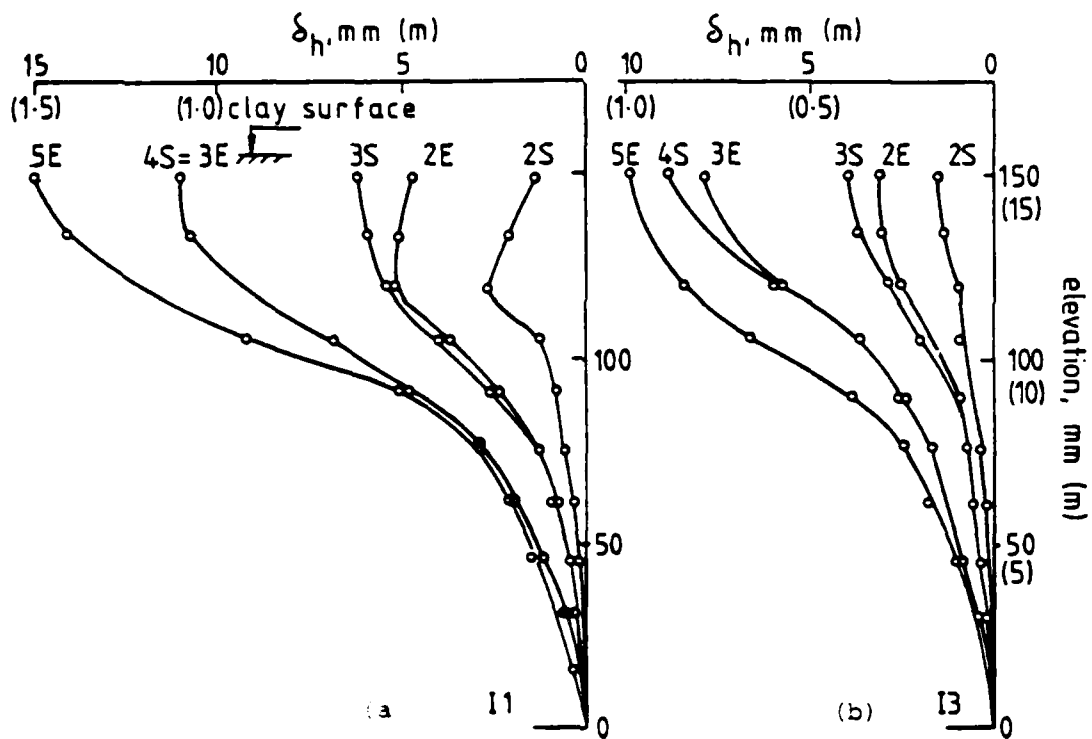


Fig. 3.13 - Equivalent inclinometer plots - test MA3

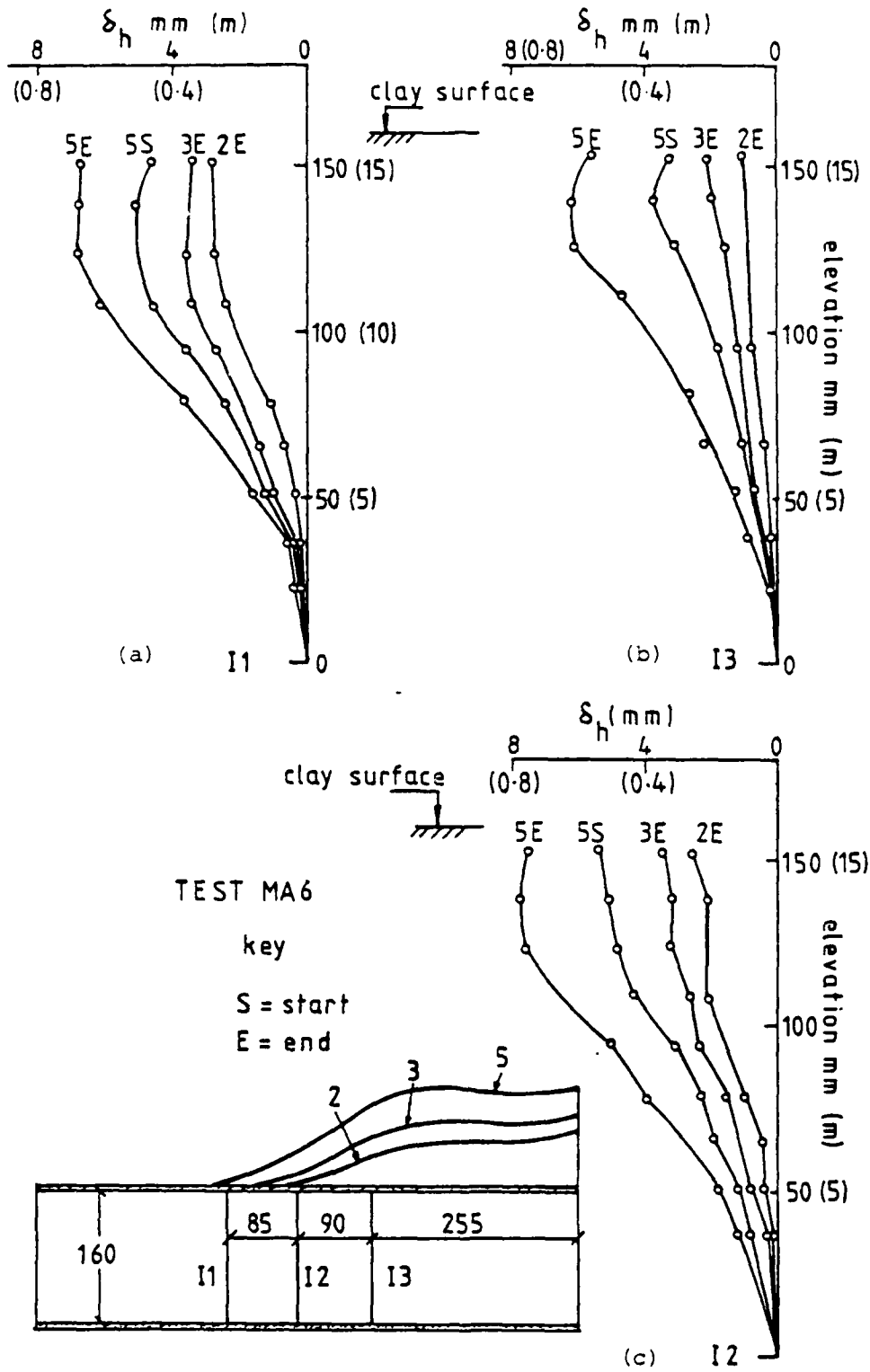
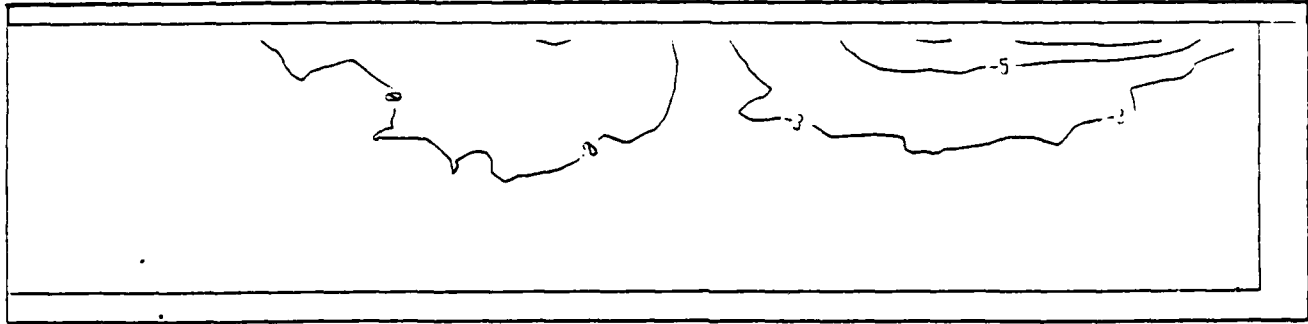
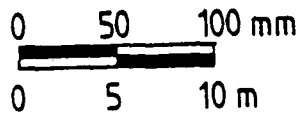
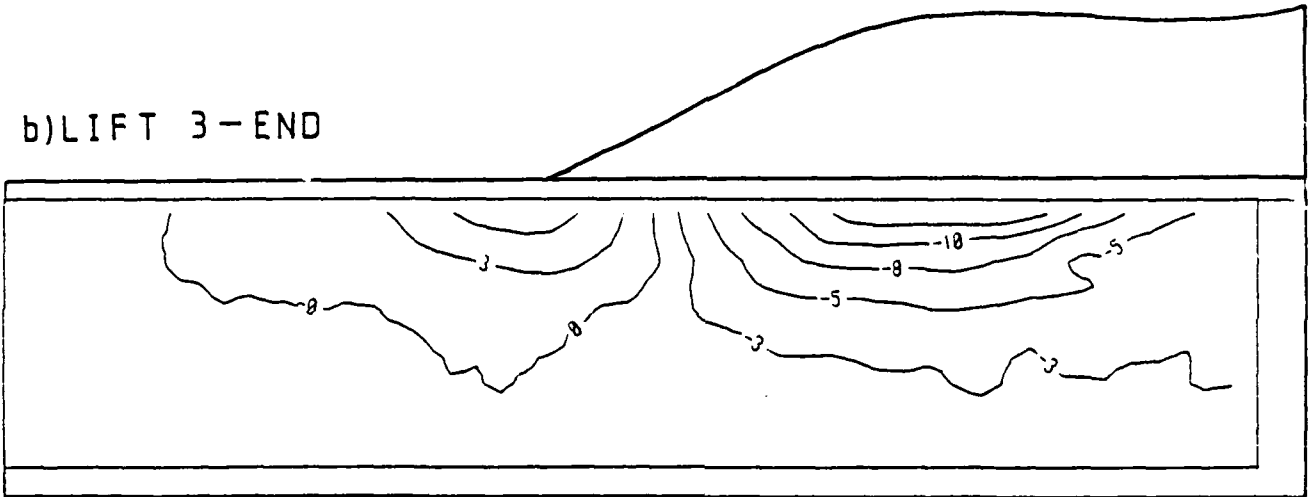


Fig. 3.19 - Equivalent inclinometer plots - test MA6

a) LIFT 3 - START



b) LIFT 3 - END



c) LIFT 5 - END

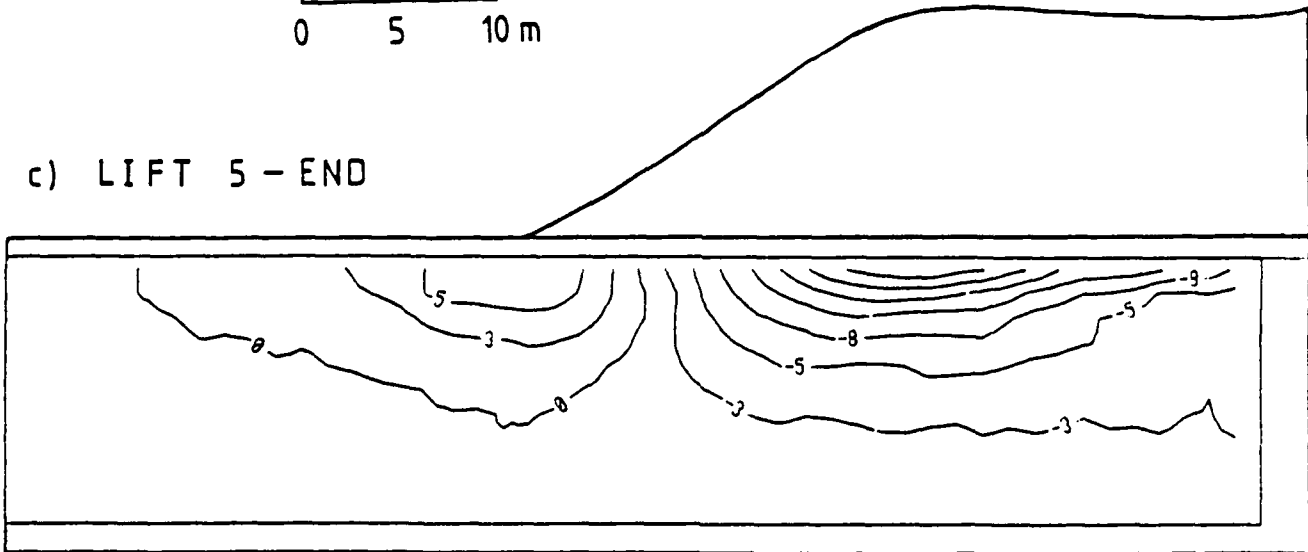
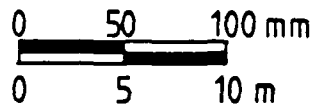
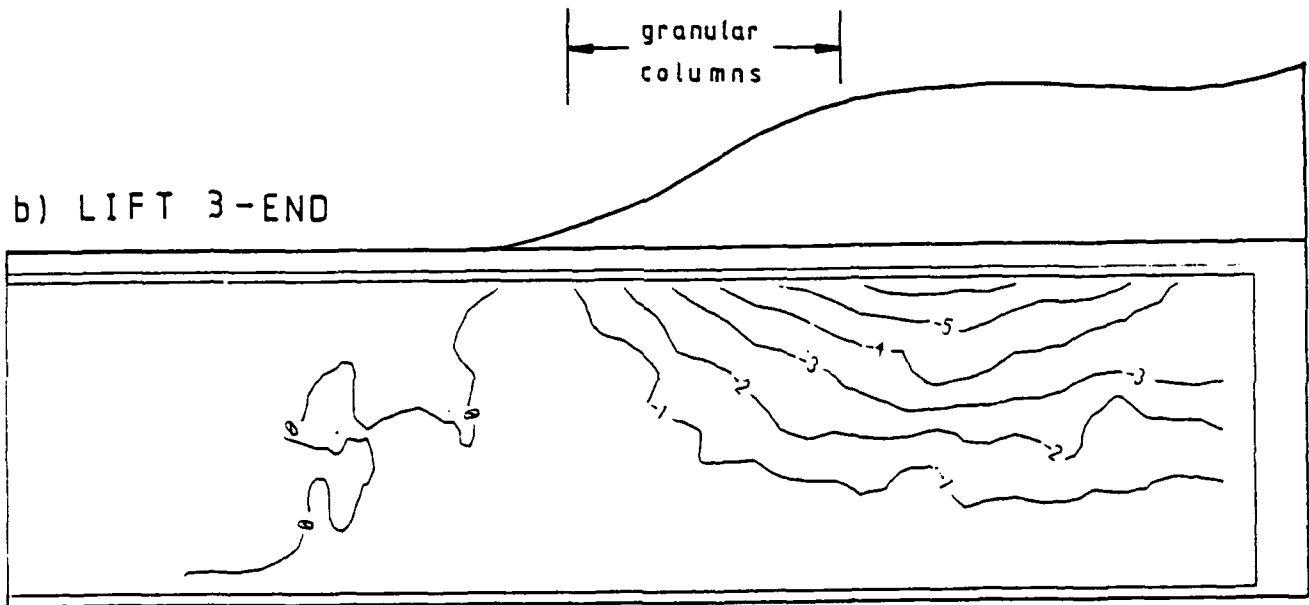


Fig. 3.20 - VERTICAL DISPLACEMENTS - TEST MA3

a) LIFT 3-START



b) LIFT 3-END



c) LIFT 5-END

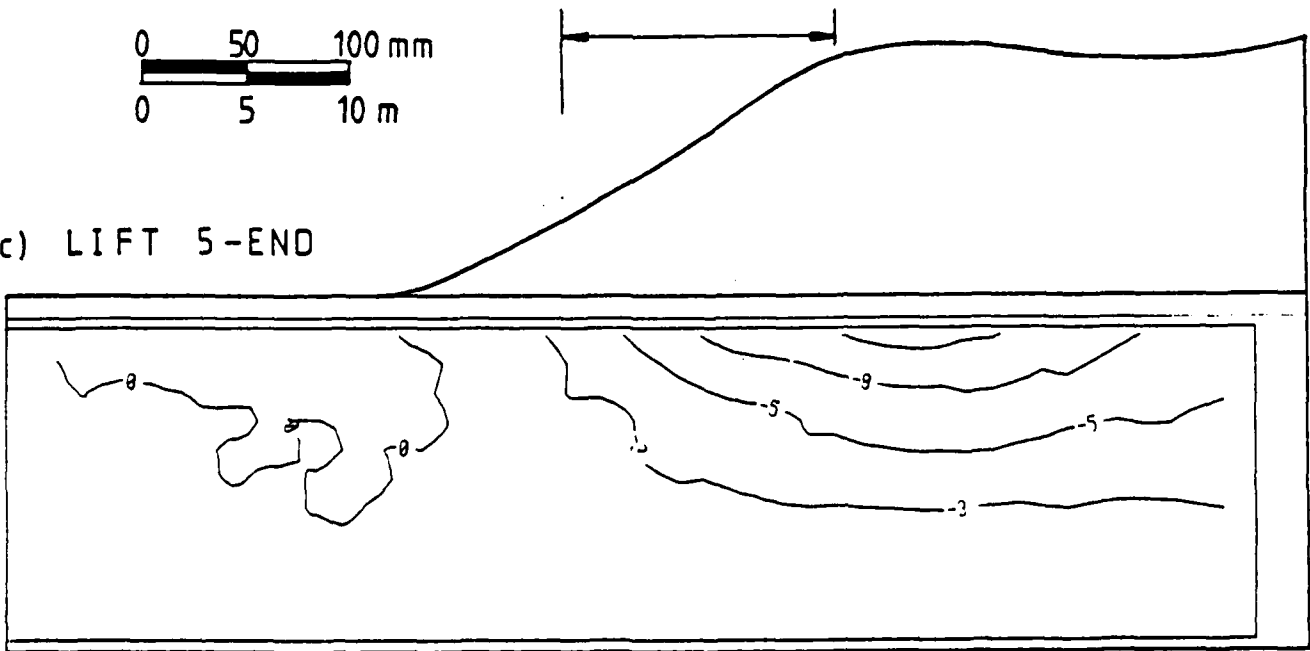
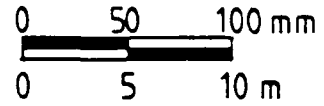
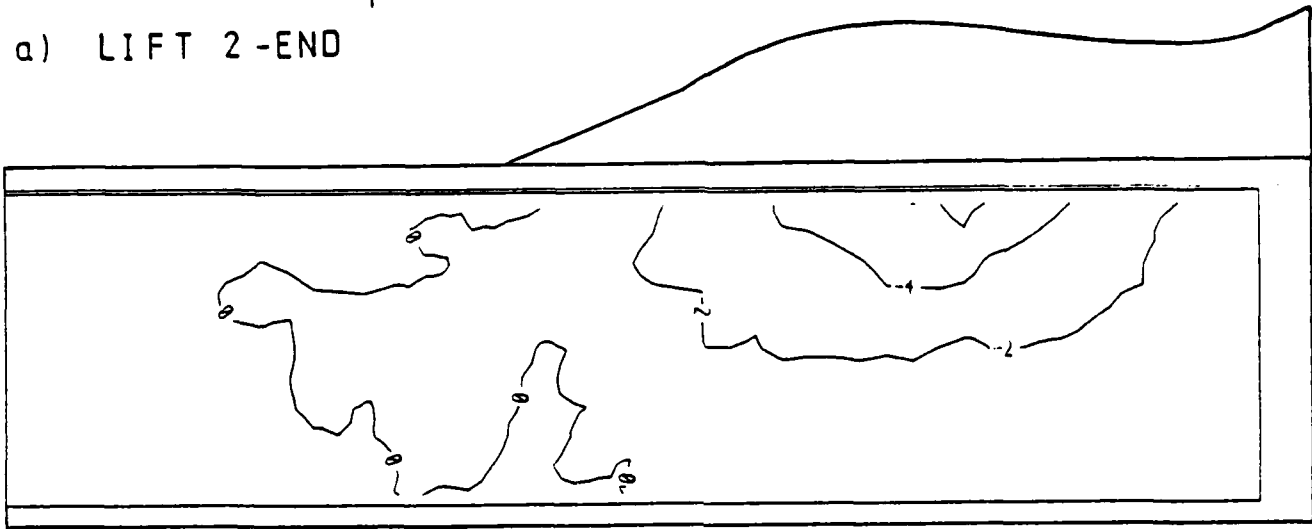


Fig. 3.21 - VERTICAL DISPLACEMENTS-TEST MA6



a) LIFT 2-*END*



b) LIFT 5-*END*

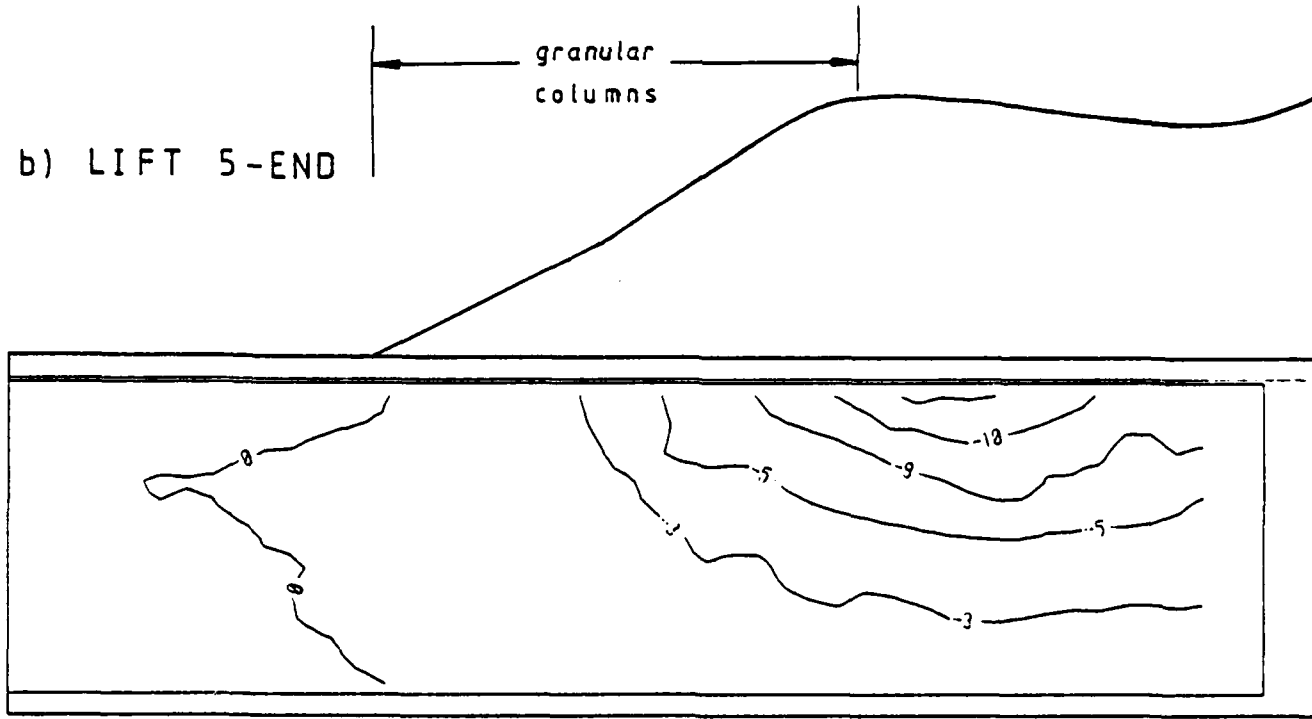
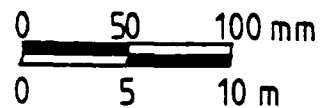
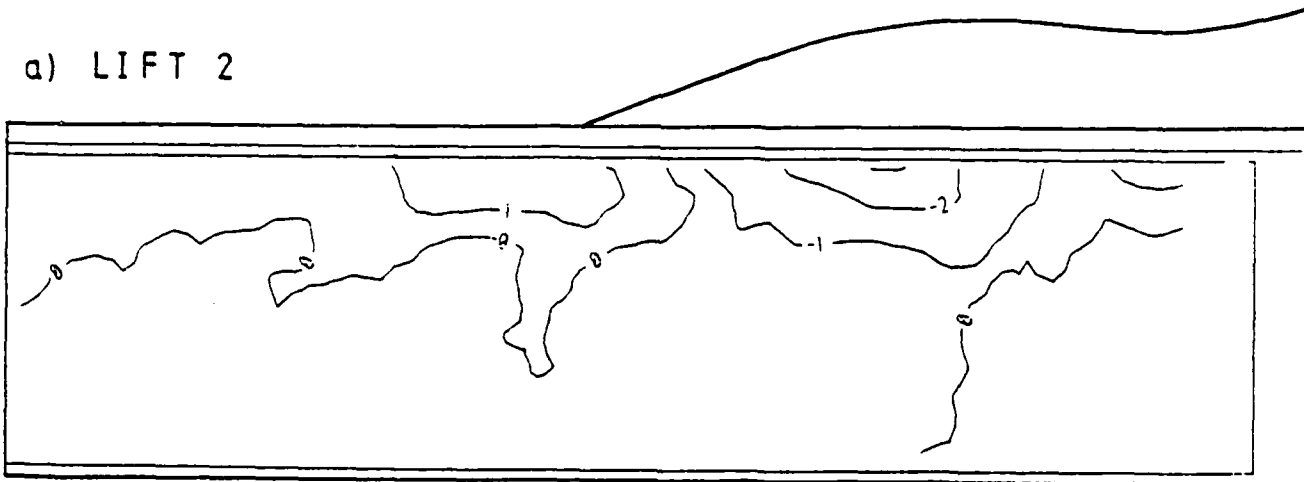


Fig. 3.22 - VERTICAL DISPLACEMENTS -TEST MA4

a) LIFT 2



b) LIFT 4

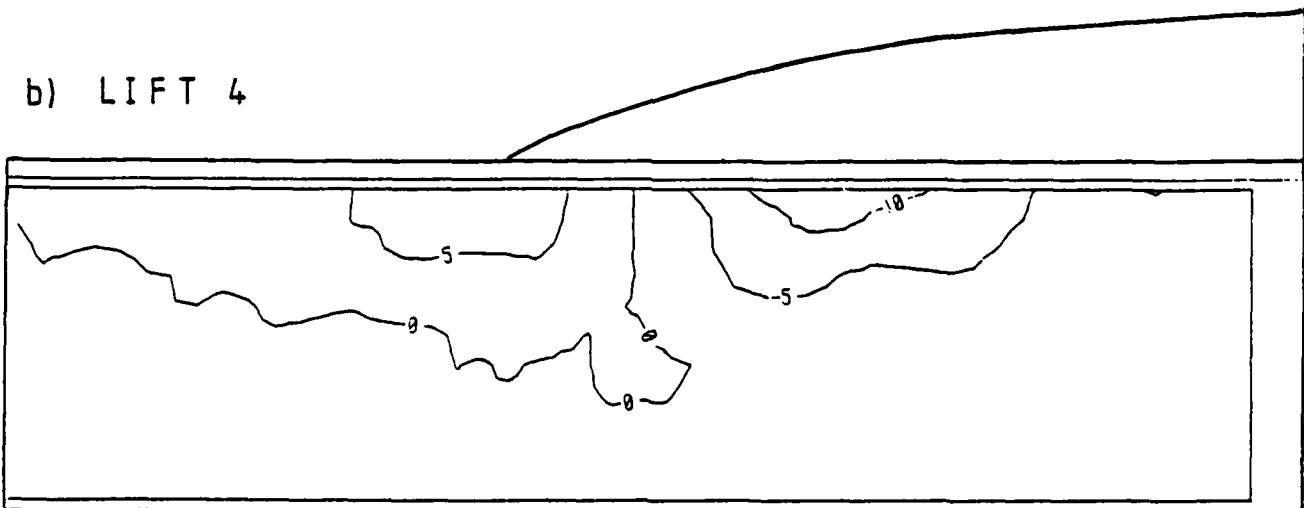


Fig. 3.23 - VERTICAL DISPLACEMENTS - TEST MA5

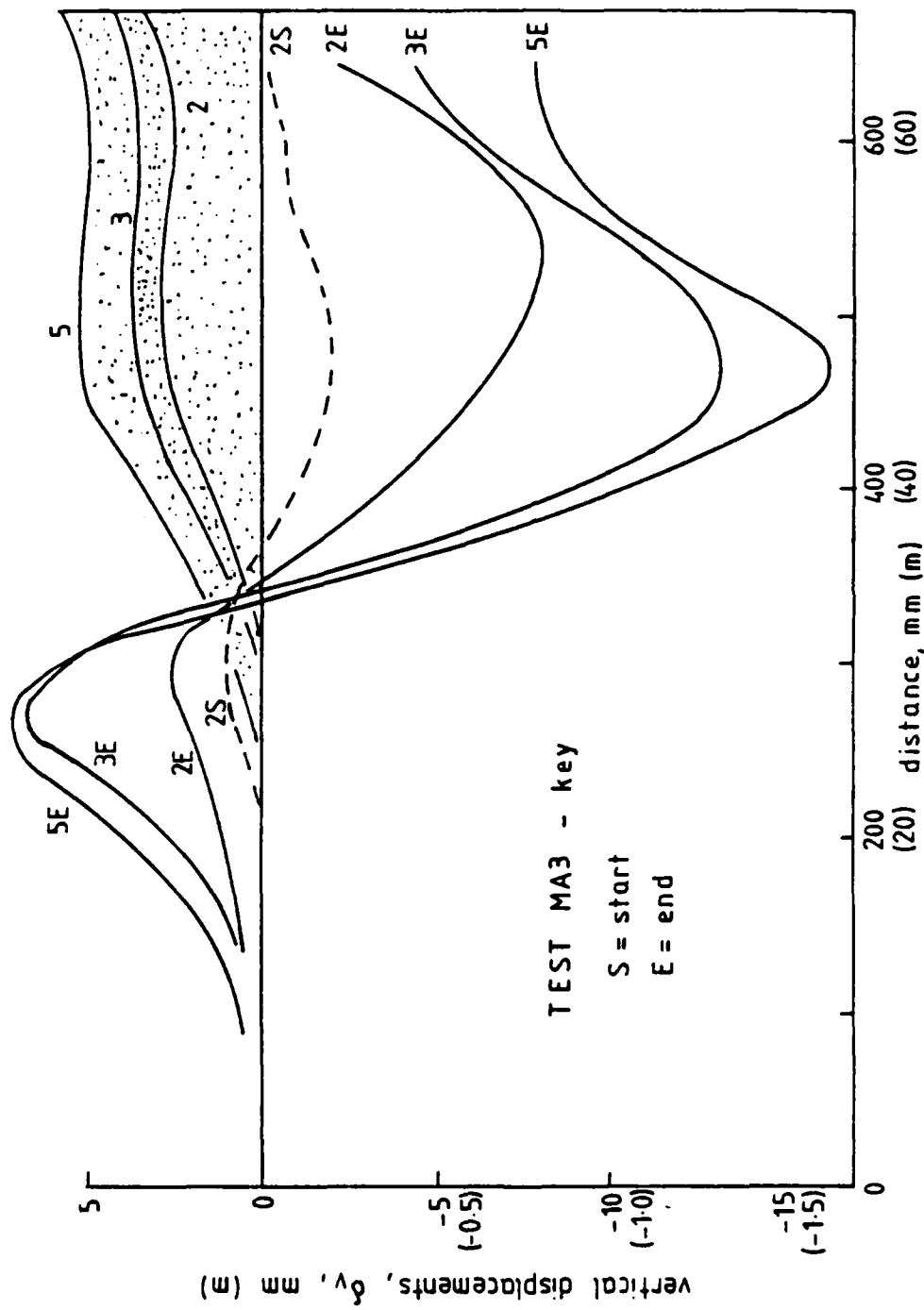


Fig. 3.24 - Vertical displacements 5 mm (0.5 m) below clay surface - test MA3

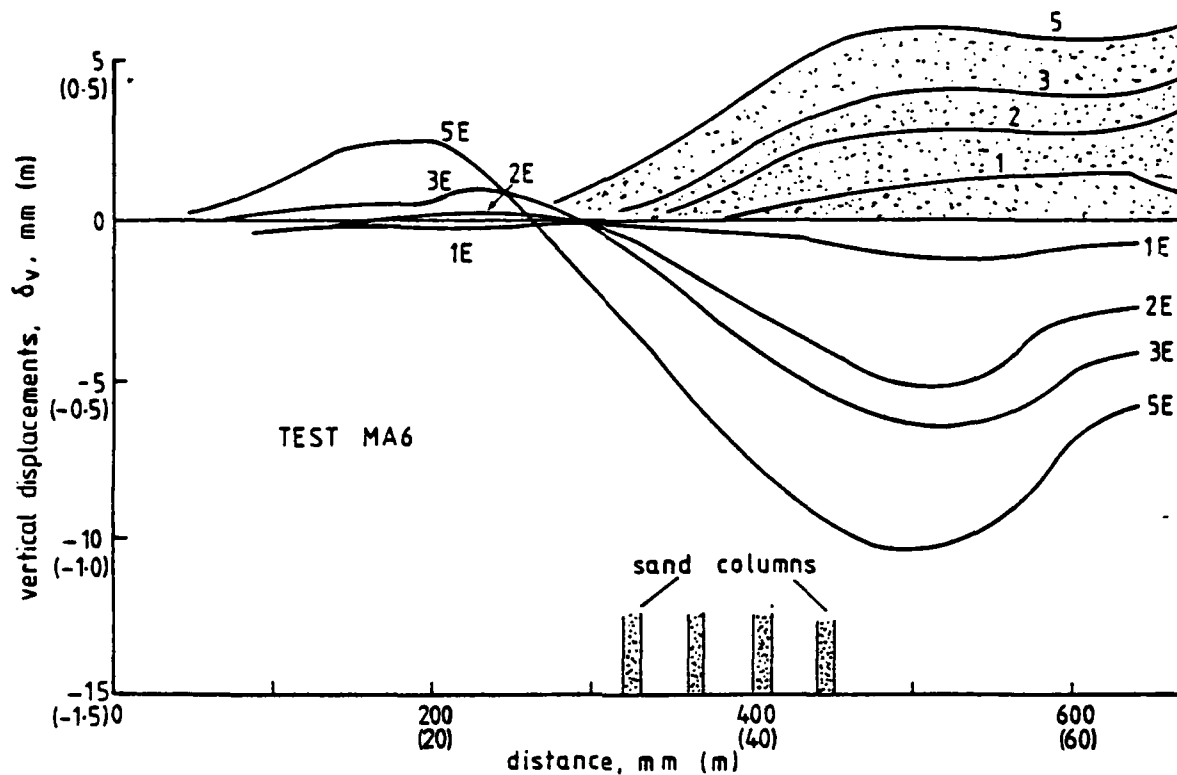


Fig. 3.25 - Vertical displacements 5 mm (0.5 m) below clay surface - test MA6

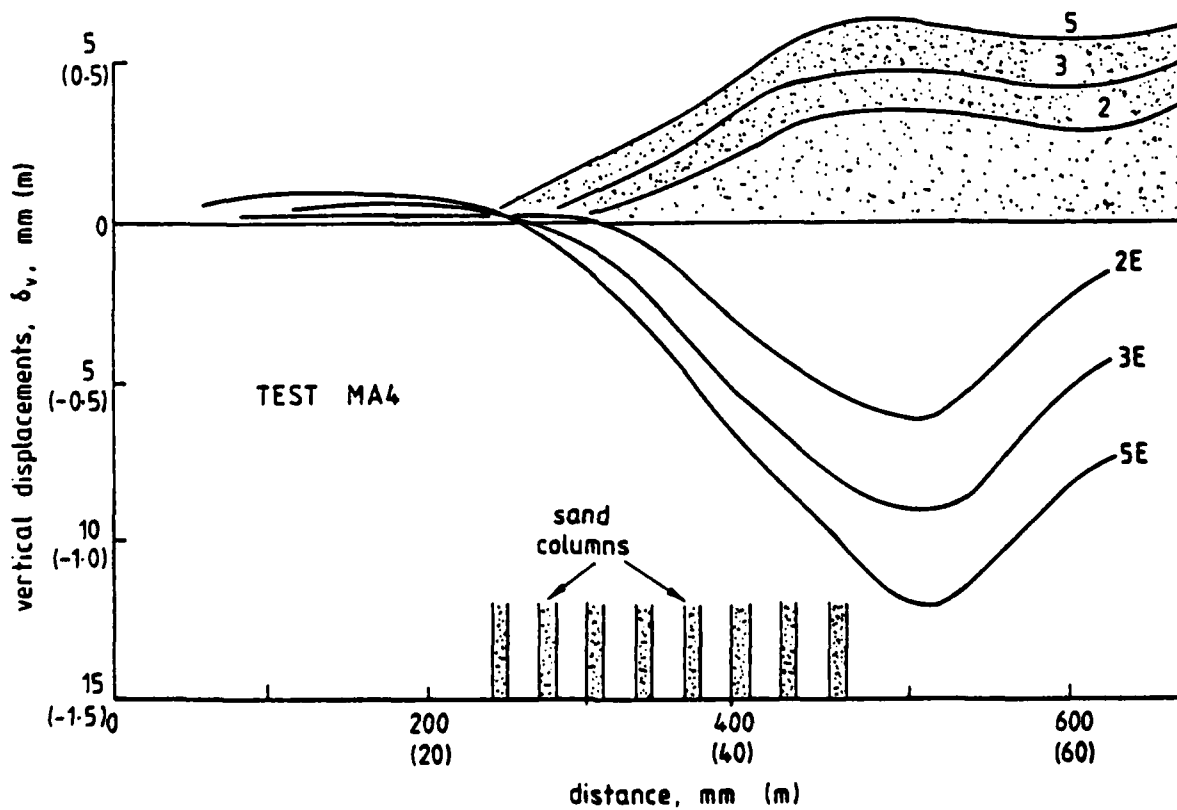


Fig. 3.26 - Vertical displacements 5 mm (0.5 m) below clay surface - test MA4

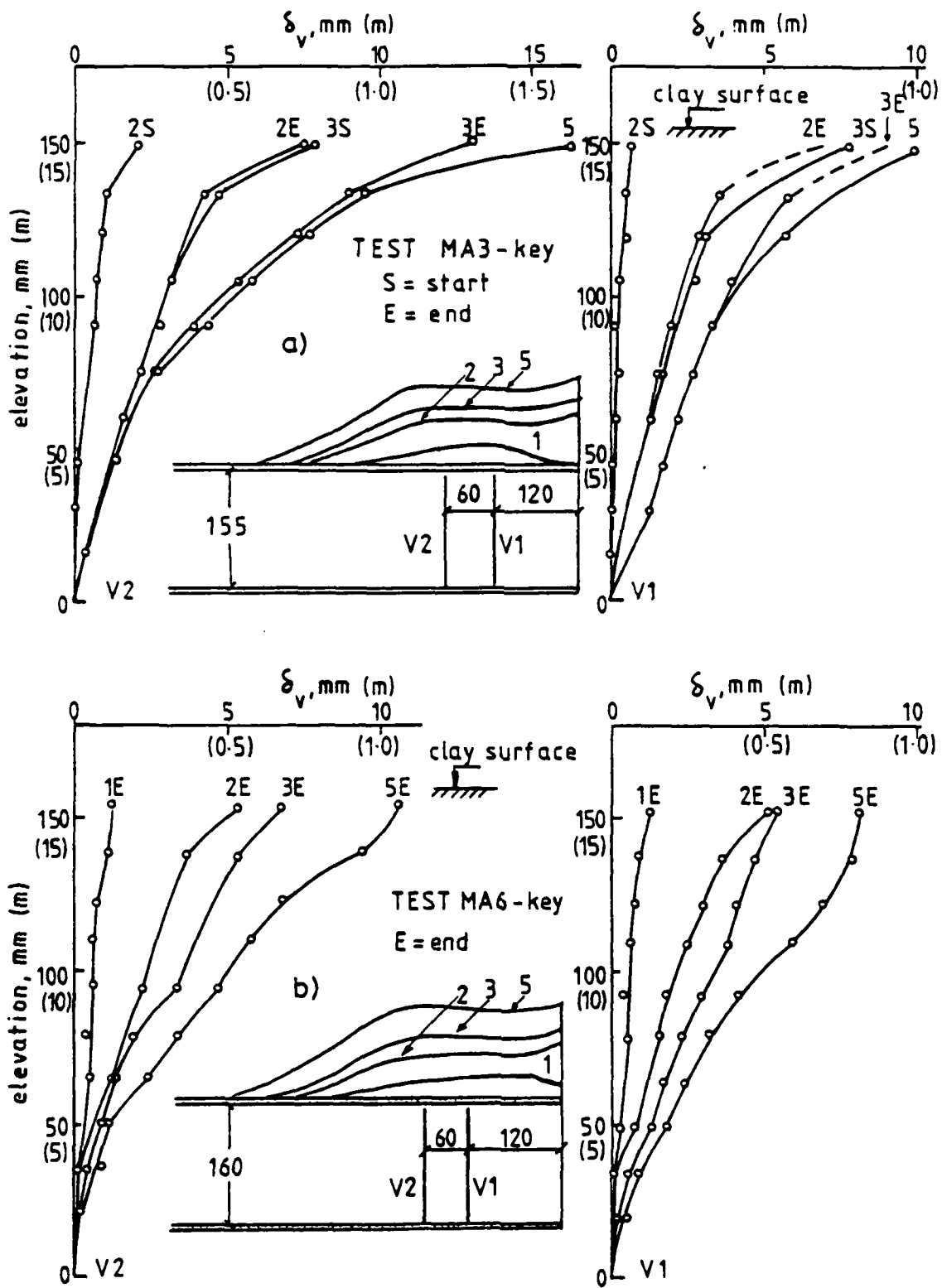
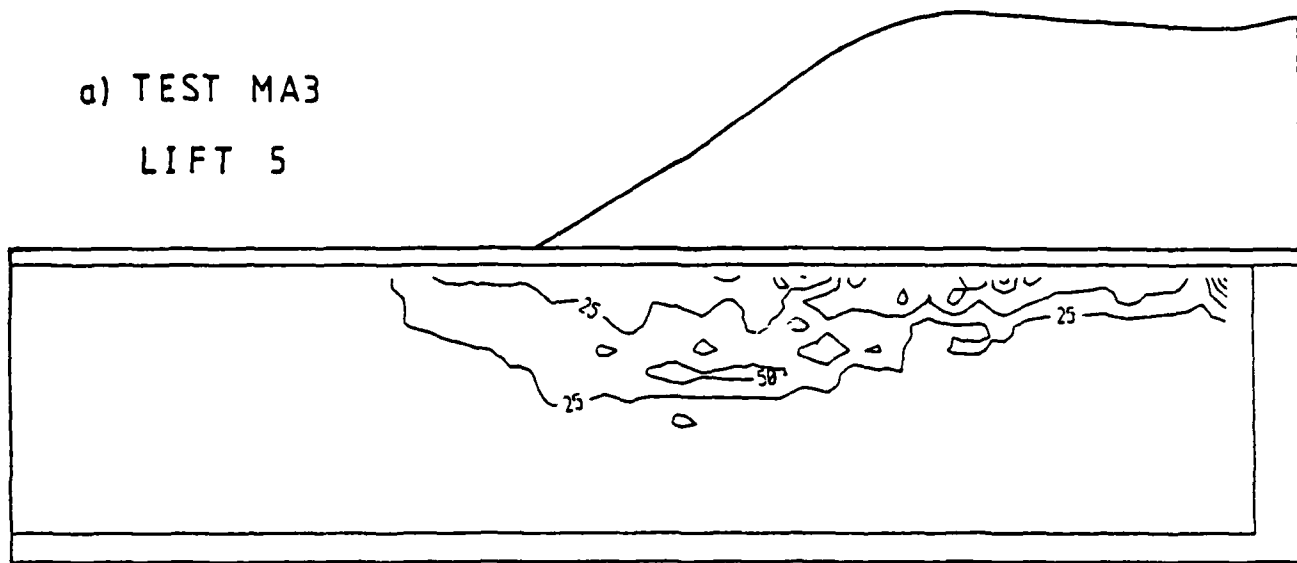


Fig. 3.27 - Variation of settlements with depth, tests MA3 and MA6

d) TEST MA3  
LIFT 5



b) TEST MA5  
LIFT 4

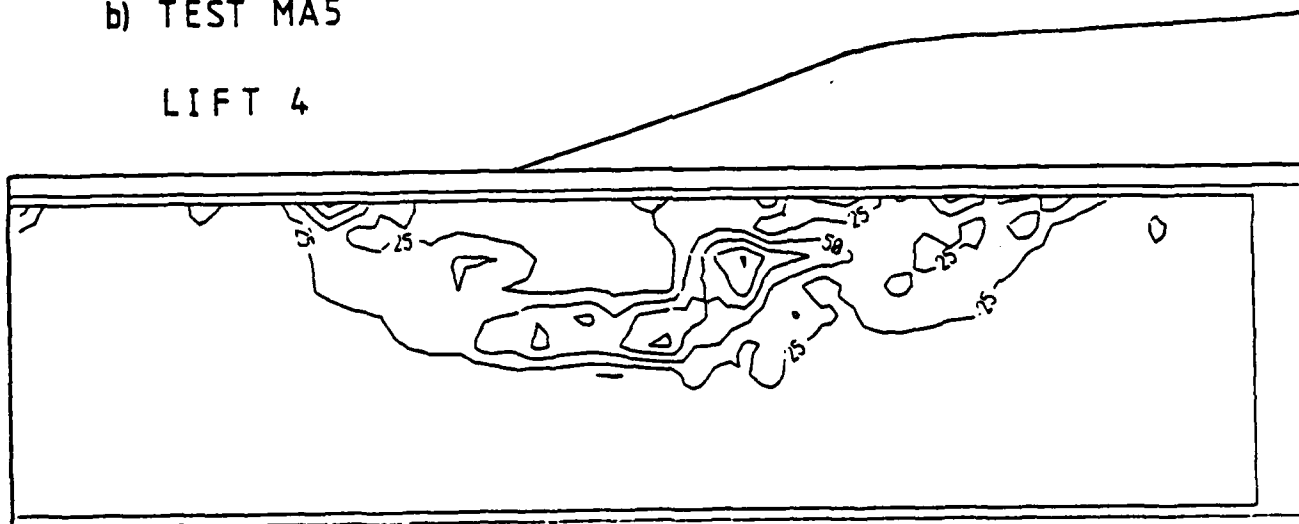


Fig. 3.28 - MAXIMUM SHEAR STRAINS

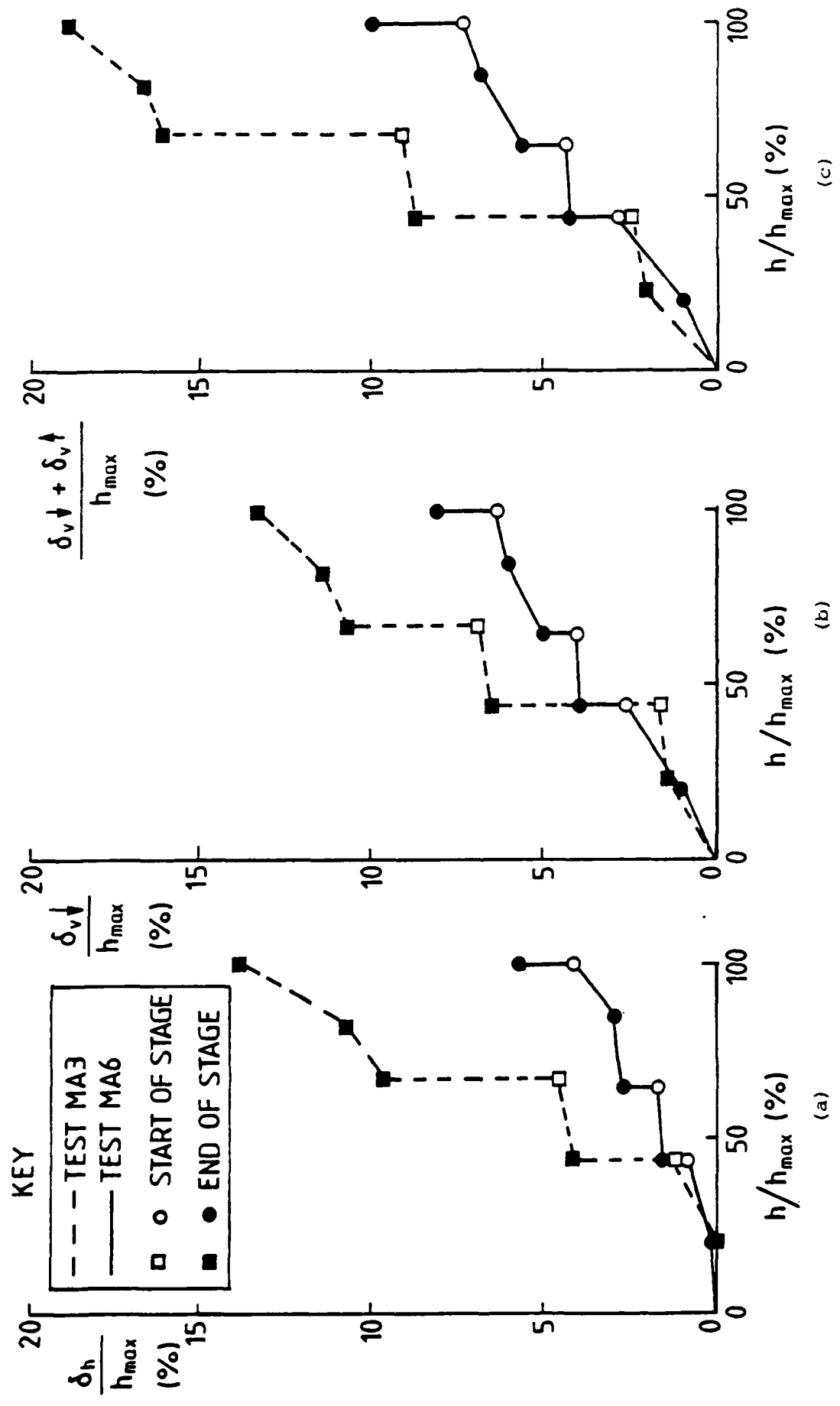


Fig. 3.29 - Non-dimensional plots of displacements against height of embankment

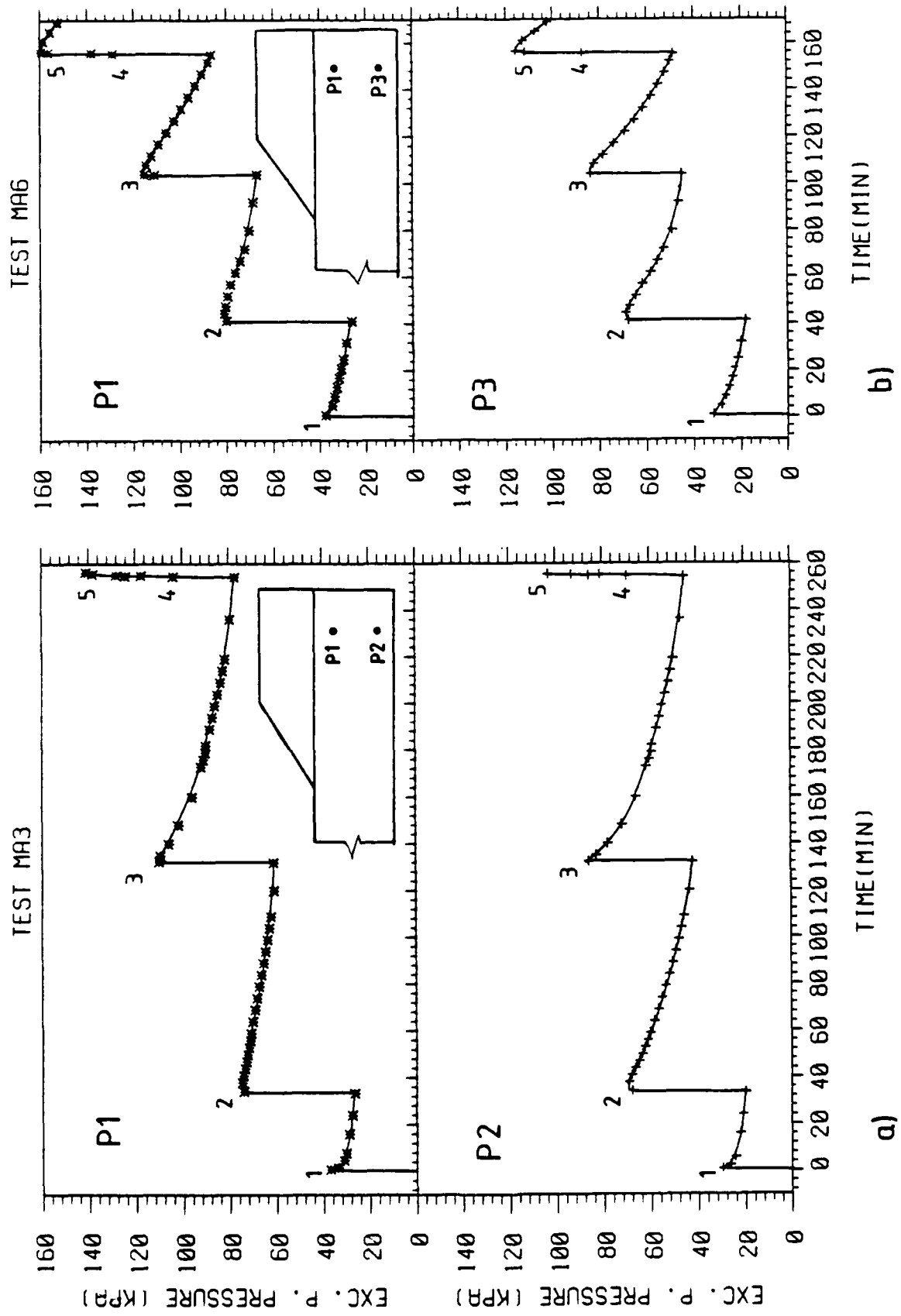


Fig. 3.30 - Excess pore pressures during tests MA3 and MA6 (for location of the transducers see Fig. 6.1)

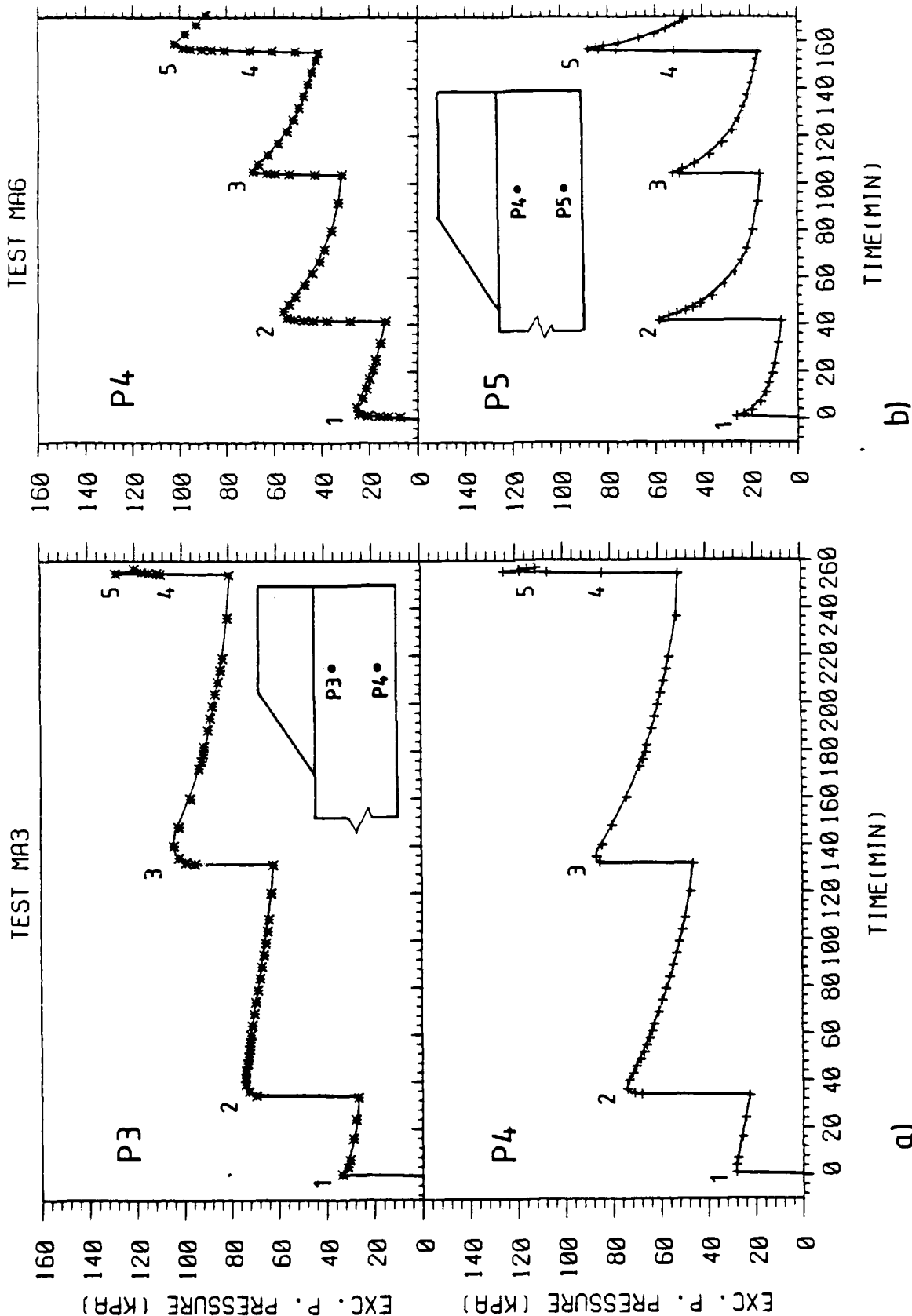


Fig. 3.31 - Excess pore pressures during tests MA3 and MA6 (for location of the transducers see Fig. 6.1)

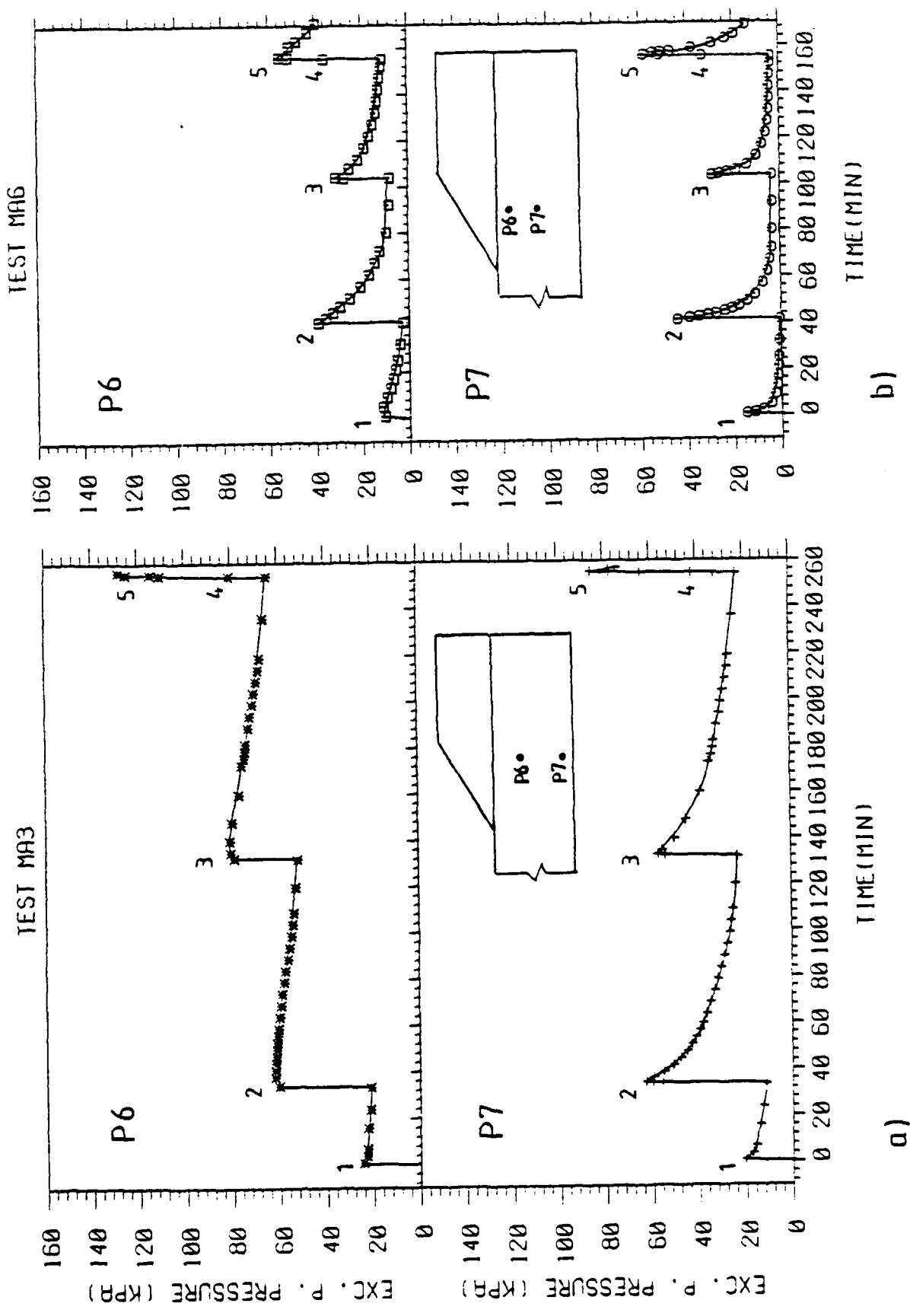
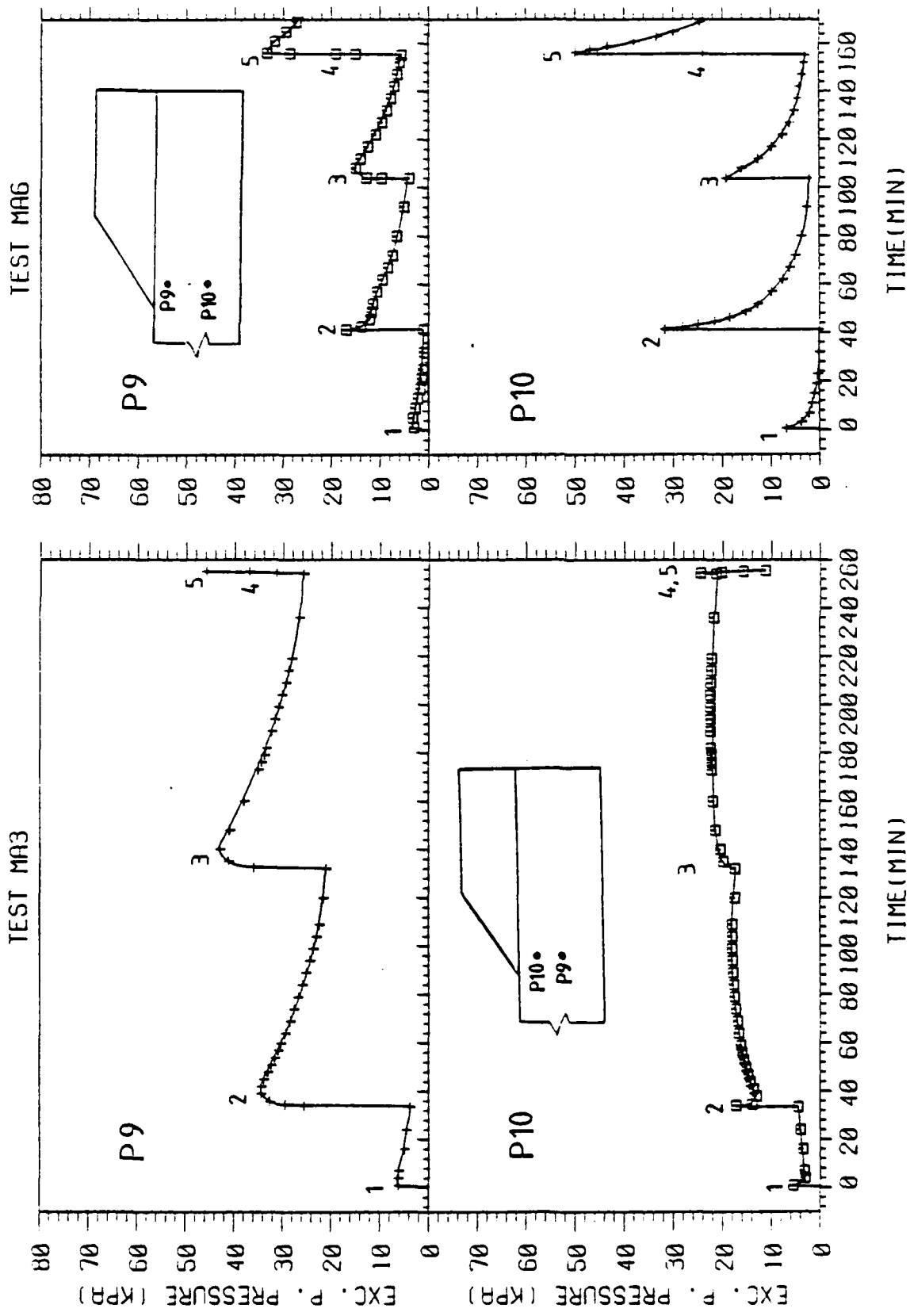


Fig. 3.12 - Excess pore pressures during tests MA3 and MAG (for location of the transducers see Fig. 6.1)



a) b)

Fig. 3.33 - Excess pore pressures during tests MA3 and MA6 (for location of the transducers see Fig. 6.1)

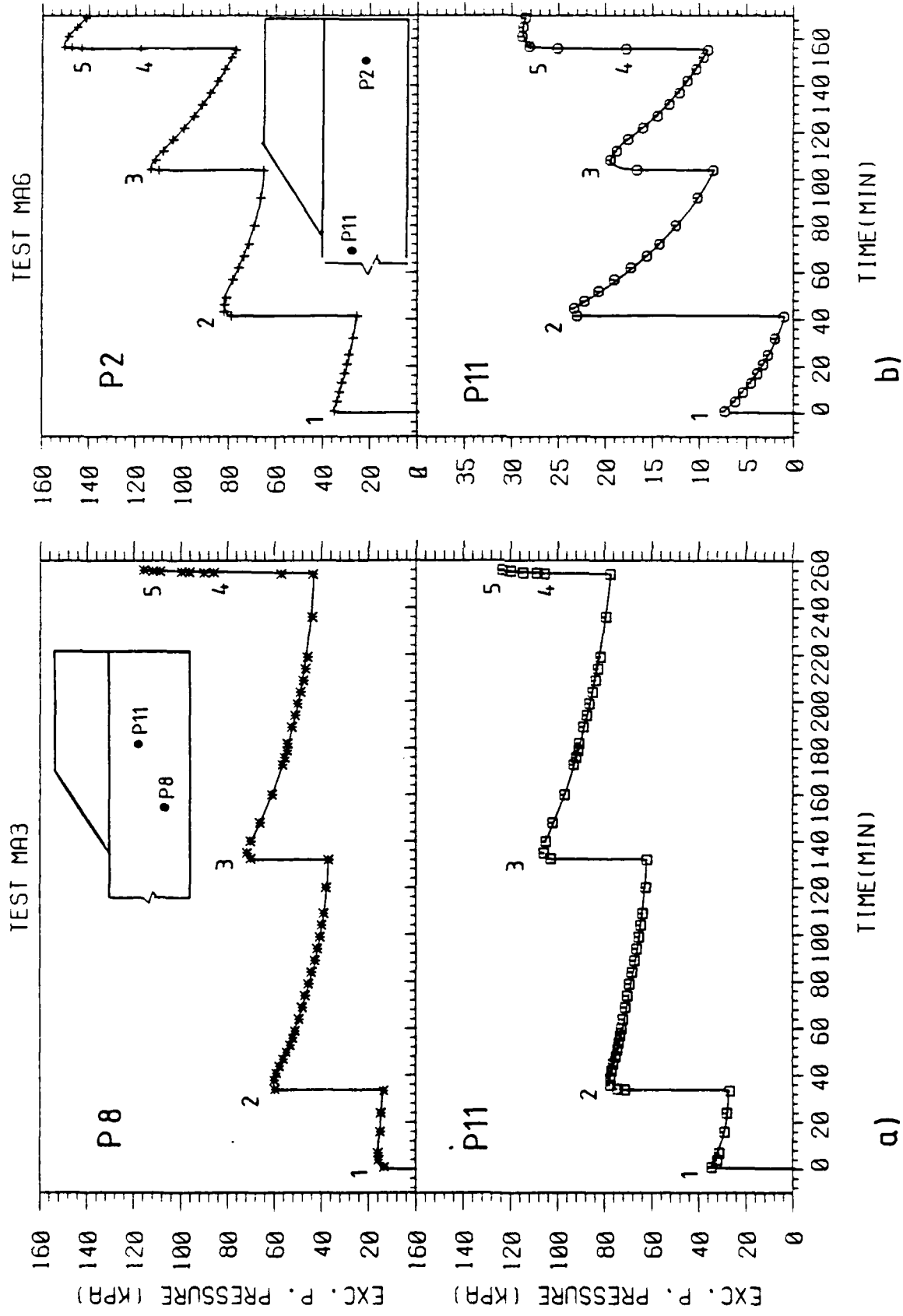
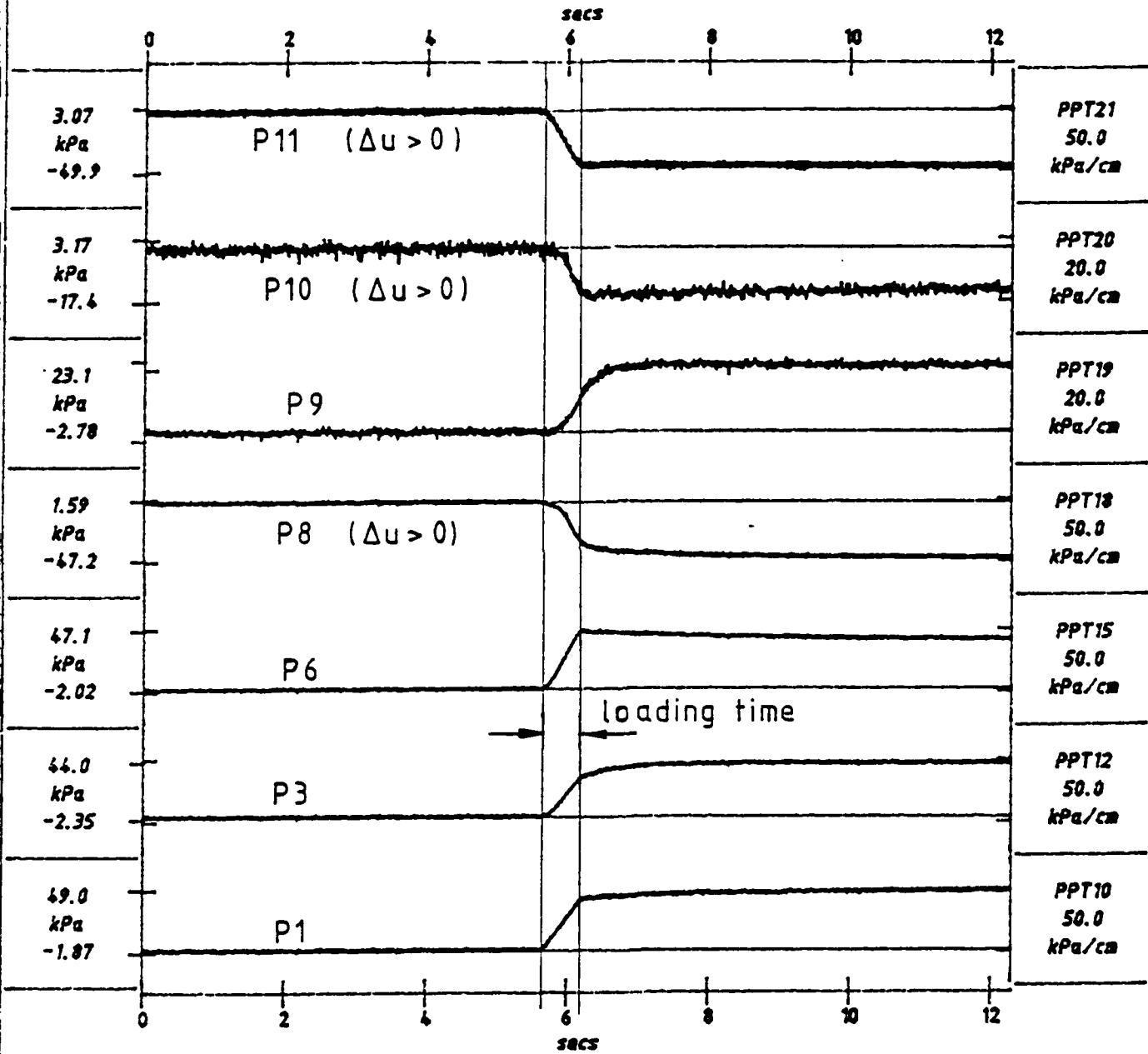


Fig. 6.1 - Excess pore pressures during tests MA3 and MA6 (for location of the transducers see Fig. 6.1)

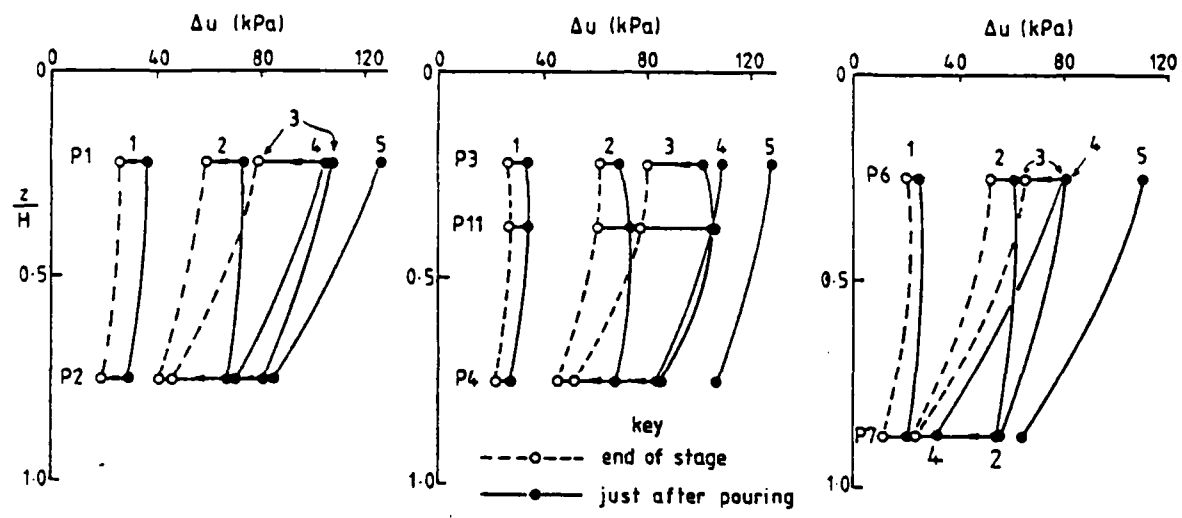
1024 raw data points plotted per transducer



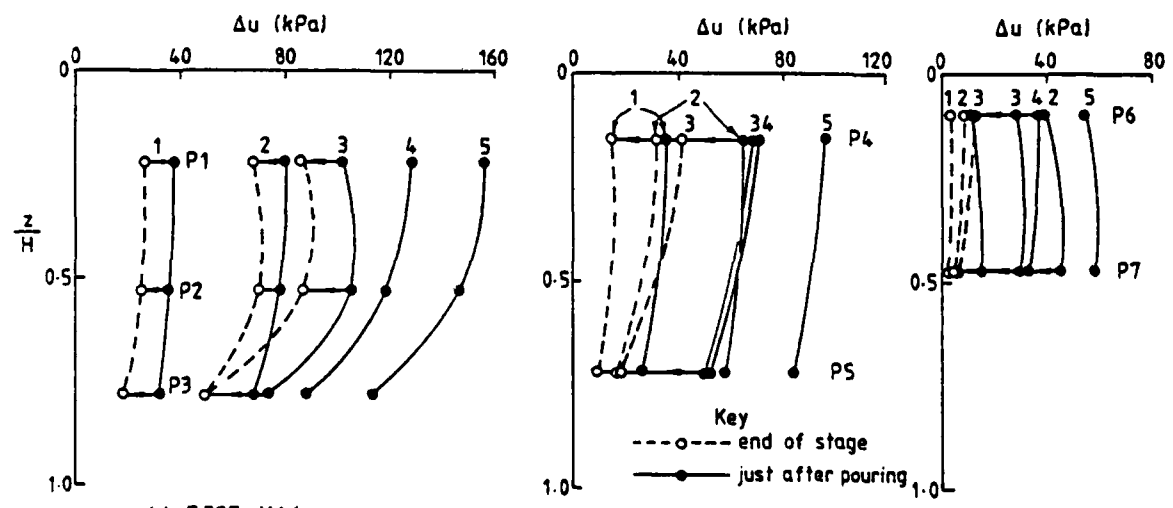
Scales : model

NOTE: excess pore pressures are positive for all transducers.

Fig. 3.35 - Pore pressure time record



a) TEST MA3

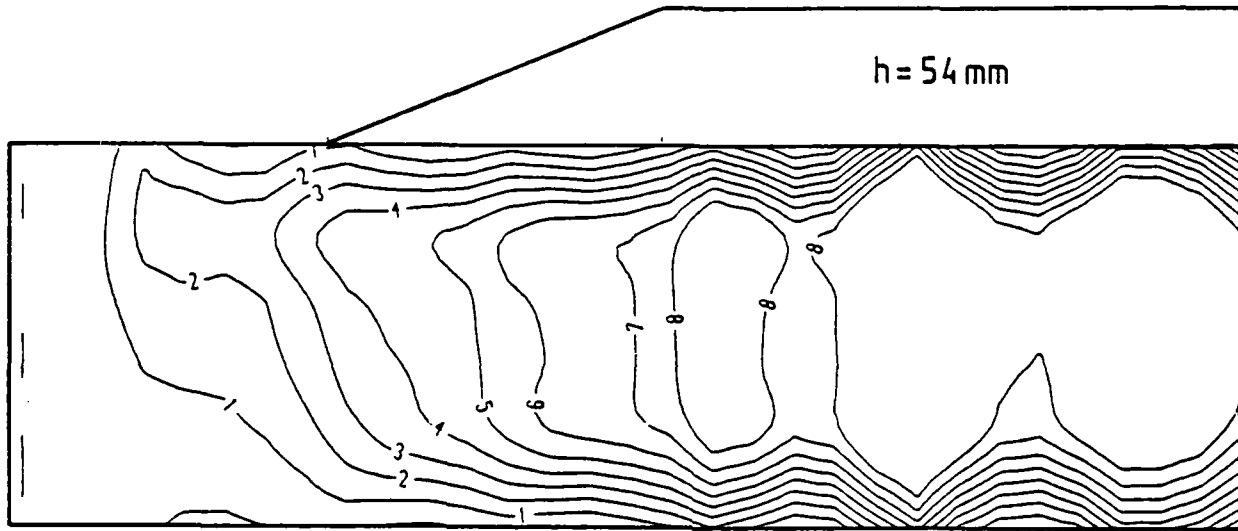


b) TEST MA6

Fig. 3.36 - Excess pore pressure profiles for tests MA3 and MA6

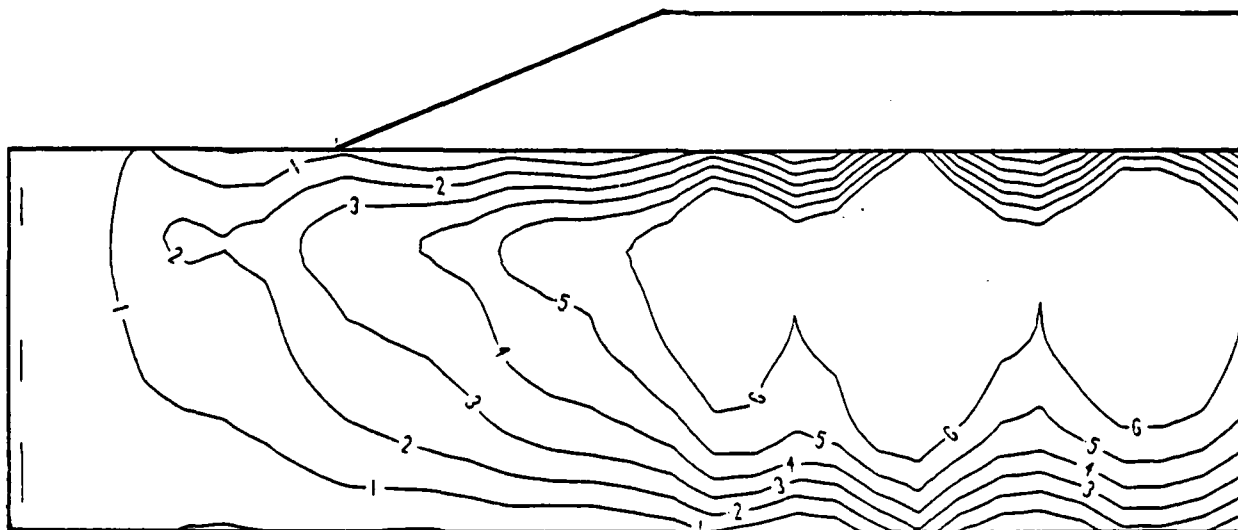
TEST MA3

$$h_u = \frac{\Delta u}{\gamma_w} \text{ (meters)}$$



a) STAGE 2 START

0 50 100 mm

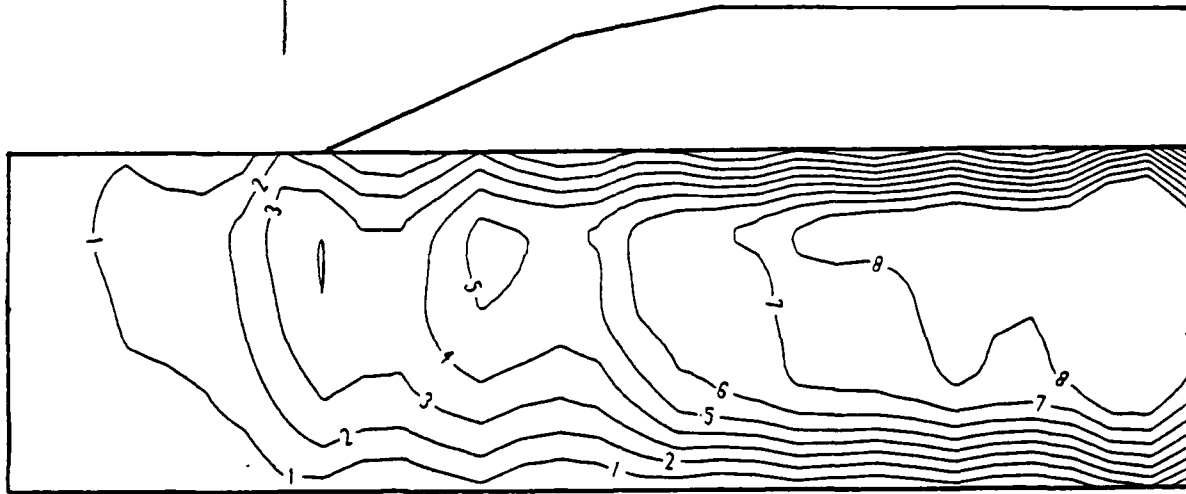


b) STAGE 2 END

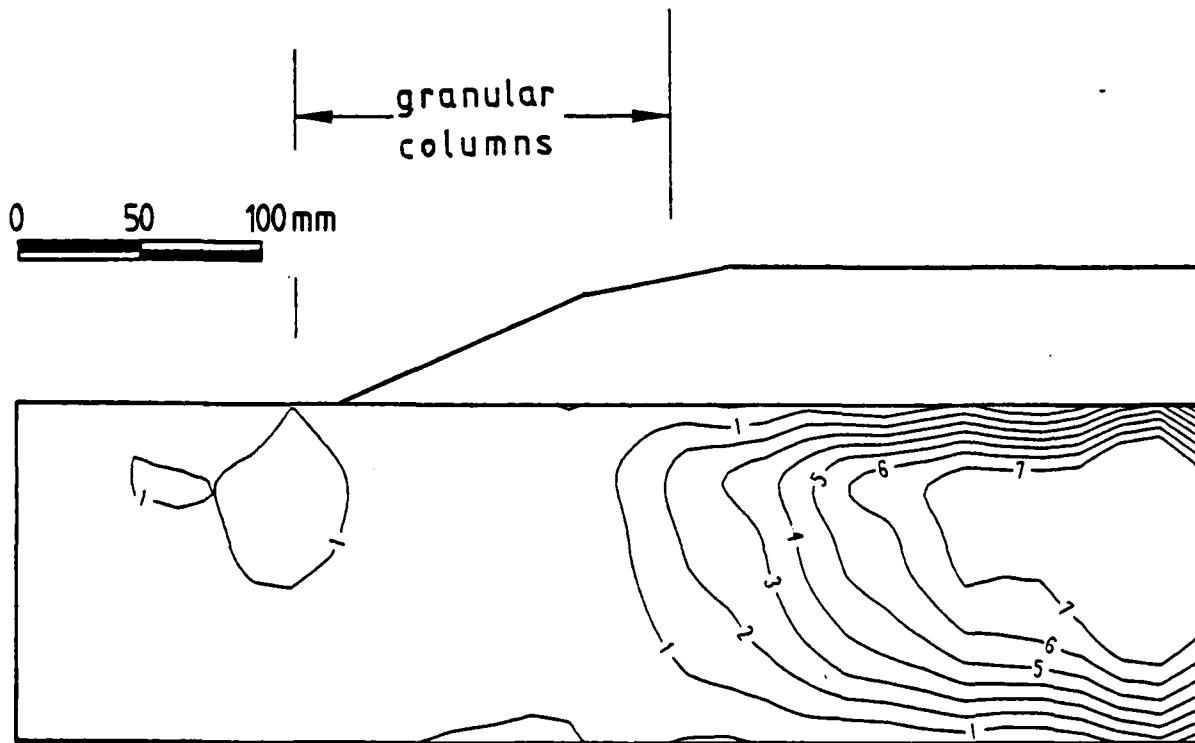
Fig. 3.37 - Excess pore pressure contours in meters of water - test MA3

TEST MA6

$$h_u = \frac{\Delta u}{\gamma_w} \text{ (meters)}$$



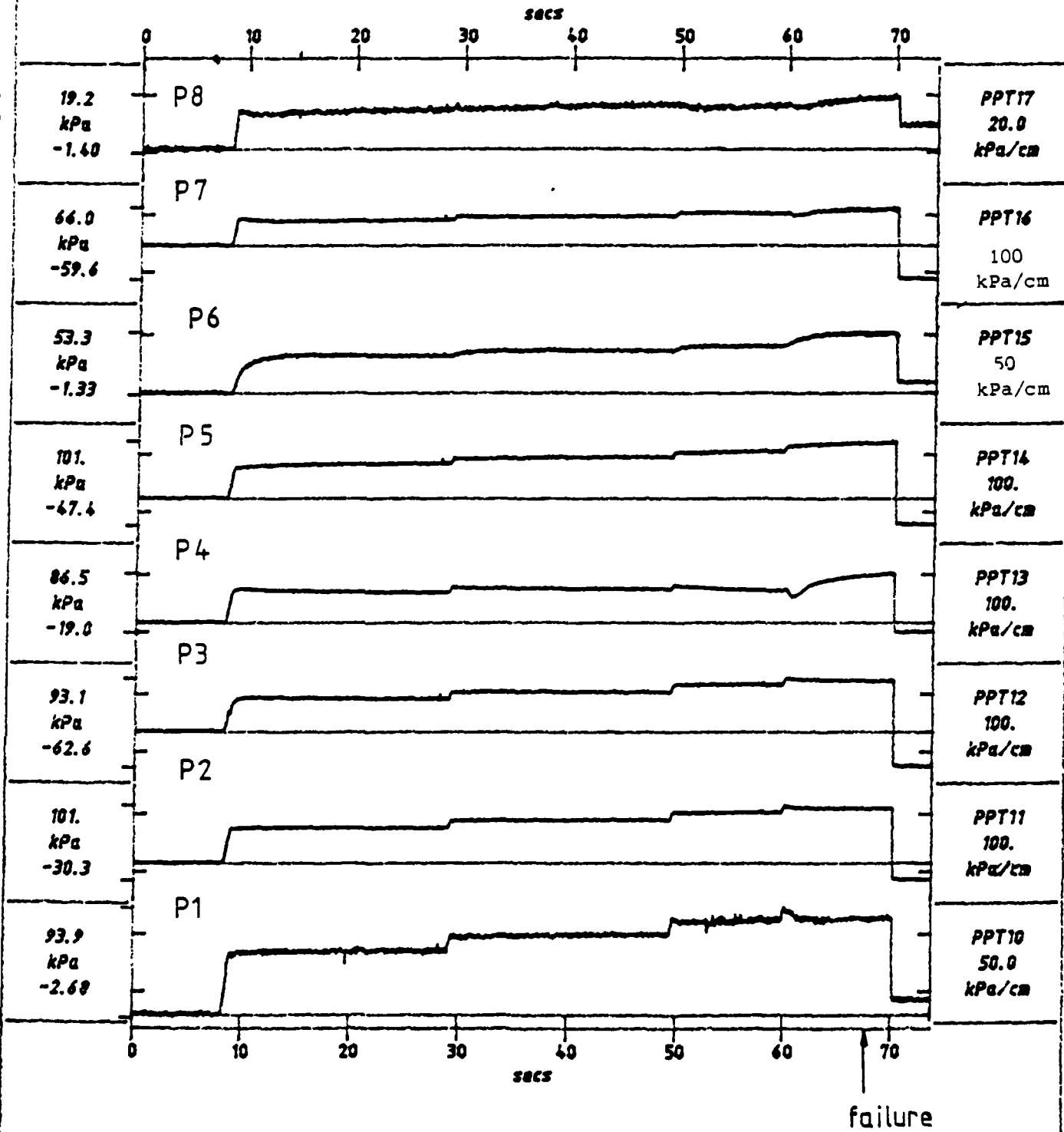
a) STAGE 2 - START



b) STAGE 2 - END

Fig. 3.38 - Excess pore pressure contours in meters of water - test MA6

1024 raw data points plotted per transducer



Scales : model

TEST MA5  
MODEL PORE P  
FLIGHT 1

SV11

PORE PRESSURES  
TIME RECORDS

FIG. NO.

3.39

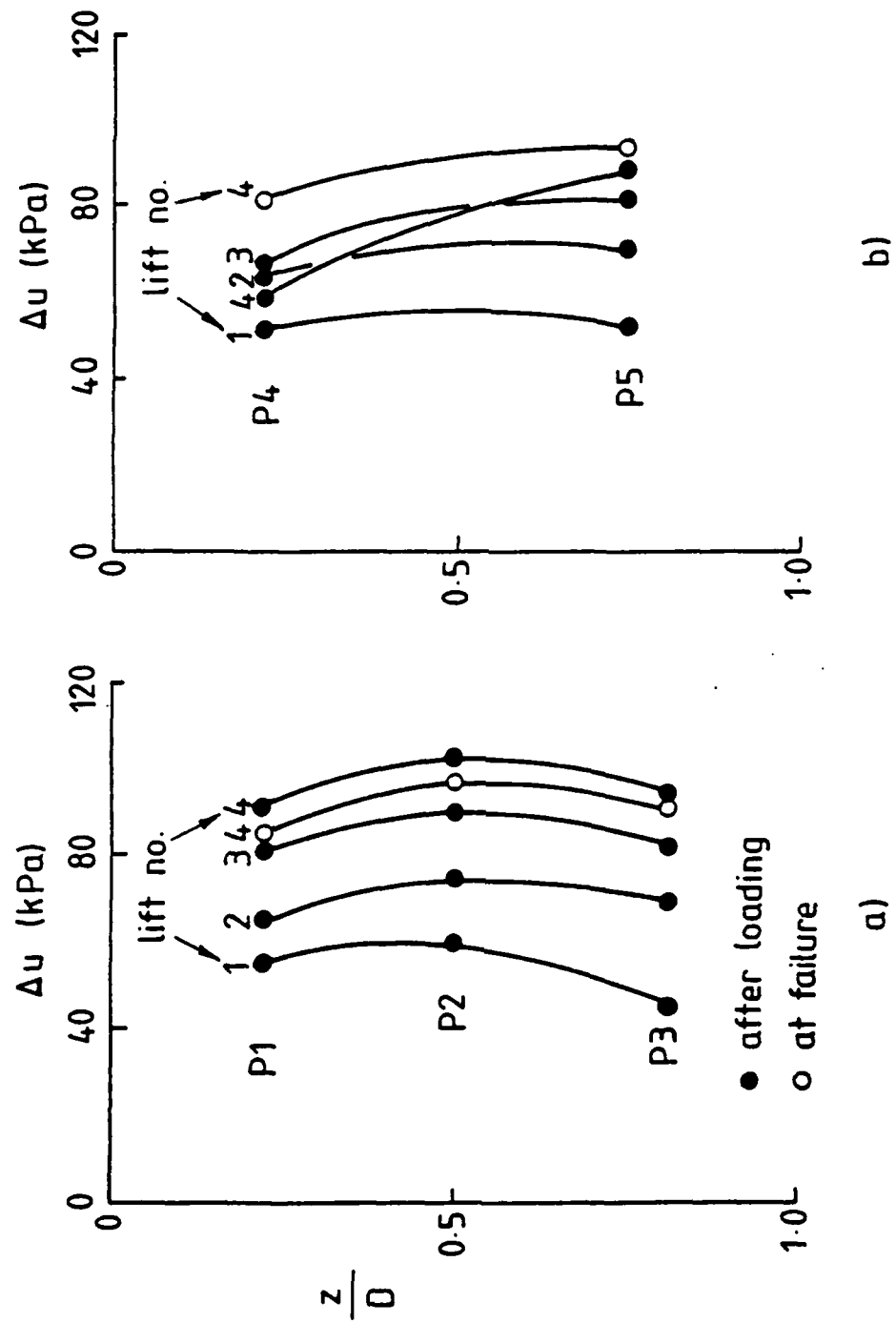


Fig. 3.40 - Excess pore pressure profiles for test MA5

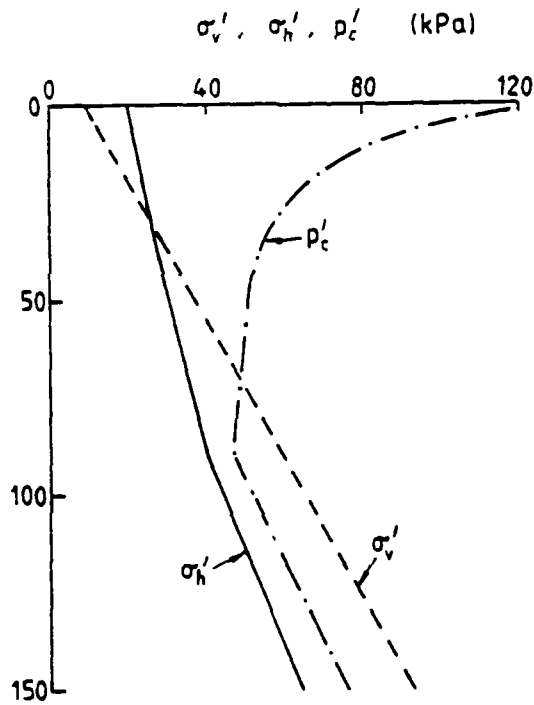
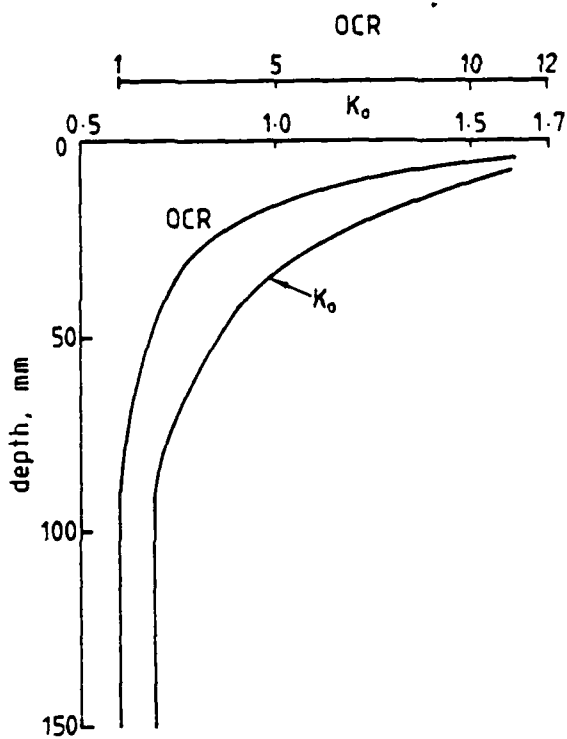


Fig. 4.1 - In situ stress state

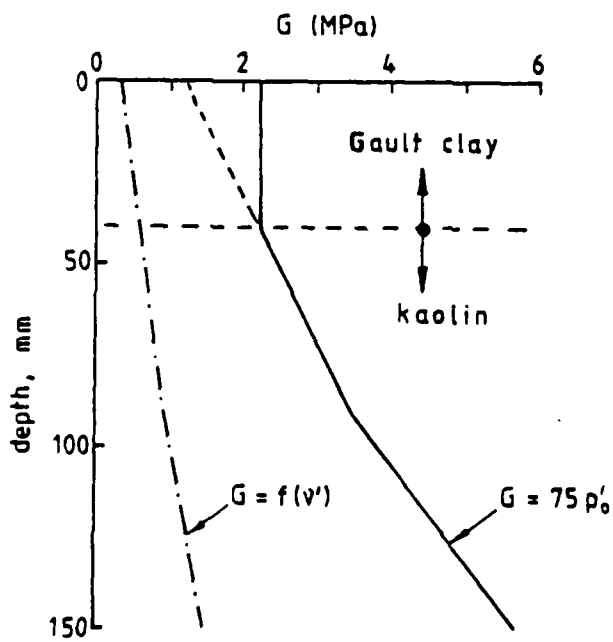


Fig. 4.2 - Variation of shear modulus with depth

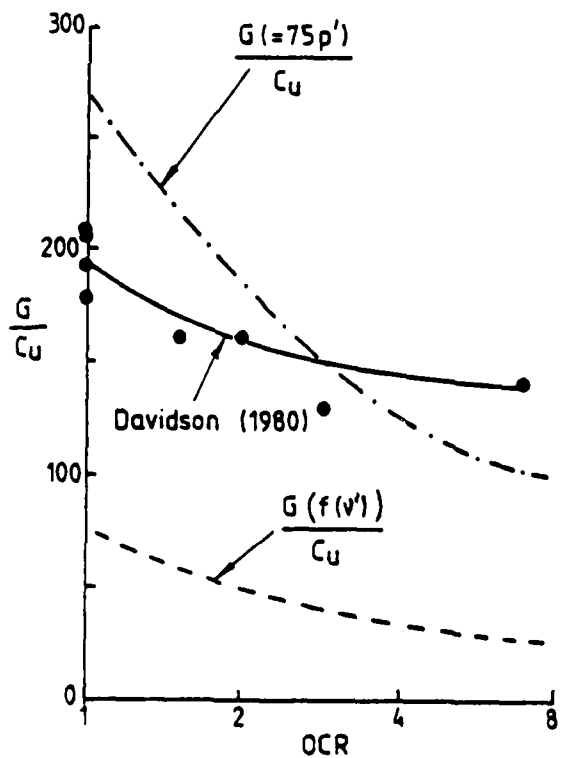
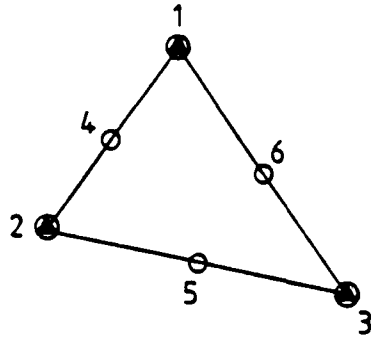


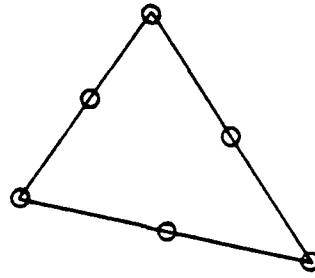
Fig. 4.3 - Variation of  $G/c_u$  with OCR

○  $\delta_x, \delta_y$  - displacements unknown

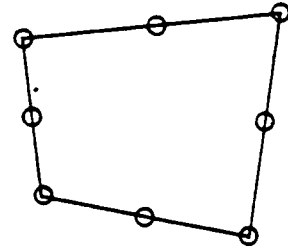
▲  $u$  - pore pressure unknown



a) LST (element type 3)  
6 nodes, 15 d.o.f.  
(for consolidation)

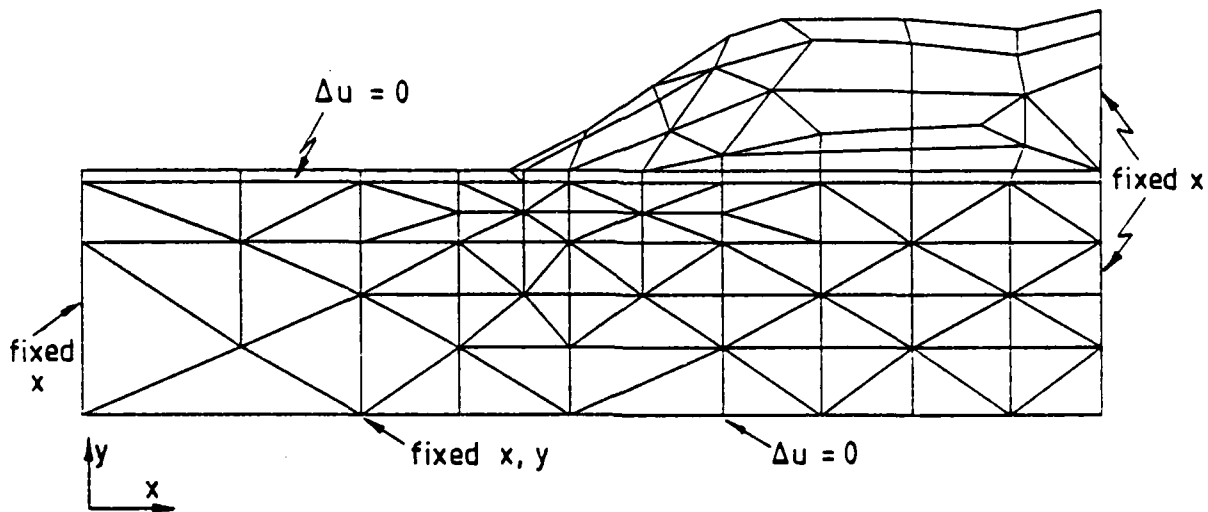


b) LST (element type 2)  
6 nodes, 12 d.o.f.



c) LSQ (element type 4)  
8 nodes, 16 d.o.f.

Fig. 4.4 - Types of elements used



TEST MA3 - F. E. MESH - 95 VERTICE NODES, 130 ELEMENTS

Fig. 4.5 - Finite element mesh

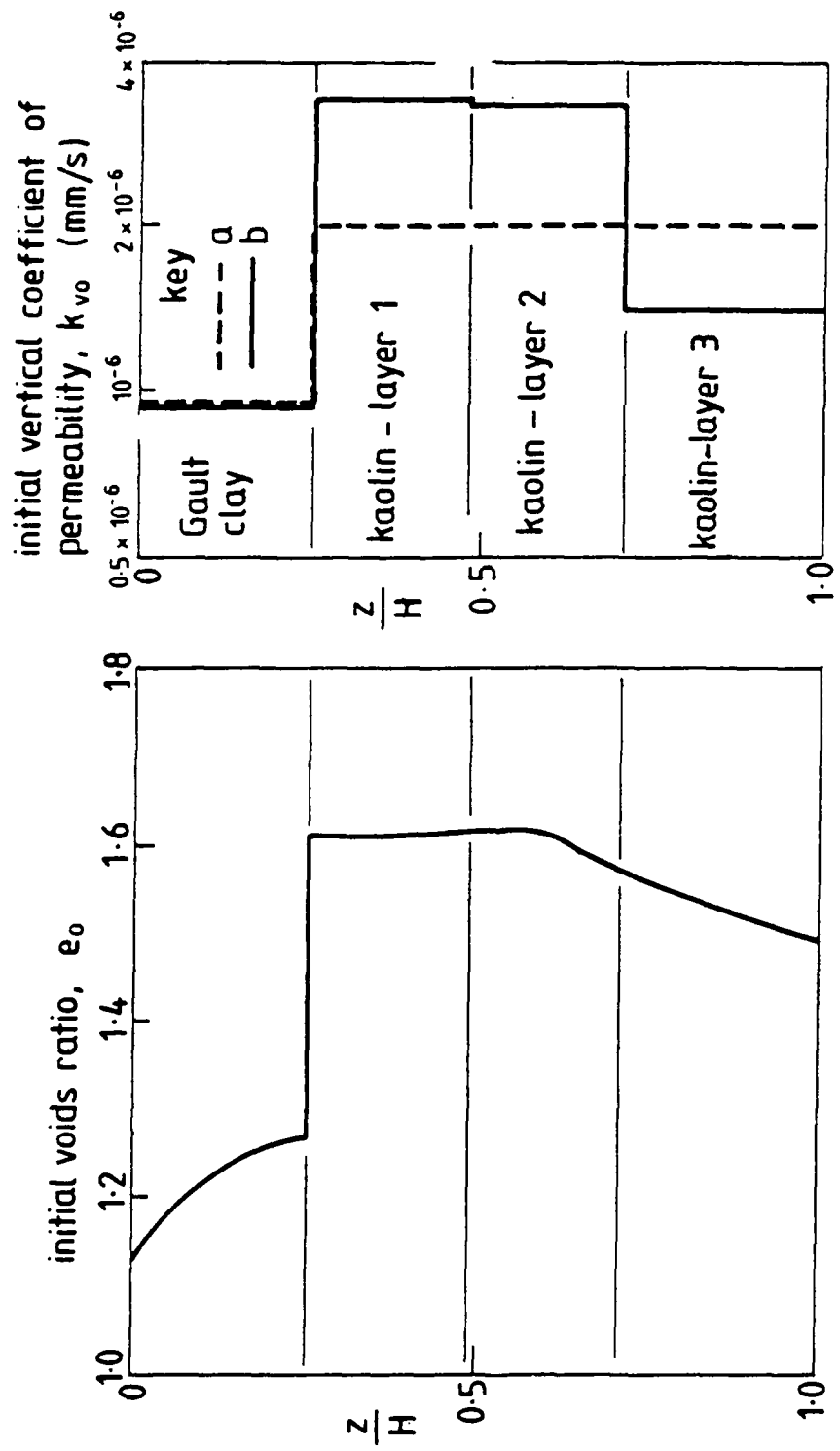
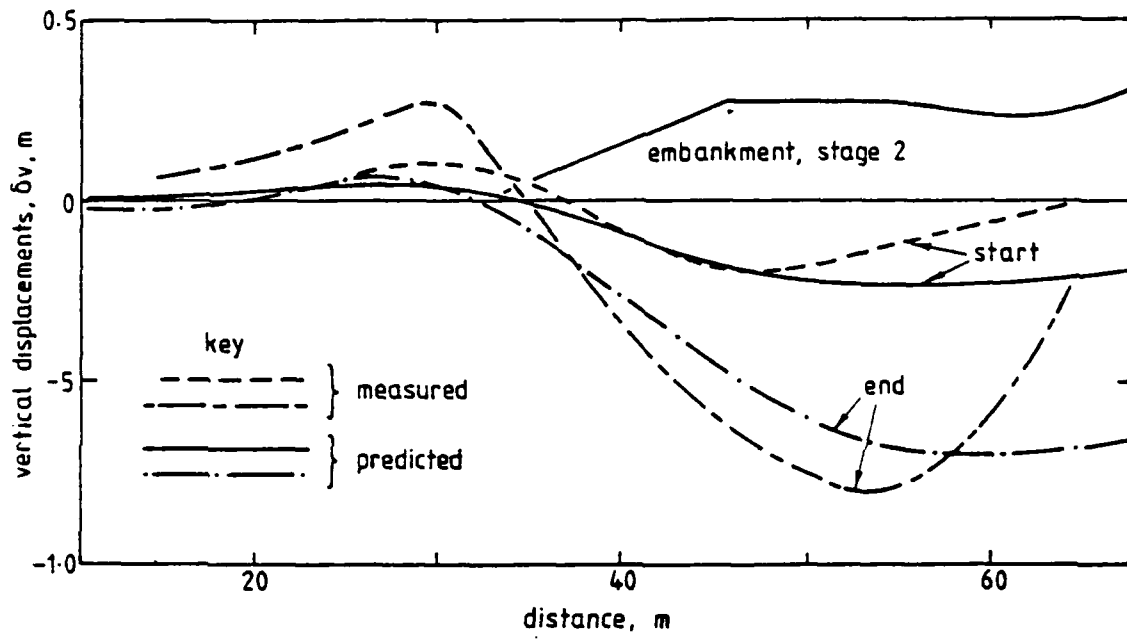
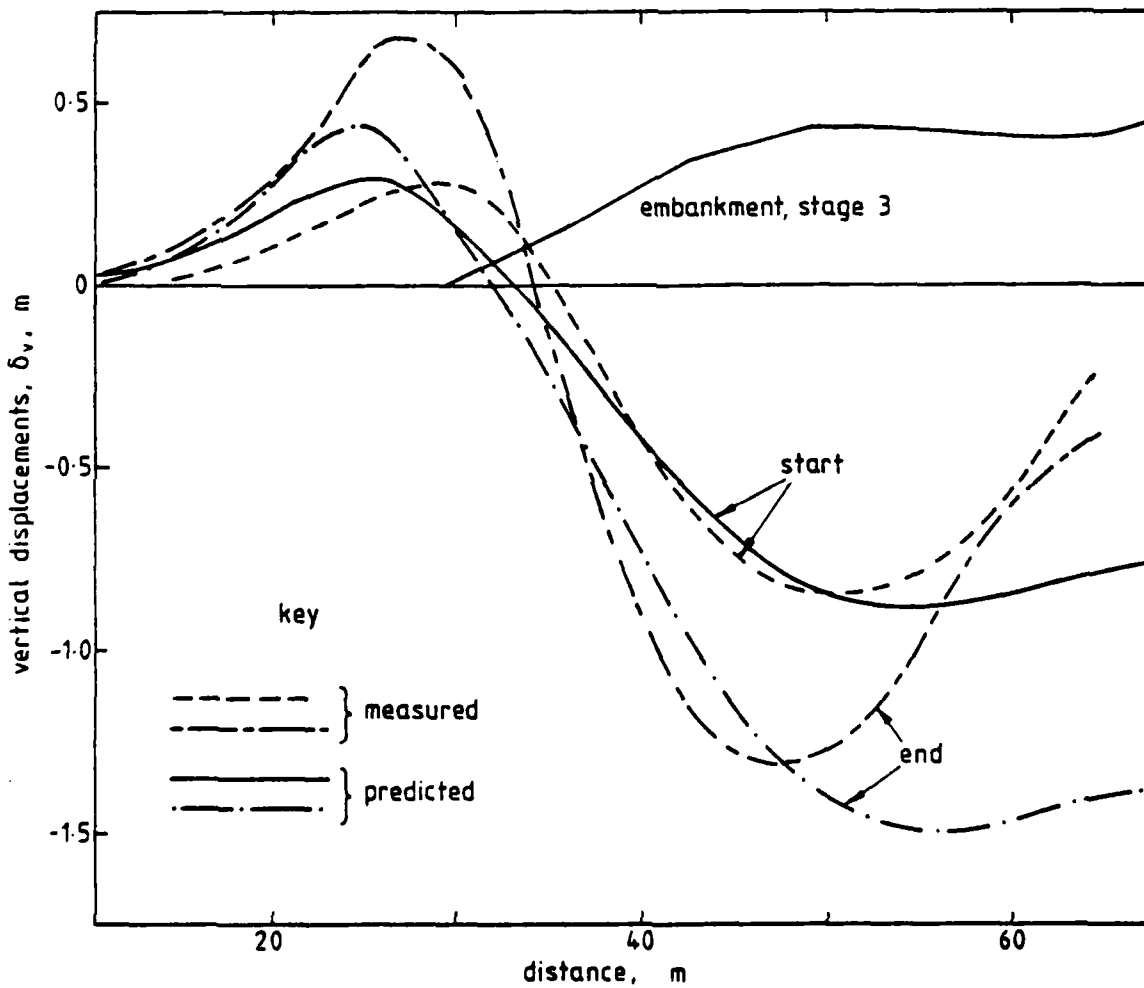


Fig. 4.6 - Distribution of voids ratio and permeability in clay foundation

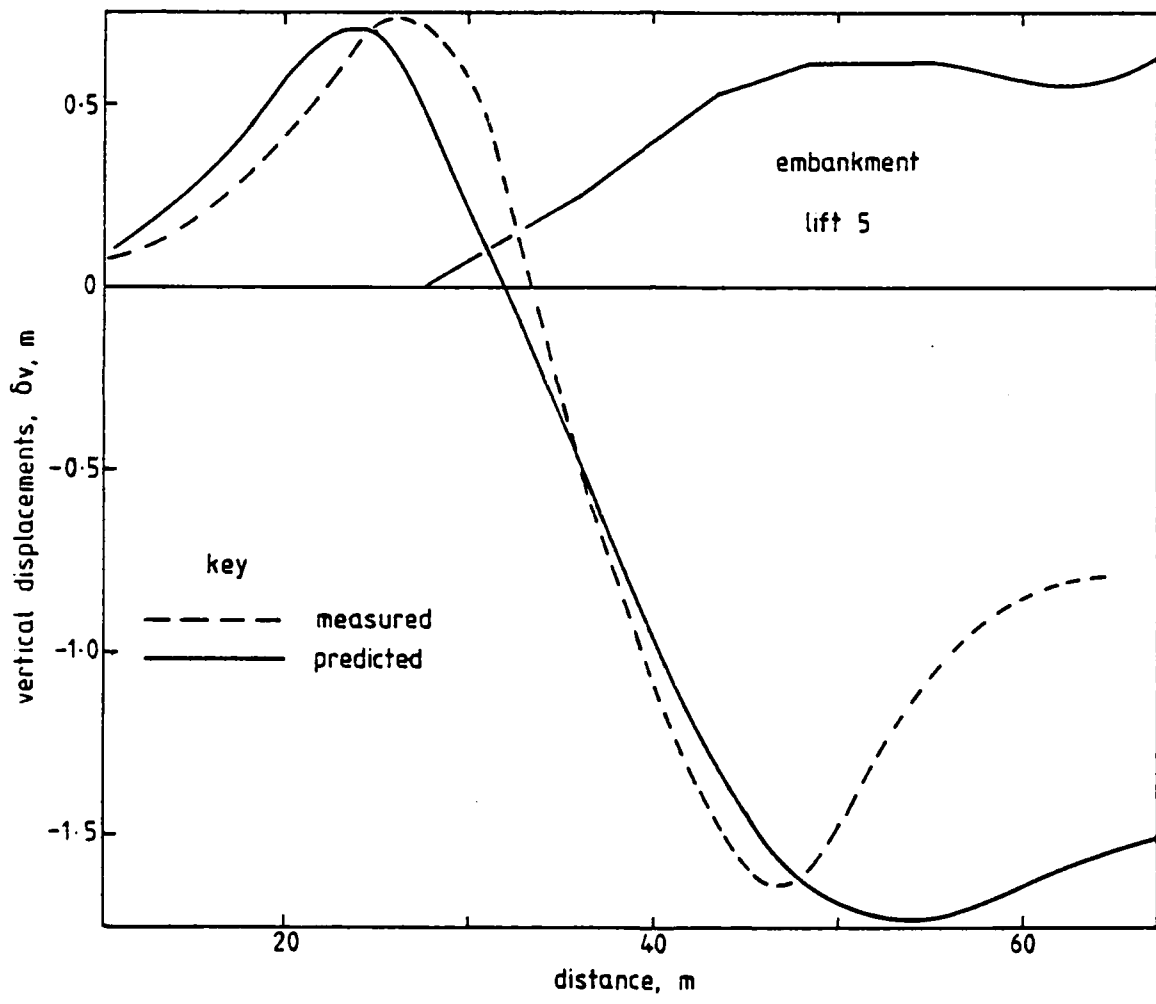


(a)



(b)

Fig. 4.7 - Predicted and measured vertical displacements at clay surface



(c)

Fig. 4.7 (contn). - Predicted and measured vertical displacements at clay surfaces

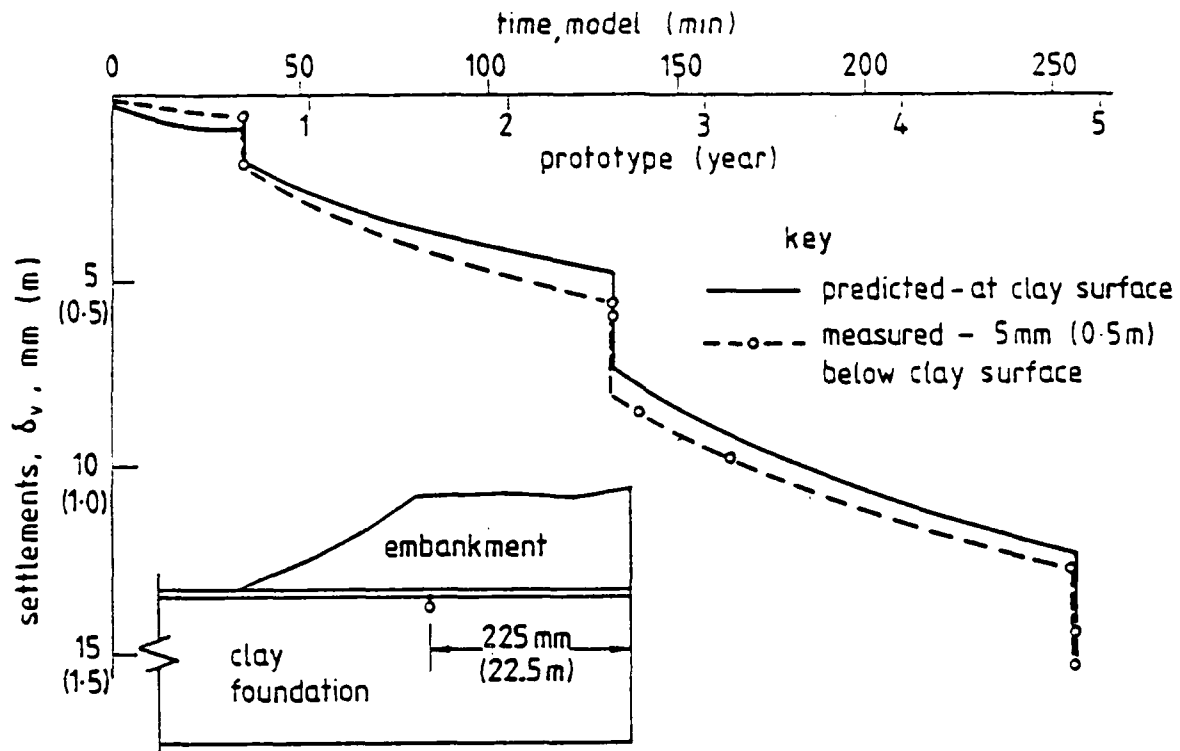


Fig. 4.8 - Predicted and measured settlements with time

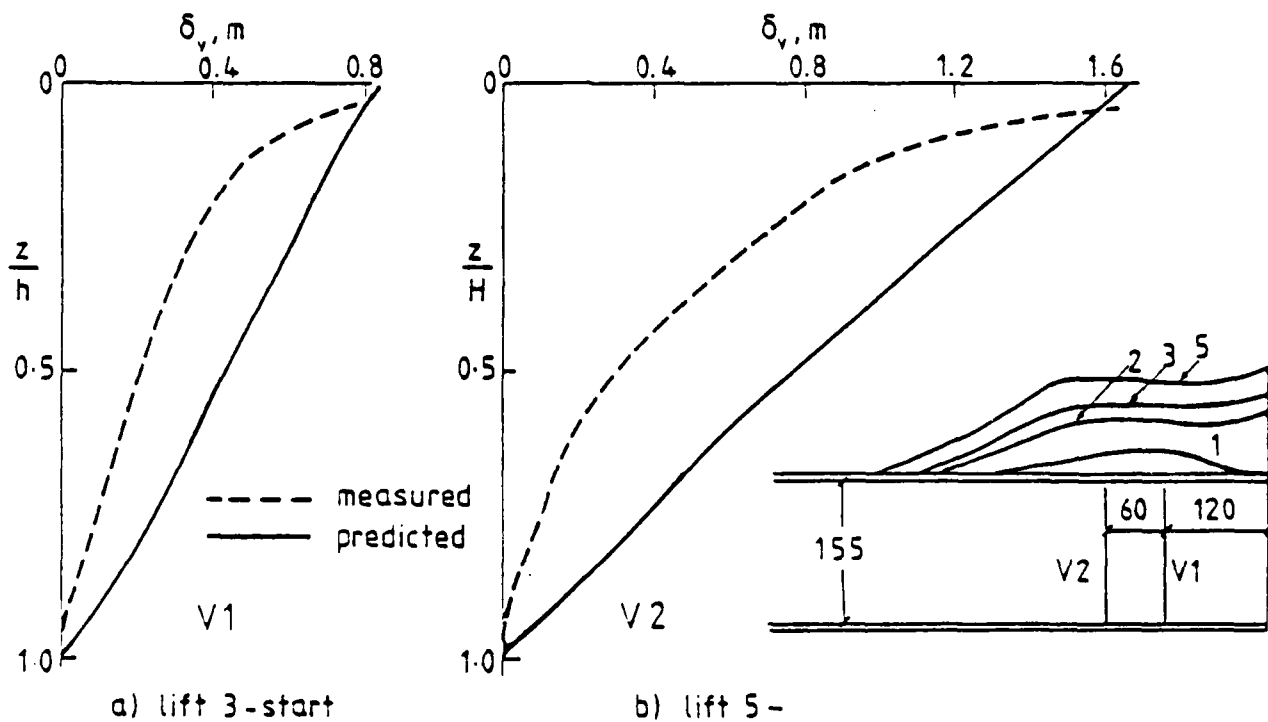


Fig. 4.9 - Predicted and measured settlements with depth

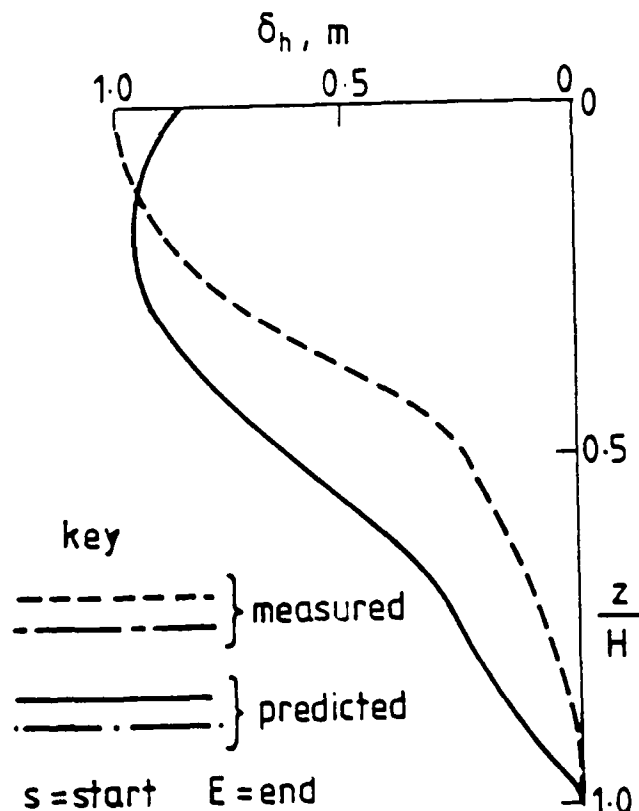
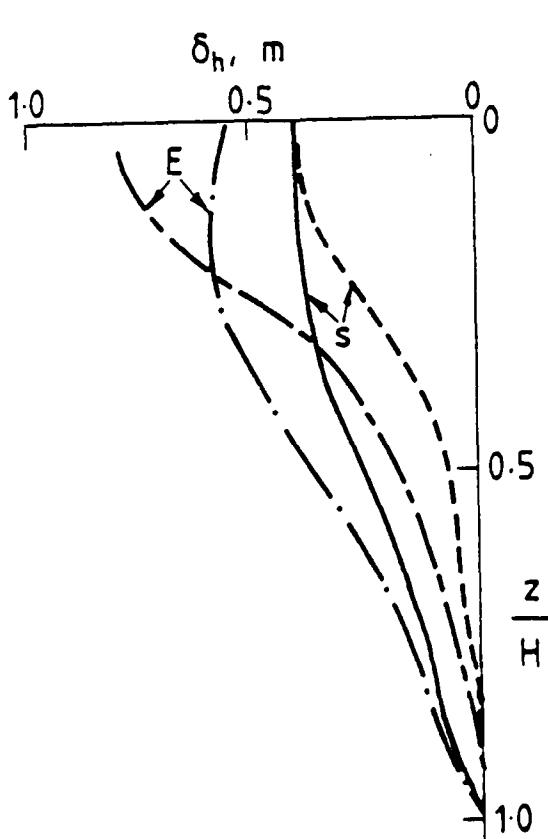
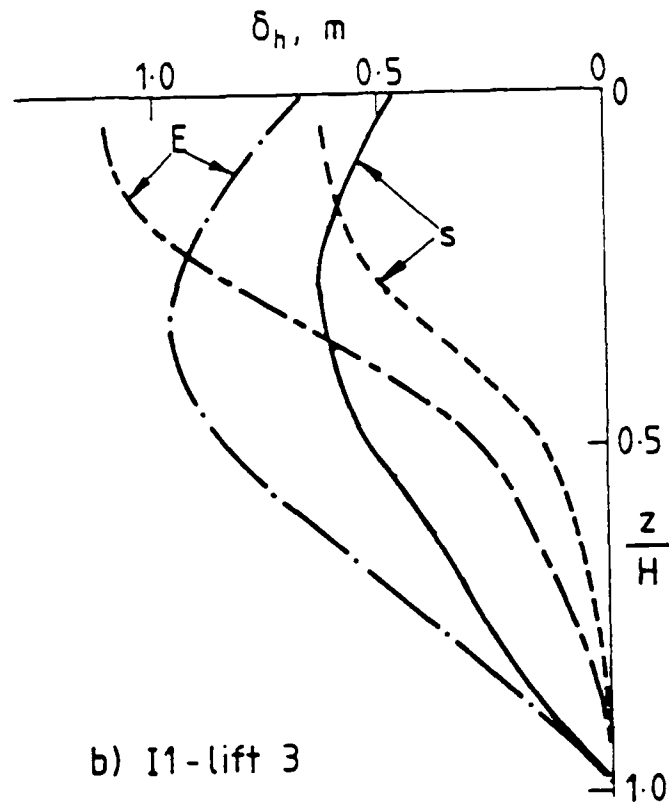
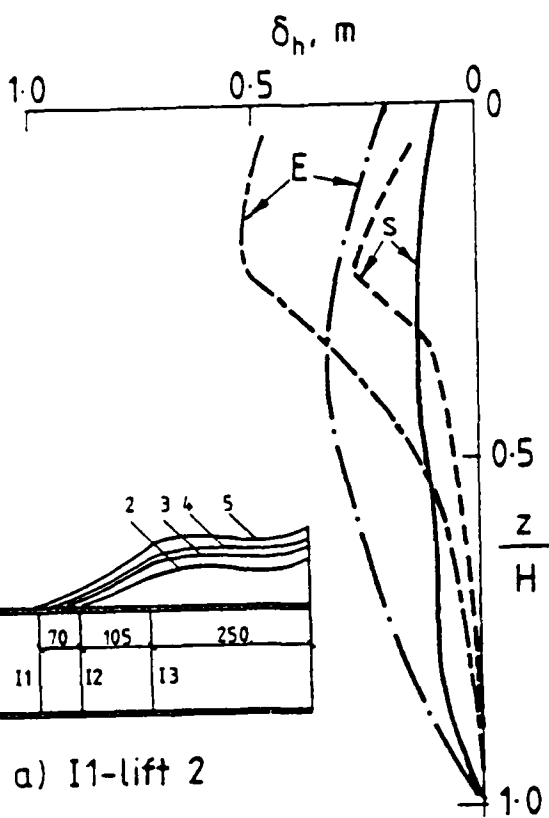


Fig. 4.10 - Equivalent inclinometer plots I1 and I3 (see location at Fig. 6.15)

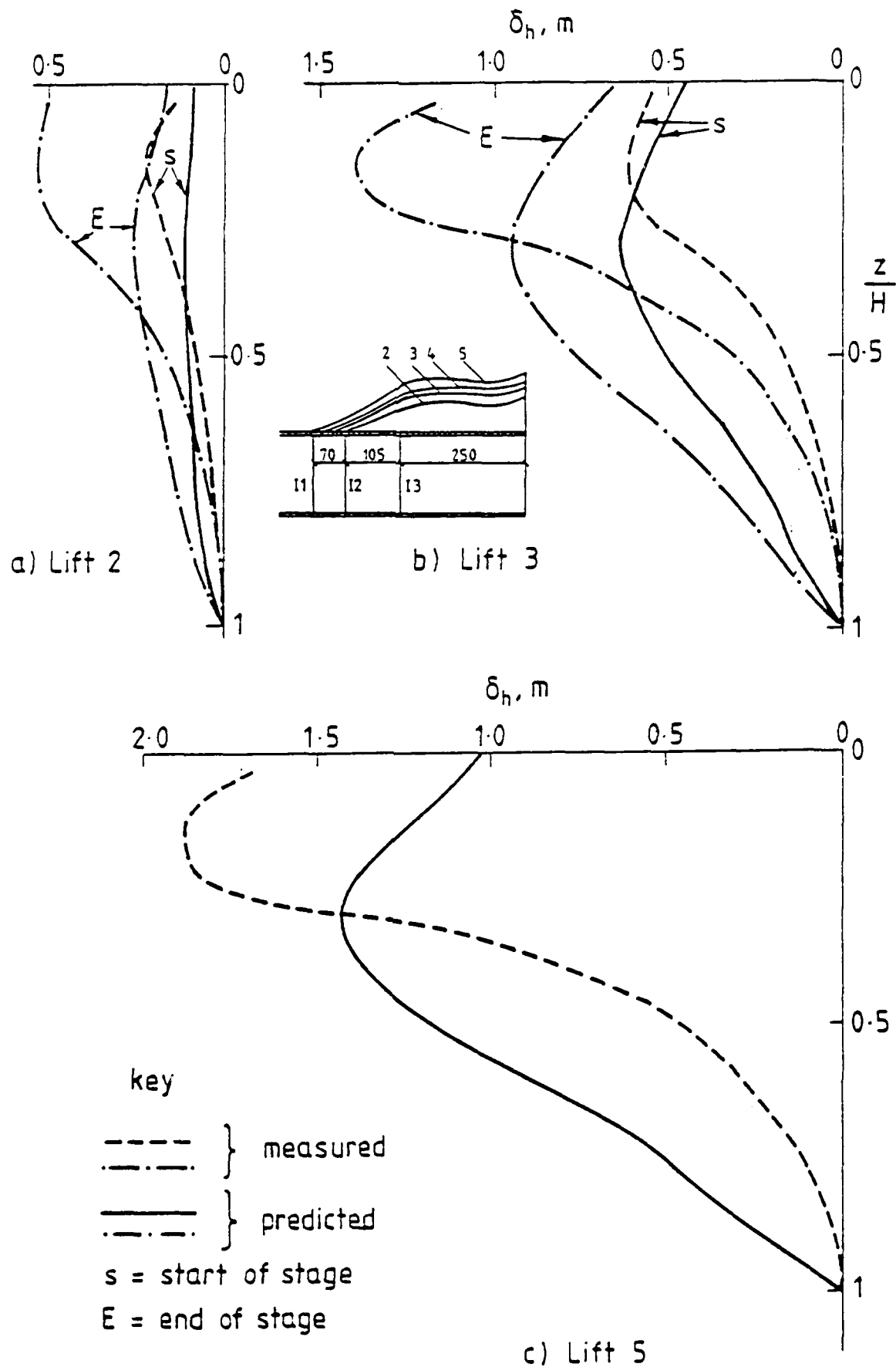
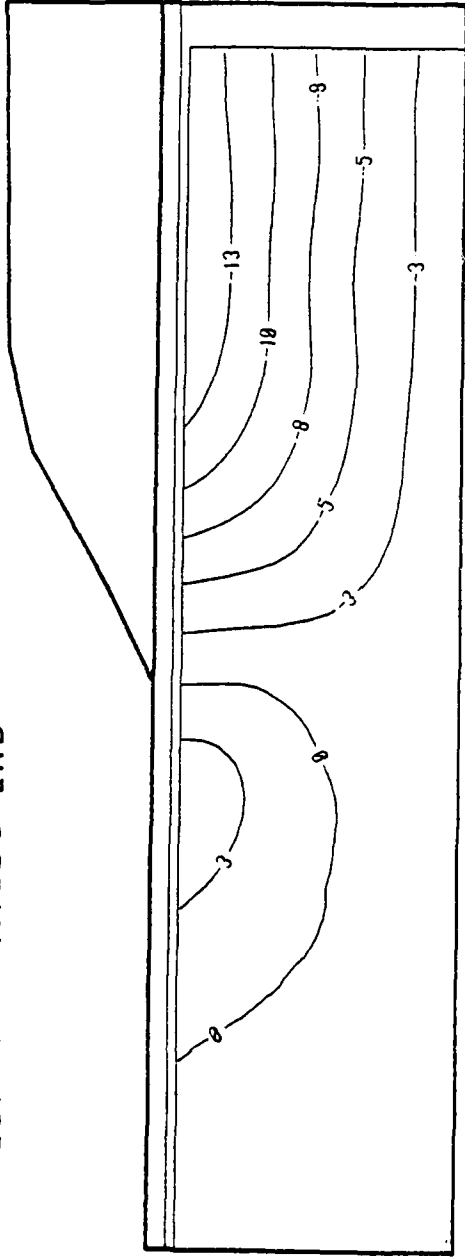
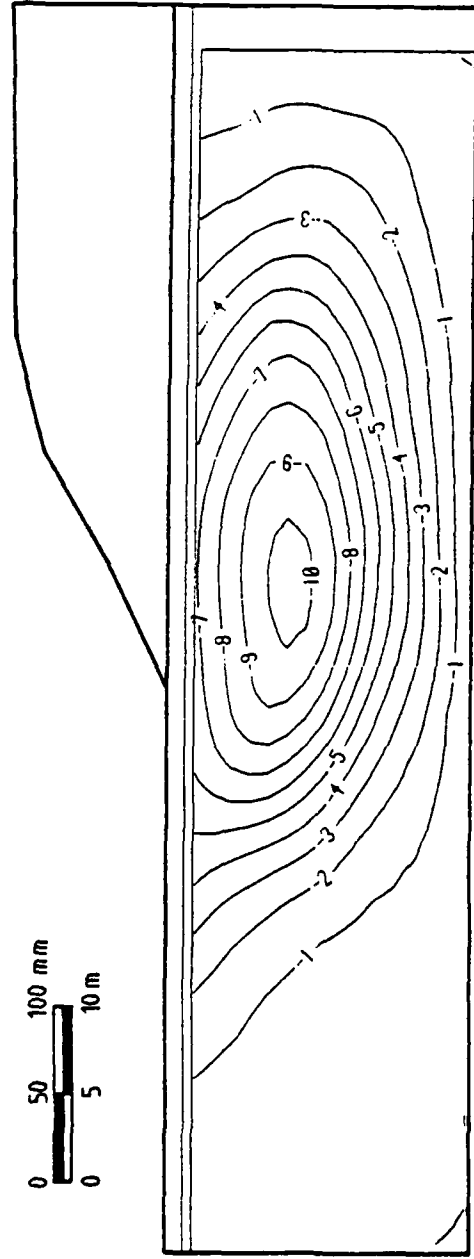


Fig. 4.11 - Equivalent inclinometer plot 12 (see location at Fig. 6.15) - predicted and measured displacements

TEST MA3-STAGE 3-END



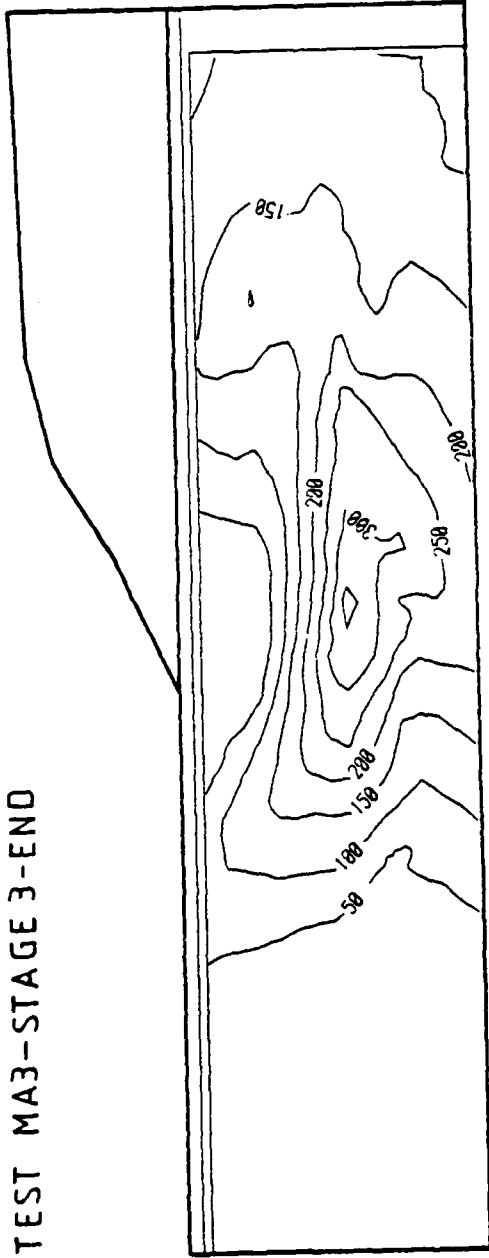
a) VERTICAL DISPLACEMENT  $\delta_v$  (mm)



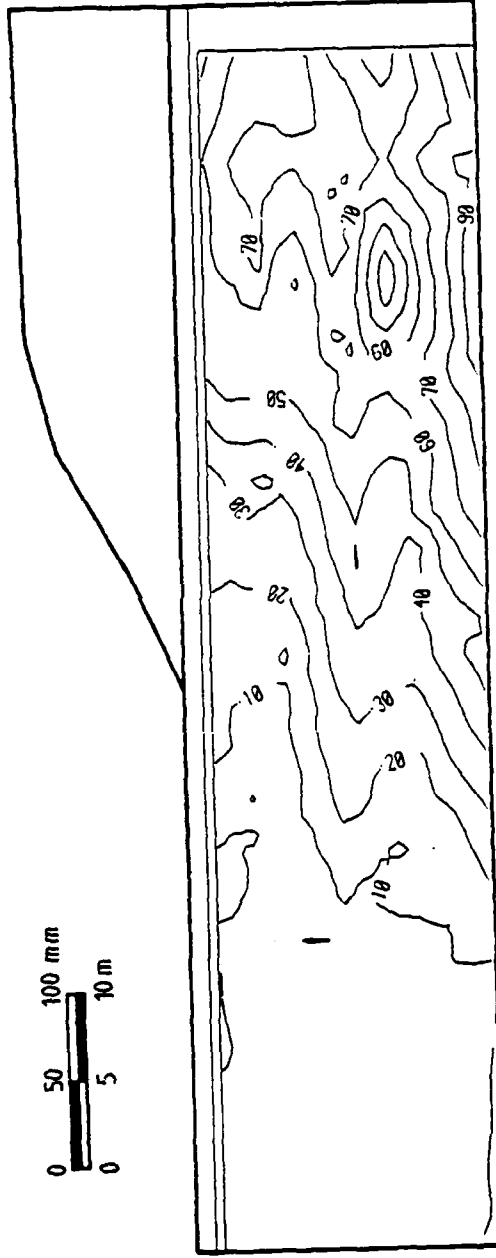
b) HORIZONTAL DISPLACEMENT  $\delta_h$  (mm)

Fig. 1.12 - Predicted vertical and horizontal displacements

TEST MA3-STAGE 3-END



a) MAXIMUM SHEAR STRAIN  $\times 10$  (%)



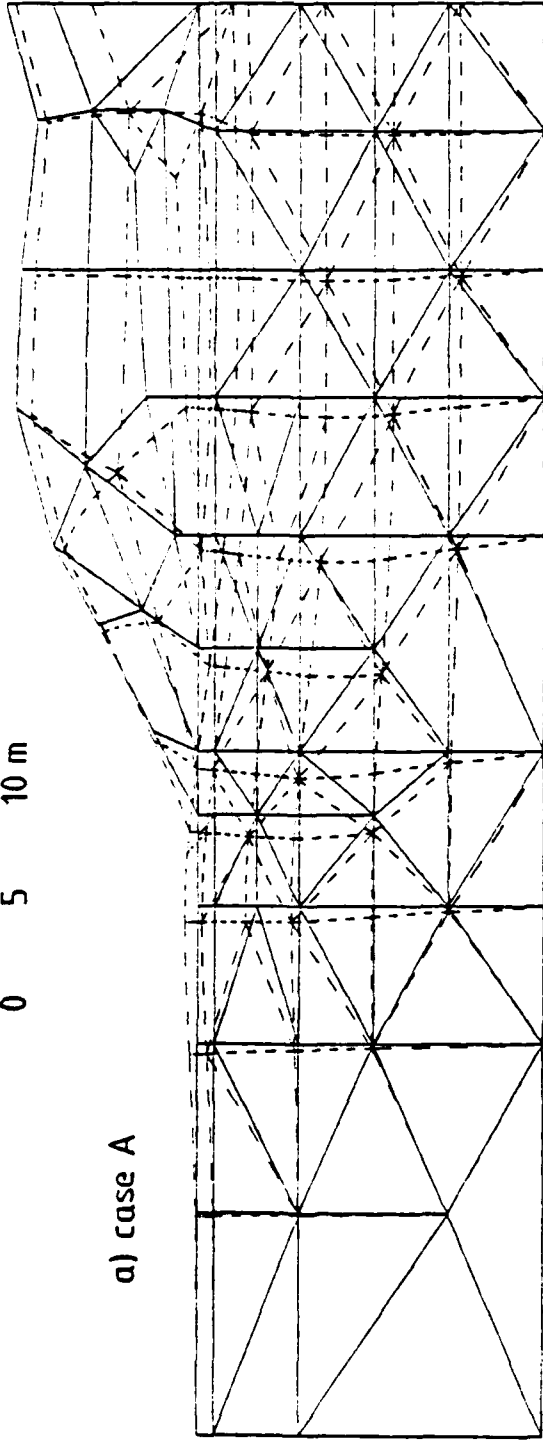
b) VOLUMETRIC STRAIN  $\times 10$  (%)

Fig. 4.13 - Predicted maximum shear and volumetric strains

0 50 100 mm  
0 5 10 m

TEST MA3

a) case A



b) case D

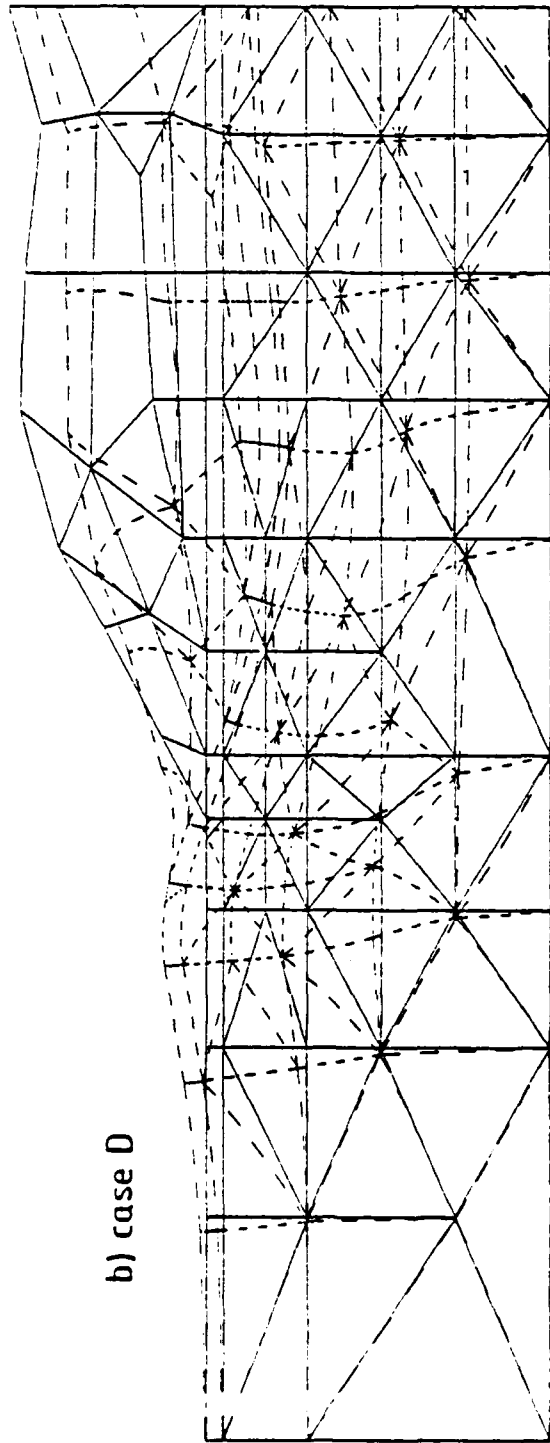


Fig. 4.14 - Deformed and undeformed meshes on completion of loading lift 3 for cases A and D - displacements magnified by 2

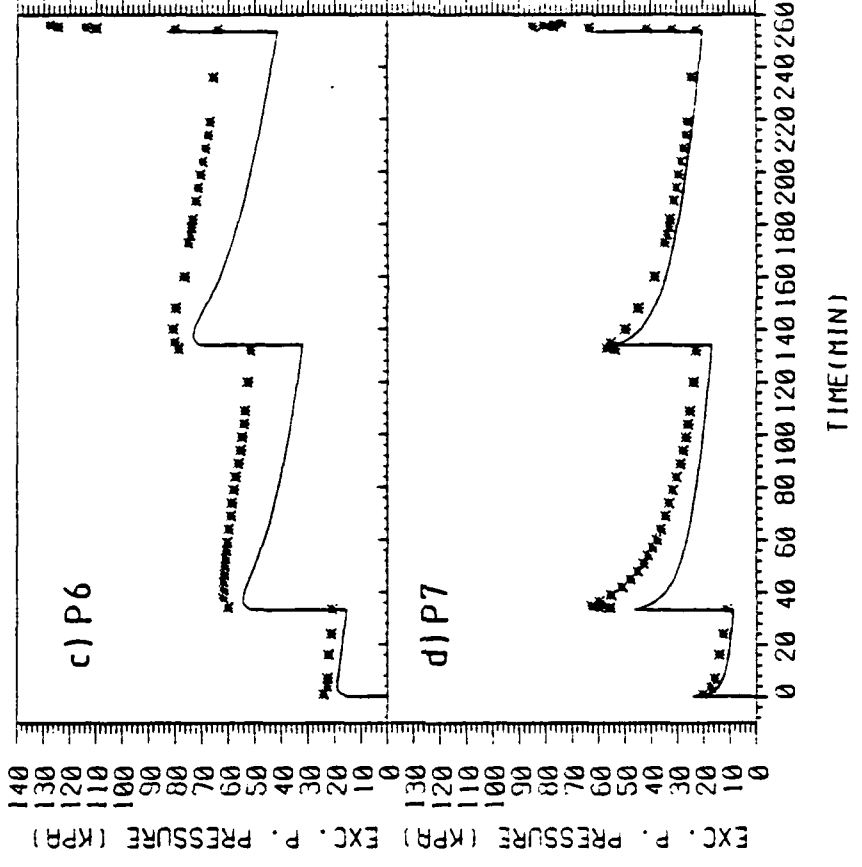
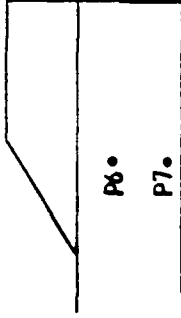
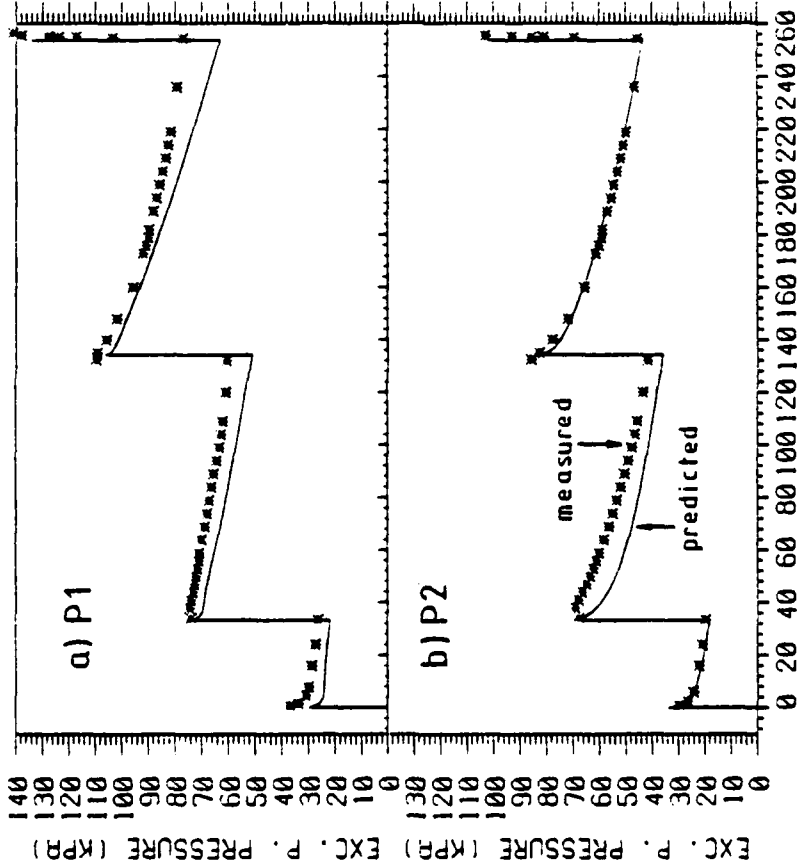
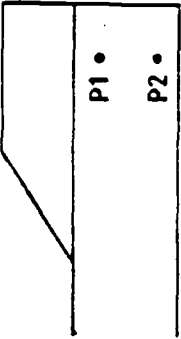


Fig. 4.15 - Measured and predicted pore pressures, transducers P1, P2, P6 and P7

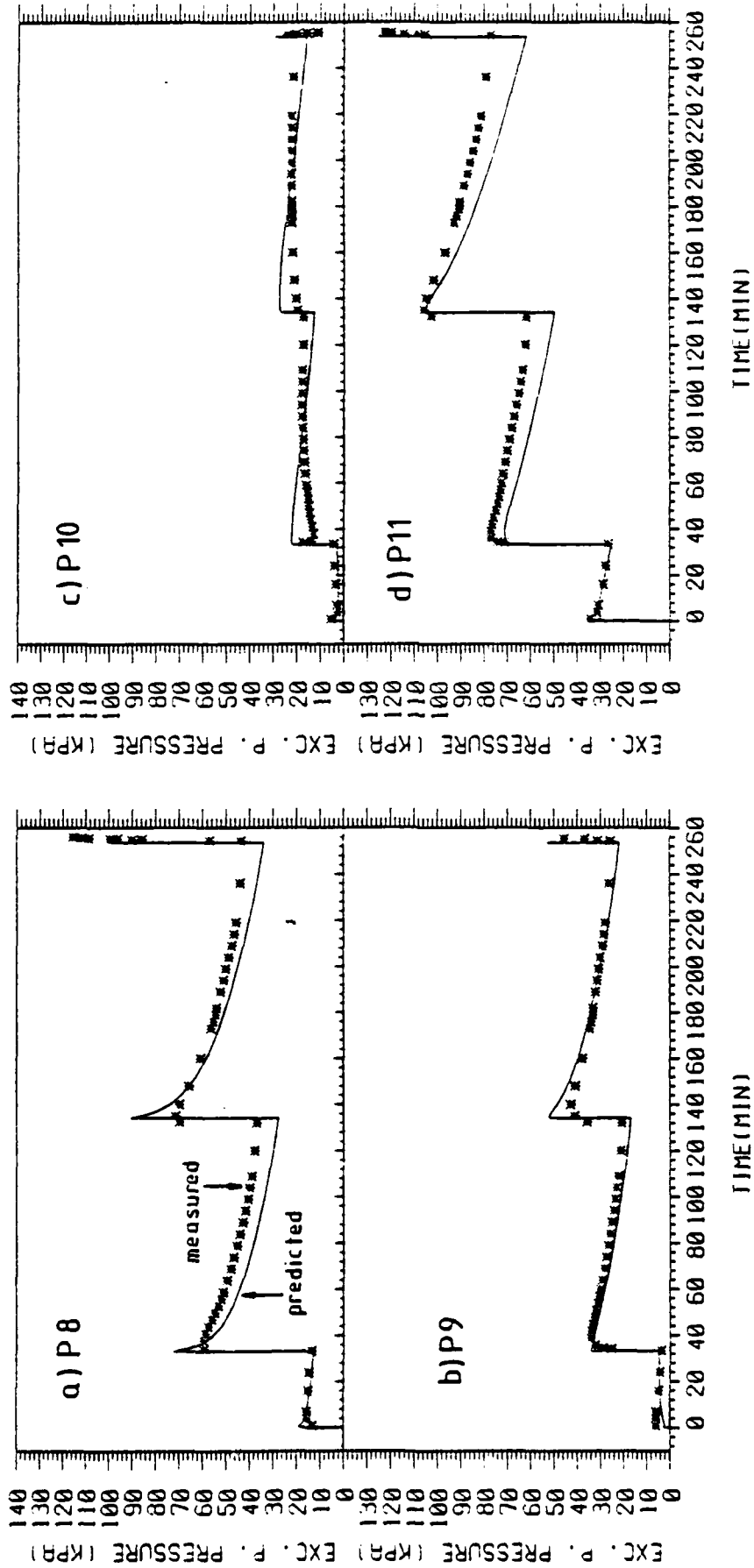
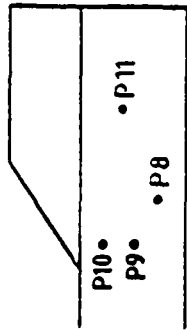


Fig. 4.16 - Measured and predicted pore pressures at transducers P8, P9, P10 and P11

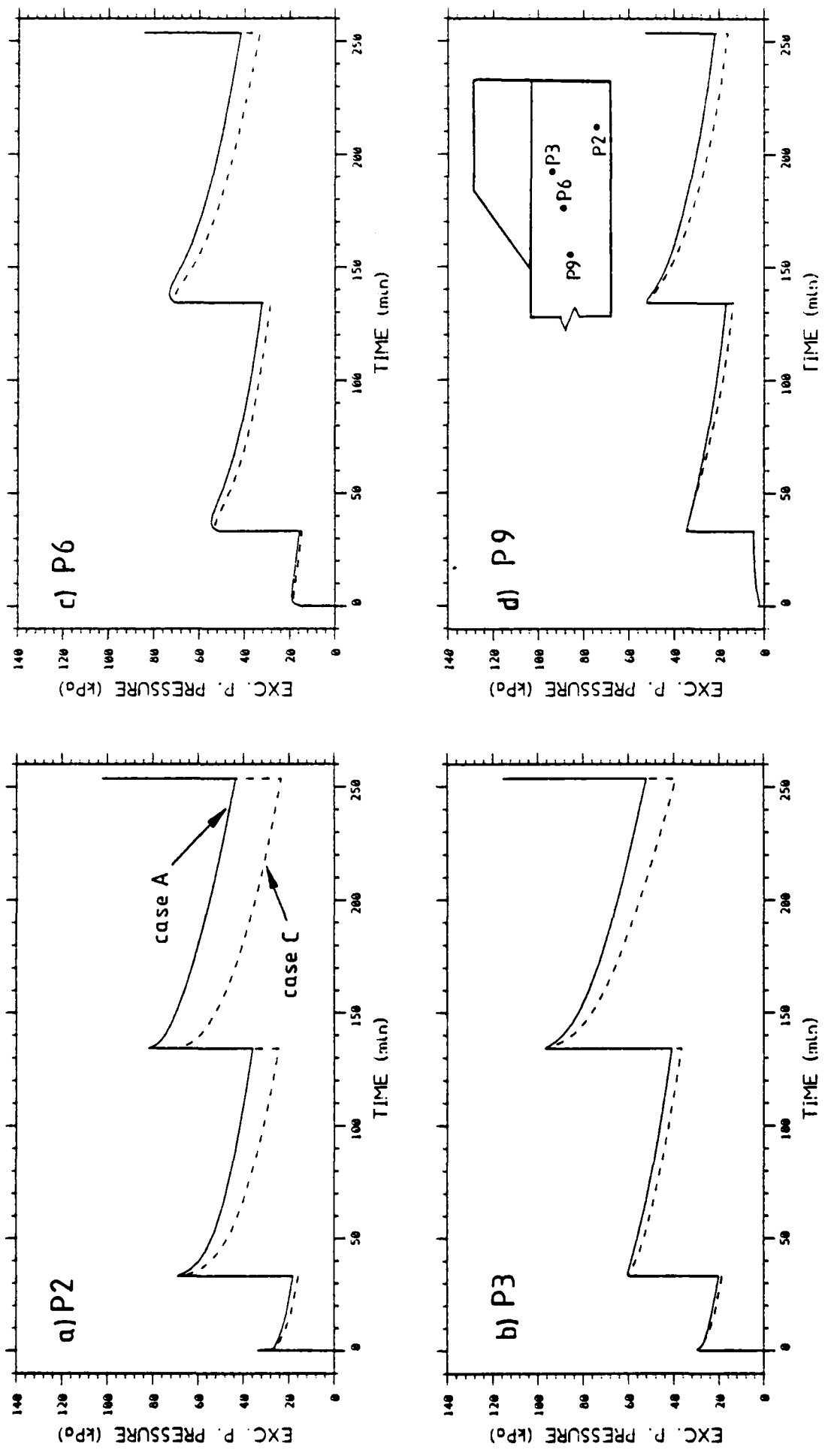
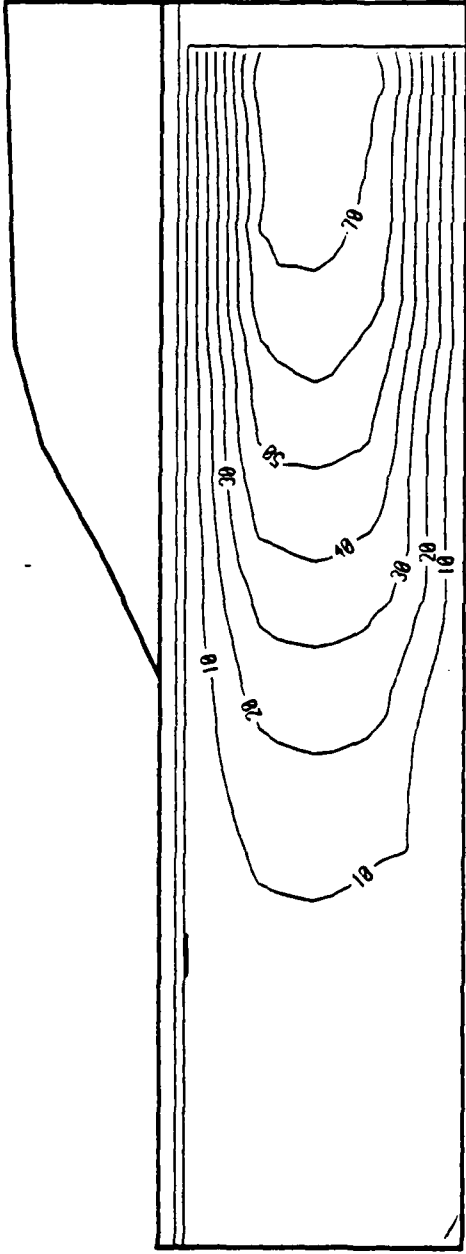


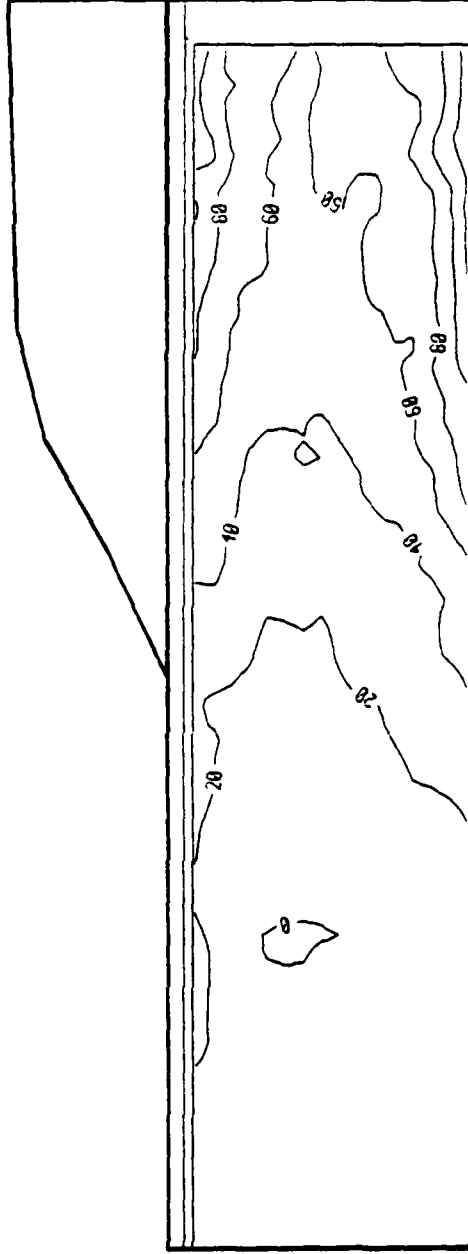
Fig. 4.17 - Influence of the hypothesis related to the permeability on the pore pressure response

0 5 10m

### TEST MA3 - STAGE 3-END



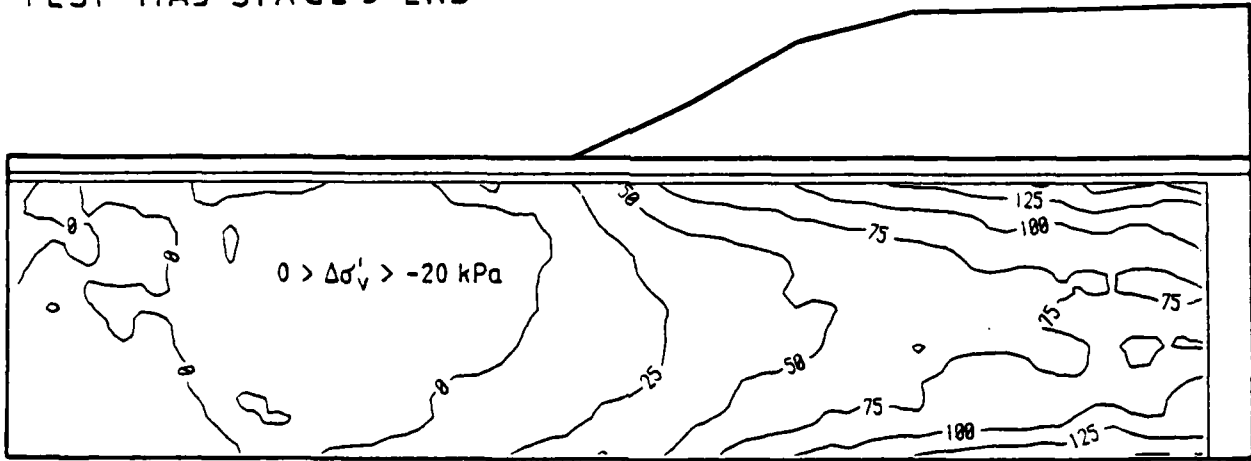
EXC PORE PRESSURE  $\Delta u$  (kPa)



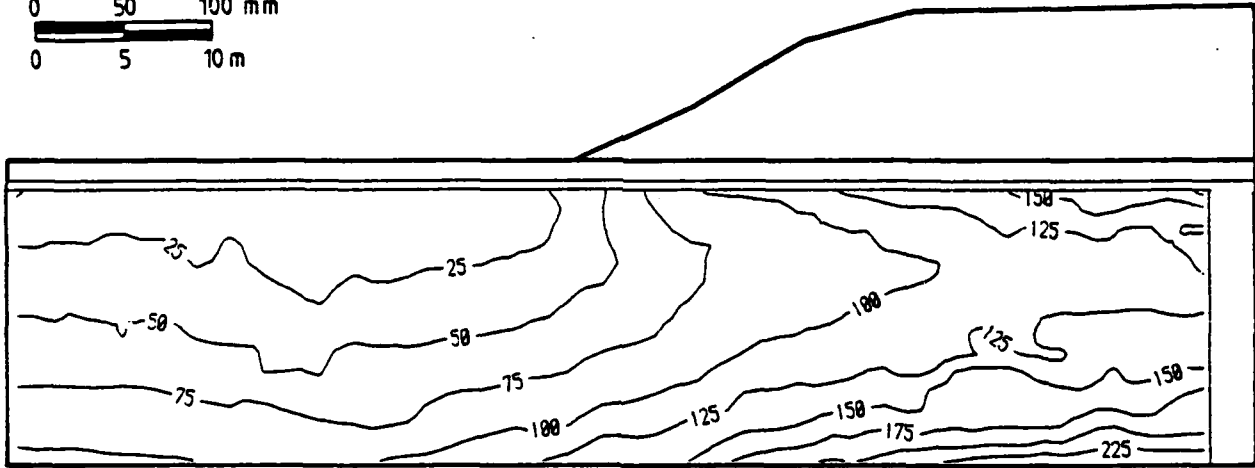
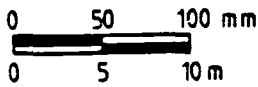
EFFECTIVE MEAN STRESS  $\Delta p'$  (kPa)

Fig. 4.18 - Predicted excess pore pressure and mean effective stresses

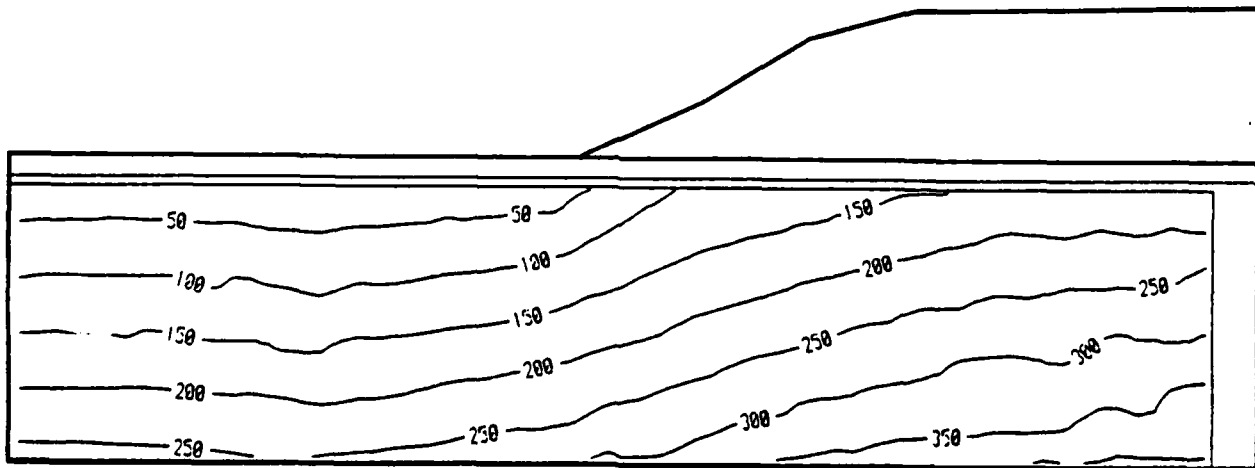
TEST MA3-STAGE 3-END



a) EFFECTIVE VERTICAL STRESS  $\Delta\sigma'_v$  (kPa)



b) EFFECTIVE VERTICAL STRESS  $\sigma'_v$  (kPa)



c) TOTAL VERTICAL STRESS  $\sigma_v$  (kPa)

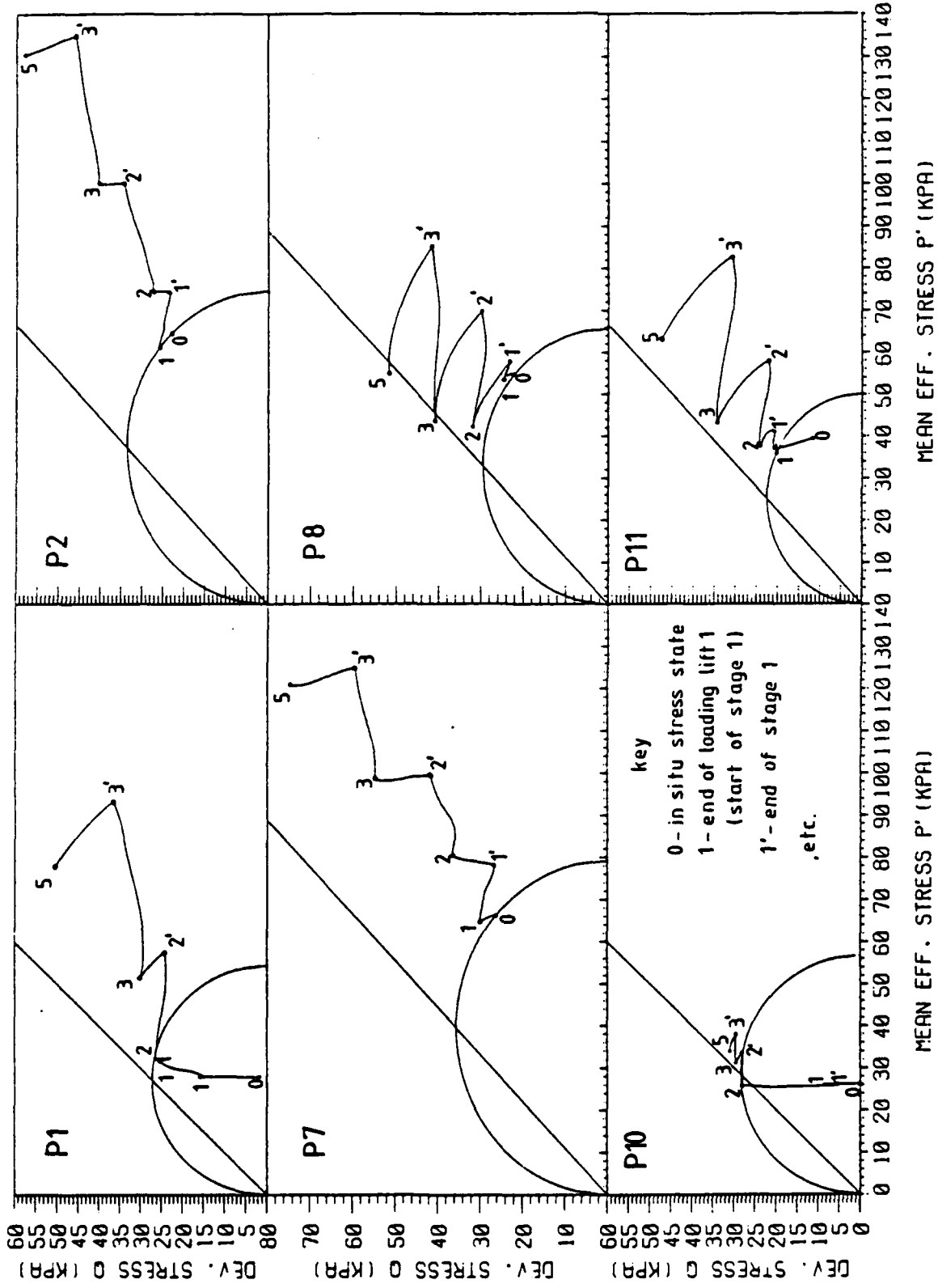


Fig. 4.20 - Computed stress paths at the location of transducers P1, P2, P7, P8, P10 and P11

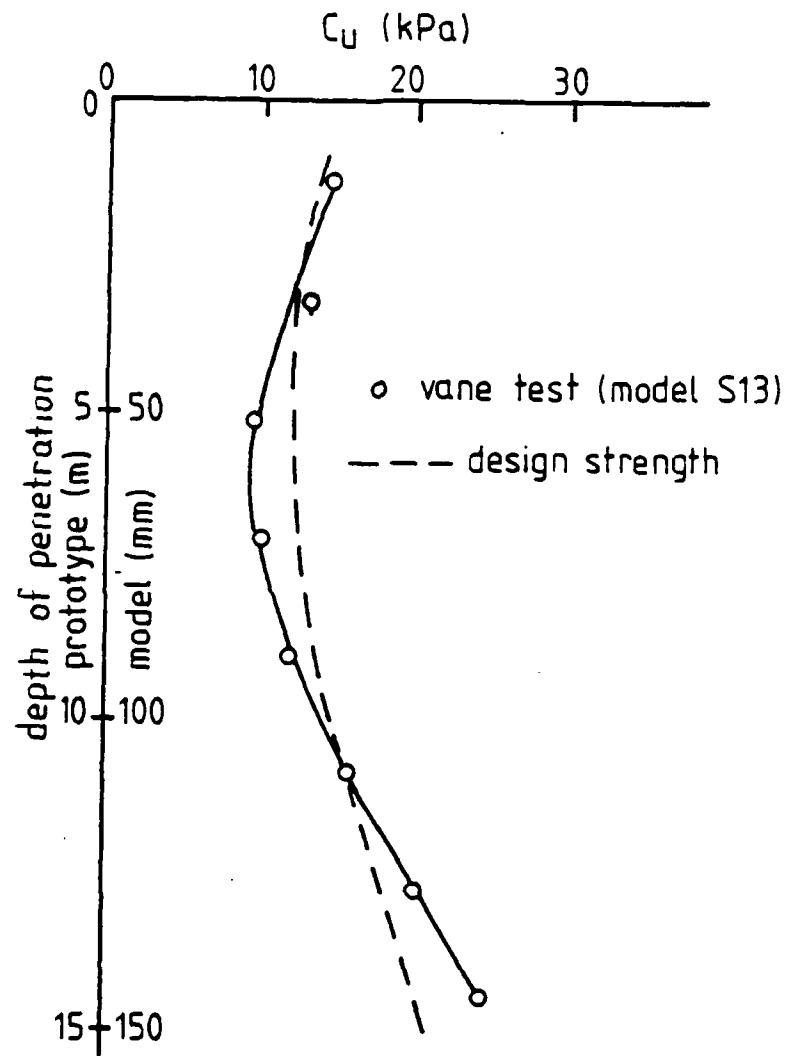


Fig. 5.1 - Predicted and measured undrained strengths

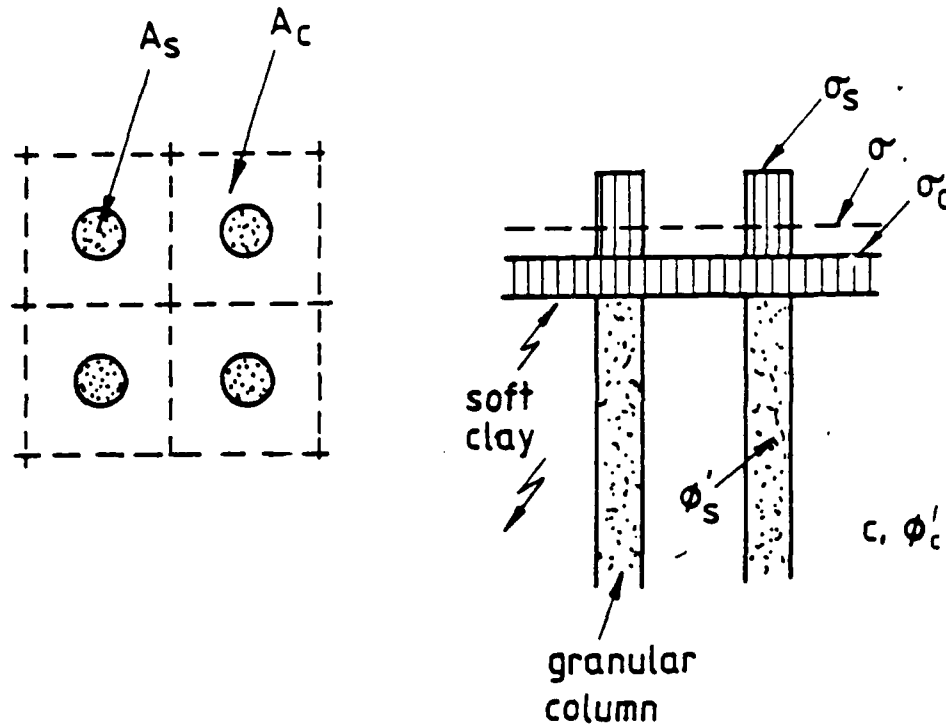


Fig. 5.2 - Stress distribution between granular column and soil

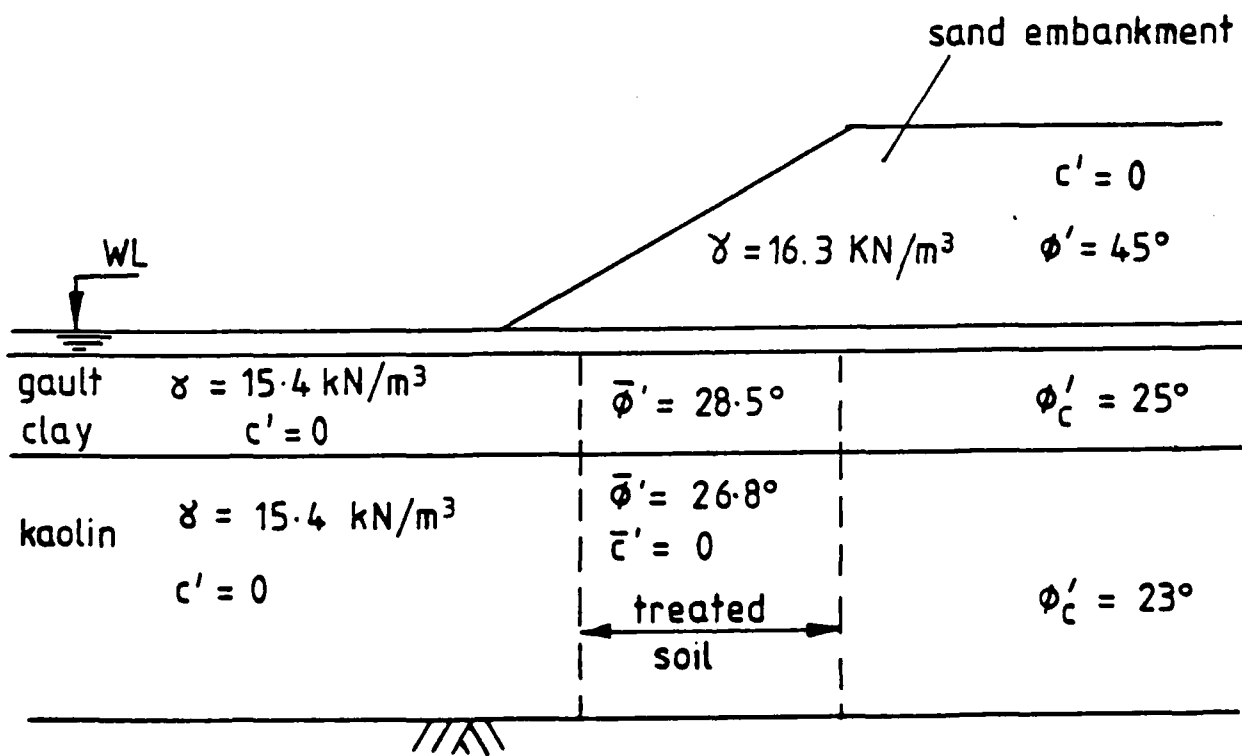


Fig. 5.3 - Soil parameters adopted for stability analyses of test MA6

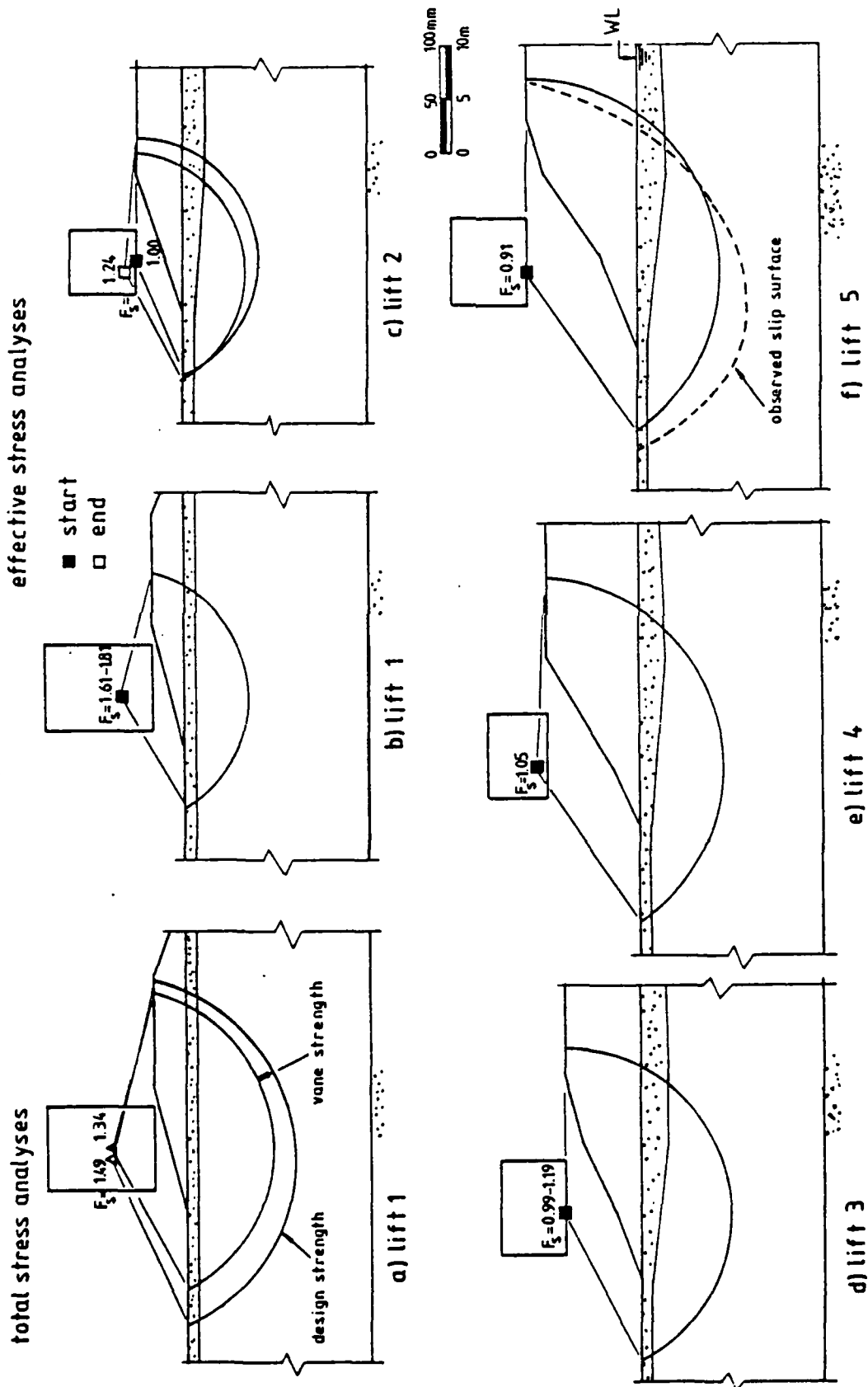


Fig. 5.4 - Stability analyses - test MA3

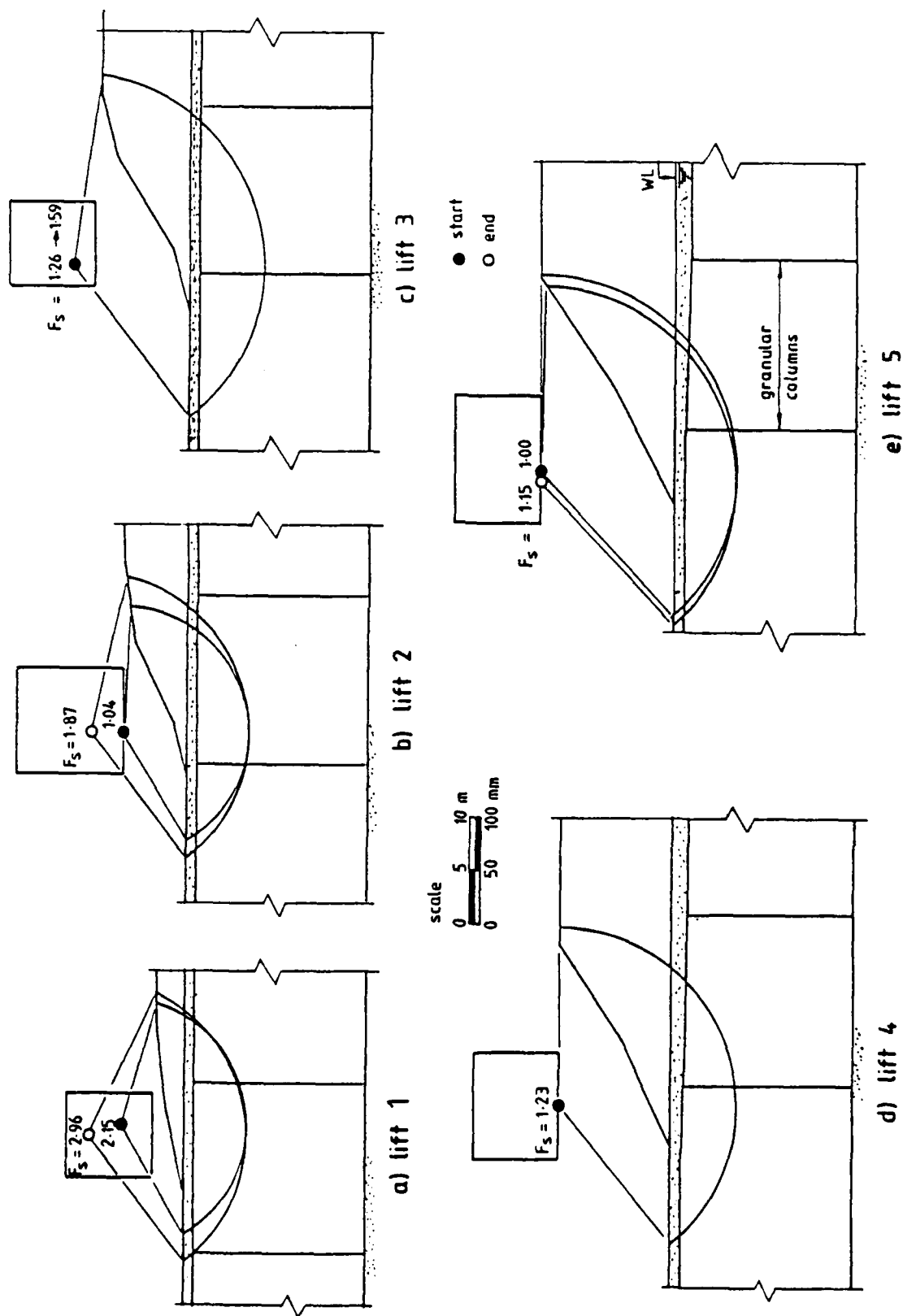


Fig. b.5 - Stability analyses - test MA6

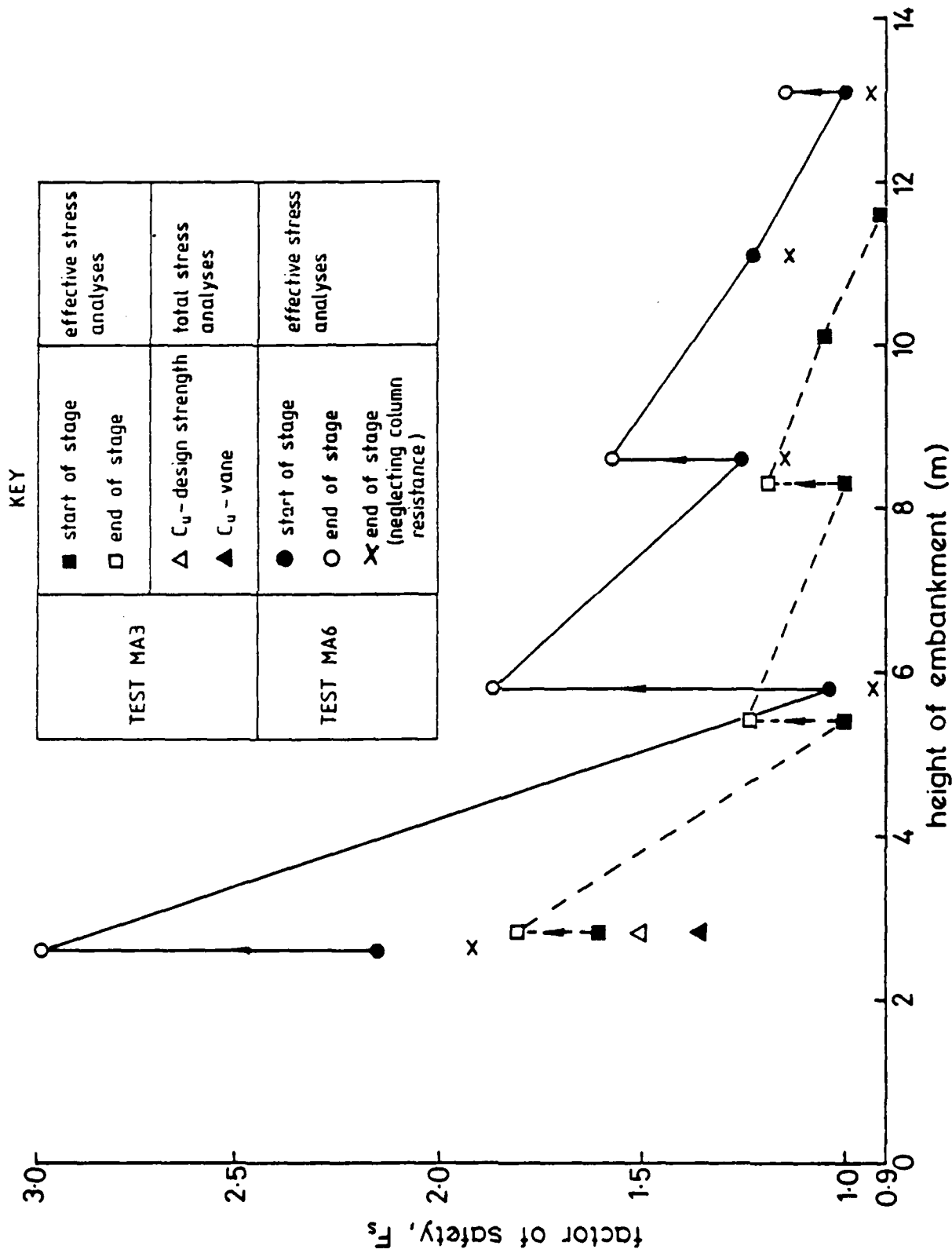
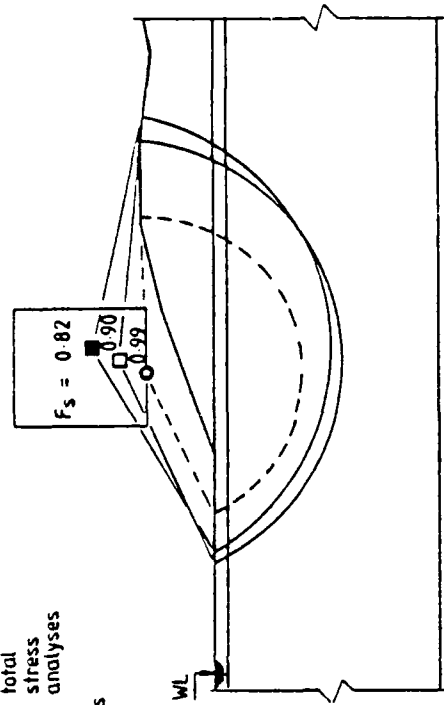


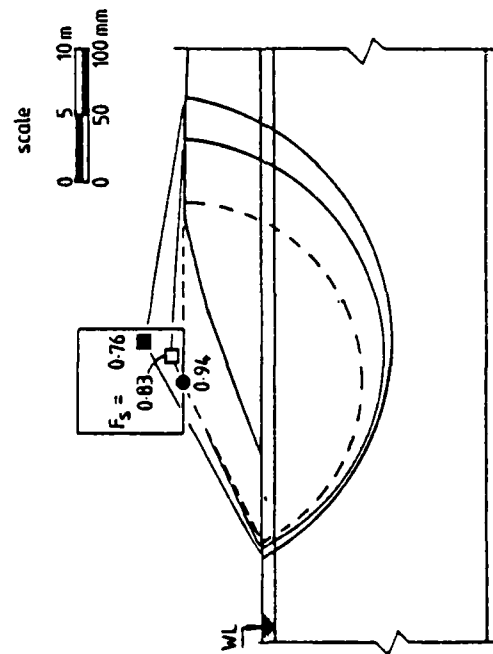
Fig. 5.6 - Variation of the factor of safety with height of embankment - stage constructed embankments MA3 and MA6

key

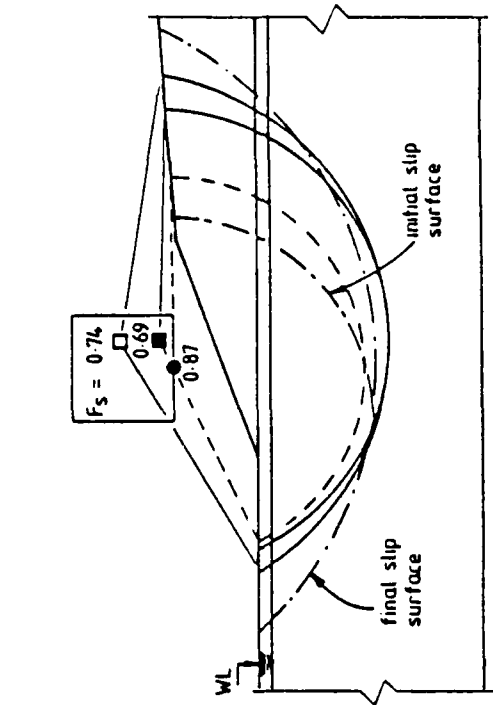
- C<sub>u</sub> design strength } total stress analyses
- C<sub>u</sub> vane strength } total stress analyses
- effective stress analyses



a) lift 1



b) lift 2



c) lift 3

d) lift 4

Fig. 5.7 - Stability analyses - test MA5

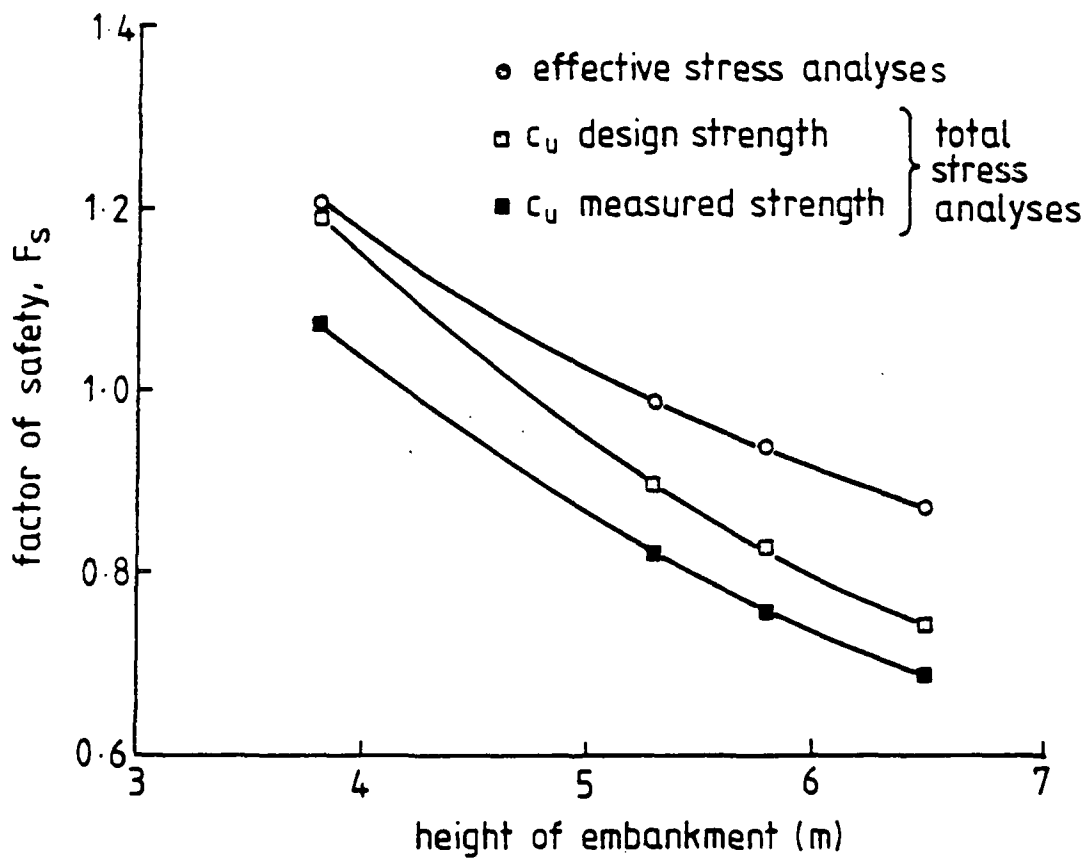


Fig. 5.8 - Variation of factor of safety with height of embankment - test MAS

**END**

**FILMED**

1-85

**DTIC**